UNIVERSITÀ DEGLI STUDI DI MILANO

Phd Program in Agriculture, Environment And Bioenergy
XXXVIII cycle

Dipartimento di Scienze Agrarie e Ambientali - Produzione, Territorio, Agroenergia

AGRO-HYDROLOGICAL MODELS FOR THE ASSESSMENT OF INNOVATIVE IRRIGATION PRACTICES IN RICE AREAS

SSD AGRI-04/A - Agricultural Hydraulics and Watershed Protection

PhD candidate: Giulio Luca Cristian Gilardi
Student ID: R13678
ORCID: 0000-0002-8207-9466

Supervisor: Prof. Arianna Facchi
Co-supervisor: Prof. Claudio Gandolfi
Coordinator: Prof. Salvatore Roberto Pilu

A.A. 2024/2025

ACKNOWLEDGEMENTS

I would like to thank Alice Mayer for introducing me, during my master's thesis, to our group's research on the San Giorgio district, including the 'semi-distributed' approach used in this study. I am also grateful to Michele Rienzner for his contribution to the same modelling framework and for developing a noteworthy groundwater level model for the district. My thanks go to Marco Romani (Ente Nazionale Risi) for supporting the analyses on San Giorgio, which sparked my interest in an 'adaptive' rice irrigation model. The support provided by ENR, essential to this study and to broader research activities, is of fundamental importance. I would like to thank AIES (Associazione Irrigazione Est Sesia) for providing discharge data and key information on irrigation practices and on the irrigation network system, not only in San Giorgio but across the wider Lomellina area.

The characterization of rice fields in the Lomellina region was carried out within a project in collaboration with ERSAF (Ente Regionale per i Servizi all'Agricoltura e alle Foreste), started during my first research fellowship. I am grateful to Marco Sciaccaluga for his contribution to the study. My sincere thanks go once again to Michele Rienzner for his expertise in measuring saturated hydraulic conductivity and developing PedoTransfer functions for rice soils. I am also grateful to Antonia Moreno Carrera for her laboratory work and for her constant encouragement. I must thank Darya Tkachenko for her participation in this research, for the fieldwork and the many activities we carried out together, and for her contribution to Chapter 4 of this manuscript.

I would like to thank Sílvia Cufí Aregay (University of Girona), the first external user of the QGIS-SWAP-Paddy tool, for her confidence in a tool still under development and for undertaking her research period abroad with us.

I would like to express my gratitude to Prof. Claudio Gandolfi, whose experience and knowledge have always been a point of reference. I also wish to thank Prof. Daniele Masseroni for the journey shared in California together with Prof. Claudio Gandolfi and Prof. Arianna Facchi, during our visit to UC Davis.

I am sincerely grateful to Prof. Arianna Facchi, my thesis supervisor, for all the opportunities she has offered me since the beginning of my academic career. Her guidance has been invaluable, and her unconditional support, even in the most difficult moments, makes her contribution especially meaningful to me.

Contents

1 Introduction

1.1 Context

1.1.1 The Lomellina Rice-Growing Area

Rice (Oryza sativa L.) is a globally consumed staple crop. Thanks to its broad environmental adaptability and socio-economic relevance, rice contributes significantly to human nutrition and plays an important role in global food security (Nayar, 2014). The majority of the world's rice is produced on irrigated land (Chauhan et al., 2017; Gassman et al., 2022). Rice accounts for 40% of all global irrigation and 17% of global ground water depletion (Patnaik et al., 2024). Water scarcity poses a challenge to the sustainability of rice production systems, as overuse of water resources and potential future reductions in water availability could further impact these intensively irrigated systems (Bouman et al., 2007; Liu et al., 2022; Silalertruksa et al., 2017). Exploring alternative irrigation strategies to conventional continuous flooding that improve irrigation efficiency at the field level while maintaining traditional gravity-based rice irrigation methods is a current research topic explored by many groups worldwide (Lampayan et al., 2015; Carrijo et al., 2017), including in Europe (Fasola and Ruiz, 1996; Gharsallah et al., 2023; Gilardi et al., 2023; Gonçalves et al., 2022; Zoffoli et al., 2023).

The north-western part of the Po Valley in Italy is the most important rice-growing area in Europe (Giuliana et al., 2024). The portion of this territory that falls in the Pavia province is called 'Lomellina' and covers more than 125,000 hectares (Figure 1). Of this, about 62,615 hectares are occupied by rice paddies. It is bordered by the Piedmont Region to the north, the Po River to the south, the Sesia River to the west, and the Ticino River to the east. Lomellina has a strong agricultural tradition, especially in rice cultivation. Together with Basso Novarese and Vercellese in the Piedmont region, it forms Italy's principal rice-growing area. Other significant agricultural uses include maize and woody crops, mainly poplars.

The paddy area in northern Italy, including the Lomellina area, is characterized by a complex geomorphological and hydrogeological structure that hosts one of the largest aquifers in Europe. Over the centuries, this land has been shaped to take advantage of the topographical gradient (north-west to south-east direction) to irrigate all the agricultural fields by gravity through an extensive network of unlined canals. This region has long been known for its abundance of surface water and its extensive network of unlined irrigation and drainage canals.

The main authority managing irrigation resources in Lomellina is the Associazione Irrigazione Est Sesia (AIES, https://www.estsesia.it/), while the Ente Nazionale Risi (ENR, https://www.enterisi.it/) is the reference authority for the agronomic practices adopted in the area.

According to the Köppen climate classification (Köppen, 1936), the Lomellina district has a humid subtropical climate (Cfa). Based on data from the Castello D'Agogna agro-meteorological station (ARPA Lombardia, https://www.arpalombardia.it/), which is the only one from the ARPA network located in the Lomellina area, the average cumulative rainfall in the period 1993 - 2024, during the agricultural season (April to September) is approximately 322 mm. The average air temperature during the same period is 20.6 °C, while the average wind speed at 2 meters is 1.5 m/s and the average daily global solar radiation is 233.3 W/m².

From a pedological prospective, in the study area there are 60 Cartographic Units (UCs) in the 1:50,000 Lombardy Region Soil Map (https://www.geoportale.regione.lombardia.it/), produced by the Ente Regionale per i Servizi all'Agricoltura e alle Foreste (ERSAF, https://www.ersaf.lombardia.it/) together with the LOSAN soils database (https://www.losan.ersaflombardia.it/) describing the characteristics of the reference soil profiles for each UC. Soils are generally characterized by a coarser texture (loam/sandy - loam) and by higher vertical percolation rates (0.7 - 2.3 cm/d) than those found in other rice-growing areas of the world (Gassman et al., 2022).

Historically, rice cultivation in Lomellina has relied on wet seeding and continuous flooding (WFL) until two-three weeks before harvest. As the WFL method traditionally adopted in the study area requires large volumes of water (Miniotti et al., 2016; Monaco et al., 2021), the increased frequency of periods of water scarcity and the competition between agricultural and non-agricultural users for water resources has led farmers to adopt water-saving techniques over the last 15 - 20 years. These include dry seeding followed by delayed flooding at the 3 - 4 leaf stage (DFL) or by turn-based irrigation (FTI) in years when water for continuous flooding after dry seeding is unavailable. Despite the benefits that dry seeding has brought to farmers (e.g., reduced working time and economic savings) it has resulted in lower groundwater levels in the early months of the irrigation season (April - May). This reduces the contribution of groundwater to river and irrigation network discharges, limiting mid-season water availability for agricultural areas downstream. Furthermore, farmers and irrigation managers perceive that competition for irrigation water between rice and other crops (e.g., maize) has increased since the introduction of this technique, especially in June and partially in July. This may be because with DFL the first flooding occurs at the beginning of June instead of April - May, and the first flooding event usually requires much more water than subsequent ones, since the soil is typically dry and the groundwater level is low.

The year 2022 was characterized by low levels of liquid and solid precipitation, and by high temperatures during the winter and spring-summer periods (AIT, 2024). This further emphasized the vulnerability of northern Italian rice systems and the urgent need to optimize irrigation management, while highlighting the buffering capacity of the first phreatic aquifer. Groundwater conditions play a crucial role in the hydrology of the Lomellina (Cesari De Maria et al., 2017; Mayer et al., 2019; Zampieri et al., 2019). In areas with shallow groundwater levels, such as the rice-growing regions of northern Italy, the interaction between the phreatic aquifer and the irrigation system (consisting of flooded paddy fields and unlined irrigation channels) creates a semi-natural, virtuous mechanism for water reuse. Percolation losses from flooded fields and channel beds raise the groundwater level, thereby reinforcing downstream river and irrigation canal discharges. This water is then reused for irrigation purposes. Furthermore, shallow groundwater levels (Figure 1) can reduce the percolation form paddy fields and thus the irrigation water required by rice during the agricultural season.

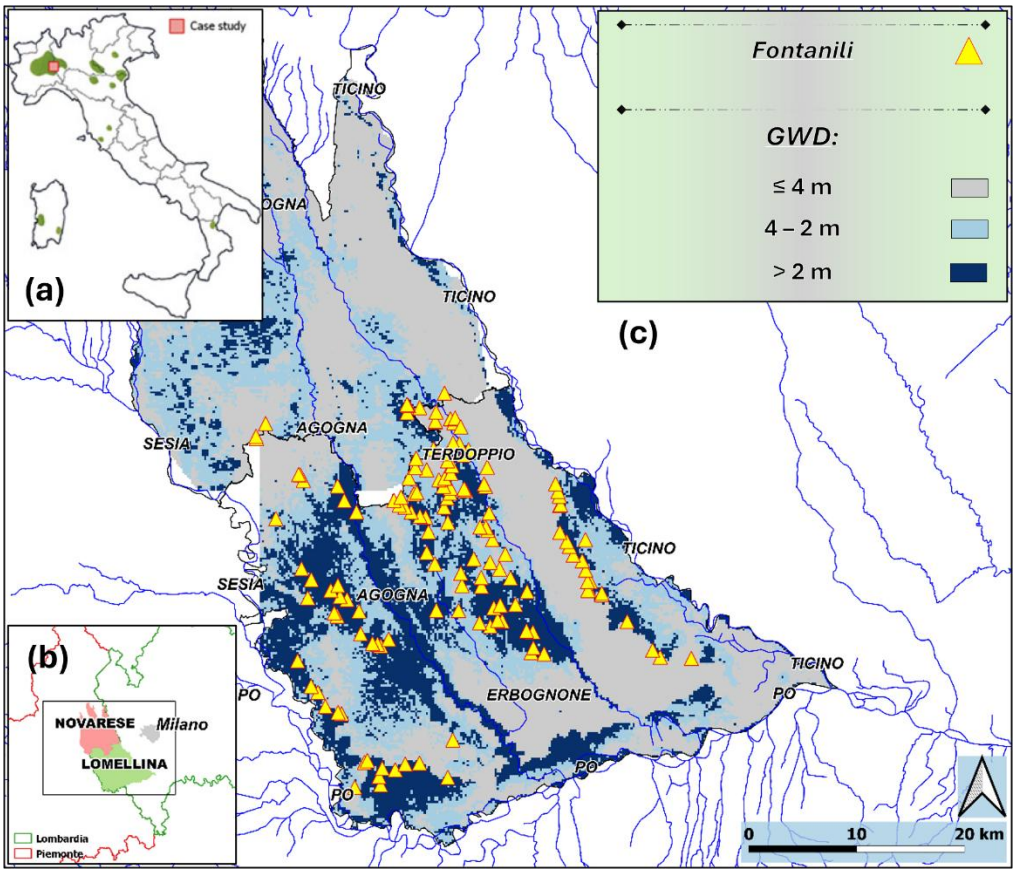

Figure 1. (a) General overview of rice-growing areas in Italy (ENR); (b) Novarese (Piedmont) and Lomellina (Lombardy) regions in the north-western part of Italy; (c) Surface hydrography and groundwater table depth (GWD, negative). Yellow triangles (Fontanili) indicate the depression springs surveyed by the Lombardy Region. Sources from https://www.geoportale.regione.lombardia.it/.

1.1.2 Alternate Wetting and Drying Rice Irrigation Strategy: Application in the Lomellina Rice-Growing Area

In many areas of the world, especially in Eastern and South-Eastern countries, Alternate Wetting and Drying (AWD) irrigation technique has been applied since the early 2000s (Lampayan et al., 2015). When AWD is adopted, paddy fields are subjected to intermittent flooding cycles, carried out only when the soil water status reaches a critical threshold, which can be expressed as a certain value of the soil water potential/content in the root zone (SWP, SWC) or as a specific water level depth (WLD) of the perched water table below the soil surface measured in a Water Tube (WT). Two types of AWD are generally described in the literature: i) 'safe', if SWP is maintained between soil saturation and -20 kPa (WLD ≤ 15 cm), or ii) 'severe', if SWP falls below -20 kPa (WLD > 15 cm) (Carrijo et al., 2017).

Many authors have studied, at the field level, the effects of AWD on different environmental and agronomical aspects, also considering its timing during the crop cycle and the severity of the threshold adopted; in Carrijo et al. (2017) 56 different studies were analyzed, including 528 comparisons between AWD and WFL. The results showed that, under a safe AWD, the yield did not significantly decrease and the achieved average reduction in water use (irrigation

+ rainfall) is, on average, 23.4%. Another relevant environmental benefit of AWD is the reduction of global warming potential (GWP), which is primarily being ascribed to the reduction of CH4, as a consequence of creating an unsuitable environment (oxidised conditions) for methanogenic soil bacteria (Liang et al., 2016; Linquist et al., 2015).

Most of the studies available in the literature have been conducted in Asia, and a comprehensive understanding of the effectiveness of AWD in contexts with different agronomic practices and pedo-climatic conditions is still needed. Recent field trials in Lomellina, conducted by the 'Centro Ricerche Riso' of the Ente Nazionale Risi (CRR-ENR) together with the University of Milan (UNIMI) and the University of Turin (UNITO), have shown that AWD can affect heavy metal dynamics in rice grain, lowering arsenic but increasing cadmium and nickel contents, with these effects closely linked to the local silty loam soil's chemistry and redox behaviour, making their uptake a key concern for its implementation in the area (Vitali et al., 2024).

During the 2019 - 2020 agricultural seasons, a safe AWD management (WLD ≥ -10/15 cm; SWP at -5 cm ≈ -5 kPa) was tested alongside WFL in a field experiment conducted within the MEDWATERICE project (PRIMA-Section 2, 2019 - 2023) at CRR-ENR. AWD reduced net irrigation water use by about 20.4% compared to WFL, without any loss in rice yield. Grain analyses showed no significant differences in total arsenic or cadmium concentrations between AWD and WFL, and all values were well below the EU maximum limits for milled rice (0.20 mg/kg for inorganic As; 0.15 mg/kg for Cd), indicating that under mild AWD thresholds heavy metal uptake did not pose a food safety concern in those seasons (Gharsallah et al., 2023).

In the RISWAGEST project (PSR Regione Lombardia, 2021 - 2022), wet seeding was combined with two AWD strategies: one safe (WLD ≥ -10/15 cm; SWP at -5 cm ≈ -5 kPa) and one strong (WLD ≥ -20/25 cm; SWP at -5 cm ≈ -20 kPa). Safe AWD achieved water savings of around 25% (1006 mm vs 1351 mm in WFL), and strong AWD of about 31% (932 mm), both without yield reduction, even in 2022, when irrigation water availability was limited. Experimental evidence from these trials showed that while AWD can significantly reduce total arsenic in rice grain (-30% with safe AWD and -37% with strong AWD compared to WFL), it may also lead to substantial increases in cadmium (from 17 µg/kg in WFL to 169 µg/kg in safe AWD and 237 µg/kg in strong AWD, both above the EU maximum limit of 0.15 mg/kg) and in nickel (from 95 µg/kg in WFL to 492 µg/kg in safe AWD and 632 µg/kg in strong AWD). These findings highlight the need for careful timing and modulation of AWD severity, taking into account soil properties and groundwater depth, to mitigate heavy metal uptake risks while still achieving water savings (Vitali et al., 2024).

The RISOSOST project (PSR, Regione Lombardia, 2023 - 2024), implemented in collaboration with CRR-ENR and involving different farm-scale case studies, designed an AWD protocol tailored to the Lomellina region (Figure 2). Following wet seeding, AWD began at the tillering stage and continued until a few weeks before harvest. The management relied on field Water Tubes (Figure 2), plastic tubes (Ø ~ 15 cm, length ~ 50 cm, fenestrated in the lower 30 cm) inserted into the soil, to monitor water depth relative to the soil surface, coupled with SmartWT (Mascherpa et al., 2025) devices developed by DiSAA-UNIMI for continuous logging and cloud transmission of water level data inside the WT. Soil moisture probes (Sentek, Australia; with sensors spanning from -5 cm to -115 cm from the soil surface) complemented the monitoring.

The AWD protocol applied a relatively severe threshold (-20 cm in WT) in early stages, a more cautious one (-15 cm in WT) during stem elongation, and a temporary suspension from booting to milk-dough stages (20 - 30 days) to reduce cadmium accumulation and avoid sterility. After the dough stage, the cautious threshold was reinstated. Monitoring points for the installation

of WTs and SmartWTs were selected by combining electromagnetic induction (EMI) soil conductivity maps and satellite imagery to identify zones with different water-holding capacities.

The number of AWD cycles was found to vary according to site conditions: few or no cycles occurred in heavier soils with shallow groundwater (around 10 - 15 cm), while cycles were more frequent (5 - 7) in lighter soils with deeper groundwater (around 1 m). This adaptive management approach reflects the trade-offs observed in RISWAGEST, even despite a reduction in the number of cycles due to the temporary suspension of AWD between the booting and milk-dough stages. However, AWD applied with the RISOSOST protocol still retains the benefits of water saving and As reduction, while mitigating the risk of Cd and Ni accumulation in the Lomellina pedo-climatic context.

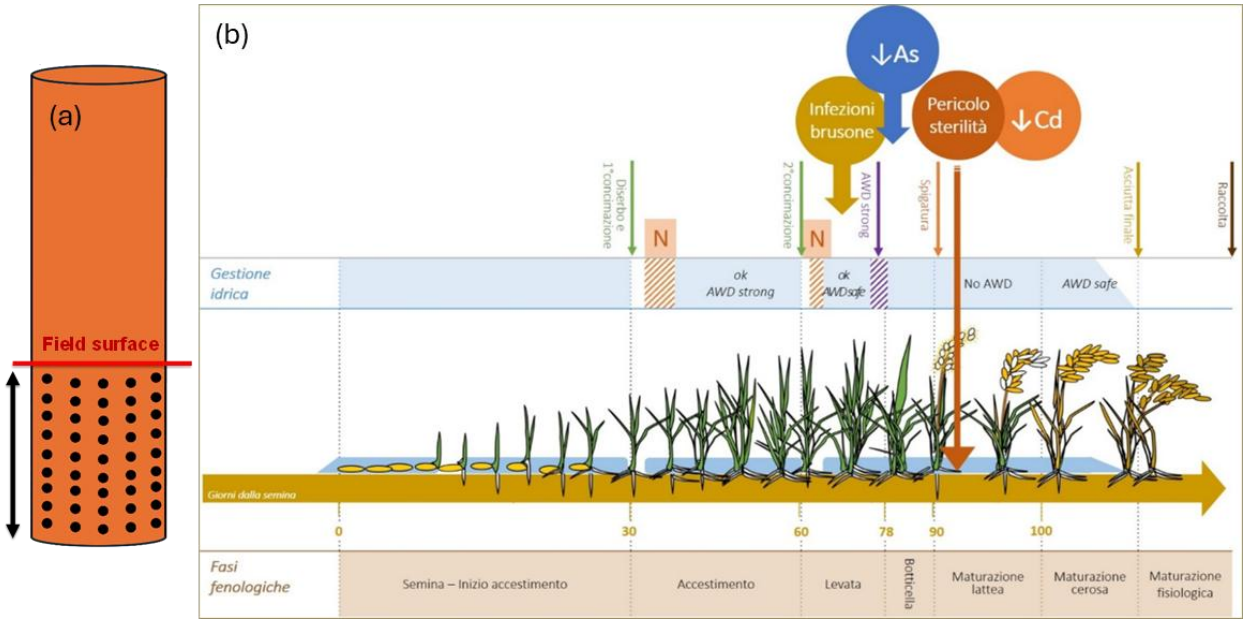

Figure 2. (a) Schematic representation of a Water Tube; (b) AWD protocol, RISOSOST project (source: ENR, Ente Nazionale Risi).

1.2 Rationale and main Material and Methods

1.2.1 Physically Based Agro-Hydrological Modelling

Water-saving irrigation strategies are usually assessed at the field level, with the objective of reducing water losses considered 'non beneficial', such as evaporation, surface runoff, seepage and deep percolation (Tuong et al., 2005). However, when considering large spatial domains, the evaluation of the effects of a massive change in irrigation strategies should include factors that are difficult to quantify, such as the interaction of irrigation and the groundwater system (Li and Ren, 2019a, 2019b; Singh et al., 2006a, 2006b). The coupling of hydrological, crop and water management models is becoming crucial in addressing the effects of new irrigation practices in agricultural areas, as it allows the investigation of the different phenomena involved in such complex systems (Siad et al., 2019; Uniyal and Dietrich, 2021). 'Physically-based' models (e.g., HYDRUS - https://www.pc-progress.com/, SWAP - https://www.swap.wur.nl/), developed to simulate water movements in the unsaturated soil on the basis of the Richards equation (Richards,

1931) are generally applied at the field level, while more 'conceptual' modelling approaches (e.g., APEX - https://epicapex.tamu.edu/, SWAT/SWAT+ - https://swat.tamu.edu/), usually based on a bucket approach, are implemented to simulate irrigation planning and management over large areas in a distributed or semi-distributed mode, as they require less data and computational effort.

Modelling offers the possibility to analyze the suitability of different irrigation techniques or management scenarios. However, to effectively explore all relevant processes occurring in complex agro-ecosystems, especially when considering different spatial scales within the same case study domain, careful attention must be paid to the physical description and parameterization of the systems under study. The unique environment of paddy areas makes it necessary to quantify water fluxes within the system using rigorous methods. This requires physically based models that can accurately describe the complex processes involved in managing the irrigation of paddy soils and capture the influence of shallow groundwater conditions on the soil water balance. However, this type of tool is missing from the literature.

The main aim of this Thesis is to develop a semi-distributed, physically based modelling framework for simulating water dynamics in rice-growing areas. This tool has been used in the Lomellina region, where the soil-crop-irrigation system was thoroughly parameterized, with particular focus on the hydrological properties of paddy soils. This framework enables various irrigation strategies alternative to wet seeding and continuous flooding to be evaluated. Particular focus is given to the wet seeding and Alternate Wetting and Drying (AWD) technique which has been shown in many parts of the world to improve water use efficiency in rice-growing areas while preserving the main functions of gravity-fed irrigation systems.

A tool such as the one developed and presented in this Thesis can be of great support to water resource planning and management in rice-growing areas, as it allows the effects of different irrigation management practices on the entire water resource system (including the aquifer system, if coupled with an aquifer flow model such as MODFLOW) to be explored. Focusing on the Lombardy-Piedmont rice-growing area (94% of Italy's rice-growing area; (ENR, 2024), this information can be extremely useful to irrigation managers (Land Reclamation and Irrigation consortia of rice-growing areas) as well as decision-makers (Lombardy and Piedmont Regional Authorities and/or Po River District Authority).

1.2.2 Soil Characterization for Agro-Hydrological Modelling in the Lomellina Rice Area

The geological formation of the Lomellina territory dates back to the Quaternary period, when the fluvioglacial activity of the Pleistocene (1.7 - 0.01 million years ago) and the subsequent fluvial processes of the Holocene (from 0.01 million years ago) progressively modelled its landscape (ERSAF, 2004). In this territory, two Landscape Systems can be identified: the fundamental level of the plain (L), consisting of the substrate formed at the end of the last Quaternary glaciation (the Würmian proglacial plain), and the fluvial valleys and terraces of the Holocene rivers (V). Within these two Systems, it is possible to identify different Landscape Sub-systems and, finally, several Landscape Units and Cartographic Units (UCs) describing the landscapes of the territory in a more detailed manner. A total of 60 UCs were identified and described in the 1:50,000 Soil Map for the Lomellina area by ERSAF.

An accurate characterization of soil hydraulic properties is essential for modelling key hydrological processes such as infiltration, evapotranspiration, runoff, and groundwater recharge. Core parameters include the soil water retention curve - $\theta(h)$ and the saturated hydraulic

conductivity - Ks, which, through Mualem's approach, are used to derive the unsaturated hydraulic conductivity curve - K(h). These parameters are critical inputs for physically based models of vadose zone water flow, widely applied in environmental, agricultural, and hydrological studies (Facchi et al., 2018; Raats and Knight, 2018).

Soil hydraulic properties can be determined through various laboratory and field methods, but their high spatial variability and the labor-intensive nature of direct measurements make large-scale application challenging (Vereecken et al., 2010). PedoTransfer Functions (PTFs) offer an alternative by estimating these properties from readily available data such as soil texture, organic matter content, and other basic characteristics (Bouma, 1989; Wösten et al., 2001). Some PTFs incorporate morphological and structural attributes to improve accuracy (Hollis et al., 2012; Ungaro et al., 2005), while others integrate measured hydraulic parameters, such as water contents at field capacity and wilting point, to better define the soil water retention curve (Ahuja et al., 1989; Saxton and Rawls, 2006). Bulk density (BD) is moderately informative on its own but strongly correlated with many soil characteristics, making it a key input for PTFs. Accurate BD measurement requires undisturbed samples, so it is often omitted from large-scale surveys in favor of disturbed samples to simplify fieldwork and reduce costs (Iovino et al., 2009). When unavailable, BD can be estimated via PTFs, but this may introduce significant uncertainty due to its central role in predicting hydraulic properties. The quality of BD predictors critically affects the reliability of PTF-derived parameters for the $\theta(h)$ and K(h) curves (Szabó et al., 2021).

PTFs vary in methodological complexity, from simple texture-based look-up tables (Schaap et al., 2001) to regression-based models (Patil et al., 2009; Tomasella and Hodnett, 1998; Vereecken et al., 1989) and, more recently, advanced machine learning approaches (Zhang and Schaap, 2017). Despite these developments, multiple regression remains the most widely used method, valued for its simplicity and the relatively small number of soil samples required (Li et al., 2007; Vereecken et al., 1989; Wösten et al., 1999).

Numerous PTFs have been developed to estimate soil hydraulic parameters, based on datasets ranging from very local (Mayer et al., 2019) to regional (Ungaro et al., 2005; Wösten et al., 1999) and even global scales (Zhang and Schaap, 2017). Most are calibrated for general agricultural soils, but are likely inadequate for rice soils, as they rarely use observational data from paddy fields. In traditional rice systems, fields are flooded from before sowing until shortly before harvest, maintaining a 5 - 12 cm water layer above the surface. These practices promote the formation of a compact, low-conductivity hardpan beneath the ploughed horizon, which restricts vertical percolation due to its lower saturated hydraulic conductivity compared to adjacent layers (Bouman et al., 2007; Facchi et al., 2018). The resulting vertical profile typically comprises a ponded water layer, a muddy surface horizon, the compact hardpan, and a subsoil weakly affected by cultivation (Wopereis et al., 1994). In such systems, the Ks of the hardpan is often the key parameter for estimating vertical percolation (Facchi et al., 2018).

The formation of the hardpan is a well-known consequence of the 'puddling' agricultural practice commonly conducted in paddy fields of Asia (Aimrun and Amin, 2009). The development of low-permeability soil layers has also been well documented in Lomellina, despite the absence of puddling practices, due to hundreds of years of plugging and monoculture rice cultivation using flood irrigation practices on the same fields. Prolonged rice cultivation and flooding irrigation, as well as biological phenomena developing in anaerobic/aerobic environments, have probably enabled clogging processes, both physical and biological. These effects have been observed in field conditions in stormwater infiltration ponds (Pedretti et al., 2024) and reproduced

mechanistically through biofilm-induced pore network modifications (Carles Brangarí et al., 2017).

Nevertheless, much more research is needed to gain sufficient knowledge to describe these phenomena. As Wösten et al. (2001) warn that applying PTFs outside their original domain can lead to inaccurate or unsatisfactory results, it is clear that paddy fields' unique soil conditions would require proper PTFs.

In a study conducted together with ERSAF and presented in this Thesis, a dataset containing soil physicochemical and hydraulic parameters measured in the laboratory for 170 soil horizons from 28 profiles sampled in rice-growing areas of Lomellina between 2012 and 2023 is presented. This database is used to validate PTFs already present in the literature by assessing their estimation accuracy for the paddy soils of this geographical area. The PTFs that guarantee the lowest estimation error are identified for all the soil hydraulic parameters, and calibration coefficients are developed where necessary. In the case of hardpan Ks specifically, a novel PTF was developed as those in the literature were found to be strongly unsuitable.

1.2.3 Metrics in Agro-Hydrological Modelling: Model Performance and Irrigation System Performance Assessment

In physically based agro-hydrological modelling, credibility rests on transparent calibration and validation against observations. To this end, widely adopted statistical indices provide complementary views of model fidelity (Moriasi et al., 2007). The Nash-Sutcliffe Efficiency (NSE, -) measures predictive skill relative to the mean of observations, ranging from $-\infty$ to 1, with values between 0 and 1 generally acceptable and 1 indicating perfect agreement. The RMSE-observations standard deviation ratio (RSR, -) normalizes error magnitude to observed variability, where lower values indicate better performance (often < 0.70 considered satisfactory). Percent Bias (PBIAS, %) quantifies systematic over- or under-estimation, with an optimal value of 0 and application-specific tolerances (e.g., $\pm$ 25% for streamflow).

When models inform on irrigation management, the simulations carried out must also reproduce and diagnose operational performance through field- and district-scale indicators (Ahmad et al., 2024). Water Application Efficiency (WAE, %) represents the ratio between the net crop irrigation water requirement and the total water delivered to the field (irrigation application plus rainfall). An ideal value of 100% indicates that supply exactly meets demand. As a field-level metric, WAE excludes conveyance losses (Bos et al., 1994; Molden, 1998). Typical application efficiencies are about 60% for surface irrigation, 75% for sprinkler systems, and up to 90% for drip irrigation (Burt et al., 1997; Pereira et al., 2012). Distribution Efficiency (DE, %) measures the fraction of water entering a system's headworks that actually reaches the fields, effectively the inverse of conveyance losses due to seepage, percolation, and operational leakage (Bos et al., 2005; Molden, 1998). While 100% is theoretical, observed values depend on lining, soil texture, and reach length: unlined canals range from roughly 60% in long sandy reaches to 80% in long clay reaches, 70 - 85% in medium reaches, and 80 - 90% in short reaches; well-maintained lined canals can consistently achieve around 95% (Burt et al., 1997; Pereira et al., 2012). However, DE in unlined channels also depends on the depth of the groundwater table and on the circulating irrigation discharge. Relative Water Supply (RWS, -) is a ratio between the total water supplied at the system inlet (including rainfall) and the total crop water requirement, providing a measure of supply adequacy at the system or district scale (Bos et al., 2005; Molden, 1998). Values close to

1.0 indicate a balance between supply and demand; 0.8 - 1.0 suggests a slight deficit; less than 0.8 indicates moderate to severe deficit; and greater than 1.2 points to oversupply.

1.3 Objectives and Organization of the Dissertation

This dissertation addresses the outlined research needs through: I) developing and applying a prototype agro-hydrological framework to assess the effects of alternative rice irrigation strategies on the water resource system at the irrigation district scale (San Giorgio di Lomellina district, about 1,000 hectares); II) using the experience gained with the prototype to develop a more flexible modelling framework integrated with a GIS, QGIS-SWAP-Paddy, suitable for simulating water flows in irrigation systems characterized by rice cultivation, also taking into account other areas (whether cultivated or not, e.g., bare soils, urban areas, etc.); III) defining the most suitable PTFs for describing the hydraulic characteristics of the Lomellina paddy soils, and IV) applying QGIS-SWAP-Paddy to quantify the impacts of AWD and other irrigation strategies on the Lomellina irrigation system water balance.

The dissertation is organized as follows:

- Chapter 2 presents the development, calibration, and application of a prototype agro-hydrological framework to a pilot irrigation district to evaluate the effects on the water resource system of different rice irrigation scenarios. This work has been published in the paper: Gilardi, G.L.C.[1], Mayer, A.[1], Rienzner, M.[1], Romani, M.[2], & Facchi, A.[1] (2023). Effect of Alternate Wetting and Drying (AWD) and Other Irrigation Management Strategies on Water Resources in Rice-Producing Areas of Northern Italy. Water, 15(12), 2150. https://doi.org/10.3390/w15122150, [1]Department of Agricultural and Environmental Sciences, University of Milan, 20133 Milan, Italy, [2]Centro Ricerche sul Riso, Ente Nazionale Risi, 27030 Castello D'Agogna, Italy;

- Chapter 3 describes the QGIS-SWAP-Paddy framework, detailing its workflow, data structure, and showing how the framework can be applied to agricultural areas including agricultural fields and irrigation networks. The framework is presented as an operational modelling tool tailored to low-land agricultural areas, particularly those dedicated to rice cultivation. This chapter will also serve as the basis for a future comprehensive manual of the developed tool, which will be accompanied by a more concise user guide, in view of its potential publication in the official repository of plugins for the open-source QGIS software. Moreover, it will be the basis for a scientific paper illustrating the tool;

- Chapter 4 focuses on the identification of the most suitable PTFs for estimating key hydraulic parameters for the Lomellina paddy soils. This work has formed the basis for the paper just submitted to Soil & Tillage Research: Tkachenko, D.[1], Rienzner, M.[1], Gilardi, G.L.C.[1], Sciaccaluga, M.[2], Brenna, S.[2], Gandolfi, C.[1], & Facchi, A.[1]. Hydro-pedotransfer functions for the main Italian rice district, [1]Department of Agricultural and Environmental Sciences, University of Milan, 20133 Milan, Italy, [2]Ente Regionale per i Servizi all'Agricoltura e alle Foreste (ERSAF), Regione Lombardia;

- Chapter 5 describes the application of the identified PTFs to the Lomellina paddy soils and the use of QGIS-SWAP-Paddy framework to assess the effects of AWD and other rice irrigation strategies to the Lomellina irrigation system. This work will serve as the basis for a forthcoming publication on the use of the tool for exploring different irrigation scenarios for the Lomellina district. In the next steps of the PROMEDRICE project (PRIMA-Section 2, 2023 - 2026), the framework will be integrated with the MODFLOW model (https://www.usgs.gov/software/modflow-6-usgs-modular-hydrologic-model/), simulating the water flows in the groundwater system of the Lomellina (under development by researchers from Earth science Department, UNIMI). The objective will be to produce an estimate of the different irrigation strategies, also under climate change conditions, on groundwater aquifer levels and therefore on water reuse in the irrigation system.

- Chapter 6 summarizes the main findings, discusses implications for irrigation management, and outlines directions for future research.

Annex 1 presents a work that was carried out alongside the main research activities presented in this Thesis, but which is closely connected to them. It illustrates the design and implementation of an extensive monitoring campaign carried out in 2021 in the San Giorgio di Lomellina paddy district to evaluate the occurrence of selected herbicides and nutrient losses in surface and groundwater under the current rice cropping strategies. Although my direct involvement in this work was limited and focused on the analysis of data collected, it provided a meaningful opportunity to contribute specific expertise and to broaden the environmental perspective on rice cultivation in the Lomellina district. This chapter is based on the Author's Accepted Manuscript of: Tediosi A., Ferrari F., Voccia D. Gharsallah O., Lamastra L., Botteri L., Rossi R., Ferrari T., Ballerini N., Gilardi G.L.C., & Facchi A. (2024) Herbicide and nutrient monitoring in surface waters and groundwater of a paddy district in northern Italy. Environmental Science and Pollution Research, 31:52963–52979. https://doi.org/10.1007/s11356-024-34692-x.

2 Development of a Prototype Agro-Hydrological Framework to Assess the Effects of Different Irrigation Management Strategies in the San Giorgio di Lomellina Irrigation District

2.1 Abstract

In rice areas with shallow aquifers, an evaluation of alternative irrigation strategies should consider the interactions between irrigation, groundwater recharge and water reuse, which are crucial for correctly evaluating the efficiency of the irrigation system. A modelling system composed of three sub-models developed within a MATLAB framework (a physically based, semi-distributed agro-hydrological model and two empirical models, the former for the channel network percolation and the latter for the groundwater level) was applied to a 1,000 ha rice district in the Padana Plain, Italy. The framework estimates the daily time series of the irrigation requirement and of the groundwater depth for each given irrigation management strategy, based on the inputs provided (agro-meteorology, crop data, soil data, irrigation practices, groundwater table depth upstream of the study area). After the calibration of the system based on a 'current state' scenario, five irrigation management strategies, relevant to the area, were compared: I) wet seeding and continuous flooding (WFL), II) wet seeding and alternate wetting and drying (AWD), III) dry seeding and delayed flooding (DFL), IV) dry seeding and fixed-turn irrigation FTI), V) early dry seeding and delayed flooding (DFLearly). Due to economic advantages, dry-seeded techniques (DFL, and FTI) are replacing the traditional WFL in northern Italy. Simulations show that dry seeding techniques lead to a drastic decrease of the water table in April/May, reducing the overall irrigation efficiency of the area. In particular, DFL (widely adopted in the area) causes a rice irrigation need in June higher than WFL, when other crops increase their water demand, exacerbating eventual water shortages in the area. AWD turned out to couple smaller irrigation needs (from June onwards) compared to WFL with a maintenance of the groundwater recharge, especially in the first part of the irrigation season, thus being a recommendable rice management strategy for the study area.

2.2 Motivation and Objectives

Historically, rice cultivation in Lomellina has been carried out using wet seeding followed by continuous flooding until two to three weeks before harvest (WFL). In response to increased water scarcity, farmers have implemented water-saving practices, including dry seeding with either delayed flooding (DFL) or intermittent flooding (FTI), both of which start at the third to fourth leaf stage. Farmers have embraced these techniques for their economic and labor-saving advantages, but they have also inadvertently accelerated the lowering of phreatic groundwater levels during the early agricultural season (April - May). This decline diminishes the contributions of shallow aquifers to river flows and unlined canals, sharpening competition for water in the critical summer months (June - July). The application of Alternate Wetting and Drying (AWD)

after wet seeding may be considered, as it can help maintain groundwater recharge in April - May and decrease irrigation requirements for rice in June - July without negatively affecting yield.

This chapter proposes the use of a modelling framework developed in MATLAB consisting of three sub-models: the first for the agricultural area, based on a semi-distributed application of the well-known physically based SWAP model (https://www.swap.wur.nl/), the second and the third, empirical, for the groundwater level dynamics and their interaction with the channel network percolation. The modelling framework, calibrated in a previous study (Mayer et al., 2019), was revised and optimized in this Thesis, and completed by a crop development model. After these steps, it was used to explore the effects on the water resource system of the San Giorgio di Lomellina district (Pavia; Figure 3) of realistic scenarios based on the adoption of specific irrigation strategies for the rice crop.

The set of the irrigation management strategies to be tested was selected in collaboration with the National Rice Authority (Ente Nazionale Risi - ENR, https://www.enterisi.it/) and discussed with the irrigation managers governing water in the district (AIES, Associazione Irrigua Est Sesia). The chosen set, besides the aforementioned WFL, AWD, DFL and FTI, also includes an early seeding DFL (beginning of April, DFLearly). The DFLearly was conceived to balance the request of farmers that want: I) to maintain the dry seeding due to economic advantages, II) to anticipate the use of water in April - May, where it is usually abundant and no other crops need it, III) to recharge the phreatic groundwater at the beginning of the agricultural season.

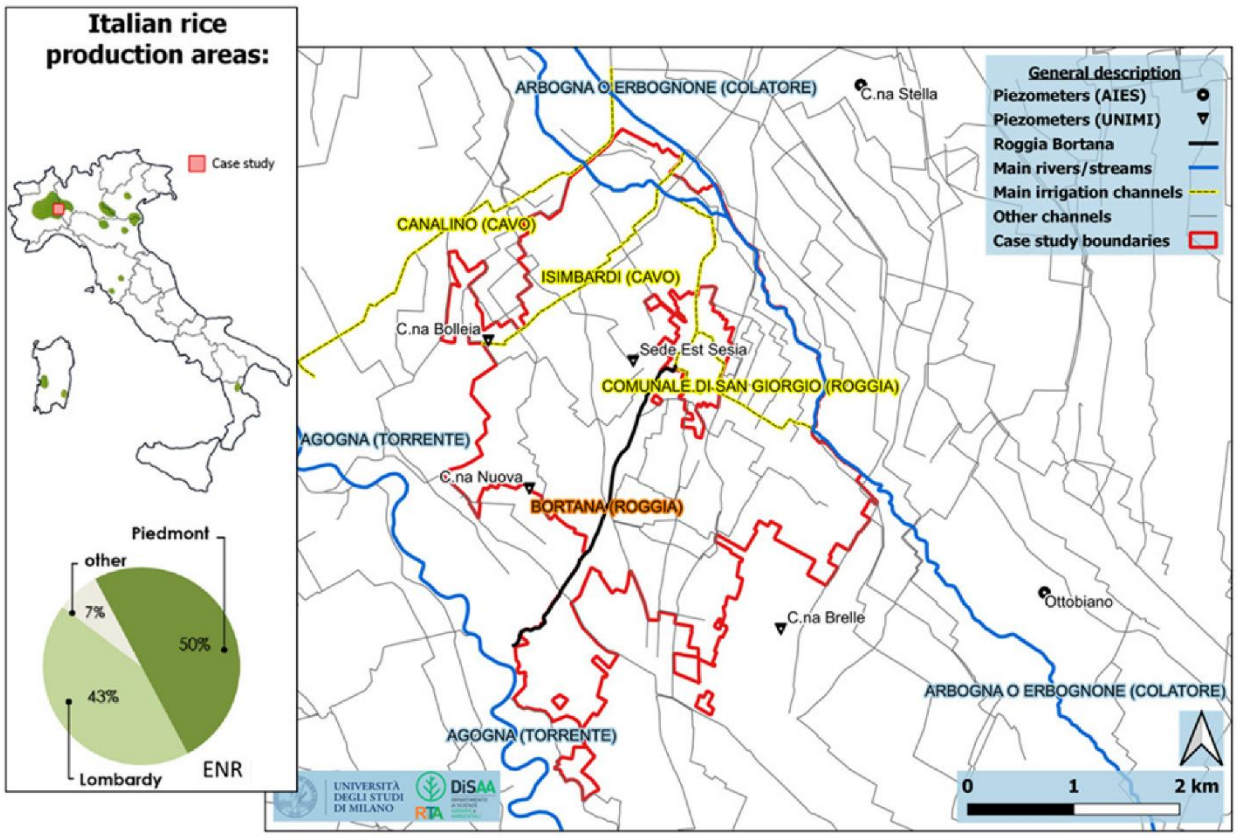

Figure 3. General overview of rice-growing areas in Italy and siting of the pilot irrigation district (San Giorgio di Lomellina, Pavia, northern Italy).

2.3 Materials and Methods

2.3.1 Pilot Irrigation District and Data Availability

The pilot irrigation district, located approximately 45 km south-west of Milan, is in the western part of the municipality of San Giorgio di Lomellina (Pavia, Italy) and covers an area of about 1,000 ha.

Hourly time series of the needed agro-meteorological variables were obtained for the period 2013 - 2020 at a station located approximately 12 km north-west of the district center (Castello d'Agogna, Pavia, Italy; Agenzia Regionale per la Protezione dell'Ambiente, ARPA Lombardia, https://www.arpalombardia.it/). In the period April - September, the average rainfall, mean air temperature, wind speed at 2 m and daily global radiation were found to be respectively: 326 mm, 21 °C, 2 m/s and 338 W/m^2.

The irrigation water diverted in the district comes from three canals (Roggia Comunale di San Giorgio - RCSG, Cavo Isimbardi - CiSi and Cavo Canalino - CCan; Figure 4) managed by Associazione Irrigazione Est Sesia - AIES (AIES, https://www.estsesia.it/). Channel network losses are not quantified; however, they have been estimated to be on average one third of the water discharges during the central part of the agricultural season by AIES. The water table strongly influences percolation losses, which are characterized by higher rates at the beginning of the season (when the water table is deeper) and lower rates at the end of the season.

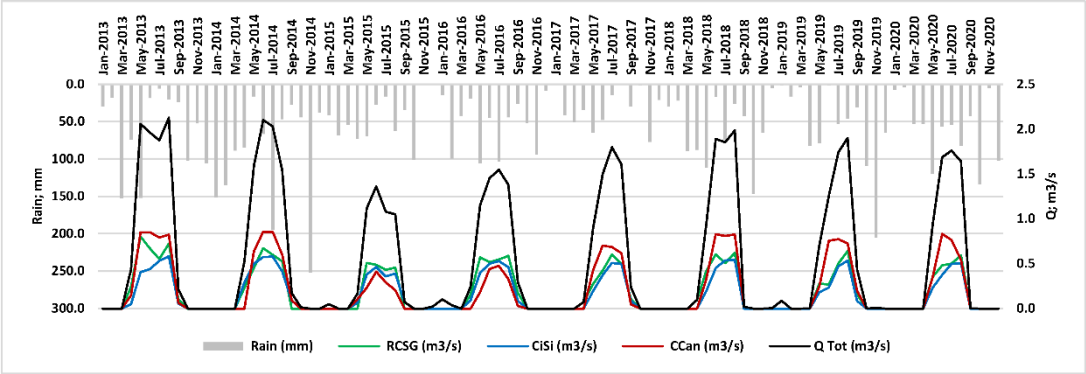

Figure 4. Monthly discharges (m^3/s) delivered by AIES in 2013 - 2020. QTot represents the sum of the discharges conveyed by three main channels of the district: Roggia Comunale di San Giorgio (RCSG), Cavo Isimbardi (CiSi) and Canalino (CCan).

As the district is bordered by two rivers (Agogna and Arbogna), the phreatic aquifer is sufficiently hydrogeologically delimited on the east and west sides of the study area, but not in the north and south directions. Groundwater level (GWL) data series representative for the regional aquifer north of the district were obtained from a piezometer located at Cascina Stella. Inside the district, GWL has, since 2015, been measured twice a week in four piezometers and in another nearby districts (Ottobiano). This data (the four piezometers installed by UNIMI and the two from AIES), together with water levels measured in the deep drainage channel Bortana, added as a constant value, were used to interpolate phreatic GWL of the district on July 15th each year during the studied period (2013 - 2020), as described in (Mayer et al., 2019). This date was chosen because

the GWL is assumed to be maximum in the district and the obtained map is used by the modelling framework to split the district into two groundwater depth (GWD) sub-areas. For each sub-area, daily spatial interpolations are used to compute two daily GWD series (shallow and deep; see Section 2.3.2). Figure 5 displays an example of a GWL map built for the day 15 July 2020, together with a comparison of the measured GWL in Cascina Stella (upstream of the pilot district) and in the district (average value) for the period 2013 - 2020 on a monthly basis.

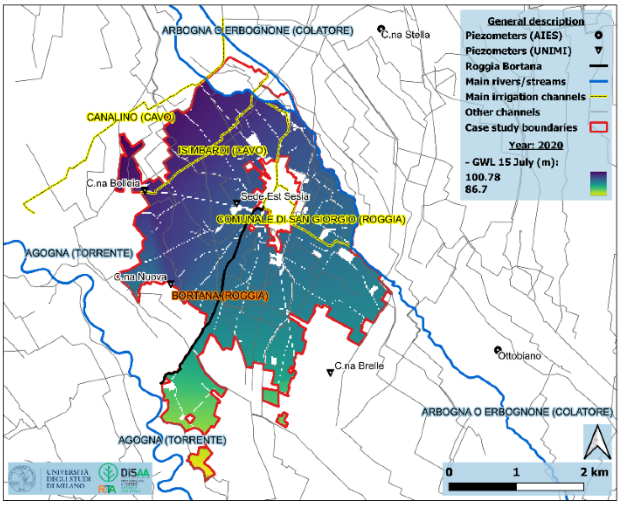

(**a**)

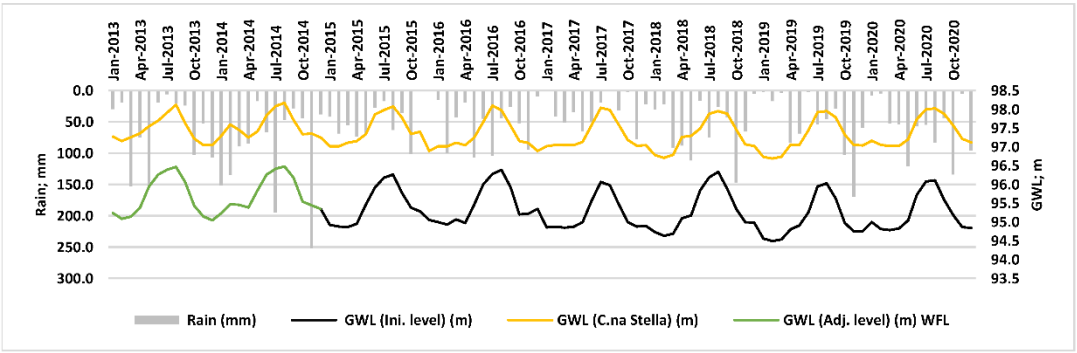

(**b**)

Figure 5. (a) Interpolated GWL (m) of 15 July map (2020); (b) Average monthly GWL (m) in San Giorgio and Cascina Stella for 2013 - 2020. Since data for the district were not available for years 2013 - 2014, the simulated values obtained from the PGL model (see Section 2.3.2) for WFL scenario are shown in green.

To describe the soils of the district area (Table 1), five units were defined starting from the 1:50,000 Lombardy Region Soil Map (https://www.geoportale.regione.lombardia.it/; Ente Regionale per i Servizi all'Agricoltura e alle Foreste - ERSAF, https://www.ersaf.lombardia.it/). Subsequently, the hydraulic properties of each horizon were estimated through PedoTransfer Functions (PTFs). The Bulk Density (BD) was estimated using the PTFs presented in (Tomasella and Hodnett, 1998), while the parameters of the soil water retention curve (θ(h)) and the saturated hydraulic conductivity (Ks) were estimated using the PTFs presented in (Ungaro et al., 2005). In order to take into account the compaction that characterizes paddy field soils, the BD for each soil

horizon and the Ks for the less conductive soil layer in the profile were corrected by means of empirical coefficients retrieved by experimental data (Mayer et al., 2019).

Table 1. Parameters of the Mualem - Van Genuchten functions. In the last column, values in parentheses indicate Ks values modified to account for the compaction of the less conductive soil layer in the profile of paddy field soils.

Unit	Depth	BD	θr	θs	α	n	λ	Ks
	cm	g/cm³	cm^3/cm^3	cm^3cm^3	1/cm	-	-	cm/d
407	0 - 25	1.74	0.0000	0.3348	0.0169	1.2859	0.2859	13.86
	25 - 50	1.77	0.0000	0.3226	0.0111	1.1940	0.1940	89.20
	50 - 75	1.77	0.0000	0.3220	0.0154	1.1610	0.1610	88.82 (0.97)
	75 - 105	1.55	0.0000	0.4034	0.0244	1.8436	0.8436	109.61
	105 - 120	1.58	0.0052	0.3926	0.0688	1.1940	0.1940	114.48
409	0 - 40	1.65	0.0000	0.3686	0.0467	1.1451	0.1451	56.78
	40 - 67	1.54	0.0008	0.4071	0.0467	1.3479	0.3479	365.84
	114 - 150	1.65	0.0496	0.3675	0.0347	1.1352	0.1352	16.33 (0.18)
	192 - 228	1.49	0.0537	0.4263	0.0470	1.6820	0.6820	283.34
410	0 - 25	1.72	0.0000	0.3400	0.0295	1.1053	0.1053	1.31
	25 - 40	1.69	0.0043	0.3537	0.0186	1.2098	0.2098	22.52
	40 - 70	1.63	0.0447	0.3761	0.0261	1.1365	0.1365	14.15 (0.15)
	70 - 100	1.68	0.0584	0.3562	0.0318	1.1319	0.1319	27.01
	100 - 160	1.62	0.0401	0.3769	0.0877	1.1940	0.1940	225.56
413	0 - 22	1.65	0.0453	0.3660	0.0697	1.1073	0.1073	2.71
	22 - 29	1.78	0.0000	0.3194	0.0295	1.1940	0.1940	28.86 (0.32)
	29 - 60	1.68	0.0541	0.3558	0.0336	1.0772	0.0772	132.60
	60 - 104	1.46	0.0252	0.4397	0.0634	1.6115	0.6115	214.05
	104 - 117	1.57	0.0000	0.3961	0.0571	1.9240	0.9240	263.97
	117 - 157	1.43	0.2235	0.4510	0.1660	1.1940	0.1940	28.78
417	0 - 35	1.72	0.0000	0.3420	0.0301	1.0922	0.0922	1.03
	35 - 40	1.74	0.0000	0.3346	0.0091	1.2955	0.2955	37.58 (0.41)
	40 - 85	1.77	0.0000	0.3239	0.0162	1.0704	0.0704	136.27
	85 - 140	1.73	0.0000	0.3389	0.0122	1.2200	0.2200	47.83

The land use map of the area is available on a yearly basis (20 m × 20 m SIARL raster maps; https://www.geoportale.regione.lombardia.it/). The rice-growing area of the district covers approximately 90% of the agricultural surface, while the remaining 10% is cultivated mainly with maize and poplar (Figure 6). The Modified Normalized Difference Water Index (MNDWI) (Xu, 2006), calculated starting from Landsat 7/8 and after 2016 from Sentinel-2 images for the period April - May, when flooding starts in wet-seeded paddies, was calculated every year to identify wet seeded and dry seeded rice areas (Mayer et al., 2019). Regarding crops, as poplar is only irrigated in the first four years out of ten and covers a very limited area in the district, the poplar area was randomly divided into young (irrigated) and mature (rainfed), following a 40 - 60% ratio. Maize, also covering a limited area, was considered to follow a fixed development cycle, with emergence on 20th April and harvest on 3rd September. As regards rice, development stages were computed through a crop module described in Section 2.3.4. Crop parameters (crop coefficients, rooting depths, Leaf Area Index) for rice, maize and poplar are the same as in (Mayer et al., 2019).

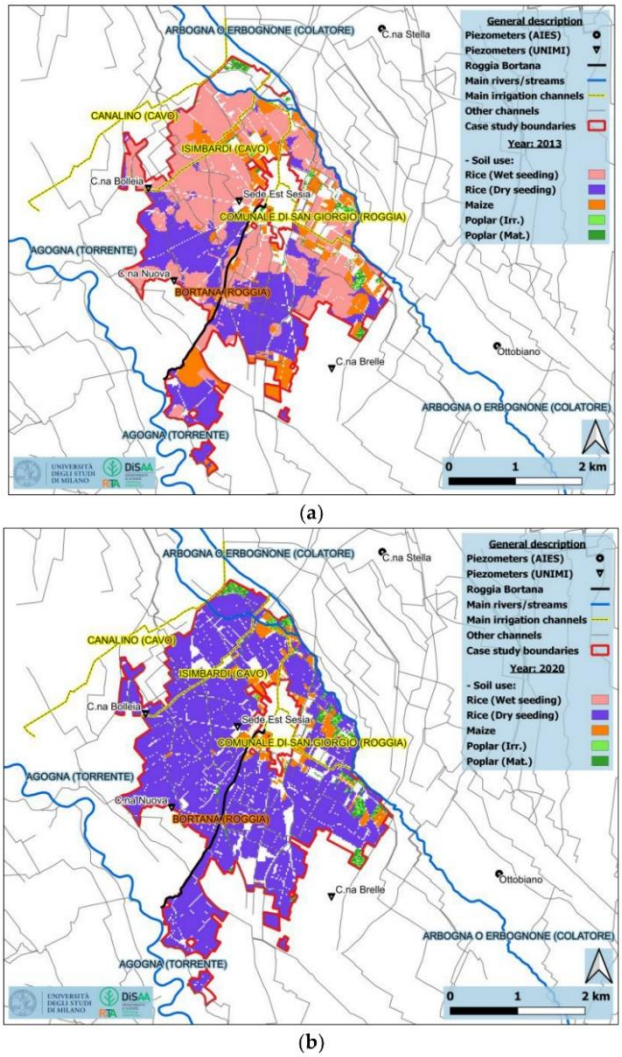

Figure 6. (a) Soil use of the year 2013; (b) Soil use of the year 2020. The transition between wet and dry seeding is particularly evident in the case study area.

2.3.2 Modelling Framework

The modelling framework consists of three sub-models: I) one for the agricultural area (SDMAA), based on the well-known SWAP model, II) one for the channel network percolation (CP), III) one for the GWL dynamics (PGL). The MATLAB code described in (Mayer et al., 2019) to integrate the three sub-models and to process the results was further developed in this study. Figure 7 illustrates the flowchart of the model framework showing the interconnections among the three sub-models.

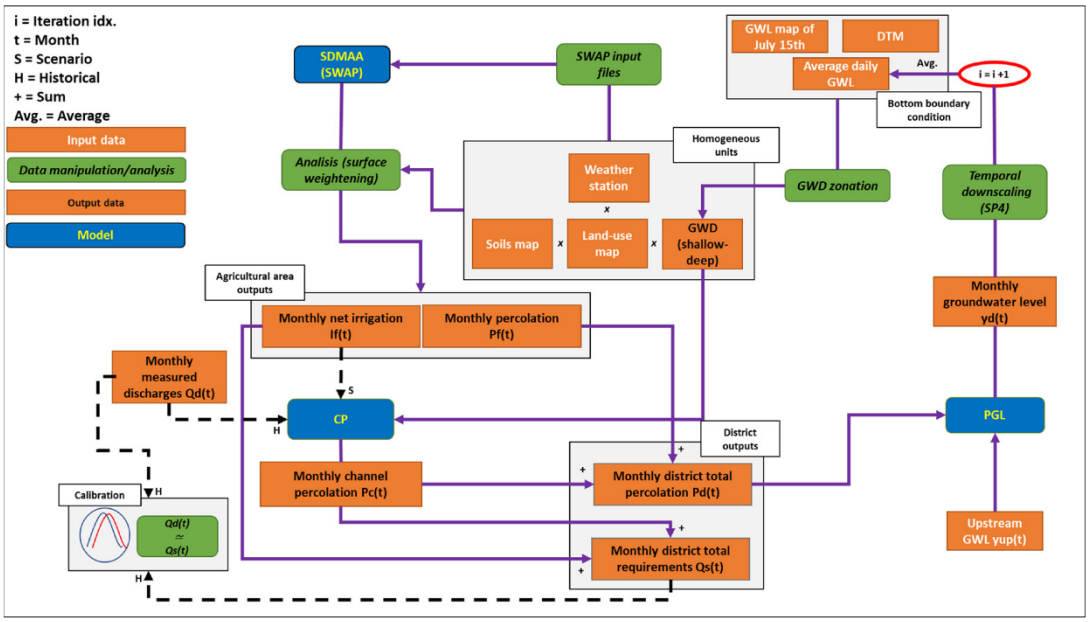

Figure 7. Flowchart framework showing the interconnections among the three sub-models (SDMAA, CP and PGL) and the input data required (GWL map of 15 July, DTM, average daily GWL, weather station, soils map, land-use map and upstream GWL). In the present study only the scenario (S) path was used, since it was not possible to rely on historical (H) measurements of the monthly measured discharges entering the district (Qd) for the simulated irrigation management alternative. The entire modelling framework, except for the SDMAA core model (SWAP), was developed in MATLAB.

For each year and iteration step, the interpolated GWL map of 15 July, along with the Digital Terrain Model - DTM (20 m × 20 m raster map; https://www.geoportale.regione.lombardia.it/), is used to create a reference GWD map to split the district into two GWD sub-areas: shallow if greater than -1 m and deep if lesser than -1 m Figure 8. Then, an interpolation of the GWD for the district is performed for each day of the simulated year and the required series for the SWAP simulations (GWD shallow and deep) are created by averaging the daily values of the GWD maps over the two reference GWD sub-areas. In this step, the actual simulation domain is also defined by overlaying each matrix (20 m × 20 m), showing the spatial distribution of the different information taken into account. SDMAA subdivides the agricultural area of the district into homogeneous simulation units, each one described by a specific set of parameters (SWAP inputs text file), considering crop type and irrigation management, soil type and GWD conditions. The water discharges provided by the three channels (RCSG, CiSi and Can) of the district are distributed homogenously over the entire agricultural area; due to the limited extension of the district, the same is done for the agro-meteorological data measured in the Castello D'Agogna meteorological station. Once the simulations for each simulation unit are

completed, the water fluxes obtained by SWAP are aggregated over a specific time step (e.g., month) to get the monthly net irrigation (I_f, mm) and the monthly percolation (P_f, mm) coming from the agricultural area. Therefore, in order to obtain the district fluxes (m^3), the aggregated results for each unit (mm) are: I) assigned to the simulation domain based on their position in the district, II) weighted (i.e., averaged) over the total cell numbers evaluated in the assigning process, III) multiplied by the total surface (total cell numbers evaluated multiplied by the cell size - 400 m^2) covered by all the simulated cells within the district domain.

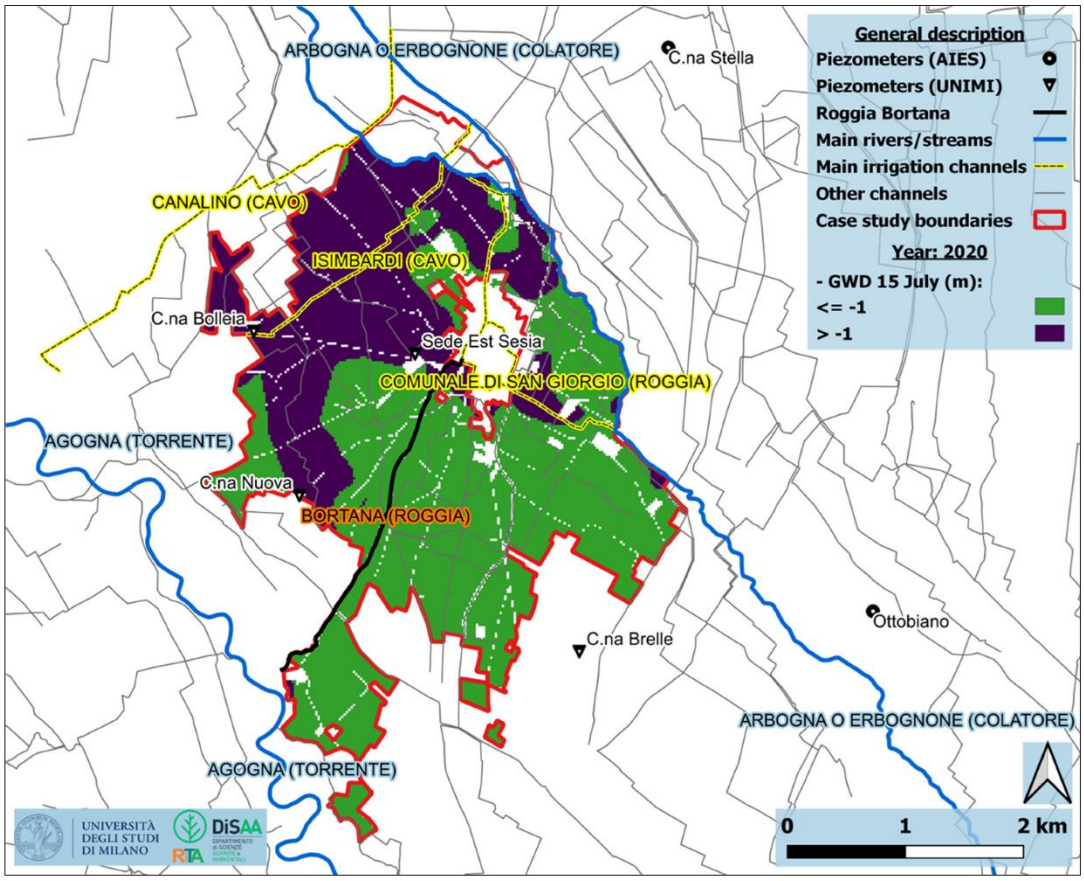

Figure 8. GWD (m) map of July 15 used by the framework to subdivide the district into two groundwater depth sub-areas: shallow if greater than -1 m and deep if lesser than -1 m.

Two empirical models complete the modelling framework - the former (PC) is used to estimate the monthly percolation from the channel network (P_c, mm) and the latter (PGL) to simulate the average monthly GWL over the district (y_d, m). In a scenario analysis, in which the monthly measured discharges entering the district (Q_d, mm) cannot be measured, P_c, which is usually highest in the early months of the irrigation season, is estimated as:

$$P_c(t) = \frac{(\alpha(t) * I_f(t))}{(1 - \alpha(t))} \quad \text{(Eq. 1)}$$

where α (-) is a loss factor, calculated as follows:

$$\alpha(t) = \begin{cases} 0.2, & t < 4 \; or \; t > 9 \\ min\left(0.4, max(0, {y_d}^i - 1.6)\right), & 4 \geq t \leq 9 \; (t = month: April \; to \; September) \end{cases} \quad \text{(Eq. 2)}$$

To reproduce the behavior that links the monthly total percolation coming from the district (P_d, mm; $P_f + P_c$) and y_d, in a context in which the district phreatic aquifer is not completely hydrologically isolated, the following theoretical model was chosen:

$$y_d(t)^i = f\left(P_d(t)^i;\, y_{up}(t);\, y_d(t-1)^i\right); \quad t = month, i = iteration \; index \quad \text{(Eq. 3)}$$

where y_d is the estimated average monthly GWL over the district and y_{up} (m) is the average monthly GWL measured in a piezometer located upstream along the main groundwater flow direction with respect to the study area (C.na Stella). In this way, by following a recursive computation scheme, in which at each iteration step the new GWL (y_d^{i+1}) is averaged with the GWL of the previous iteration step (y_d^i), the modelling system can simulate scenarios and/or past years for which GWL data are not available. Since the PGL works at a monthly time step, whereas the time step of the GWD series required for the SWAP is daily, the framework also downscales the monthly estimated values to a daily time resolution using an ad-hoc set of fourth-order polynomial curves (SP4) suited for producing daily data series having a monthly average equal to the value of the parent monthly series.

2.3.3 Model Calibration

The modelling framework was calibrated using historical data for the period 2015 - 2016 (Mayer et al., 2019). For that period, five agricultural soil uses (wet and dry seeded rice, maize, mature and young poplar) were considered; two concerned the rice crop, since WFL and FTI strategies were both used for rice irrigation in the district (WFL with decreasing importance from 2013 onwards).

The calibration of the SDMAA model consisted in a manual tuning of the parameters related to irrigation management, in particular irrigation amount and application turns, and was conducted together with the calibration of the parameters involved in the PC model. In the calibration process, the objective was to minimize the differences between Q_d and the simulated monthly district total requirements (Q_s, mm; $I_f + P_c$), paying particular attention to the central months of the irrigation season (June, July and August). Specifically, the difference between the measured Q_d and the simulated Q_s in 2015 was used to calibrate the groundwater depth at which channel percolation reaches its maximum (Eq. 2). The Nash-Sutcliff Model Efficiency (NSME) (Moriasi et al., 2007) computed over the whole 2015 - 2016 period was 0.67, reaching 0.80 when considering just the months characterized by the major channel water losses (April - July).

The calibration of the parameters included in the PGL model was performed automatically, through the MATLAB 'lsqnonlin.m' function, by comparing the available measured GWD and the estimated GWD for the period 2015 - 2016. The NSME index, averaged over the two GWD (shallow and deep), was 0.89 for the whole two-years period, while it was 0.98 when considering only the irrigation season (15 April - 15 September) of the same two years.

2.3.4 Simulated Scenarios

The simulation scenarios are defined by the irrigation management practice adopted for the rice crops in the whole district. As described in the introduction, the irrigation practices selected for the assessment are: I) wet seeding and continuous flooding (WFL), II) wet seeding and Alternated Wetting and Drying (AWD), III) dry seeding and delayed flooding (DFL), IV) dry seeding and fixed turn irrigation (FTI), V) early seeding DFL (DFLearly).

Given the nature of the scenario analysis implemented, maize and poplar crop development stages, crop parameters and irrigation management remained the same as described in (Mayer et al., 2019) in all of the simulations performed. Maize is border irrigated when a critical threshold of depletion of the Readily Available Water in the root zone (RAW) is reached: I) in the case of shallow groundwater, irrigation starts when 60% of RAW is consumed and an irrigation depth of 110 mm is applied, II) in the case of deep groundwater, irrigation starts when 70% of the RAW is consumed and an irrigation depth of 180 mm is applied. For young poplar (irrigated), two flooding irrigations with a fixed irrigation depth of 150 mm are prescribed, the first at the end of June and the second towards the end of July. For mature poplar (rainfed), no irrigation is simulated, as indicated by AIES.

For the two main types of rice (wet and dry seeded) a crop development model was implemented using a degree-day approach analogous to the one used in SWAP from seeding to harvest; moreover, a simple algorithm to determine a likely seeding date for the crop was also implemented. The model allows us to adapt the simulated irrigation management to the differences in crop development occurring each year, associating eventual changes in the irrigation strategy (e.g., from flooding to turned irrigation) to specific values of the crop Development Stage (DVS). For each year, the seeding date was identified verifying the achievement of a minimum temperature threshold ($T_{seeding}$, °C) in a forward five-days moving window built from a minimum seeding date (D_{min}) up to a maximum seeding date (D_{max}). When D_{max} is reached, even if the air temperature criterion is not satisfied, seeding is forced to occur. The minimum air temperature condition is verified as follows:

$$\frac{\sum_{i=D_{min}}^{D_{min}+4} T_{mean}}{5} \geq T_{seeding} \qquad \text{(Eq. 4)}$$

where T_{mean} (°C) is the daily mean air temperature. Three different growing stages were used to describe the development of rice: I) from seeding to emergence, II) from emergence to flowering (DVS from 0 to 1), III) from flowering to complete ripening/harvest (DVS from 1 to 2). The thermal contribution of the day (T_{eff}, °C) was computed using the following procedure:

$$T_{eff} = \begin{cases} 0, & T_{mean} < T_{base} \\ T_{mean} - T_{base}, & T_{base} \leq T_{mean} \leq T_{cutoff} \\ T_{cutoff} - T_{base}, & T_{mean} > T_{cutoff} \end{cases} \qquad \text{(Eq. 5)}$$

where T_{base} and T_{cutoff} (°C) are the minimum and the maximum temperatures for crop development in a specific growing stage range. Finally, to estimate the DVS value of the crop on a specific day, an integration is performed using the equation:

$$DVS^{i+1} = DVS^{i} + \frac{T_{eff}}{T_{sum}} \quad \text{(Eq. 6)}$$

where i (-) is the day index, while T_{sum} (°C) is the thermal amount defined to satisfy the achievement of a growing stage. The model was calibrated with the support of the ENR using the year 2020 as the reference and with the aim of obtaining an average crop cycle of around 140 days, with seeding in late April and harvesting around mid-September ($T_{seeding}$, T_{base} = 10 °C, T_{cutoff} = 40 °C, T_{sum}-DVS: 0 - 1 = 1051 °C, T_{sum}-DVS: 1 - 2 = 752 °C). D_{max} was set to be D_{min} plus 30 days for each seeding type. Each scenario inherits its crop development based on the seeding type: i) wet seeding for WFL and AWD, ii) dry seeding for DFL, FTI and DFLearly. D_{min} for wet seeding was set to 30th April and for dry seeding to 23rd April. Lastly, DFLearly D_{min} was anticipated to 5th April.

With respect to the implementation of the irrigation strategies explored in the scenarios, data were taken from the actual practices adopted by the farmers in northern Italy and, in the case of AWD, from two recent experimentations carried out at CRR-ENR (Centro Ricerche sul Riso; Castello D'Agogna, Pavia, Italy).

In WFL, as an average over the territory, 12 cm of ponded water is maintained on the fields from about five days before seeding until ripening, apart from a few dry periods necessary for plant emergence and other agronomic practices (typically two before and one after the tillering stage, as suggested by ENR).

DFL and FTI are designed based on the currently implemented on-farm practices adopted in northern Italy. In DFL, rice is dry seeded and fields are flooded from the tillering phase up to the ripening phase maintaining about 12 cm of ponding water in the fields. The FTI is managed at the same way as the DFL in the first part of the season (dry seeding), but from the tillering phase onwards, apart from an initial flooding period of about 10 days, rice is irrigated with an eight-day rotation and 120 mm per irrigation event. According to the information provided by AIES, an eight-day rotation is still representative of good surface water availability for the district.

Concerning AWD, an experimental platform was set up in the agricultural season 2021 - 2022 at the CRR-ENR to test wet seeding and two different AWD strategies, one safer and one stronger in terms of soil water status critical thresholds of intervention, compared to the traditional WFL (Vitali et al., 2024). Irrigation water use was monitored by the installation of flow meters, and all the other soil water balance components were quantified. In the safe implementation of AWD, the water level depth (WLD) below the field surface, measured in a perforated Water Tube, could not fall below -10/15 cm (corresponding to a SWP at -5 cm of approximately -5 kPa), while in the stronger implementation, the WLD could fall as low as -20/25 cm (SWP at -5 cm of approximately -20 kPa). In the field trials, the safe AWD and the strong AWD resulted in saving 25% and 31% of water, respectively, over two years, without showing any drop in production despite a period with scarce water availability for irrigation in 2022, which forced a longer AWD cycle than planned. Moreover, during the agricultural season 2019 - 2020, the safer AWD was compared with WFL and DFL in a previous experiment carried out at CRR-ENR. At the field scale, water savings of AWD and DFL were found to about 20% and 14% compared to WFL, without penalizing rice production (Gharsallah et al., 2023). Regarding the implementation in the model, AWD is managed as WFL in the early part of the season (wet seeding) and intermittent flooding only starts from the tillering stage, when irrigation is performed to reach 12 mm of standing water only if the soil reaches a critical moisture level of -10 kPa at 5 cm below the surface.

No experimental data are available for DFLearly, which is designed in this study to find a compromise between the request of farmers who would like to keep dry seeding due to economic

advantages and the need to anticipate the use of water in April - May, recharging the phreatic groundwater at the beginning of the agricultural season. DFLearly maintains the same irrigation scheduling of DFL (dry seeding and flooding from the tillering phase up to the ripening) but implements an earlier seeding date (5th April) than the original DFL (23rd April). Anticipating seeding could lead to an earlier rise in the water table in the first part of the irrigation season, limiting the negative effects of dry seeding.

Hence, in the final configuration used in this study, the model considers 40 simulation units: four crop types cultivated in the area (rice, maize, young and mature poplar), five soil units and two GWD (shallow and deep). Each specific rice irrigation alternative (WFL, AWD, DFL, FTI and DFLearly) is applied to all the rice area cropped within the district, while surfaces devoted to maize and poplar remain unchanged. To correct the estimated mean monthly groundwater level over the district (recursive averaging of y_d^{i+1} and y_d^i) based on the simulated monthly total percolation coming from the district (P_d), five iterations for each year are performed (i = 5). PC and PGL models use a 30-day time-step, thus the same period is used to aggregate the water fluxes obtained by SWAP in the SDMAA model.

2.3.5 Performance Indicators

Three indicators (-) were used to support the analysis of results (Water Application Efficiency - WAE, Distribution Efficiency of the irrigation network - DE and Relative Water Supply - RWS) (Bos et al., 2005, 1994; Burt et al., 1997; Molden, 1998; Pereira et al., 2012) calculated both for the whole irrigation season (April - September) and for the most critical month of the irrigation season (June). The equations used to calculate the indicators are:

$$WAE = \frac{ETp_f}{(I_f + R)} \quad \text{(Eq. 7)}$$

$$DE = \frac{I_f}{Q_s} \quad \text{(Eq. 8)}$$

$$RWS = \frac{(Q_s + R)}{ETp_f} \quad \text{(Eq. 9)}$$

where ET_{pf} (mm) is the potential evapotranspiration from the agricultural area, I_f (mm) is the net irrigation supplied to the agricultural area, R (mm) is the rainfall, and Q_s (mm; $I_f + P_c$) is the simulated monthly district total requirement.

2.4 Results and Discussion

2.4.1 Rice Development Stages (DVS)

Rice development stages obtained for the period 2013 - 2020 are shown in Figure 9. Apart from DFLearly in 2013, the minimum seeding date (D_{min}) imposed for each rice seeding

type/scenario (dry, wet and DFLearly) and year combination was satisfied; the temperature threshold ($T_{seeding}$) of 10 °C was generally met in D_{min}.

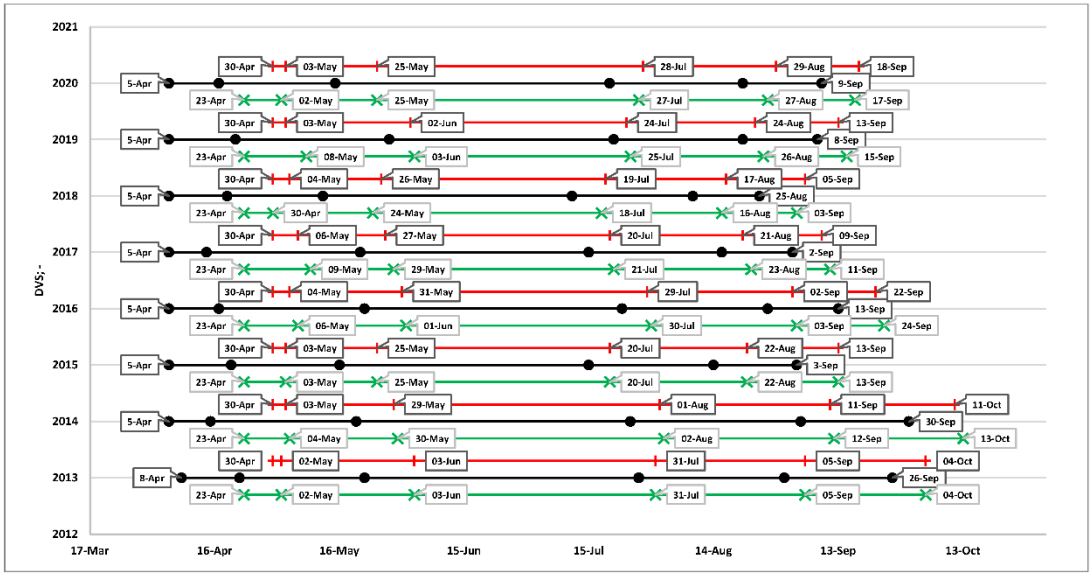

Figure 9. DVS of rice for 2013 - 2020. Lines in black show DVS for DFLearly. For each year, the line above the black one reports the development of the scenarios with wet seeding (WFL/AWD, in red), while the line below the black one illustrates the development of the scenarios with dry seeding (DFL/FTI, in green). The labels indicate (from left to right): I) seeding, II) emergence (DVS = 0), III) beginning of tillering (DVS = 0.20), IV) flowering (DVS = 1), V), ripening (DVS = 1.65) and VI) complete ripening/harvesting (DVS = 2). For DFLearly, just the DVS = 0 and DVS = 2 labels are shown.

2.4.2 Groundwater Depths (GWD)

The daily GWD values for all the scenarios are shown in Figure 10. DFL and FTI lead to a drastic decrease in water table levels in the first months of the season, slowing their rise towards their peaks (late July - August). In contrast, water table depths in AWD overlap with those in WFL in the early part of the season and only begin to diverge from the tillering phase (late May - early June). However, from this point onwards, the depths in AWD will never reach the values of WFL, DFL and DFLearly, showing a deeper condition in the middle months of the irrigation season. This is also the case in FTI, which shows similar groundwater dynamics to AWD in the middle months of the season, although in this scenario the groundwater levels seem to be more influenced by the presence/absence of rain. As expected, early seeding in DFLearly contributes to a rise in groundwater levels at the beginning of the irrigation season to an extent that it is closely linked to rainfall events in the early months of the season compared to the wet seeding scenarios (WFL and AWD). In WFL, the groundwater depths are clearly less influenced by the amount and seasonal patterns of rainfall but depend mainly on the high percolation coming from the agricultural area imposed by the continuous flooding condition. Under good conditions of water availability in rivers and canals, wet seeding is the best option to store water resources in the phreatic aquifer at the beginning of the irrigation season, and it is best to make them available for the agricultural area in the following months.

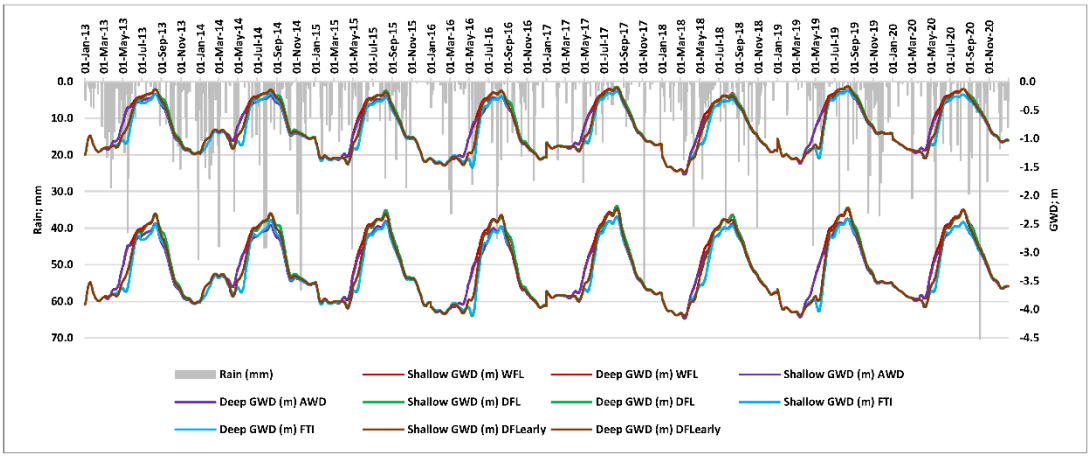

Figure 10. Daily GWD (shallow and deep; m) simulated for all the scenarios in 2013 - 2020.

2.4.3 Water Requirements (Q_s)

The average (2013 - 2020) seasonal (April - September) and critical (June) district total requirements (Q_s: sum of net irrigation from the agricultural area - I_f and the percolation from the channel network - P_c) are reported in Figure 11. The highest seasonal district water use is observed in WFL (19.7 Mm3), followed by AWD and DFLearly (about -16%), DFL (-19%) and FTI (-32%). The lower DFL and FTI requirements are clearly related to the adoption of dry seeding, which limits water applications to the field in the early months of the irrigation season. When looking at June, however, the water consumption in DFL (+25%) exceeds that required by FTI and DFLearly (about +5%), WFL (4.9 Mm3) and AWD (-28%). This happens because with dry seeding, paddy fields are flooded later in the season, and their filling occurring when the groundwater level is low and the soil is dry, requires a huge volume of water. Among the dry seeded scenarios, FTI and DFLearly limit this occurrence: the first strategy because of the turned application of irrigation water, which lowers the volumes applied, and the second due to an earlier flooding of the paddies (about 10 days earlier). AWD lower irrigation demand is linked to the adoption of wet seeding (shallower groundwater depth) but also to the start of the alternate wetting and drying scheduling at the rice tillering phase (around the end of May).

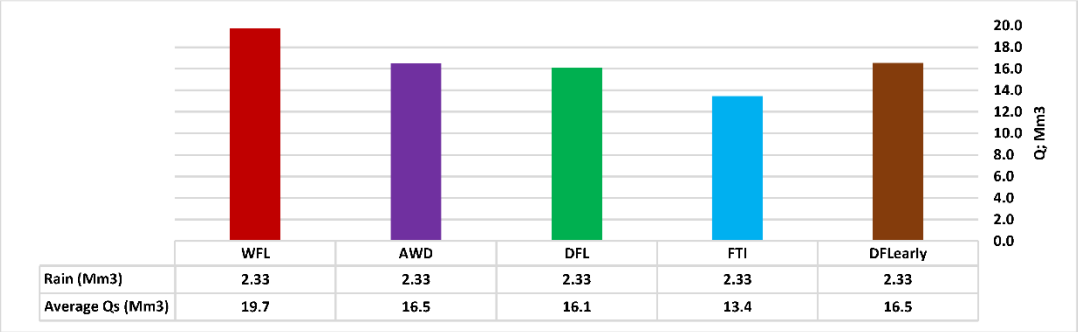

	WFL	AWD	DFL	FTI	DFLearly
Rain (Mm3)	2.33	2.33	2.33	2.33	2.33
Average Qs (Mm3)	19.7	16.5	16.1	13.4	16.5

(a)

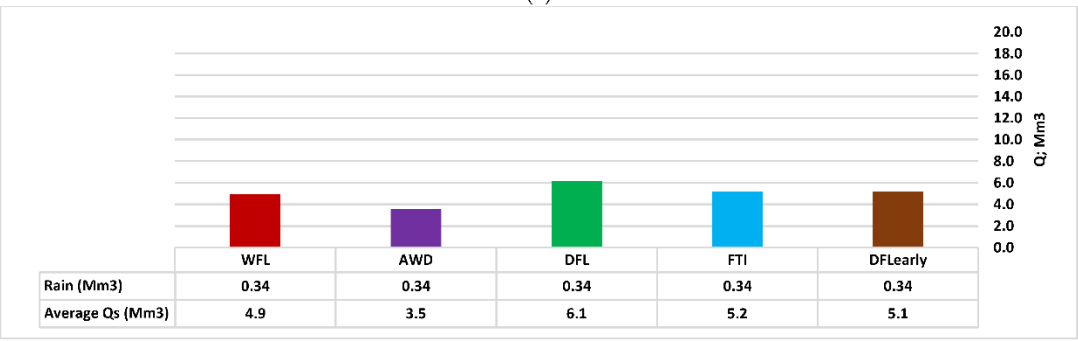

	WFL	AWD	DFL	FTI	DFLearly
Rain (Mm3)	0.34	0.34	0.34	0.34	0.34
Average Qs (Mm3)	4.9	3.5	6.1	5.2	5.1

(b)

Figure 11. Average seasonal (April - September) Q_s (Mm^3) simulated for all the scenarios in 2013 - 2020; (b) Average critical (June) Q_s (Mm^3) simulated for all the scenarios in 2013 - 2020.

The monthly Q_s are reported in Figure 12. DFL peak demand always surpasses the other simulated scenarios, overtaking them when the critical month of June or the late spring-early summer months are particularly dry. This is the case of the 2019 data, which is characterized by an extremely dry June, while in 2020 the presence of higher rainfall narrows the differences in total demand of the district between DFL and the other scenarios.

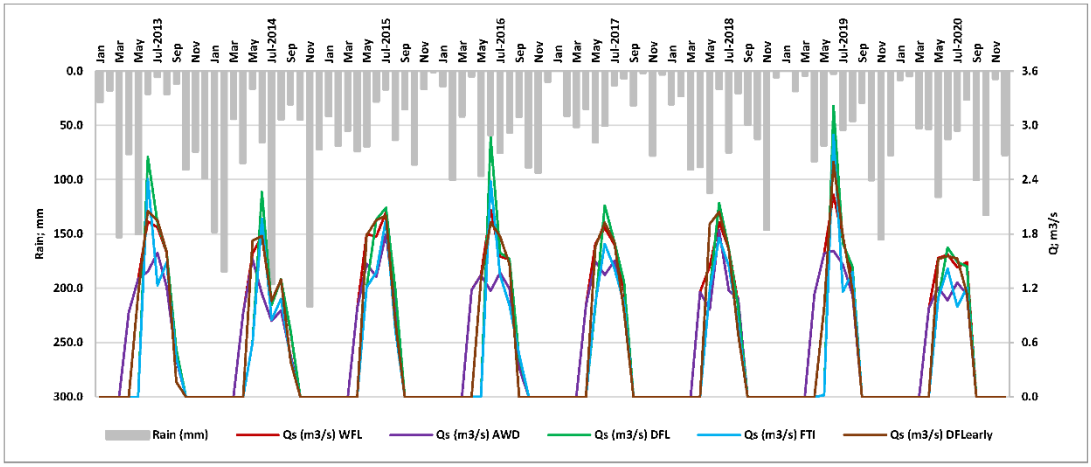

Figure 12. Monthly Q_s (m^3/s) simulated for all the scenarios in 2013 - 2020.

2.4.4 Water Application Efficiency (WAE)

The average seasonal and critical (June) WAE are shown in Figure 13. During the season, FTI obtains the best WAE (0.43), followed by AWD (0.37), DFL and DFLearly (about 0.33) and WFL (0.29), which remains rather distant. On the other hand, when looking at the average WAE values for June, AWD (0.41) far exceeds FTI (0.32), DFLearly (0.28), WFL (0.26) and DFL (0.25). AWD is the only scenario in which WAE values remain relatively stable in both periods, showing a more efficient use of irrigation water at field level. FTI also shows good WAE values, but the fixed irrigation rotation scheme adopted in this technique seems to perform less well in the critical months of the irrigation season than the scheduling adopted in AWD, which is more linked to the actual rice water requirements. The good seasonal performance of the other dry seeding scenarios (DFL and DFLearly) seems to be more related to the adoption of dry seeding, which limits water consumption than to a real efficient use of water, given the very low WAE value in June. However, DFLearly seems to benefit from early seeding, showing slightly higher efficiency than DFL in June. As far as the efficiency of water use at field level is concerned, from the results presented, WFL is the least reliable scenario among those simulated.

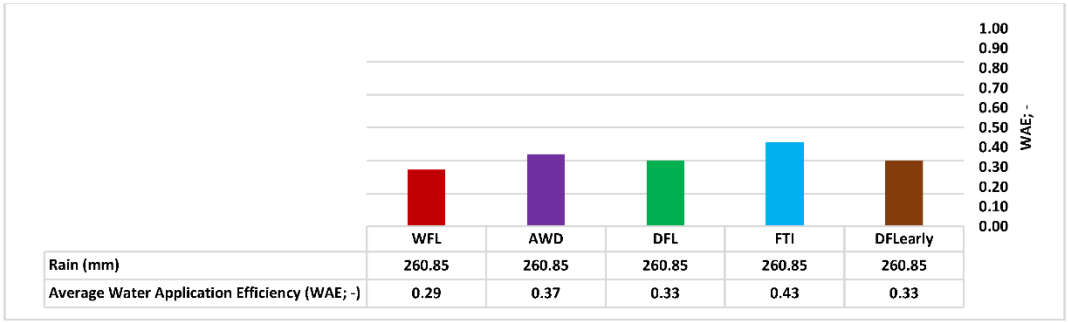

(a)

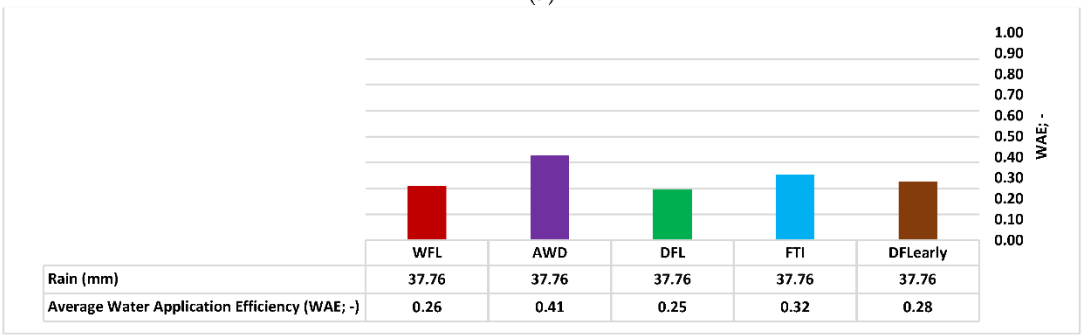

(b)

Figure 13. (a) Average seasonal (April - September) WAE (-) calculated for all the scenarios in 2013 - 2020; (b) Average critical (June) WAE (-) calculated for all the scenarios in 2013 - 2020.

2.4.5 Distribution Efficiency (DE)

Figure 14 displays the average seasonal and critical (June) DE of the irrigation network. DFL, WFL and DFLearly show a rather high seasonal DE (around 0.80), while AWD and FTI remain lower (around 0.70). During the whole season, continuous flooding techniques are clearly advantaged, as the shallower groundwater table limits the percolation from the channel network.

In June, the flooding technique performs better, especially WFL (0.78) and DFLearly (0.72), but the dry seeding adopted in DFL (0.68) penalizes this scenario in the most critical month. On the contrary, DFLearly continues to benefit from the early rise of the groundwater table due to early seeding. Deep groundwater depth conditions strongly influenced FTI (0.68) and AWD (0.66) efficiencies in June. In terms of channel efficiency, these latter two scenarios are the least performing of those simulated in both the aggregation periods.

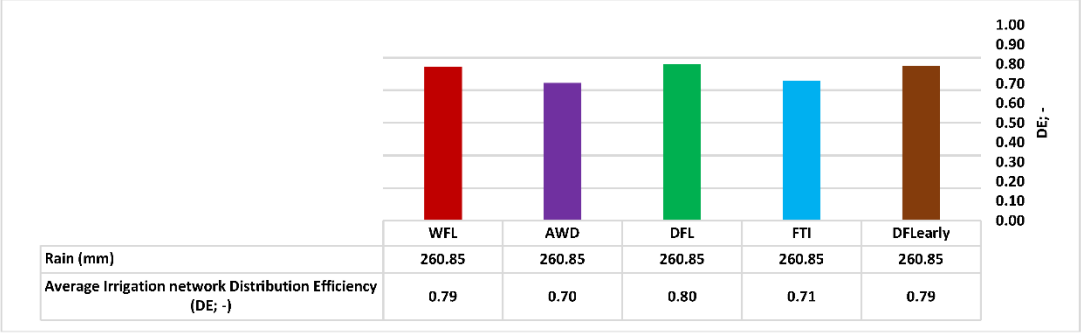

	WFL	AWD	DFL	FTI	DFLearly
Rain (mm)	260.85	260.85	260.85	260.85	260.85
Average Irrigation network Distribution Efficiency (DE; -)	0.79	0.70	0.80	0.71	0.79

(a)

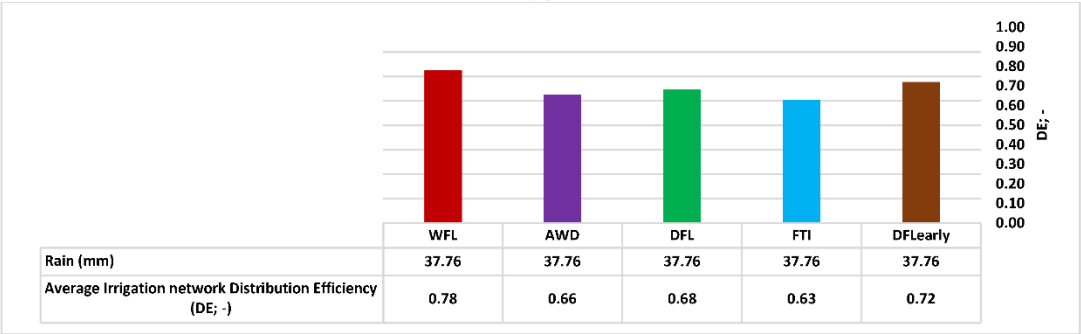

	WFL	AWD	DFL	FTI	DFLearly
Rain (mm)	37.76	37.76	37.76	37.76	37.76
Average Irrigation network Distribution Efficiency (DE; -)	0.78	0.66	0.68	0.63	0.72

(b)

Figure 14. Average seasonal (April - September) DE (-) calculated for all the scenarios in 2013 - 2020; (b) Average critical (June) DE (-) calculated for all the scenarios in 2013 - 2020.

2.4.6 Relative Water Supply (RWS)

RWS values are more connected to the overall efficiency of the irrigation strategies applied in the territory, since they consider both the irrigation efficiency of the agricultural land and the irrigation water losses in the channel system (Eq. 9). The average seasonal and critical (June) RWS values are shown in Figure 15. In the simulated period, FTI (3.13) achieves the best seasonal RWS, closely followed by DFL (3.64) and AWD and DFLearly (about 3.70), showing a more efficient irrigation water use at the district level compared to WFL (4.33). However, in June, DFL (6.02) and FTI (5.13) show the worst RWS, while AWD (3.57) performs the best, followed by DFLearly (4.85) and WFL (4.89). Despite good seasonal values, the scenarios adopting dry seeding (DFL and FTI) are again adversely affected by the deeper groundwater depth conditions they experience in the early part of the season and close to the critical month of June, and thus by greater channel percolation that causes higher irrigation requirements, with a small exception for DFLearly due to the early seeding adopted. On the contrary, shallower groundwater levels in the case of WFL

decrease channel percolation and raise the overall district water use efficiency. AWD seems to be the most robust scenario, with good performance both seasonally and in the critical month.

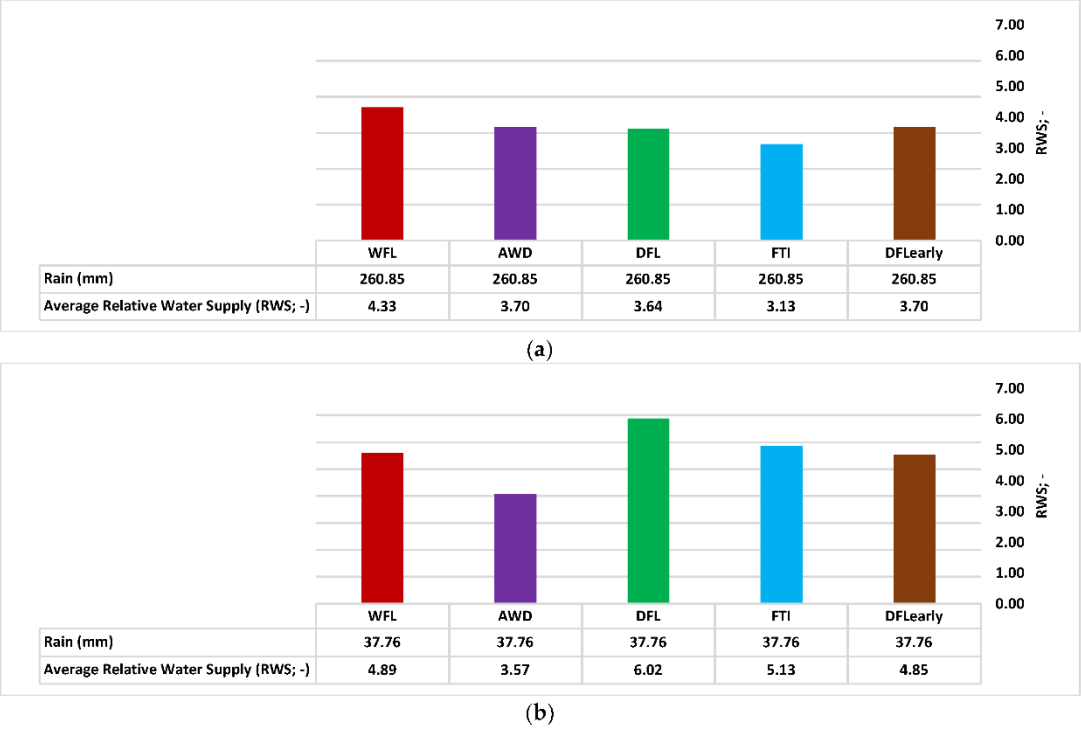

Figure 15. (a) Average seasonal (April - September) RWS (-) calculated for all the scenarios in 2013 - 2020; (b) Average critical (June) RWS (-) calculated for all the scenarios in 2013 - 2020.

2.5 Conclusions

The modelling work conducted in this study once again highlighted the strong connection between irrigation management and groundwater table in rice-growing areas characterized by shallow aquifers, which makes it complex to estimate the actual efficiency of irrigation management alternatives over vast agricultural areas without the implementation of articulated agro-hydrological tools such as the one proposed in this chapter.

Recently, many portions of the rice-growing area in the Padana Plain are facing a lowering of the groundwater table at the beginning of the agricultural season due to a massive conversion to dry-seeded irrigation techniques. However, even if this strategy is able to reduce the total irrigation volume used during the irrigation season (April - September), as demonstrated for DFL scenario in this study, it does not allow to decrease the irrigation demand in the most critical month of the season (June), leading to an even higher irrigation demand when compared with WFL, and AWD. The calculated RWS values for DFL clearly show a less efficient district water use compared to the other scenarios simulated.

DFLearly can benefit from an anticipated seeding date than its original formulation, showing a better RWS than DFL in the critical month of the season, which is comparable to that of WFL but still far from the one achieved with AWD. However, rice varieties different from those used at the present time should be identified to meet appropriate thermal conditions for

germination and/or to avoid yield and product quality losses if the grain-filling period falls during high temperature periods.

Although FTI performs better than DFL and DFLearly throughout the irrigation season, mainly due to a reduction of irrigation volumes applied at the field level, in June/July the dry seeding technique adopted and the rigid irrigation scheme employed severely penalize its performance in terms of water use and, consequently, in the calculated RWS index.

A safe AWD, applied after wet seeding, seems to be a suitable solution to reduce irrigation demand for rice after the tillering phase (late May - early June) while maintaining good groundwater recharge, especially in the early part of the season (until the end of May). AWD achieves good performances on a seasonal basis, in particular in June, when it records by far the highest RWS value. AWD simulated water savings compared to WFL (16%) are less than those found at the field level at CRR-ENR (25% in 2021 - 2022 and 20% in 2019 - 2020) and reported in the meta-analysis in Carrijo et al. (2017) (23.4%), which are indeed in good agreement with each other. The coarser texture and the overall deeper water table condition in the San Giorgio di Lomellina pilot district are likely responsible for the lower water savings compared to those measured at CRR-ENR. In addition, it is important to highlight that all the considered studies refer to results obtained in field trials, which do not consider water distribution network losses. In any case, based on the results obtained, we can state that, if implemented over large agricultural areas, AWD could be a good option to cope with low groundwater levels at the beginning of the season and to appease the exasperated competition for water among crops that the rice-growing area of northern Italy has been experiencing in recent years.

3 The QGIS-SWAP-Paddy Agro-Hydrological Modelling Framework: a Tool for Evaluating the Impact of Different Irrigation Strategies in Rice-Growing Regions of Northern Italy

3.1 Abstract

Rice-growing areas are characterized by complex interactions between field-scale water demand, channel network distribution efficiency, and aquifer recharge. This study introduces a physically based, spatially explicit framework that integrates field-scale and channel network processes within a single modelling workflow. The framework harmonizes multi-source spatial data into simulation units defined by thematic map intersections within a chosen simulation domain, ensuring consistent parameterization and reproducibility. Semi-distributed SWAP simulations generate key agro-hydrological variables, among which irrigation requirements and deep percolation fluxes. The channel module represents both 'major' linear and 'minor' diffuse components of a typical irrigation network in lowland agricultural areas, estimating channel percolation losses and circulating discharges under historical and scenario conditions, and redistributing them spatially while preserving the domain-scale channel efficiency. The modular design of the framework allows for multi-year and sub-domain assessments, making it adaptable to many irrigated plain contexts. Although the framework was developed and applied in this Thesis primarily to simulate the water balance of large-scale rice-growing areas, its approach and the models used make it suitable for simulating the water balance of any agricultural area or bare soil.

3.2 Motivation and Objectives

A modelling framework that links the description of the main characteristics of lowland agricultural areas (soil units, soil use and irrigation techniques, groundwater table conditions, agro-meteorological constraints, channel irrigation network structure) with the simulation of the agro-hydrological balance at field scale has been developed. Written in Python, the framework takes advantage of the environment provided by the open-source software QGIS (https://qgis.org/) to translate the spatialized information contained in a GeoPackage database (https://www.geopackage.org/) into physically based simulations performed by the agro-hydrological model SWAP (https://www.swap.wur.nl/) for each simulation unit in which the territory is divided. The main objective of the framework is to simplify the implementation of the physical description of a simulation domain within an integrated tool that functions similarly to a relational database. Successively, this data used for the simulation of 'current status' or 'what if' scenarios. In addition to the agricultural area, the framework enables the simulation of the water losses coming from the channel network. This is particularly useful in the case of agricultural areas with unlined channels like many rice-growing regions in northern Italy and all over the world.

The idea developed by the novel modelling framework is based on previous studies conducted in the Lomellina region, in particular regarding the San Giorgio di Lomellina rice district. The San Giorgio district is located about 45 kilometers southwest of Milan, spanning

roughly 1,000 hectares in the Lombardy main rice area. For this area, an integrated modelling prototype, composed of four sub-models (one for the agricultural area, one for the rice phenology, one for the phreatic groundwater levels, and the last one for the channel network) was developed, calibrated and used to simulate 'what if scenarios'. While this prototype captures the main factors for assessing irrigation efficiency in rice-growing areas, it was built with fixed parameters specific to for the San Giorgio irrigation district (rigidity) and could not be easily adapted elsewhere (non-transferability). The new modelling architecture is built to resolve both limitations.

To explain the modelling framework developed, showing the various steps involved in its application to a case study as well as the main results produced, the current situation of the San Giorgio di Lomellina district for the period 2018 - 2020 is used as an example. The input data and model parameters for the district result from the calibration described in Chapter 5 of this manuscript, which reports the work done for the entire Lomellina region (over 125,000 hectares, mostly cultivated with rice). Within the time period considered, two major rice irrigation management strategies were present in the San Giorgio district: I) the traditional wet seeding and continuous flooding (WFL), II) a raw dry seeding and intermittent flooding technique (FTI). Other productive soil uses include maize and poplar. Moreover, the district is characterized by 12 different soil units, 2 groundwater depth zones (shallow and deep) and 1 representative agro-meteorological station. The simulation area contains 15 channel traits that can be defined as the 'primary network', with a length of around 14 km.

3.3 Materials and Methods

3.3.1 QGIS, Python and GeoPackage databases

QGIS offers the possibility of writing custom script and plugins using the Python programming language, taking advantage of geoprocessing tools and software already available in its environment, like GDAL/OGR (https://gdal.org/en/stable/), or creating something original using Python libraries, such as GeoPandas (https://geopandas.org/en/stable/), or external software like the SWAP agro-hydrological model.

Historically, most databases used in the GIS context are based on the relational data model, which stores data in a structured format (i.e. tables consisting of rows and column), and uses SQL (Structured Query Language) to query, manipulate, and update data. SQLite (https://sqlite.org/) is a serverless database that operates by reading and writing data to ordinary disk files, such as .sqlite files. A database container specifically designed by the Open Geospatial Consortium (https://www.ogc.org/) to work with spatial data is the GeoPackage.

A vector feature could be defined as an object characterized by attributes, which include information describing its properties (e.g., text or numeric entries), and a geometry, that details its position and shape in space; a virtual representation of a real-world entity georeferenced to a specific Coordinate Reference System (CRS). Multiple features sharing the same geometry type (e.g., polygon) and similar attributes can be organized into a vector table (or map). On the contrary, a raster matrix is a spatial data model that represents the world as a regular grid of cells, each storing a value that describes the attribute of the corresponding geographic location.

3.3.2 Framework Workflow

The framework outlines two distinct groups of processes that occur within the simulation domain (i.e., the boundary of the geographical area under investigation): I) processes that take place in the agricultural area, and II) processes involving the channel network.

The first group of processes relies on a semi-distributed application of the SWAP model to estimate both irrigation requirements and deep percolation within the agricultural area. The second group of processes incorporates an ad hoc algorithm developed to estimate percolation and, consequently, the net and/or gross discharge circulating within the channel network.

In simulations based on historical data, the measured gross irrigation discharge at the inlet of the simulation domain, provided by the Irrigation Consortium, is used as input to derive the corresponding net irrigation requirement (i.e. irrigation water availability for the agricultural area). Conversely, in scenario analyses where historical data are unavailable, the framework starts with the estimated net irrigation requirement coming from the agricultural area and computes the corresponding gross discharge (i.e. net irrigation plus channel network percolation).

Figure 16 shows the steps followed by the framework to: 1) semi-distribute the SWAP model simulations within the simulation domain, and 2) describe the channel network of a simulation domain. Each simulation domain is stored in a simulation database (.gpkg) and is identified by a unique id (*gis_cod_domain*).

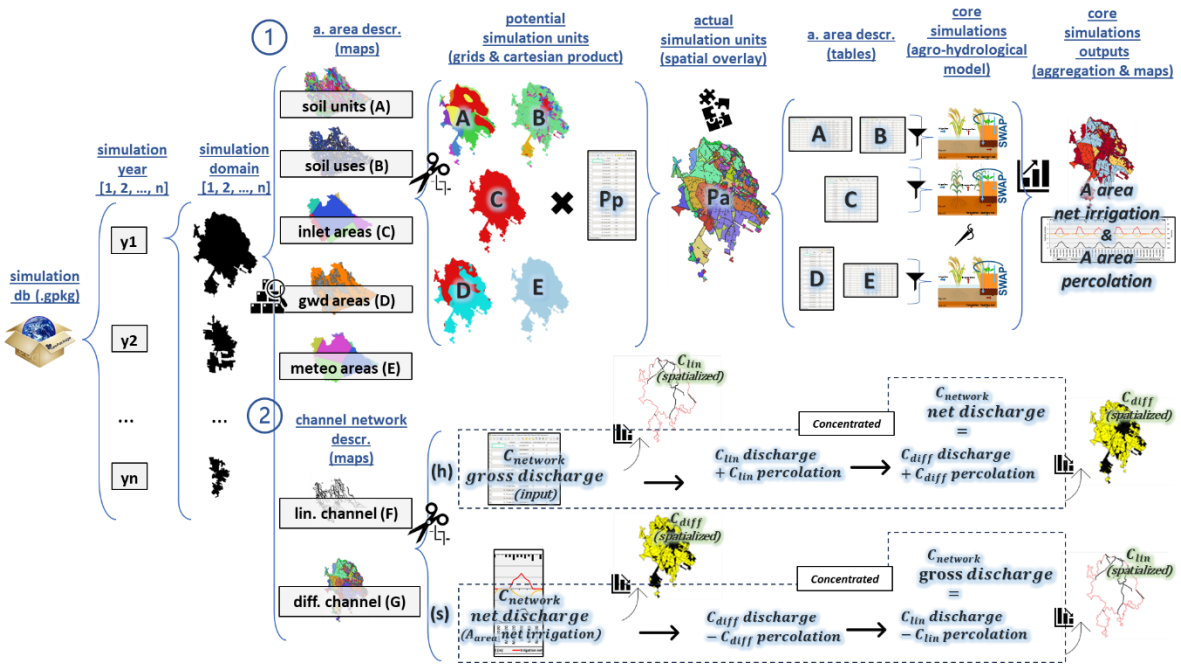

Figure 10. A schematic overview of the steps followed by the framework to: (1) semi-distribute the SWAP model within the agricultural area, and (2) describe the channel network of a simulation domain; both for a user defined simulation year.

3.3.2.1 Agricultural area model

The modelling framework operates on a daily simulation time step and is designed to perform agro-hydrological simulations in a semi-distributed manner, identifying individual simulation units (fields or areas defined by unique physical characteristics or management practices) within one or more simulation domains/sub-domains.

Input data and simulation unit definition

The input vector maps describing the agricultural area (soil units, soil use and irrigation techniques, groundwater table conditions, and agro-meteorological constraints) are collected from the same simulation database. Each map serves as a spatial register for a specific property of the agricultural area (e.g., a land use map indicating crop locations) and may vary by simulation year. All maps must include a *gis_cod* attribute for each feature, linking its geometry to parameterizations or time series stored in the required input tables.

Maps may differ in spatial extent, contain gaps, or include a user-defined 'no data' *gis_cod*. They must spatially overlap the simulation domain; geometries exceeding domain boundaries and with a 'no data' *gis_cod* are excluded. Each feature contributes to defining potential simulation units, but to be included in the core simulations, it must be described in the input tables. All maps and domains must use a projected CRS in meters.

The framework constructs the potential simulation units table by computing the Cartesian product of all unique *gis_cod* values across the input maps, each combination pointing to a specific set of parameters and time series. Spatial overlay of all themes determines the geometry of actual simulation units, stored in an actual simulation units map, each with an associated area (m^2). The *gis_cod* values of these units are then linked to their parameterizations or time series in five input tables (*swap3236_soilunit*, *swap3236_soiluse*, *swap3236_inlet_daily*, *swap3236_gwd_daily*, and *swap3236_meteo_daily*). Data are filtered by *gis_cod* (and simulation year, if needed) to prepare the required inputs for field-scale simulations.

SWAP model integration

The framework is built upon SWAP (Soil Water Atmosphere Plant) version 3.2.36 (Kroes et al., 2008), previously applied in studies on the San Giorgio di Lomellina irrigation district. SWAP is a one-dimensional, vertically oriented agro-hydrological model simulating water, solute, and heat transport in the vadose zone, accounting for soil-atmosphere-crop-irrigation interactions (Heinen et al., 2024). The simulation domain extends from above the vegetation canopy to the interface between unsaturated soil and the phreatic groundwater table.

During execution, the framework dynamically updates SWAP input files according to the agricultural area description. While SWAP offers extensive capabilities, the current configuration focuses on irrigation needs and deep percolation in lowland agricultural areas. Certain parameters are hardcoded in the provided SWAP files but can be modified by experienced users if required.

Irrigation regimes and rice field management

The framework supports two SWAP irrigation scheduling modes: I) User-defined fixed irrigation applications, and II) Crop-related irrigation scheduling with dynamically defined timing and depth criteria

It is designed to simulate continuously or intermittently flooded rice fields, with maximum ponding water level as a key management parameter. When this threshold is reached, SWAP removes surplus water, enabling controlled drying periods (ponding level = 0). To regulate ponding levels, excess input water may be supplied; net irrigation requirements are calculated as total irrigation input minus daily simulated runoff at the field scale.

The approach assumes that in flat areas, unsaturated zone fluxes are primarily one-dimensional and vertical, and that surface water connections between contiguous units are negligible at the territorial scale (runoff is generated at field level but not routed between units).

Output processing

Simulation results (e.g., net irrigation height) are stored in a structured tabular format analogous to a relational database, where each record corresponds to a variable, time step, and spatial unit. Results are aggregated monthly for the entire simulation domain, with values (e.g., net irrigation volumes) weighted by the relative area (square meters) of each simulation unit.

3.3.2.2 Channel network model

The channel network model operates on a monthly time step and is structured in two distinct phases. In the first phase, a concentrated water balance is calculated for the entire simulation domain. Inputs and equations used in the concentrated model are specified in Section 3.3.4.2. In the second phase, this balance is spatially distributed across the individual elements of the channel network. The distribution distinguishes between the primary linear channel network, which represents the main infrastructure such as medium- and large-sized canals, and the secondary diffuse channel network, which consists of the smaller channels branching from the primary network to supply individual fields. These smaller channels are generally difficult to map directly. Details on the algorithm used to spatialize the channel network balance items are provided in Section 3.3.4.3.

Input data and network components definition

The primary linear channel network is defined through a linear channel network map provided by the user, containing the geometries of the main canals. This map may extend beyond the boundaries of the simulation domain and is cropped to match the domain geometry. Each segment within the domain is assigned a reference length (meters). The secondary diffuse channel network is reconstructed from the actual simulation units map and from areas identified by the user where such smaller channels are likely to occur (e.g. only where there is rice). As with the agricultural area maps, all channel network geometries must use a projected coordinate reference system in meters and must spatially overlap the simulation domain. Features outside the domain with no relevant data are excluded from the analysis. The groundwater depth series required to run the channel network model are calculated directly by the framework based on the series provided in the agricultural area description (i.e. monthly average weighted for the areas of belonging).

Historical and scenario balance computation

In simulations based on historical data, the framework retrieves the monthly gross channel discharge at the inlet of the simulation domain from the channel network table stored in the simulation database. The net channel discharge is obtained by subtracting the estimated channel percolation from the gross discharge, representing the irrigation water effectively available to the agricultural area. In scenario simulations, where historical measurements are not available, the process is reversed. The framework begins with the aggregated monthly net irrigation estimated for the agricultural area and the gross channel discharge is reconstructed by adding the estimated channel percolation, representing the total irrigation water entering the domain at the inlet structure.

Spatial distribution of flows and losses

The spatial distribution of the concentrated monthly balance outputs (percolation losses and net/gross discharges) is applied to the geometries contained in the channel network input maps.

This is achieved using a weighting system that varies according to the network component. For the primary linear network, weights are based on the length and hierarchical order of the canals. For the secondary diffuse network, weights are based on the area and irrigation application of each actual simulation unit. This methodology enables potential integration with distributed groundwater flow models such as MODFLOW (https://www.usgs.gov/software/modflow-6-usgs-modular-hydrologic-model/). Such integration is particularly relevant in contexts where losses from the unlined channel network contribute significantly to the recharge of the phreatic aquifer, alongside recharge from the agricultural area.

3.3.2.3 *Folder System*

In addition to the simulation database, the framework needs a folder system to carry out the steps required during a run (Figure 17). Inside a user-defined root directory, the main working folder of the tool (*db*) is placed, within which all the necessary subfolders are located (*file*, *grid*, *sim* and *table*). The file folder stores all the files related to the available core agro-hydrological models (currently, only SWAP 3.2.36 - *swap3236* - is implemented). This folder contains three different sub-folders, namely: *bin*, where the core model executable is located (swap.exe), *crp*, where the files describing the crops to be simulated are located (.crp), and *swp*, containing the starting templates files (SWP, IRG, GWD and ET0) for the framework to write the remaining core model simulation input files (main SWAP input file - .swp, IRGFIL - .irg, BBCFIL - .bbc and METFIL - .0YY). The grid and the sim folders will contain all the supporting files needed, respectively, to build the simulation units within the agricultural area and to run the core agro-hydrological simulations. These folders share a similar system of subfolders, constructed as follows: I) name of the simulation database > II) name of the table in which the simulation domain is located > III) year of simulation > IV) unique id identifier of the simulation domain (*gis_cod_domain*). Inside the table directory tree, the user must locate the GeoPackage file containing the simulation database. Inside the table folder, the framework allows the user to store several databases within different folders to store more than one case study.

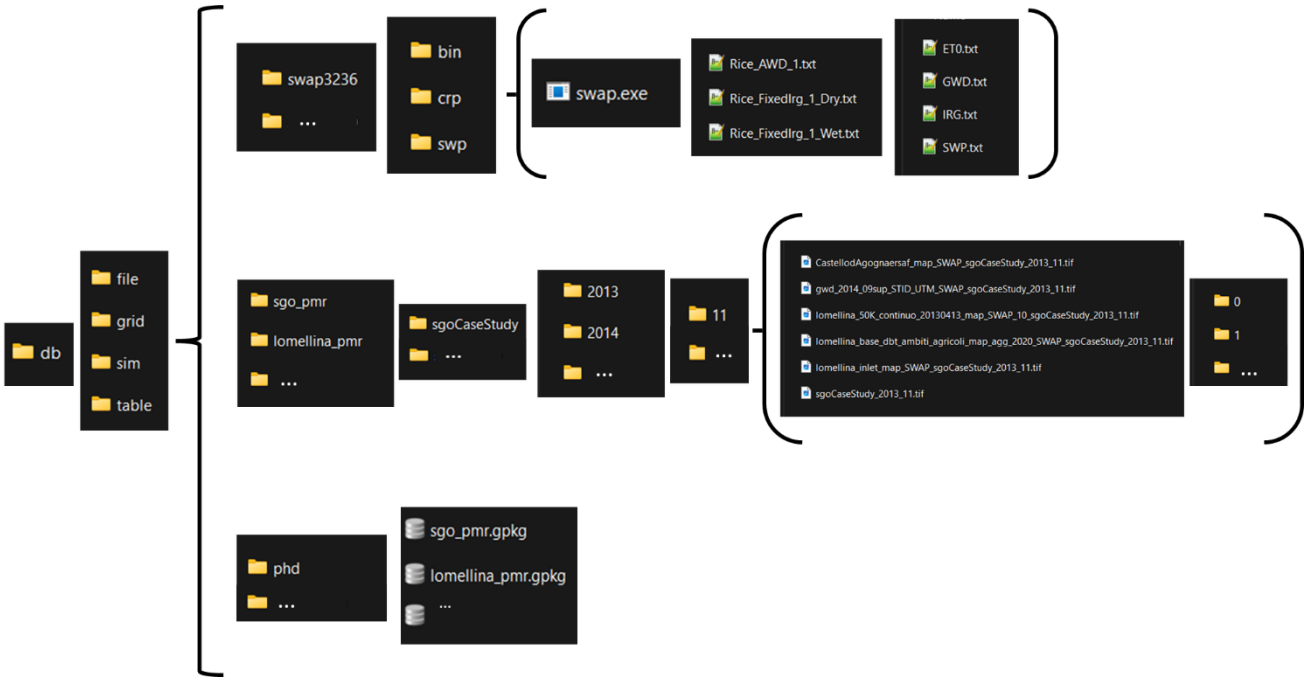

Figure 17. Root directory of the framework: main working folder (db), and subfolders (file, grid, sim, table).

3.3.3 Agricultural Area Model

3.3.3.1 Agricultural Area Description (Input Maps and Tables)

Soil Unit Map and Soil Hydraulic Parameters

The soil unit map (Figure 18) shows the spatial distribution of the pedological units, which are referred to as Cartographic Units (CUs) for the purposes of this study. Depending on the scale of application, a CU represents an area in which one or more homogeneous soil types (along with their corresponding observed typical soil profiles) occur. Over time, parental material, geomorphology, agrometeorological conditions, the presence of water, fauna and land uses combine to originate the soil types mapped in the CUs of pedological maps. The observed typical soil profiles for each CU are characterized by different soil horizon types, depth, physicochemical and hydraulic characteristics. If needed, the framework enables users to define alternative descriptions of the same soil type/soil profile in its linked input table, based on eventual changes due to agricultural management, such as puddling in paddy fields. This is achieved by using two different *gis_cod* attributes within the same input table, one referring to the soil unit map (*gis_cod_soilunit*) and the other to the soil use map (*gis_cod_soiluse*).

The *swap3236_soilunit* input table (Figure 19) stores the parameters required to describe the features depicted in the soil unit input vector map. SWAP uses a near saturation modification to the Mualem - Van Genuchten functions to describe the soil water retention function - θ(h) and the soil unsaturated hydraulic conductivity function - K(θ) (Schaap and Van Genuchten, 2006). Currently, the framework allows the user to use just the SWSOPHY = 0 option (Mualem - van Genuchten parameters), so the user must define the required parameters (ISOILLAY, ISUBLAY,

HSUBLAY - cm, HCOMP - cm, NCOMP, ISOILLAY1, ORES - cm3/cm3, OSAT - cm3/cm3, ALFA - 1/cm, NPAR, KSAT - cm/d, LEXP, ALFAW - 1/cm, H_ENPR - cm) for each soil layer that constitute the simulated soil profile. The framework writes all the required parameters by replacing the string *soilunit_table_1* (profile discretization) and soilunit_table_2 (hydraulic parameters) within the SWAP main input file (Figure 20, file .swp). The current architecture of the framework does not consider the hysteresis of soil water retention function or similar media scaling (file .swp).

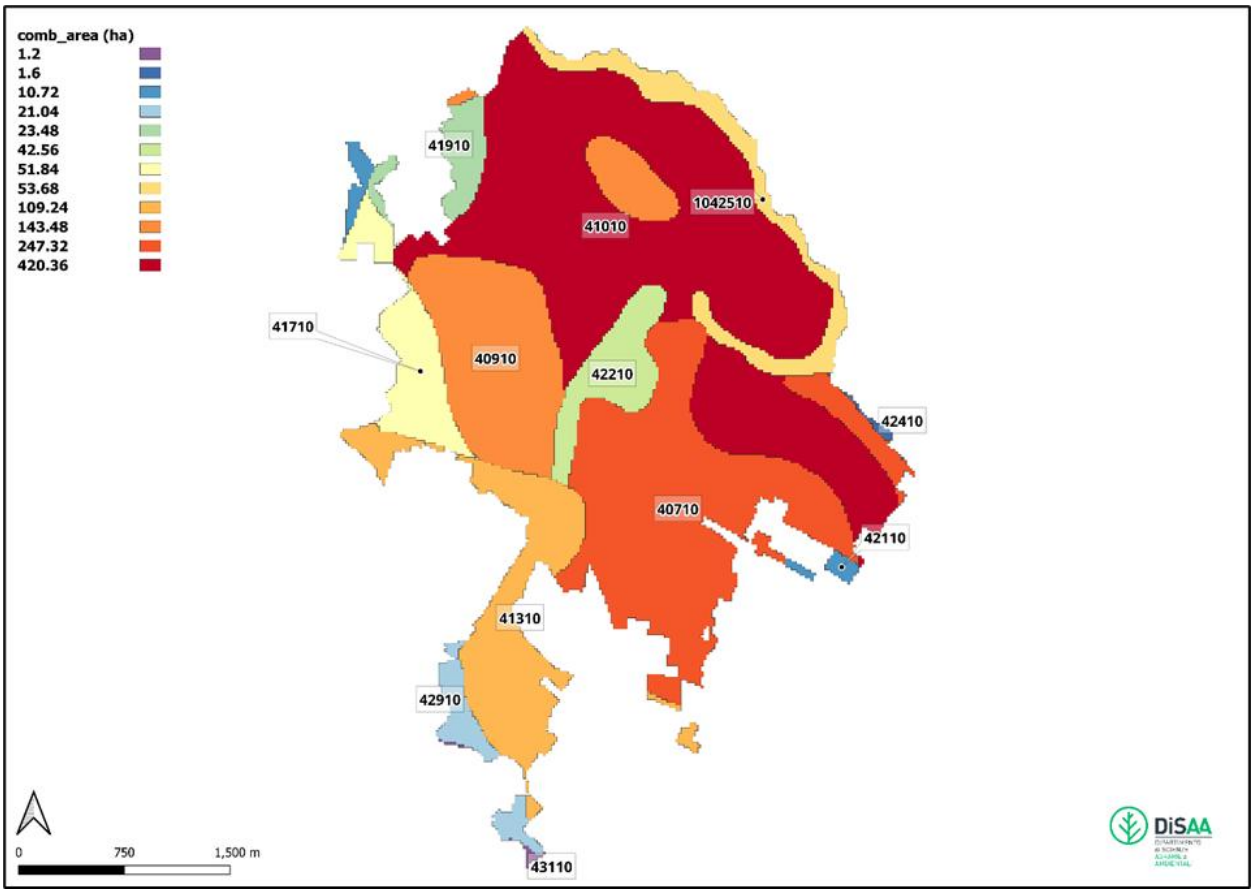

Figure 18. Example of a map showing soil units spatial distribution within the agricultural area of a simulation domain (San Giorgio di Lomellina; gis_cod_domain = 11).

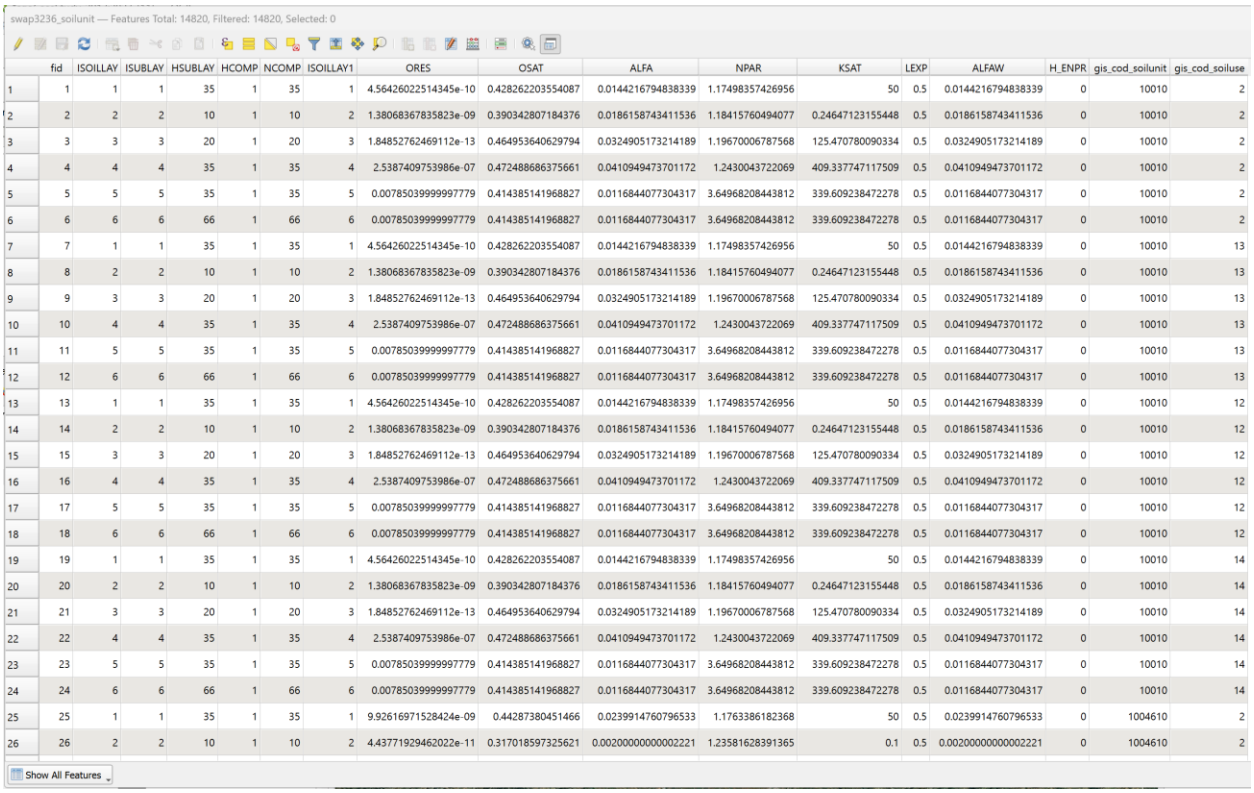

swap3236_soilunit — Features Total: 14820, Filtered: 14820, Selected: 0

	fid	ISOILLAY	ISUBLAY	HSUBLAY	HCOMP	NCOMP	ISOILLAY1	ORES	OSAT	ALFA	NPAR	KSAT	LEXP	ALFAW	H_ENPR	gis_cod_soilunit	gis_cod_soiluse
1	1	1	1	35	1	35	1	4.56426022514345e-10	0.428262203554087	0.0144216794838339	1.17498357426956	50	0.5	0.0144216794838339	0	10010	2
2	2	2	2	10	1	10	2	1.38068367835823e-09	0.390342807184376	0.0186158743411536	1.18415760494077	0.24647123155448	0.5	0.0186158743411536	0	10010	2
3	3	3	3	20	1	20	3	1.84852762469112e-13	0.464953640629794	0.0324905173214189	1.19670006787568	125.470780090334	0.5	0.0324905173214189	0	10010	2
4	4	4	4	35	1	35	4	2.5387409753986e-07	0.472488686375661	0.0410949473701172	1.2430043722069	409.337747117509	0.5	0.0410949473701172	0	10010	2
5	5	5	5	35	1	35	5	0.00785039999997779	0.414385141968827	0.0116844077304317	3.64968208443812	339.609238472278	0.5	0.0116844077304317	0	10010	2
6	6	6	6	66	1	66	6	0.00785039999997779	0.414385141968827	0.0116844077304317	3.64968208443812	339.609238472278	0.5	0.0116844077304317	0	10010	2
7	7	1	1	35	1	35	1	4.56426022514345e-10	0.428262203554087	0.0144216794838339	1.17498357426956	50	0.5	0.0144216794838339	0	10010	13
8	8	2	2	10	1	10	2	1.38068367835823e-09	0.390342807184376	0.0186158743411536	1.18415760494077	0.24647123155448	0.5	0.0186158743411536	0	10010	13
9	9	3	3	20	1	20	3	1.84852762469112e-13	0.464953640629794	0.0324905173214189	1.19670006787568	125.470780090334	0.5	0.0324905173214189	0	10010	13
10	10	4	4	35	1	35	4	2.5387409753986e-07	0.472488686375661	0.0410949473701172	1.2430043722069	409.337747117509	0.5	0.0410949473701172	0	10010	13
11	11	5	5	35	1	35	5	0.00785039999997779	0.414385141968827	0.0116844077304317	3.64968208443812	339.609238472278	0.5	0.0116844077304317	0	10010	13
12	12	6	6	66	1	66	6	0.00785039999997779	0.414385141968827	0.0116844077304317	3.64968208443812	339.609238472278	0.5	0.0116844077304317	0	10010	13
13	13	1	1	35	1	35	1	4.56426022514345e-10	0.428262203554087	0.0144216794838339	1.17498357426956	50	0.5	0.0144216794838339	0	10010	12
14	14	2	2	10	1	10	2	1.38068367835823e-09	0.390342807184376	0.0186158743411536	1.18415760494077	0.24647123155448	0.5	0.0186158743411536	0	10010	12
15	15	3	3	20	1	20	3	1.84852762469112e-13	0.464953640629794	0.0324905173214189	1.19670006787568	125.470780090334	0.5	0.0324905173214189	0	10010	12
16	16	4	4	35	1	35	4	2.5387409753986e-07	0.472488686375661	0.0410949473701172	1.2430043722069	409.337747117509	0.5	0.0410949473701172	0	10010	12
17	17	5	5	35	1	35	5	0.00785039999997779	0.414385141968827	0.0116844077304317	3.64968208443812	339.609238472278	0.5	0.0116844077304317	0	10010	12
18	18	6	6	66	1	66	6	0.00785039999997779	0.414385141968827	0.0116844077304317	3.64968208443812	339.609238472278	0.5	0.0116844077304317	0	10010	12
19	19	1	1	35	1	35	1	4.56426022514345e-10	0.428262203554087	0.0144216794838339	1.17498357426956	50	0.5	0.0144216794838339	0	10010	14
20	20	2	2	10	1	10	2	1.38068367835823e-09	0.390342807184376	0.0186158743411536	1.18415760494077	0.24647123155448	0.5	0.0186158743411536	0	10010	14
21	21	3	3	20	1	20	3	1.84852762469112e-13	0.464953640629794	0.0324905173214189	1.19670006787568	125.470780090334	0.5	0.0324905173214189	0	10010	14
22	22	4	4	35	1	35	4	2.5387409753986e-07	0.472488686375661	0.0410949473701172	1.2430043722069	409.337747117509	0.5	0.0410949473701172	0	10010	14
23	23	5	5	35	1	35	5	0.00785039999997779	0.414385141968827	0.0116844077304317	3.64968208443812	339.609238472278	0.5	0.0116844077304317	0	10010	14
24	24	6	6	66	1	66	6	0.00785039999997779	0.414385141968827	0.0116844077304317	3.64968208443812	339.609238472278	0.5	0.0116844077304317	0	10010	14
25	25	1	1	35	1	35	1	9.92616971528424e-09	0.44287380451466	0.0239914760796533	1.1763386182368	50	0.5	0.0239914760796533	0	1004610	2
26	26	2	2	10	1	10	2	4.43771929462022e-11	0.317018597325621	0.00200000000002221	1.23581628391365	0.1	0.5	0.00200000000002221	0	1004610	2

Show All Features

Figure 19. Example swap3236_soilunit input table showing the parameters needed to describe soil profiles within the agricultural area of a simulation domain (San Giorgio di Lomellina; gis_cod_domain = 11).

```
*******************************************************************************
* Part 4: Vertical discretization of soil profile

* Specify the following data (maximum MACP lines):
* ISOILLAY = number of soil layer, start with 1 at soil surface, [1..MAHO, I]
* ISUBLAY  = number of sub layer, start with 1 at soil surface, [1..MACP, I]
* HSUBLAY  = height of sub layer, [0.0..1000.0 cm, R]
* HCOMP    = height of compartments in this layer, [0.0..1000.0 cm, R]
* NCOMP    = number of compartments in this layer (= HSUBLAY/HCOMP), [1..MACP, I]

ISOILLAY ISUBLAY HSUBLAY HCOMP NCOMP
soilunit_table_1

* end of table
*******************************************************************************
*******************************************************************************
* Part 5: Soil hydraulic functions

* Switch for Mualem - van Genuchten parameters or detailed tabels:
  SWSOPHY = 0   ! 0 = Mualem - van Genuchten parameters
                ! 1 = Detailed tables

* If SWSOPHY = 0, specify for each soil layer (maximum MAHO):
* ISOILLAY1 = number of soil layer, as defined in part 4 [1..MAHO, I]
* ORES   = Residual water content, [0..0.4 cm3/cm3, R]
* OSAT   = Saturated water content, [0..0.95 cm3/cm3, R]
* ALFA   = Shape parameter alfa of main drying curve, [0.0001..1 /cm, R]
* NPAR   = Shape parameter n, [1..4 -, R]
* KSAT   = Saturated vertical hydraulic conductivity, [1.d-5..1000 cm/d, R]
* LEXP   = Exponent in hydraulic conductivity function, [-25..25 -, R]
* ALFAW  = Alfa parameter of main wetting curve in case of hysteresis, [0.0001..1 /
* H_ENPR = Air entry pressure head [-40.0..0.0 cm, R]

ISOILLAY1 ORES OSAT ALFA NPAR KSAT LEXP ALFAW H_ENPR
soilunit_table_2

* --- end of table

* If SWSOPHY = 1, specify names of input files [A80] with soil hydraulic tables for
  FILENAMESOPHY = 'topsoil_sand_B2.csv', 'subsoil_sand_O2.csv'
*******************************************************************************
```

Figure 20. SWAP main input file (.swp); SOIL WATER SECTION: Part 4 - Vertical discretization of soil profile; Part 5 - Soil hydraulic functions.

Soil Use Map, Crop Parameters and Irrigation Management

The soil use map (Figure 21) shows the spatial distribution of the different crops (and their crop-related irrigation management definded in the file .crp) and/or semi-natural areas in the simulation domain. In the current configuration of the framework, crops and their crop-related irrigation management can be defined, starting from their associated input table, by intersecting not just soil uses (*gis_cod_soiluse*) but also groundwater depth areas (*gis_cod_gw*). This makes it possible to differentiate crop properties (e.g. biometric parameters) and automated irrigation management even under different groundwater conditions existing in a simulation domain.

All the needed data about the features charted in the soil use input vector map are contained inside the *swap3236_soiluse* input table (Figure 22). Three different types of attributes are required: I) CROPSTART, CROPEND, CROPNAME, CROPFIL, CROPTYPE (involved in crop rotation scheme during simulation period definition), II) PONDMX (involved Runoff and pond management) and III) VAP_node.

The framework allows the definition of a single crop rotation scheme during simulation period (Figure 23, file .swp). Regarding CROPFIL, the framework creates a direct connection between the simulated crop and the SWAP crop input file (.crp), allowing the user to fully manage the parameterization of the crop file without making any dynamic modifications. Currently, the framework has only been tested to work with the so-called simple crop module. The simple crop module is designed to provide appropriate upper boundary conditions, in terms of water movement, without dealing with the actual growth of a crop. Within the simple crop input file, all parameters related to the estimation of interception and evapotranspiration, as well as the management of the crop-related irrigation scheduling, are defined by the user according to the

development stage (DVS, -). Inside the crop input file (.crp, not shown), the user can define an automatic scheduled irrigation regime by setting Irrigation time criteria (I - daily Stress, II - depletion of Readily Available Water, III - depletion of Totally Available Water, IV - depletion Water Amount, V - pressure head or moisture content, and VI - fixed weekly irrigation, rootzone to field capacity) and irrigation depth criteria (I - back to Field Capacity, and II - fixed Irrigation Depth).

In SWAP surface runoff (q_{runoff}, cm) is calculated using the formula:

$$q_{runoff} = \frac{1}{\gamma}\left(max(0,(h_0 - h_{0,threshold}))\right)^{\beta} \qquad \text{(Eq. 10)}$$

where:

- h_0 (cm) is the ponding depth of water on the soil surface,
- $h_{0,threshold}$ (cm) is a user-defined critical ponding depth,
- γ (cmβ-1 d) and β (-) are, respectively, a resistance and an exponent parameter in the empirical relation.

Two paths are available to customize runoff management in the main SWAP input file (Figure 24, file .swp): I) define a single constant threshold (swpondmx = 0) or II) a time dependent threshold (swpondmx = 1). In the first case, the framework replaces the string *XXXX* for the PONDMX parameter with the desired value, while in the second, it replaces the string *pondmx_table* with the user-supplied input table values (DATEPMX and PONDMXTB, see Section Inlet Areas Map and Irrigation Time Series). Considering the specific case for which the tool was developed (flooded rice fields), the framework is tailored to treat $h_{0,threshold}$ as a fundamental part of irrigation management. The idea is to move surplus water away from fields if the target pond values $h_{0,threshold}$ is reached and to allow the user to carry out controlled drying periods ($h_{0,threshold} = 0$). Since it is often necessary to supply excess water to correctly maintain $h_{0,threshold}$ during simulaton at the field level, the actual irrigation water requirement ($Net\ irrigation$, cm) of the field is then calculated as:

$$\boldsymbol{Net\ irrigation_d} = \begin{cases} Irrigation_d - q_{runoff\,d}, & Irrigation_d - q_{runoff\,d} \geq 0 \\ 0, & Irrigation_d - q_{runoff\,d} < 0 \end{cases} \qquad \text{(Eq. 11)}$$

where

- $Irrigation$ (cm) is the irrigation water applied by the user (fixed irrigation applications) or simulated by SWAP (crop-related irrigation scheduling),

- d (-) is the day of the simulation year.

Regarding VAP_node, the framework asks the user to define a minimum and a maximum node (cm, negative) in which evaluate outputs from the soil profile output file (.vap) (see Section 3.3.3.3). The current configuration does not implement Runon (SWRUNON = 0, file .swp).

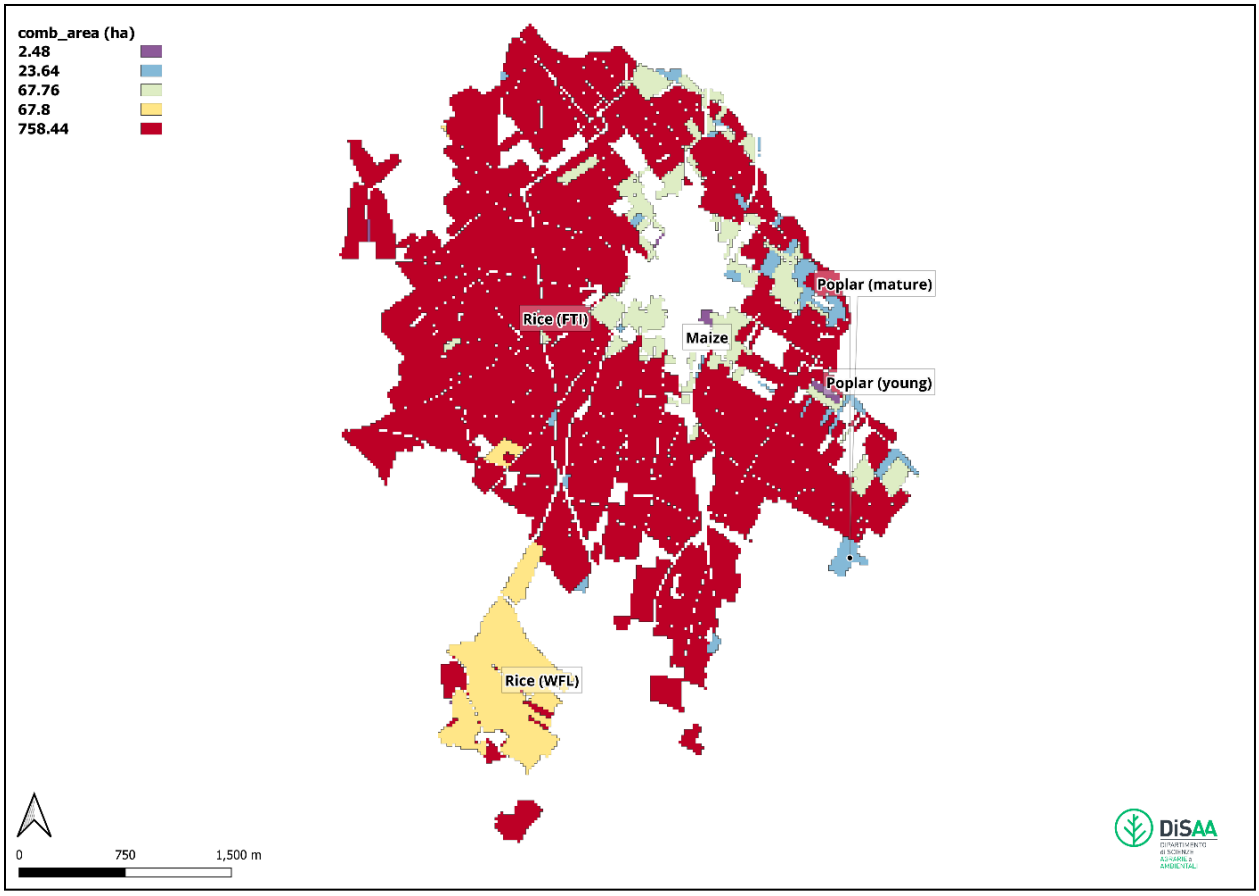

Figure 21. Example of a map showing crops spatial distribution within the agricultural area of a simulation domain (San Giorgio di Lomellina; gis_cod_domain = 11). In particular, the map illustrates the considered productive soil uses in 2020, including Rice (WFL), Rice (FTI), Maize, young Poplar (irrigated), and mature Poplar (not irrigated).

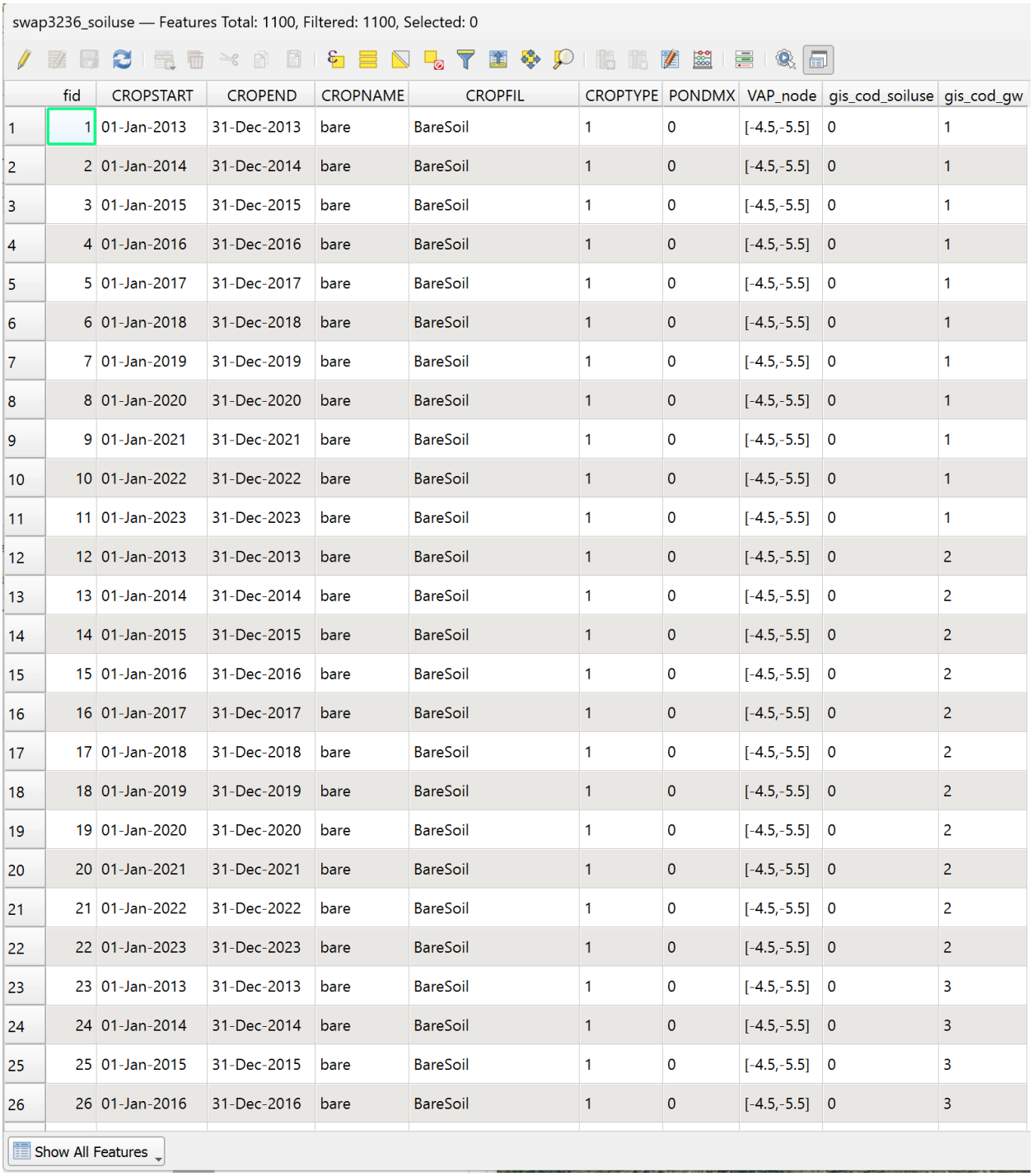
swap3236_soiluse — Features Total: 1100, Filtered: 1100, Selected: 0

	fid	CROPSTART	CROPEND	CROPNAME	CROPFIL	CROPTYPE	PONDMX	VAP_node	gis_cod_soiluse	gis_cod_gw
1	1	01-Jan-2013	31-Dec-2013	bare	BareSoil	1	0	[-4.5,-5.5]	0	1
2	2	01-Jan-2014	31-Dec-2014	bare	BareSoil	1	0	[-4.5,-5.5]	0	1
3	3	01-Jan-2015	31-Dec-2015	bare	BareSoil	1	0	[-4.5,-5.5]	0	1
4	4	01-Jan-2016	31-Dec-2016	bare	BareSoil	1	0	[-4.5,-5.5]	0	1
5	5	01-Jan-2017	31-Dec-2017	bare	BareSoil	1	0	[-4.5,-5.5]	0	1
6	6	01-Jan-2018	31-Dec-2018	bare	BareSoil	1	0	[-4.5,-5.5]	0	1
7	7	01-Jan-2019	31-Dec-2019	bare	BareSoil	1	0	[-4.5,-5.5]	0	1
8	8	01-Jan-2020	31-Dec-2020	bare	BareSoil	1	0	[-4.5,-5.5]	0	1
9	9	01-Jan-2021	31-Dec-2021	bare	BareSoil	1	0	[-4.5,-5.5]	0	1
10	10	01-Jan-2022	31-Dec-2022	bare	BareSoil	1	0	[-4.5,-5.5]	0	1
11	11	01-Jan-2023	31-Dec-2023	bare	BareSoil	1	0	[-4.5,-5.5]	0	1
12	12	01-Jan-2013	31-Dec-2013	bare	BareSoil	1	0	[-4.5,-5.5]	0	2
13	13	01-Jan-2014	31-Dec-2014	bare	BareSoil	1	0	[-4.5,-5.5]	0	2
14	14	01-Jan-2015	31-Dec-2015	bare	BareSoil	1	0	[-4.5,-5.5]	0	2
15	15	01-Jan-2016	31-Dec-2016	bare	BareSoil	1	0	[-4.5,-5.5]	0	2
16	16	01-Jan-2017	31-Dec-2017	bare	BareSoil	1	0	[-4.5,-5.5]	0	2
17	17	01-Jan-2018	31-Dec-2018	bare	BareSoil	1	0	[-4.5,-5.5]	0	2
18	18	01-Jan-2019	31-Dec-2019	bare	BareSoil	1	0	[-4.5,-5.5]	0	2
19	19	01-Jan-2020	31-Dec-2020	bare	BareSoil	1	0	[-4.5,-5.5]	0	2
20	20	01-Jan-2021	31-Dec-2021	bare	BareSoil	1	0	[-4.5,-5.5]	0	2
21	21	01-Jan-2022	31-Dec-2022	bare	BareSoil	1	0	[-4.5,-5.5]	0	2
22	22	01-Jan-2023	31-Dec-2023	bare	BareSoil	1	0	[-4.5,-5.5]	0	2
23	23	01-Jan-2013	31-Dec-2013	bare	BareSoil	1	0	[-4.5,-5.5]	0	3
24	24	01-Jan-2014	31-Dec-2014	bare	BareSoil	1	0	[-4.5,-5.5]	0	3
25	25	01-Jan-2015	31-Dec-2015	bare	BareSoil	1	0	[-4.5,-5.5]	0	3
26	26	01-Jan-2016	31-Dec-2016	bare	BareSoil	1	0	[-4.5,-5.5]	0	3

Show All Features

Figure 22. Example swap3236_soiluse input table showing the parameters needed to describe soil uses within the agricultural area of a simulation domain (San Giorgio di Lomellina; gis_cod_domain = 11).

```
*******************************************************************************************
* Part 1: Crop rotation scheme during simulation period

* Specify information for each crop (maximum MACROP):
* CROPSTART  = date of crop emergence, [dd-mmm-yyyy]
* CROPEND    = date of crop harvest, [dd-mmm-yyyy]
* CROPNAME   = crop name, [A40]
* CROPFIL    = name of file with crop input parameters without extension .CRP, [A40]
* CROPTYPE   = type of crop model: simple = 1, detailed general = 2, detailed grass = 3

CROPSTART CROPEND CROPNAME CROPFIL CROPTYPE
soiluse_table

* End of table
*******************************************************************************************
```

Figure 23. SWAP main input file (.swp); CROP SECTION: Part 1 - Crop rotation scheme during simulation period.

```
*******************************************************************************
* Part 2: Ponding, runoff and runon

* Ponding threshold
* time-dependent threshold of ponding layer is optional and dependent on the presence of
* the input parameter swPondmx. Only when swPondmx is present and has a value of 1, then:
* - a table must be supplied with dates and values for days when pondmx changes value.
* - the value for RSRO must be larger than 0.01 d.
  swPondmx = XXXX

* In case of time dependent threshold (swpondmx = 1), then specify date DATEPMX [dd-mmm-yyyy] and
* threshold for ponding PONDMXTB [cm], maximum MAIRG records:
* The threshold value is determined by linear interpolation between date-values.

DATEPMX PONDMXTB
pondmx_table

* End of table

* In case of a constant threshold (swpondmx = 0 or absent), then specify PONDMX:
  PONDMX  = XXXX  ! In case of ponding, minimum thickness for runoff, [0..1000 cm, R]

* Runoff
  RSRO    =  0.01 ! Drainage resistance for surface runoff [0.001..1.0 d, R]
  RSROEXP =  10.0 ! Exponent in drainage equation of surface runoff [0.1..10.0 -, R]

* Runon
* Specify whether runon data are provided in extra input file
  SWRUNON = 0  ! 0 = No input of runon data
               ! 1 = Runon data are provided in extra input file

* If SWRUNON = 1, specify name of file with runon input data
* This file may be an output *.inc file (with only 1 header) of a previous Swap-simulation
  RUFIL = 'runon.inc' ! File name with extension [A80]
*******************************************************************************
```

Figure 24. SWAP main input file (.swp); SOIL WATER SECTION: Part 2 - Ponding, runoff and runon.

Inlet Areas Map and Irrigation Time Series

Inlet areas map (Figure 25) provides a way to distribute fixed irrigation applications and, if required, a certain time dependent ponding threshold within the agricultural area based on distinct zones that can be considered as irrigation water distribution areas (*gis_cod_inlet*, e.g. areas served by specific channels or with different farm management). If not needed, inlet areas could also coincide with the entire simulation domain and give the user the possibility to define a certain irrigation management from its related input table by intersecting only soil uses (*gis_cod_soiluse*) and groundwater depth areas (*gis_cod_gw*).

Inside the *swap3236_inlet_daily* input table (Figure 26) it is possible to define the attributes related to: I) the fixed irrigation management (IRDATE, IRDEPTH, IRCONC and IRTYPE) and II) the time dependent ponding threshold (PONDMXTB, see Section Soil Use Map, Crop Parameters and Irrigation Management). To do this, SWIRFIX and SWIRGFIL values are set to 1

in the SWAP main file (Figure 27, file .swp). So, the framework asks the user to define a table with IRDATE, IRDEPTH, IRCONC and IRTYPE series. Then, the framework overwrites the string *inlet_table* with the fixed irrigation applications table asked to the user into an irrigation file called IRG (IRGFIL).

Currently, the data reported in the *swap3236_inlet_daily* input table must represent a series of daily values (also not consecutive) and must always be present for the simulation year, and for all the *gis_cod_inlet*, *gis_cod_soiluse* and *gis_cod_gw* combinations represented in the respective input vector maps. When fixed irrigation management is not necessary, the user could define just one, or even more, row with IRDEPTH values equal to zero. In a similar way, it is possible to define PONDMXTB values to dynamically manage the simulated ponding threshold, even in case of no irrigation (IRDEPTH = 0) and/or when irrigation should be controlled by the crop-related irrigation management (CROPFIL, file .crp). This allows, for each day of the year of simulation, to manage irrigation applications by mixing the fixed irrigation management, the time dependent ponding threshold and the crop-related irrigation management. This approach provided the flexibility needed to simulate complex rice irrigation regimes, including Alternate Wetting and Drying (AWD).

Figure 25. Example of a map showing inlet spatial distribution within the agricultural area of a simulation domain (San Giorgio di Lomellina; gis_cod_domain = 11). In this case, inlet areas coincide with the entire simulation domain.

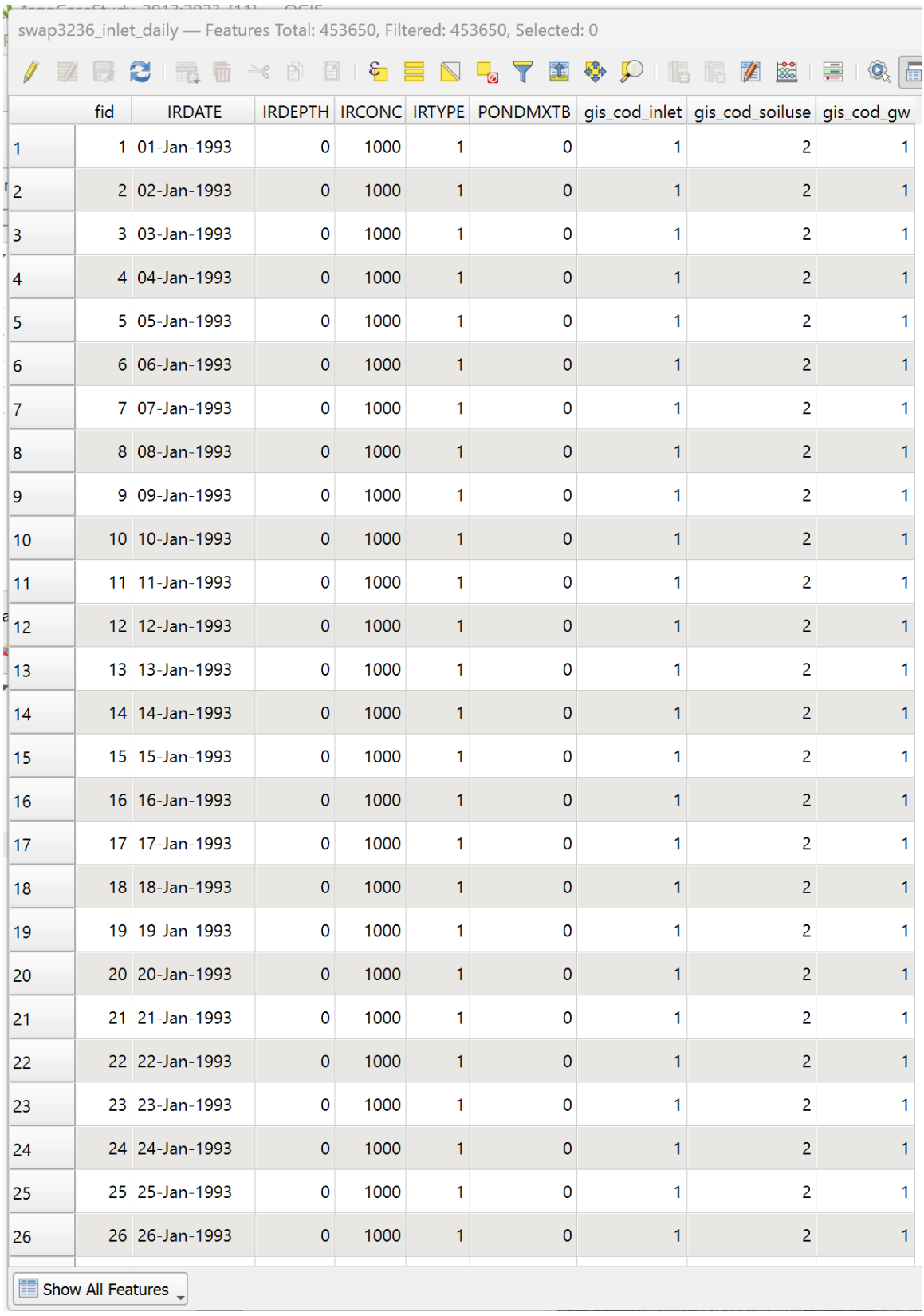

	fid	IRDATE	IRDEPTH	IRCONC	IRTYPE	PONDMXTB	gis_cod_inlet	gis_cod_soiluse	gis_cod_gw
1	1	01-Jan-1993	0	1000	1	0	1	2	1
2	2	02-Jan-1993	0	1000	1	0	1	2	1
3	3	03-Jan-1993	0	1000	1	0	1	2	1
4	4	04-Jan-1993	0	1000	1	0	1	2	1
5	5	05-Jan-1993	0	1000	1	0	1	2	1
6	6	06-Jan-1993	0	1000	1	0	1	2	1
7	7	07-Jan-1993	0	1000	1	0	1	2	1
8	8	08-Jan-1993	0	1000	1	0	1	2	1
9	9	09-Jan-1993	0	1000	1	0	1	2	1
10	10	10-Jan-1993	0	1000	1	0	1	2	1
11	11	11-Jan-1993	0	1000	1	0	1	2	1
12	12	12-Jan-1993	0	1000	1	0	1	2	1
13	13	13-Jan-1993	0	1000	1	0	1	2	1
14	14	14-Jan-1993	0	1000	1	0	1	2	1
15	15	15-Jan-1993	0	1000	1	0	1	2	1
16	16	16-Jan-1993	0	1000	1	0	1	2	1
17	17	17-Jan-1993	0	1000	1	0	1	2	1
18	18	18-Jan-1993	0	1000	1	0	1	2	1
19	19	19-Jan-1993	0	1000	1	0	1	2	1
20	20	20-Jan-1993	0	1000	1	0	1	2	1
21	21	21-Jan-1993	0	1000	1	0	1	2	1
22	22	22-Jan-1993	0	1000	1	0	1	2	1
23	23	23-Jan-1993	0	1000	1	0	1	2	1
24	24	24-Jan-1993	0	1000	1	0	1	2	1
25	25	25-Jan-1993	0	1000	1	0	1	2	1
26	26	26-Jan-1993	0	1000	1	0	1	2	1

Figure 26. Example of swap3236_inlet_daily input table showing the parameters needed to describe different inlet areas within the agricultural area of a simulation domain (San Giorgio di Lomellina; gis_cod_domain = 11).

```
*******************************************************************************************
* Part 2: Fixed irrigation applications

* Switch for fixed irrigation applications
  SWIRFIX = 1    ! SWIRFIX = 0: no irrigation applications are prescribed
                 ! SWIRFIX = 1: irrigation applications are prescribed

* If SWIRFIX = 1, specify:

* Switch for separate file with fixed irrigation applications
  SWIRGFIL  = 1  ! SWIRGFIL = 0: data are specified in the .swp file
                 ! SWIRGFIL = 1: data are specified in a separate file

* If SWIRGFIL  = 0 specify information for each fixed irrigation event (max. MAIRG):
* IRDATE   = date of irrigation, [dd-mmm-yyyy]
* IRDEPTH  = amount of water, [0.0..100.0 cm, R]
* IRCONC   = concentration of irrigation water, [0.0..1000.0 mg/cm3, R]
* IRTYPE   = type of irrigation: sprinkling = 0, surface = 1

      IRDATE   IRDEPTH     IRCONC   IRTYPE
  05-jan-1980       0.5     1000.0        1
* end of table

* If SWIRGFIL  = 1, specify name of file with data of fixed irrigation applications:
  IRGFIL = 'IRG'      ! File name without extension .IRG [A16]
*******************************************************************************************
```

Figure 27. SWAP main input file (.swp); CROP SECTION: Part 2 - Fixed irrigation applications.

Groundwater Depth Areas Map and Time Series

Groundwater depth areas map (Figure 28) defines zones in which a specific lower boundary condition is imposed during field agro-hydrological simulations. To guide the definition of the groundwater depth zones for the San Giorgio distrct, the approach proposed by (Mayer et al., 2019) was used. This approach involves using groundwater data at the peak of the irrigation season to characterize the study area as having either low (shallow, at or below -1 m from field level) or high (deep, at or below -1 m from field level) groundwater depth. For each polygon provided inside the groundwater depth areas map (i.e. shallow or deep) a time series of groundwater depths (m, negative) must be provided. The framework will select the correct data from its associated input table based on the groundwater depth area *gis_cod* attribute (*gis_cod_gw*).

The *swap3236_gwd_daily* input table (Figure 29) contains the daily time series needed (DATE5, GW) to characterize all the different features depicted into the groundwater depth areas input vector map. The framework defines the bottom boundary conditions inside a bottom boundary input file (Figure 30, .bbc), thus using the option SWBBCFILE = 1 in the main SWAP input file (.swp). The file is called GWD (BBCFIL). Bottom boundary conditions considered in SWAP are listed in the BBCFIL file; currently the modelling framework considers two of them: I) prescribed soil water pressure head of bottom compartment (SWBOTB = 5), and II) free drainage of soil profile (SWBOTB = 7). The choice between the two options is left to the user: if all the GW values provided for the simulation year and a specific *gis_cod_gw* consist of no data (user-defined), free drainage is imposed, otherwise prescribed pressure head is assumed. When SWBOTB equals 5, the framework calculates the bottom compartment pressure head (HBOT5) by adding user-provided groundwater depths (negative) to the total soil profile thickness. If SWBOTB is 7, the bottom compartment flux (cm/d) matches the hydraulic conductivity of the lowest compartment. Depending on the choice made by the user, the framework overwrites the string *XXXX* to define the right SWBOTB value (5 or 7) and print the estimated HBOT5 replacing the string *gwd_table*.

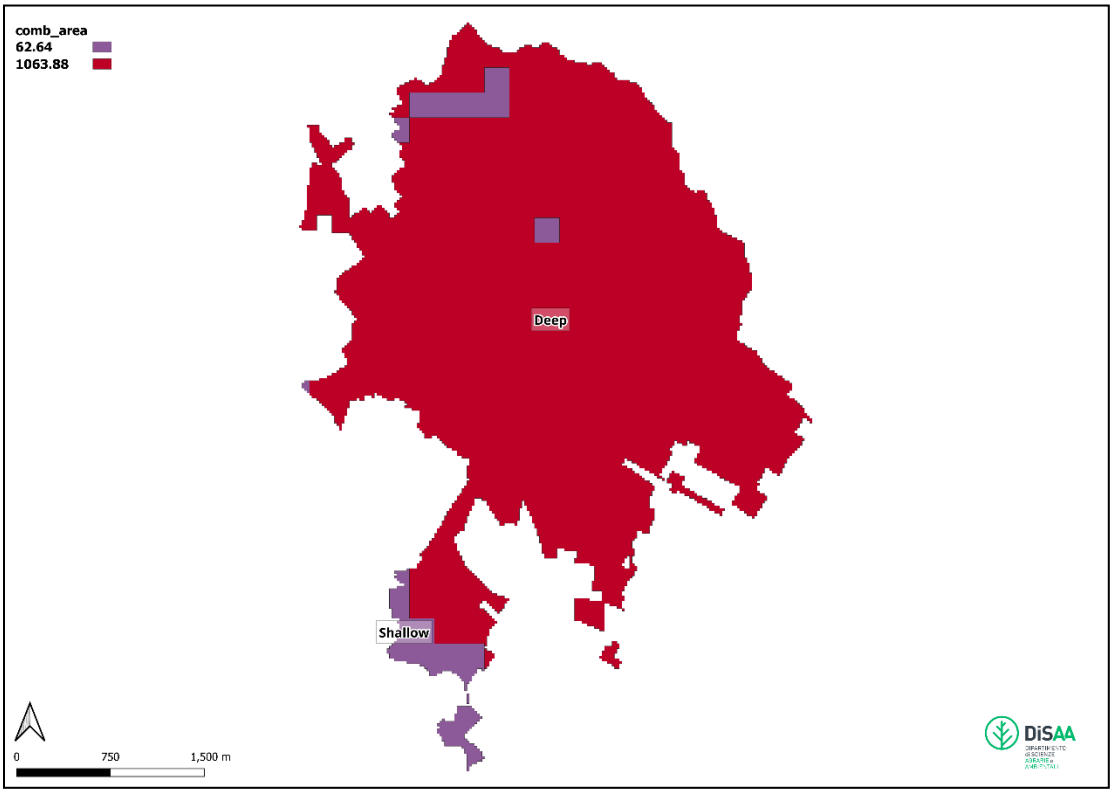

Figure 28. Example of a map showing groundwater depth areas spatial distribution within the agricultural area of a simulation domain (San Giorgio di Lomellina; gis_cod_domain = 11).

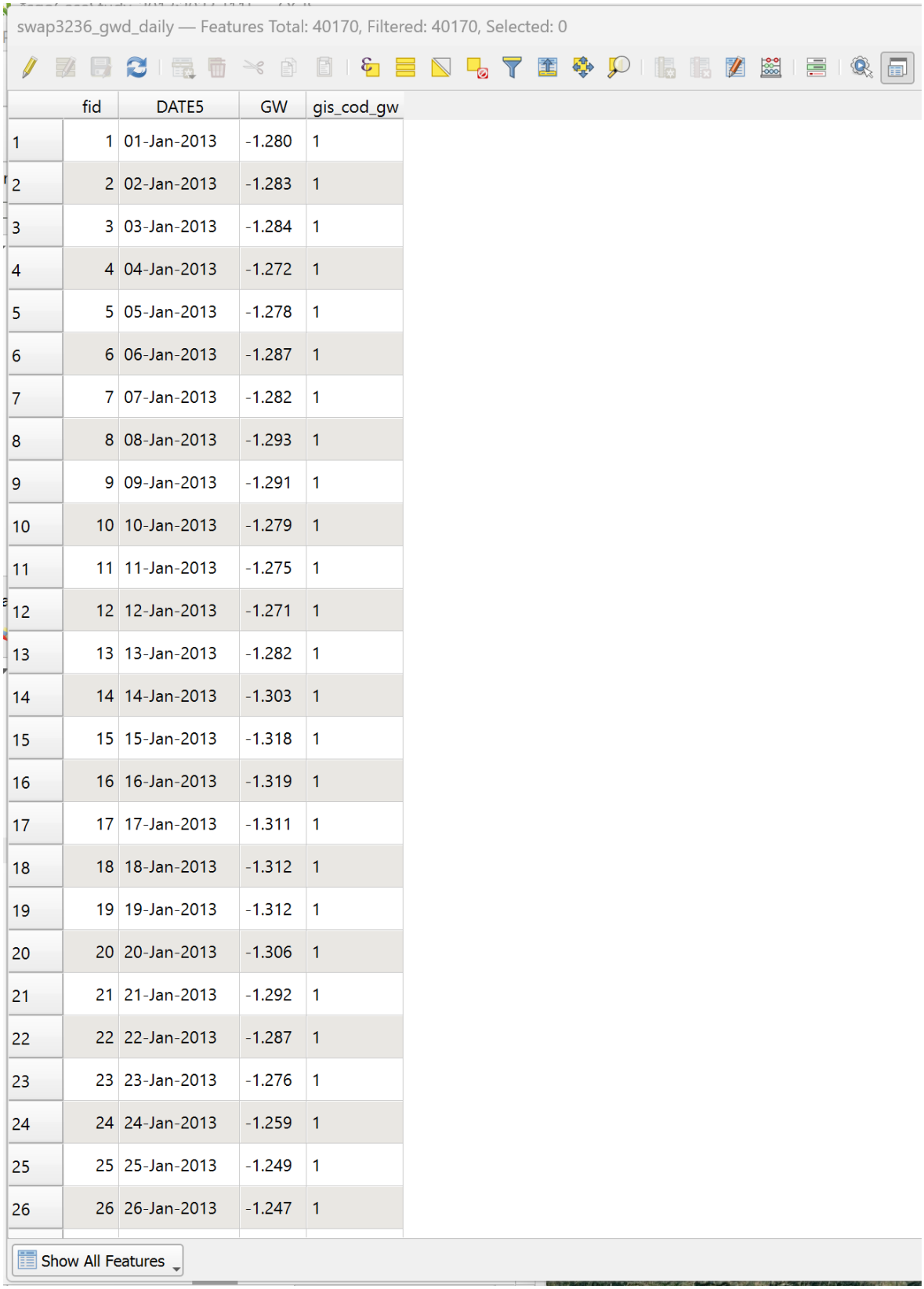

	fid	DATE5	GW	gis_cod_gw
1	1	01-Jan-2013	-1.280	1
2	2	02-Jan-2013	-1.283	1
3	3	03-Jan-2013	-1.284	1
4	4	04-Jan-2013	-1.272	1
5	5	05-Jan-2013	-1.278	1
6	6	06-Jan-2013	-1.287	1
7	7	07-Jan-2013	-1.282	1
8	8	08-Jan-2013	-1.293	1
9	9	09-Jan-2013	-1.291	1
10	10	10-Jan-2013	-1.279	1
11	11	11-Jan-2013	-1.275	1
12	12	12-Jan-2013	-1.271	1
13	13	13-Jan-2013	-1.282	1
14	14	14-Jan-2013	-1.303	1
15	15	15-Jan-2013	-1.318	1
16	16	16-Jan-2013	-1.319	1
17	17	17-Jan-2013	-1.311	1
18	18	18-Jan-2013	-1.312	1
19	19	19-Jan-2013	-1.312	1
20	20	20-Jan-2013	-1.306	1
21	21	21-Jan-2013	-1.292	1
22	22	22-Jan-2013	-1.287	1
23	23	23-Jan-2013	-1.276	1
24	24	24-Jan-2013	-1.259	1
25	25	25-Jan-2013	-1.249	1
26	26	26-Jan-2013	-1.247	1

Figure 29. Example swap3236_gwd_daily input table showing the parameters needed to describe different groundwater depth areas within the agricultural area of a simulation domain (San Giorgio di Lomellina; gis_cod_domain = 11).

```
*******************************************************************************************
* Filename: swap.bbc
* Contents: SWAP 4 - Main input data
*******************************************************************************************
* Comment area:
* Testbank of SWAP: build with template of bbc-file
*
*******************************************************************************************

*** BOTTOM BOUNDARY SECTION ***

*******************************************************************************************
* Bottom boundary condition

* Select one of the following options:
  SWBOTB = XXXX               ! 1  Prescribe groundwater level
                              ! 2  Prescribe bottom flux
                              ! 3  Calculate bottom flux from hydraulic head of deep aquifer
                              ! 4  Calculate bottom flux as function of groundwater level
                              ! 5  Prescribe soil water pressure head of bottom compartment
                              ! 6  Bottom flux equals zero
                              ! 7  Free drainage of soil profile
                              ! 8  Free outflow at soil-air interface

* Options 1-5 require additional bottom boundary data below

*******************************************************************************************

*******************************************************************************************
* SWBOTB = 5     Prescribe soil water pressure head of bottom compartment

* Specify DATE [dd-mmm-yyyy] and bottom compartment pressure head HBOT5 [-1.d10..1000 cm, R]:

DATE5 HBOT5
gwd_table

* End of table
*******************************************************************************************

* End of input file .BBC     !
```

Figure 30. SWAP bottom boundary input file (.bbc); BOTTOM BOUNDARY SECTION.

Agro-Meteorological Areas Map and Time Series

All the diverse areas of influence of the different agro-meteo stations must be reported in the agro-meteorological areas map (Figure 31). The associated agro-meteo time series is selected from its input table based just on a single *gis_cod* attribute (*gis_cod_meteo*). If not necessary, the input areas could also coincide with the entire simulation domain, as in the case study of San Giorgio di Lomellina.

The *swap3236_meteo_daily* input table (Figure 32) stores the required daily time series of agro-meteorological variables. The framework works with daily weather data (SWMETDETAIL = 0 and SWRAIN = 0, Figure 33, file .swp), written into a separate file called ET0 (METFIL, Figure 33, file .swp) and with the extension .0YY (Figure 34, where YY stands for the last two digits of the simulation year). The framework overwrites the string *meteo_table* with all the necessary information: station name (Station, -), day of the month (DD, n), month of the year (MM, n), simulation year (YYYY, n), solar radiation (RAD, kJ/m^2), air temperature (Tmin and Tmax, °C), air humidity (HUM, kPa), wind speed (WIND, m/s), daily rainfall (RAIN, mm/d) and reference evapotranspiration (ETref, mm/d). SWAP offers two methods to estimate the reference evapotranspiration in the main SWAP input file (Figure 33, file. swp): I) one involving the use of Penman Monteith equation (Allen et al., 1998) (SWETR = 0), and II) one in which the user provides directly ETref values as input (SWETR = 1). The framework currently works only with the second of these two options (SWETR = 1). No distribution of daily Tp and Ep according to

sinus wave (SWETSINE = 0, file .swp) is currently set and no snow accumulation and melt is simulated (SWSNOW = 0, file .swp).

Figure 31. Example of a map showing agro-meteorological areas spatial distribution within the agricultural area of a simulation domain (San Giorgio di Lomellina; gis_cod_domain = 11). In this case, inlet areas coincide with the entire simulation domain.

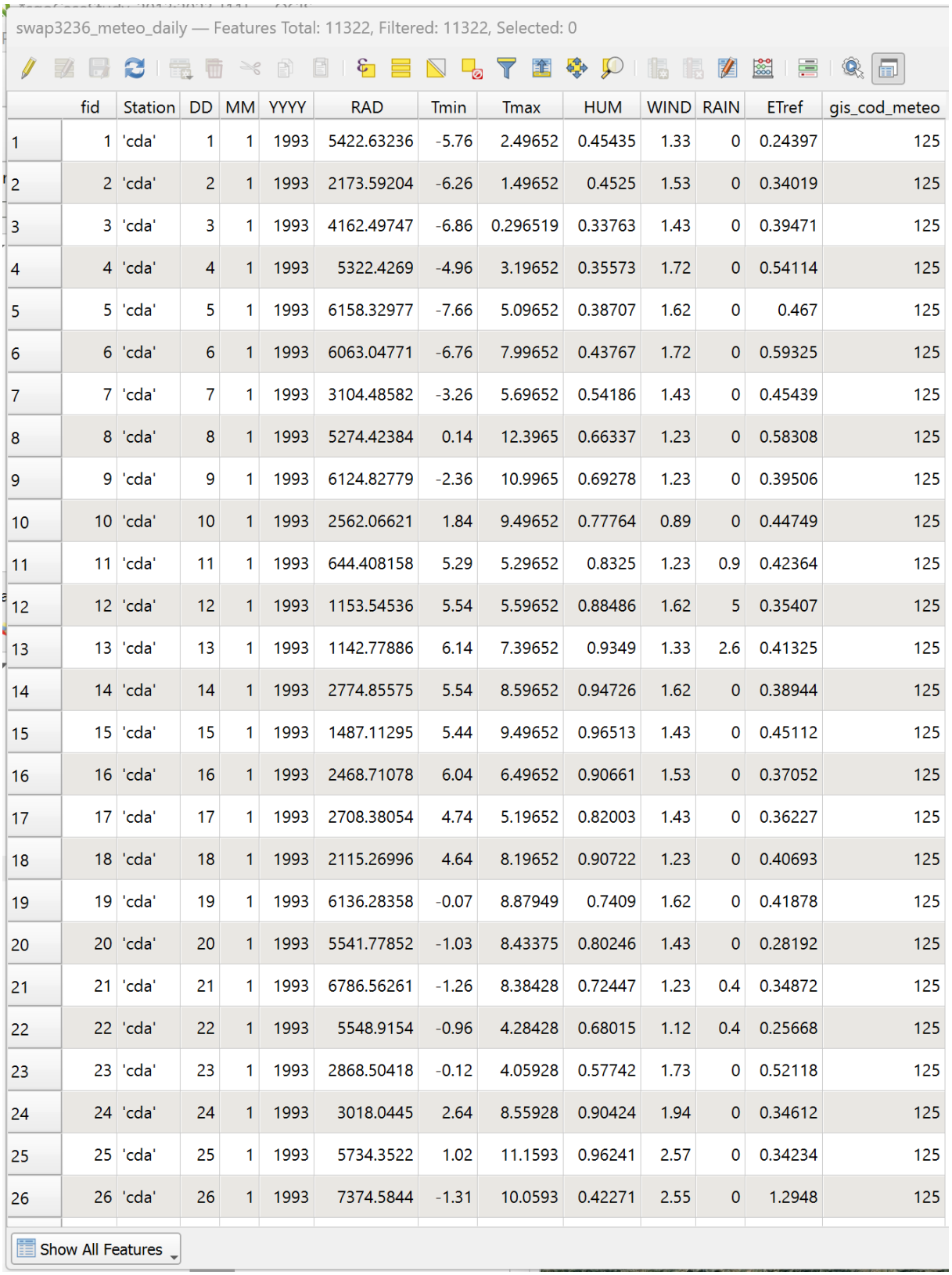

swap3236_meteo_daily — Features Total: 11322, Filtered: 11322, Selected: 0

	fid	Station	DD	MM	YYYY	RAD	Tmin	Tmax	HUM	WIND	RAIN	ETref	gis_cod_meteo
1	1	'cda'	1	1	1993	5422.63236	-5.76	2.49652	0.45435	1.33	0	0.24397	125
2	2	'cda'	2	1	1993	2173.59204	-6.26	1.49652	0.4525	1.53	0	0.34019	125
3	3	'cda'	3	1	1993	4162.49747	-6.86	0.296519	0.33763	1.43	0	0.39471	125
4	4	'cda'	4	1	1993	5322.4269	-4.96	3.19652	0.35573	1.72	0	0.54114	125
5	5	'cda'	5	1	1993	6158.32977	-7.66	5.09652	0.38707	1.62	0	0.467	125
6	6	'cda'	6	1	1993	6063.04771	-6.76	7.99652	0.43767	1.72	0	0.59325	125
7	7	'cda'	7	1	1993	3104.48582	-3.26	5.69652	0.54186	1.43	0	0.45439	125
8	8	'cda'	8	1	1993	5274.42384	0.14	12.3965	0.66337	1.23	0	0.58308	125
9	9	'cda'	9	1	1993	6124.82779	-2.36	10.9965	0.69278	1.23	0	0.39506	125
10	10	'cda'	10	1	1993	2562.06621	1.84	9.49652	0.77764	0.89	0	0.44749	125
11	11	'cda'	11	1	1993	644.408158	5.29	5.29652	0.8325	1.23	0.9	0.42364	125
12	12	'cda'	12	1	1993	1153.54536	5.54	5.59652	0.88486	1.62	5	0.35407	125
13	13	'cda'	13	1	1993	1142.77886	6.14	7.39652	0.9349	1.33	2.6	0.41325	125
14	14	'cda'	14	1	1993	2774.85575	5.54	8.59652	0.94726	1.62	0	0.38944	125
15	15	'cda'	15	1	1993	1487.11295	5.44	9.49652	0.96513	1.43	0	0.45112	125
16	16	'cda'	16	1	1993	2468.71078	6.04	6.49652	0.90661	1.53	0	0.37052	125
17	17	'cda'	17	1	1993	2708.38054	4.74	5.19652	0.82003	1.43	0	0.36227	125
18	18	'cda'	18	1	1993	2115.26996	4.64	8.19652	0.90722	1.23	0	0.40693	125
19	19	'cda'	19	1	1993	6136.28358	-0.07	8.87949	0.7409	1.62	0	0.41878	125
20	20	'cda'	20	1	1993	5541.77852	-1.03	8.43375	0.80246	1.43	0	0.28192	125
21	21	'cda'	21	1	1993	6786.56261	-1.26	8.38428	0.72447	1.23	0.4	0.34872	125
22	22	'cda'	22	1	1993	5548.9154	-0.96	4.28428	0.68015	1.12	0.4	0.25668	125
23	23	'cda'	23	1	1993	2868.50418	-0.12	4.05928	0.57742	1.73	0	0.52118	125
24	24	'cda'	24	1	1993	3018.0445	2.64	8.55928	0.90424	1.94	0	0.34612	125
25	25	'cda'	25	1	1993	5734.3522	1.02	11.1593	0.96241	2.57	0	0.34234	125
26	26	'cda'	26	1	1993	7374.5844	-1.31	10.0593	0.42271	2.55	0	1.2948	125

Show All Features

Figure 32. Example of swap3236_meteo_daily input table showing the parameters needed to describe different agro-meteorological areas within the agricultural area of a simulation domain (San Giorgio di Lomellina; gis_cod_domain = 11).

```
*** METEOROLOGY SECTION ***

*******************************************************************************
* General data

* File name
  METFIL = 'ET0' ! File name of meteorological data without extension .YYY, [A200]
                 ! Extension is equal to last 3 digits of year, e.g. 003 denotes year 2003

* Use of reference evapotranspiration data from meteorological file instead of basic data
  SWETR  =  1    ! Switch, use reference ET values of meteo file [Y=1, N=0]

* If SWETR = 0, specify:
  LAT    =   52.0       ! Latitude of meteo station, [-60..60 degrees, R, North = +]
  ALT    =   10.0       ! Altitude of meteo station, [-400..3000 m, R]
  ALTW   =    2.0       ! Altitude of wind speed measurement (10 m is default) [0..99 m, R]

* Use of detailed meteorological records for both ET and rainfall (< 1 day) in stead of daily values
  SWMETDETAIL = 0       ! Switch, use detailed meteorological records of both ET and rainfall [Y=1, N=0]

* In case of detailed meteorological weather records (SWMETDETAIL = 1), specify:
  NMETDETAIL = 10       ! Number of weather data records per day, [1..96 -, I]

* In case of daily meteorological weather records (SWMETDETAIL = 0):
  SWETSINE = 0          ! Switch, distribute daily Tp and Ep according to sinus wave [Y=1, N=0]

  SWRAIN =  0           ! Switch for use of actual rainfall intensity (only if SWMETDETAIL = 0):
                        ! SWRAIN = 0: Use daily rainfall amounts
                        ! SWRAIN = 1: Use daily rainfall amounts + mean intensity
                        ! SWRAIN = 2: Use daily rainfall amounts + duration
                        ! SWRAIN = 3: Use short time rainfall intensities, as supplied in separate file

* If SWRAIN = 1, then specify mean rainfall intensity RAINFLUX [0.d0..1000.d0 mm/d, R]
* as function of time TIME [0..366 d, R], maximum 30 records
   TIME    RAINFLUX
    1.0        20.0
  360.0        20.0
* End of table

* If SWRAIN = 3, then specify file name of file with detailed rainfall data
  RAINFIL = 'RAIN'   ! File name of detailed rainfall data without extension .YYY, [A200]
                     ! Extension is equal to last 3 digits of year, e.g. 003 denotes year 2003
*******************************************************************************
```

Figure 33. SWAP main input file (.swp); METEOROLOGY SECTION: General data.

```
*******************************************************************************
* Filename: ET0.00
* Contents: SWAP - Meteorological data
*******************************************************************************
* Comment area:
*
*
*******************************************************************************
    Station   DD MM YYYY     RAD    Tmin    Tmax     HUM    WIND    RAIN    ETref
*             nr nr   nr    kJ/m2      C       C     kPa     m/s      mm       mm
*******************************************************************************
meteo_table
```

Figure 34. SWAP meteo input file (.0YY).

3.3.3.2 Potential and Actual Simulation Units for the Agricultural Area

Once maps describing the agricultural area have been retrieved, the *gis_cod* attribute is translated into a grid .tif file and warped over the simulation domain, so as to obtain input grid maps that share a specific extension and cell size (user defined). The process of spatially overlaying multiple input vector maps, which may have varying extents and resolutions, requires a data homogenization step over the selected simulation domain. This procedure ensures that the geometries of the input vector maps can be effectively intersected by standardizing them onto a

grid with uniform number of rows and columns. However, critical considerations (Johnson and Clarke, 2021) are involved in this process, particularly with regard to selecting an appropriate resolution to accurately represent all input data, and to the algorithm employed for the resampling operation. Currently, this framework uses the GDAL library to perform these operations (https://gdal.org/en/stable/programs/gdalwarp.html); users have the option to choose between two specific algorithms: I) nearest neighbour (near) resampling, and II) mode/majority (mode) resampling.

Once this process has been completed, the framework calculates the Cartesian product (Pp) of all the unique *gis_cod* values represented in the input grid maps to reconstruct the potential simulation units table (*comb_key_table*, Figure 35). A potential simulation unit is a unique set of *gis_cod* values taken from all the input grid maps, pointing to a specific set of parameters and associated time series stored into the input tables. The potential simulation units table contains a number of columns equal to the number of input grid maps considered (A, B, C, D, E); the number of rows is given by the product of the counts of all unique *gis_cod* values found in each input grid map, thereby representing every possible combination of codes across the different maps. A potential simulation unit does not yet have a spatial extent (no geometry) in the agricultural area of the simulation domain.

comb_key_table_sgoCaseStudy_2020_11 — Features Total: 192, Filtered: 192, Selected: 1

	fid	swap3236_soilunit	swap3236_soiluse	swap3236_inlet_daily	swap3236_gwd_daily	swap3236_meteo_daily
1	1	40710	0	1	1	125
2	2	40710	0	1	2	125
3	3	40710	1	1	1	125
4	4	40710	1	1	2	125
5	5	40710	2	1	1	125
6	6	40710	2	1	2	125
7	7	40710	9	1	1	125
8	8	40710	9	1	2	125
9	9	40710	12	1	1	125
10	10	40710	12	1	2	125
11	11	40710	15	1	1	125
12	12	40710	15	1	2	125
13	13	40710	224	1	1	125
14	14	40710	224	1	2	125
15	15	40710	311	1	1	125
16	16	40710	311	1	2	125
17	17	40910	0	1	1	125
18	18	40910	0	1	2	125
19	19	40910	1	1	1	125
20	20	40910	1	1	2	125
21	21	40910	2	1	1	125
22	22	40910	2	1	2	125
23	23	40910	9	1	1	125
24	24	40910	9	1	2	125

Show All Features

Figure 35. An example comb_key table; it stores the Cartesian product (Pp) of all the unique gis_cod values represented in the input grid maps evaluated for the agricultural area of a simulation domain (San Giorgio di Lomellina; gis_cod_domain = 11).

The evaluation of the spatial relationship between all the *gis_cod* represented in the input grid maps is performed by spatially overlaying all the different input grid maps. In fact, each potential simulation unit is a tuple of *gis_cod* values drawn from all input grid maps (e.g., A = 41010, B = 12, C = 1, D = 2, E = 125). To evaluate their spatial relationship, the framework locates the cells in each map where these codes occur at the same geographic position; cells are then overlaid to form a composite cell representation of the intersection. This overlay verifies the unit's spatial existence in the domain and serves as the basis for subsequent analysis. Due to the nature of the process, the actual simulation units map generally contain less simulation units than the potential one, because it is not always possible to perform a spatial intersection of all the input grid maps for a given set of *gis_cod* values.

Therefore, an actual simulation unit consists not just of a set of *gis_cod* values, but also of a unique geometry that locates it within the agricultural area of the simulation domain. During this process, the selected cells are transformed into polygons and, together with the attributes of the potential simulation unit, are concatenated to create a single actual simulation units map (*comb_key_eff_table*, Figure 36). With a defined geometry, each actual simulation unit can be associated with an area (*comb_area*, m²) and acquire a unique id (*comb_index*).

Finally, when actual simulation units are defined, the framework links the actual simulation units map *gis_cod* values to their parameterization or associated time series contained inside the input tables.

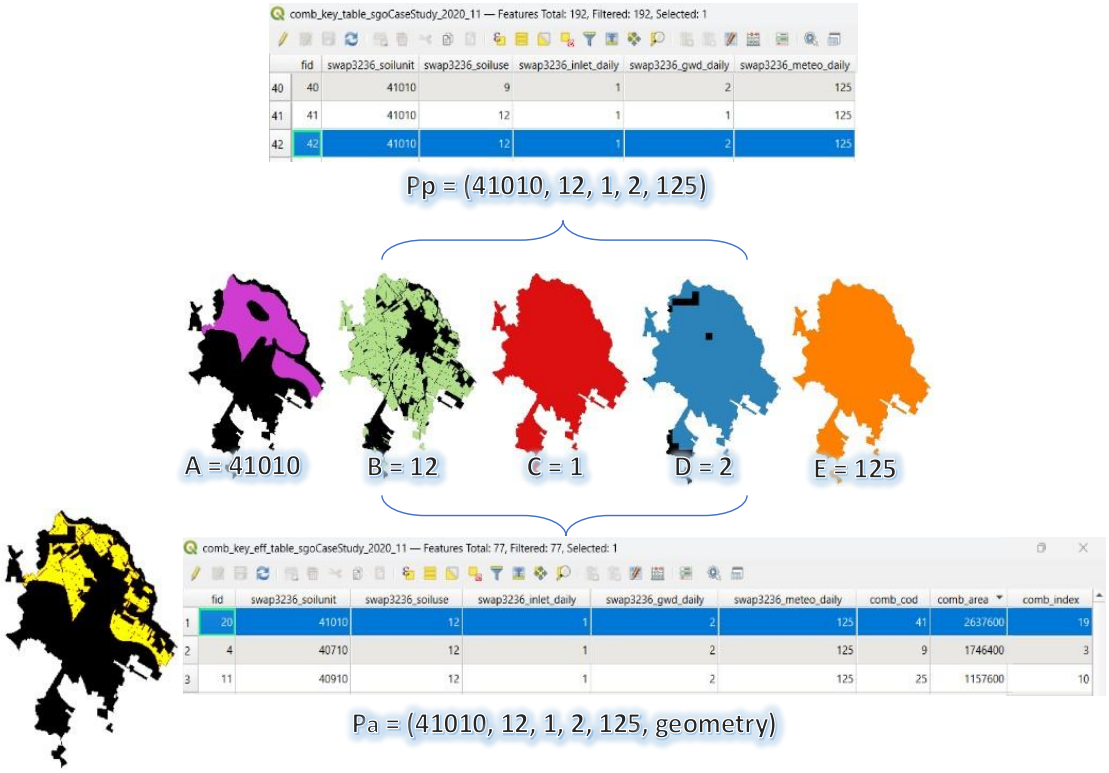

Figure 36. Above - An example of spatial overlay operation starting from the values stored by the framework in the comb_key table and all the input grid maps; Below - An example comb_key_eff table; it stores al the actual simulation units constructed by the framework to describe the agricultural area of a simulation domain (San Giorgio di Lomellina; gis_cod_domain = 11).

3.3.3.3 Agro-Hydrological Simulations for the Agricultural Area

SWAP uses the well-known Richards' equation (Richards, 1931) to simulate soil water one-dimensional vertical flow in unsaturated-saturated soil conditions. By applying specific boundary conditions at the top (i.e. atmosphere and crop constraints) and at the bottom (i.e. transient unsaturated-saturated soil interface conditions) of the SWAP simulation domain (from above the vegetation canopy to the interface between unsaturated soil and the phreatic groundwater table), the model numerically solves, in space and time, the Richards' equation for given relationships between θ, h, and K (i.e. the retention function - θ(h) and the hydraulic conductivity function - K(θ)). Parameters involved in the numerical solution of Richards' equation are those listed in Figure 37 (file .swp). No preferential flow due to macropores and no reduction to soil water flow due to frost are currently considered in the framework (file .swp).

To initiate the soil water balance resolution, SWAP requires the definition of an initial pressure head for each node in the computational mesh created for the simulated soil profile. SWAP offers different initial soil moisture conditions (Figure 38, file .swp). Out of these, the framework currently allows only the use of the second option (SWINCO = 2). Therefore, the framework overwrites the string *XXXX* with the groundwater depth value reported by the user for the first simulation day of the year.

Before conducting the core agro-hydrological simulations, the framework translates the saved parameters or time series into the required SWAP model simulation input files. These files include the main SWAP input file (.swp), the CROPFIL (.crp), the IRGFIL (.irg), the BBCFIL (.bbc), and the METFIL (.0YY). The model executable (swap.exe) is then copied inside its respective core model simulation folder and the agro-hydrological simulations are performed.

The framework is designed to run SWAP in a single folder, writing input and reading output files in the same directory. The Section Environment in the main SWAP input file (.swp) is formatted as in Figure 39. The basic simulation period of the framework is annual (Figure 39, file .swp). The framework replaces the string *XXXX* in TSTART and TEND definition with the actual value of the simulation year. Output dates of the model are meant to be daily, with NPRINTDAY and PERIOD set to 1 (Figure 40, file .swp). Output files configuration is provided in Figure 40 (file .swp). The only outputs that the framework expects to evaluate at the end of the model simulations are the soil profile output file - .vap, the crop growth output file - .crp and the incremental water balance output file - .inc; all these are named result (OUTFIL). In its current configuration, the framework does not simulate lateral drainage (SWDRA = 0, file .swp), solute transport (SWSOLU = 0, file .swp) and heat flow within the soil (SWHEA = 0, file .swp).

```
*******************************************************************************
* Part 11 Numerical solution of Richards' equation

  DTMIN         = 1.0d-6     ! Minimum timestep, [1.d-7..0.01 d, R]
  DTMAX         = 0.2        ! Maximum timestep, [ 0.01..0.5 d, R]
  GWLCONV       = 100.0      ! Maximum dif. groundwater level between iterations, [1.d-5..1000 cm, R]
  CritDevh1Cp   = 1.0d-2     ! Maximum relative difference in pressure heads per compartment, [1.0d-10..0.1 -, R]
  CritDevh2Cp   = 1.0d-1     ! Maximum difference in pressure heads per compartment, [1.0d-10..1.0 cm, R]
  CritDevPondDt = 1.0d-4     ! Maximum water balance error of ponding layer, [1.0d-6..0.1 cm, R]
  MaxIt         = 30         ! Maximum number of iteration cycles, [5..100 -, I]
  MaxBackTr     = 3          ! Maximum number of back track cycles within an iteration cycle, [1..10 -,I]

* Switch for mean of hydraulic conductivity, [1..4 -, I]:
* 1 = unweighted  arithmic mean; 2 = weighted  arithmic mean
* 3 = unweighted geometric mean; 4 = weighted geometric mean
  SWkmean = 1

* Switch for explicit/implicit solution Richards equation with hydraulic conductivity, [1..2 -, I]:
  SWkImpl = 0   ! 0 = explicit solution
                ! 1 = implicit solution
*******************************************************************************
```

Figure 37. SWAP main input file (.swp); SOIL WATER SECTION: Part 11 - Numerical solution of Richards' equation.

```
*******************************************************************************************
* Part 1: Initial soil moisture condition

 SWINCO = 2 ! Switch, type of initial soil moisture condition:
            ! 1 = pressure head as function of depth is input
            ! 2 = pressure head of each compartment is in hydrostatic equilibrium
            !     with initial groundwater level
            ! 3 = read final pressure heads from output of previous Swap simulation

* If SWINCO = 1, specify (maximum MACP):
* ZI = soil depth, [-10000..0 cm, R]
* H  = initial soil water pressure head, [-1.d10..1.d4 cm, R]

      ZI          H
    -0.5      -93.0
  -195.0      120.0
* End of table

* If SWINCO = 2, specify:
  GWLI    = XXXX  ! Initial groundwater level, [-10000..100 cm, R]

* If SWINCO = 3, specify:
  INIFIL = 'result.end'   ! name of final with extension .END [a200]
*******************************************************************************************
```

Figure 38. SWAP main input file (.swp); SOIL WATER SECTION: Part 1 - Initial soil moisture condition.

```
*******************************************************************************************
* Part 1: Environment

  PROJECT    = 'main'          ! Project description, [A80]
  PATHWORK   = '.\'            ! Path to work folder, [A80]
  PATHATM    = '.\'            ! Path to folder with weather files, [A80]
  PATHCROP   = '.\'            ! Path to folder with crop files, [A80]
  PATHDRAIN  = '.\'            ! Path to folder with drainage files, [A80]
  SWSCRE     = 0               ! Switch, display progression of simulation run:
                               !   SWSCRE = 0:  no display to screen
                               !   SWSCRE = 1:  display water balance to screen
                               !   SWSCRE = 2:  display daynumber to screen
  SWERROR    = 0               ! Switch for printing errors to screen [Y=1, N=0]
*******************************************************************************************
*******************************************************************************************
* Part 2: Simulation period
*
  TSTART  = 01-jan-XXXX ! Start date of simulation run, give day-month-year, [dd-mmm-yyyy]
  TEND    = 31-dec-XXXX ! End   date of simulation run, give day-month-year, [dd-mmm-yyyy]
*******************************************************************************************
```

Figure 39. SWAP main input file (.swp); GENERAL SECTION: Part 1 - Environment, Part 2 - Simulation period.

```
*******************************************************************************************
* Part 3: Output dates

* Number of output times during a day
  NPRINTDAY = 1        ! Number of output times during a day, [1..1000, I]

* If NPRINTDAY = 1, specify dates for output of state variables and fluxes
  SWMONTH = 0          ! Switch, output each month, [Y=1, N=0]

* If SWMONTH = 0, choose output interval and/or specific dates
  PERIOD = 1           ! Fixed output interval, ignore = 0, [0..366, I]
  SWRES  = 0           ! Switch, reset output interval counter each year, [Y=1, N=0]
  SWODAT = 0           ! Switch, extra output dates are given in table, [Y=1, N=0]

* If SWODAT = 1, list specific dates [dd-mmm-yyyy], maximum MAOUT dates:
  OUTDATINT =
  31-Jan-1980
  31-Dec-1982
* End of table

* Output times for overall water and solute balances in *.BAL and *.BLC file
* Output can be provided at a fixed date in a year or at different dates:
  SWYRVAR = 0          ! SWYRVAR = 0: each year output of balances at the same date
                       ! SWYRVAR = 1: output of balances at different dates

* If SWYRVAR = 0 specify fixed date:
  DATEFIX = 31 12      ! Specify day and month for output of yearly balances, [dd mm]

* If SWYRVAR = 1 specify all output dates [dd-mmm-yyyy], maximum MAOUT dates:
  OUTDAT =
  31-dec-1981
  31-dec-1982
* End of table
*******************************************************************************************
*******************************************************************************
* Part 4: Output files

* General information
  OUTFIL   = 'result' ! Generic file name of output files, [A16]
  SWHEADER = 0        ! Print header at the start of each balance period, [Y=1, N=0]

* Optional files
  SWVAP  = 1        ! Switch, output profiles of moisture, solute and temperature, [Y=1, N=0]
  SWBLC  = 0        ! Switch, output file with detailed yearly water balance, [Y=1, N=0]
  SWATE  = 0        ! Switch, output file with soil temperature profiles, [Y=1, N=0]
  SWBMA  = 0        ! Switch, output file with water fluxes, only for macropore flow, [Y=1, N=0]
  SWDRF  = 0        ! Switch, output of drainage fluxes, only for extended drainage, [Y=1, N=0]
  SWSWB  = 0        ! Switch, output surface water reservoir, only for extended drainage, [Y=1, N=0]

* Output for water quality models (PEARL, ANIMO) or other specific use (SWAFO to DZNEW)

* Optional output files
  SWAFO  = 0        ! Switch, output file with formatted hydrological data
                    ! SWAFO = 0: no output
                    ! SWAFO = 1: output to a file named *.AFO
                    ! SWAFO = 2: output to a file named *.BFO

  SWAUN  = 0        ! Switch, output file with unformatted hydrological data
                    ! SWAUN = 0: no output
                    ! SWAUN = 1: output to a file named *.AUN
                    ! SWAUN = 2: output to a file named *.BUN

* Critical deviation of water balance; in case of larger deviation, an error file is created (*.DWB.CSV)
  CRITDEVMASBAL = 0.00001  ! Critical Deviation in water balance during PERIOD [0.0..1.0 cm, R]

* If SWAFO = 1 or 2, or SWAUN = 1 or 2: fine vertical discretization can be lumped
  SWDISCRVERT = 0   ! SWDISCRVERT = 0: no conversion
                    ! SWDISCRVERT = 1: convert vertical discretization,

* If SWDISCRVERT = 1 then specify:
  NUMNODNEW = 6     ! New number of nodes [1..macp, I, -]
* List thickness of each compartment, total thickness should correspond to Soil Water Section, part 4
  DZNEW     = 10.0 10.0 10.0 20.0 30.0 50.0 ! thickness of compartments [1.0d-6...5.0d2, cm, R]
*******************************************************************************
```

Figure 40. SWAP main input file (.swp); GENERAL SECTION: Part 3 - Output dates, Part 4 - Output files.

3.3.4 Channel Network Model

3.3.4.1 Channel Network Description (Input Maps and Tables)

The framework needs two elements to describe the channel network: I) a linear channel network map (Figure 41), showing what the user defines as the main channel network geometries, and II) a list of *gis_cod_soiluse* identifying soil uses, marking uses/areas within the provided soil use map where it is reasonable to find smaller channels that feed from the main network and serve agricultural areas. These smaller channels, forming the diffuse channel network map, are generally difficult to map and their geometries are derived from actual simulation units map. Moreover, the framework derives the groundwater depth series for the channel network model from the agricultural area description, using monthly area-weighted averages (see Section Groundwater Depth Areas Map and Time Series).

In addition to geometries, linear channel network map attributes contain (Figure 42), for each channel trait: I) the *type* attribute, and II) the simulation domain attribute. The *type* attribute is an input to define a weight, one for each month of the simulation year, then used by the framework to spatialize the channel network balance (see Section 3.3.4.3), while the simulation domain attribute is a column, named with the value of a simulation domain id (*gis_cod_domain*), that define if a specific channel trait should be considered (IN) or not (OUT) for a specific simulation domain. This attribute allows the user to define a single linear channel network map, within the same simulation database, that is valid for multiple simulation domains. In the same way as maps relating to the agricultural area, the linear geometries of the channel network can also be provided to the framework with a greater extension of the chosen simulation domain. Once cropped using the simulation domain geometry, each trait of the linear channel network map acquires a reference length (*comb_ length*, m) a unique id (*comb_index*).

Moreover, the framework asks whether the simulation should use historical gross irrigation discharge data, which are typically measured or externally estimated, or must run as a scenario in a context where monthly discharge data is unavailable. In a historical simulation, the framework retrieves the monthly input discharge for the model from the channel network table (*simple_channel_model_monthly*, Figure 43), which is stored in the simulation database. In a scenario simulation, instead, the monthly input discharge for the model is matched with the aggregated monthly net irrigation coming from the agricultural area. Historical and scenario simulations differ in how the balance terms of the channel network are calculated. In the first case, the objective is to estimate the channel net discharge (i.e. irrigation water availability for the agricultural area), while in the second case the objective is to reconstruct the channel gross discharge (i.e. irrigation water entering the simulation domain). The channel network table attributes are: I) IRDATE, representing the month, II) DISCHARGE_IN, that is the monthly discharge value in m^3/s, and III) *gis_cod_domain*, reporting the value of the simulation domain id to which the data belongs (*gis_cod_domain*).

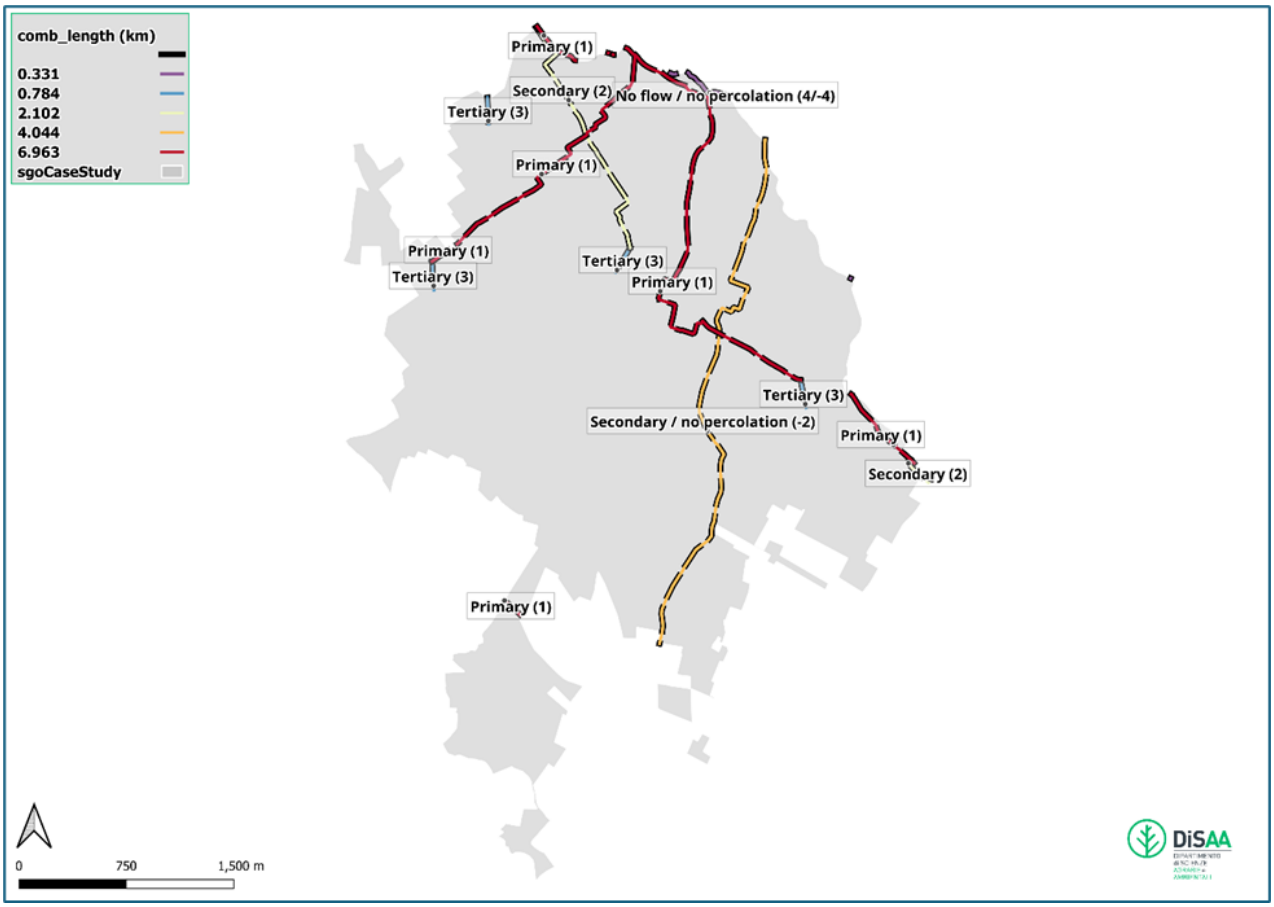

Figure 41. Example of a linear channel network map showing traits (geometries) of the main channel network within a simulation domain (San Giorgio di Lomellina; gis_cod_domain = 11).

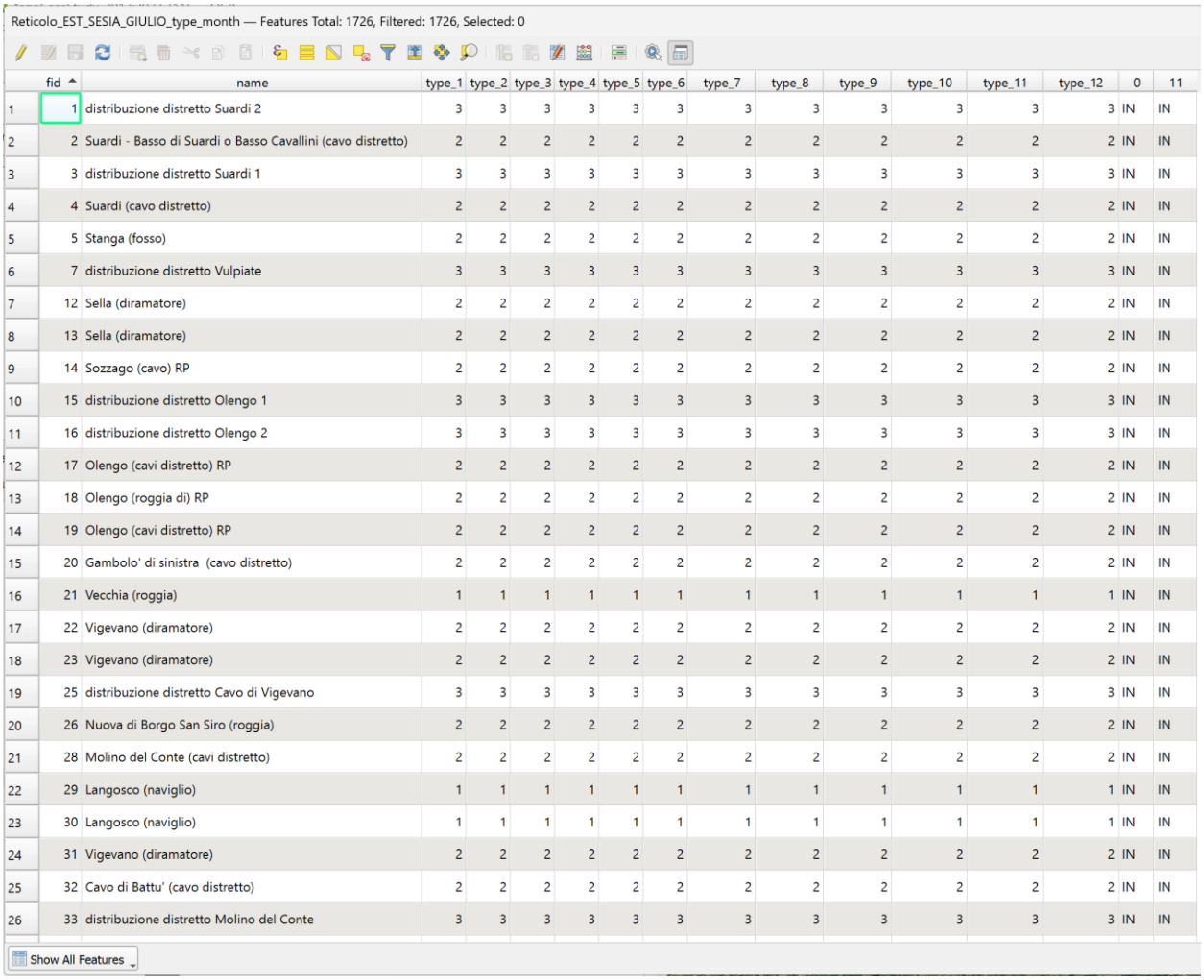
Reticolo_EST_SESIA_GIULIO_type_month — Features Total: 1726, Filtered: 1726, Selected: 0

	fid	name	type_1	type_2	type_3	type_4	type_5	type_6	type_7	type_8	type_9	type_10	type_11	type_12	0	11
1	1	distribuzione distretto Suardi 2	3	3	3	3	3	3	3	3	3	3	3	3	IN	IN
2	2	Suardi - Basso di Suardi o Basso Cavallini (cavo distretto)	2	2	2	2	2	2	2	2	2	2	2	2	IN	IN
3	3	distribuzione distretto Suardi 1	3	3	3	3	3	3	3	3	3	3	3	3	IN	IN
4	4	Suardi (cavo distretto)	2	2	2	2	2	2	2	2	2	2	2	2	IN	IN
5	5	Stanga (fosso)	2	2	2	2	2	2	2	2	2	2	2	2	IN	IN
6	7	distribuzione distretto Vulpiate	3	3	3	3	3	3	3	3	3	3	3	3	IN	IN
7	12	Sella (diramatore)	2	2	2	2	2	2	2	2	2	2	2	2	IN	IN
8	13	Sella (diramatore)	2	2	2	2	2	2	2	2	2	2	2	2	IN	IN
9	14	Sozzago (cavo) RP	2	2	2	2	2	2	2	2	2	2	2	2	IN	IN
10	15	distribuzione distretto Olengo 1	3	3	3	3	3	3	3	3	3	3	3	3	IN	IN
11	16	distribuzione distretto Olengo 2	3	3	3	3	3	3	3	3	3	3	3	3	IN	IN
12	17	Olengo (cavi distretto) RP	2	2	2	2	2	2	2	2	2	2	2	2	IN	IN
13	18	Olengo (roggia di) RP	2	2	2	2	2	2	2	2	2	2	2	2	IN	IN
14	19	Olengo (cavi distretto) RP	2	2	2	2	2	2	2	2	2	2	2	2	IN	IN
15	20	Gambolo' di sinistra (cavo distretto)	2	2	2	2	2	2	2	2	2	2	2	2	IN	IN
16	21	Vecchia (roggia)	1	1	1	1	1	1	1	1	1	1	1	1	IN	IN
17	22	Vigevano (diramatore)	2	2	2	2	2	2	2	2	2	2	2	2	IN	IN
18	23	Vigevano (diramatore)	2	2	2	2	2	2	2	2	2	2	2	2	IN	IN
19	25	distribuzione distretto Cavo di Vigevano	3	3	3	3	3	3	3	3	3	3	3	3	IN	IN
20	26	Nuova di Borgo San Siro (roggia)	2	2	2	2	2	2	2	2	2	2	2	2	IN	IN
21	28	Molino del Conte (cavi distretto)	2	2	2	2	2	2	2	2	2	2	2	2	IN	IN
22	29	Langosco (naviglio)	1	1	1	1	1	1	1	1	1	1	1	1	IN	IN
23	30	Langosco (naviglio)	1	1	1	1	1	1	1	1	1	1	1	1	IN	IN
24	31	Vigevano (diramatore)	2	2	2	2	2	2	2	2	2	2	2	2	IN	IN
25	32	Cavo di Battu' (cavo distretto)	2	2	2	2	2	2	2	2	2	2	2	2	IN	IN
26	33	distribuzione distretto Molino del Conte	3	3	3	3	3	3	3	3	3	3	3	3	IN	IN

Show All Features

Figure 42. Example of linear channel network table showing traits (attributes) of the main channel network within a simulation domain (San Giorgio di Lomellina; gis_cod_domain = 11).

simple_channel_model_monthly — Features Total: 264, Filtered: 264, Selected: 0

	fid	IRDATE	DISCHARGE_IN	gis_cod_domain
1	1	15-Jan-2013	65.92897757	0
2	2	15-Feb-2013	66.90188547	0
3	3	15-Mar-2013	60.92389155	0
4	4	15-Apr-2013	83.48905807	0
5	5	15-May-2013	127.0848117	0
6	6	15-Jun-2013	186.4228001	0
7	7	15-Jul-2013	192.708051	0
8	8	15-Aug-2013	173.9770133	0
9	9	15-Sep-2013	74.23849994	0
10	10	15-Oct-2013	56.59709451	0
11	11	15-Nov-2013	53.10123456	0
12	12	15-Dec-2013	61.89190231	0
13	13	15-Jan-2014	65.92897757	0
14	14	15-Feb-2014	66.90188547	0
15	15	15-Mar-2014	60.92389155	0
16	16	15-Apr-2014	83.48905807	0
17	17	15-May-2014	127.0848117	0
18	18	15-Jun-2014	186.4228001	0
19	19	15-Jul-2014	192.708051	0
20	20	15-Aug-2014	173.9770133	0
21	21	15-Sep-2014	74.23849994	0
22	22	15-Oct-2014	56.59709451	0
23	23	15-Nov-2014	53.10123456	0
24	24	15-Dec-2014	61.89190231	0
25	25	15-Jan-2015	65.92897757	0
26	26	15-Feb-2015	66.90188547	0

Show All Features

Figure 43. Example simple_channel_model_monthly input table showing monthly gross discharges (m^3/s) entering the main channel network within a simulation domain (San Giorgio di Lomellina; gis_cod_domain = 11).

3.3.4.2 Concentrated Model Calculations

The framework directly deals with two components: a linear discharge, circulating within the main channel network geometries, and a diffuse discharge, serving the minor channel network that develop within the agricultural area. However, in this step, the two discharges are non-spatialized along the primary channel network or over the agricultural area territory. The equations involved in the estimation are reported below:

$$\begin{cases} historical, & \begin{cases} \boldsymbol{C_{network}\ gross\ discharge_t} = C_{lin}\ discharge_t = channel\ network\ table_t \\ C_{diff}\ discharge_t = C_{lin}\ bal\ discharge_t \end{cases} \\ scenario, & \begin{cases} C_{lin}\ discharge_t = C_{diff}\ bal\ discharge_t \\ \boldsymbol{C_{network}\ net\ discharge_t} = C_{diff}\ discharge_t = \boldsymbol{A_{area}\ net\ irrigation_t} \end{cases} \end{cases} \quad \text{(Eq. 12)}$$

$$C_{lin}\ bal\ discharge_t = \begin{cases} C_{lin}\ discharge_t + C_{lin}\ percolation_t, & historical \\ \boldsymbol{C_{network}\ gross\ discharge_t} = C_{lin}\ discharge_t - C_{lin}\ percolation_t, & scenario \end{cases} \quad \text{(Eq. 13)}$$

$$C_{diff}\ bal\ discharge_t = \begin{cases} \boldsymbol{C_{network}\ net\ discharge_t} = C_{diff}\ discharge_t + C_{diff}\ percolation_t, & historical \\ C_{diff}\ discharge_t - C_{diff}\ percolation_t, & scenario \end{cases} \quad \text{(Eq. 14)}$$

$$\boldsymbol{C_{network}\ percolation_t} = C_{lin}\ percolation_t + C_{diff}\ percolation_t \quad \text{(Eq. 15)}$$

where

- $C_{lin|diff}\ discharge$ (m^3/s) is the input discharge for the channel model for each, linear or diffuse, component of the channel network,
- $channel\ network\ table$ (m^3/s) equals the monthly discharge retrieved by the framework for a specific simulation domain starting from the simulation database (historical),
- $A_{area}\ net\ irrigation$ (m^3/s) equals the aggregated monthly net irrigation coming from the agricultural area of the simulation domain,

- $C_{lin|diff}\ bal\ discharge$ (m^3/s) equals the estimated net discharge (historical) or gross discharge (scenario) for each, linear or diffuse, component of the channel network,
- $C_{lin|diff}\ percolation$ (m^3/s, negative) equals the estimated percolation for each, linear or diffuse, component of the channel network (Eq. 16),

- $C_{network}\ gross\ discharge$ (m^3/s) equals the irrigation water entering at the inlet of a simulation domain before channel network percolation losses,

- $C_{network}\ net\ discharge$ (m^3/s) equals the irrigation water availability for the agricutural area net of channel network percolation losses,
- $C_{network}\ percolation$ (m^3/s) equals the total percolation coming from the whole channel network,

- t (-) is the month of the simulation year.

In flat agricultural areas with unlined channels, it is reasonable to assume that the diffuse minor channel network is located downstream of the linear component, receiving water from the main channel network and transferring irrigation water to each field within the agricultural area. Ideally, during an historical simulation, the monthly discharge available at the inlet of a simulation domain ($C_{network}\ gross\ discharge/channel\ network\ table$) enters the linear channel network ($C_{lin}\ discharge$) and only reaches the diffuse component after losing a fraction of the water due to percolation ($C_{lin}\ bal\ discharge$). From there ($C_{diff}\ discharge$), in the route of connecting the diffuse component to the agricultural area's fields (satisfy $A_{area}\ net\ irrigation$), further water is lost through percolation ($C_{diff}\ bal\ discharge/C_{network}\ net\ discharge$). The same path, in case of a scenario simulation, is reconstructed backwards ($C_{lin|diff}\ bal\ discharge \geq C_{lin|diff}\ discharge$). Basically, in the first case, the model estimates the channel network net discharge ($C_{network}\ net\ discharge$, i.e. irrigation water availability for the agricultural area), while in the second case, the model reconstructs the channel network gross discharge ($C_{network}\ gross\ discharge$, i.e. irrigation water entering at the inlet of simulation domain).

The two components of the network (linear and diffuse) can be parameterized differently, enabling users to work on the efficiency of these two systems separately within the same simulation domain. For the two components, the percolation term is calculated as:

$$C_{lin|diff}\ percolation_t = -\begin{cases} C_{lin|diff}\ discharge_t * \alpha_{lin|diff_t}, & historical \\ \dfrac{\left(\alpha_{lin|diff_t} * C_{lin|diff}\ discharge_t\right)}{\left(1 - \alpha_{lin|diff_t}\right)}, & scenario \end{cases} \quad \text{(Eq. 16)}$$

$$\alpha_{lin|diff_t} = \begin{cases} \alpha min_{lin|diff_t}, & mod_1 \\ min\left(\alpha max_{lin|diff_t}, \quad max\left(0, \quad GWDc_{lin|diff_t} - GWD_t\right)\right), & mod_2 \\ mod_1, \quad \boldsymbol{A_{area}\ net\ irrigation_t} \leq 0 & \\ mod_2, \quad \boldsymbol{A_{area}\ net\ irrigation_t} > 0, & mod_3 \end{cases} \quad \text{(Eq. 17)}$$

where

- $\alpha_{lin|diff}$ (-, between 0 and 1) equals the estimated loss factor for each, linear or diffuse, component of the channel network,
- $\alpha max_{lin|diff}$ (-, between 0 and 1) equals the maximum value of $\alpha_{lin|diff}$ for each, linear or diffuse, component of the channel network,

- $\alpha min_{lin|diff}$ (-, between 0 and 1) equals the minimum value of $\alpha_{lin|diff}$ for each, linear or diffuse, component of the channel network,

- GWD (m, negative) equals the aggregated monthly average groundwater depth within the agricultural area,
- $GWDc_{lin|diff}$ (m, negative) equals the critical groundwater depth above which losses from each, linear or diffuse, component of the channel network should be equal to zero.

An explanation of the steps followed to derive the equation developed for calculating $C_{lin|diff}\ percolation$ (Eq. 16) in case of a scenario simulation is given in Mayer et al. (2019). To calculate the loss factor $\alpha_{lin|diff}$, the user can select one of three modes for each month within the same simulation year. In the first two, the user can specify: mod1) where $\alpha_{lin|diff}$ is equal to the fixed value $\alpha min_{lin|diff}$ (e.g., 0.2), or mod2) where $\alpha_{lin|diff}$ varies from a minimum value of zero ($GWD \geq GWDc_{lin|diff}$) to a maximum value $\alpha max_{lin|diff}$ (e.g., 0.4, $GWD < GWDc_{lin|diff}$). The former is useful for imposing fixed loss rates, which could be preferable in months outside the irrigation season, while the latter is useful in months when the depth of the groundwater table reduces percolation from the channel network, as is often the case during the irrigation season. The third mode is a combination of the previous two and is designed for scenario simulations where it is not possible to determine in advance whether a given month will fall within or outside the irrigation season. When $A_{area}\ net\ irrigation \leq 0$, the framework uses mod1 calculation, when $A_{area}\ net\ irrigation > 0$ the framework uses mod2 calculation.

3.3.4.3 Spatialized Model Calculations

The framework distributes the concentrated monthly balance outputs of the channel network model ($C_{lin|diff}\ discharge$ and $C_{lin|diff}\ percolation$) over the geometries ($geom$) contained inside the input maps of the channel network description (the linear channel network map and the diffuse channel network map). This is performed using a system of weights which varies depending on the channel network component (linear or diffuse). This is achieved by implementing the equations shown below:

$$C_{lin|diff}\ conc_t[geom_i] = C_{lin|diff}\ conc_t * \left(\frac{w_{lin|diff_t}[geom_i]}{\sum_{i=1}^{n} w_{lin|diff_t}[geom_i]}\right), with\ i = comb\_index \quad \text{(Eq. 18)}$$

$$w_{lin|diff_t}[geom_i] = \begin{cases} linear, & length[geom_i] * order_t[geom_i] \\ diffuse, & \begin{cases} area[geom_i], & \sum A_{area}\ \boldsymbol{net\ irrigation_t}[geom_i] \leq 0 \\ area[geom_i] * \boldsymbol{A_{area}\ net\ irrigation_t}[geom_i], & \sum A_{area}\ \boldsymbol{net\ irrigation_t}[geom_i] > 0 \end{cases} \end{cases} \quad \text{(Eq. 19)}$$

$$C_{lin|diff}\ bal\ discharge_t[geom_i] = \begin{cases} C_{lin|diff}\ discharge_t[geom_i] + C_{lin|diff}\ percolation_t[geom_i], & historical \\ C_{lin|diff}\ discharge_t[geom_i] - C_{lin|diff}\ percolation_t[geom_i], & scenario \end{cases} \quad \text{(Eq. 20)}$$

where

- $C_{lin|diff}\ conc$ is an alias for $C_{lin|diff}\ discharge$ and $C_{lin|diff}\ percolation$,

- $w_{lin|diff}[geom_i]$ (-) equals the estimated weight for each trait of the linear channel network map or for each actual simulation unit polygon in the diffuse channel network map,
- $length[geom_i]$ (m) equals the length of each trait of the linear channel network,
- $order[geom_i]$ (-, between 0 and 3) equals an arbitrary flow/percolation rate exaggeration factor that aims to return a hierarchical order, if present, or a condition of no water flow/no percolation for each trait of the linear channel network map. Currently, $order$ values are calculated as depicted in Table 2. In the future, these could be values established by the user based on empirical evidence collected for the case study area,
- $area[geom_i]$ (m^2) equals the area of each actual simulation unit.

Table 2. Method of assigning a flow/percolation rate exaggeration factor (order) starting from the linear channel network map type monthly attribute (user defined - linear channel network table).

Value (discharge)	**Descr.** (discharge)	**Value** (percolation)	**Descr.** (percolation)	***type*** (linear channel network map)
3	primary	3	primary	1
2	secondary	2	secondary	2
1	tertiary	1	tertiary	3
0	no flow	0	no percolation	4
3	primary	0	no percolation	-1
2	secondary	0	no percolation	-2
1	tertiary	0	no percolation	-3
0	no flow	0	no percolation	-4

The proposed algorithm for the channel linear system tries to model extensive channel networks, such as those found in large, lowland agricultural areas with highly intricate layouts, where direct measurement of local efficiency and channel network flow dynamics is generally impractical. Discharges and percolation ($C_{lin|diff}\ conc[geom_i]$) are assumed to be proportional to the length ($length[geom_i]$) and the hierarchical order ($order[geom_i]$) of each channel trait ($geom_i$). Moreover, the algorithm identifies segments exhibiting discharges without percolation (where *type* is negative and order value is 0), as in non-buried channels or in cases of negligible losses (also in case of clogging). By linearizing discharges and percolation values across the entire simulation domain, the method allows the network's overall efficiency, constant at the simulation domain scale ($\alpha_{lin|diff}$ loss factor remains the same), to be allocated heterogeneously to individual channel network trait, thus without altering the aggregate system balance ($C_{network}\ gross\ discharge$, $C_{network}\ net\ discharge$, and $C_{network}\ percolation$). Moreover,

the capacity to adjust the hierarchical order (or channel *type*) on a monthly timescale provides a mechanism to incorporate temporal variability in channel behavior.

In the diffuse channel system, positioned downstream of the principal linear network and serving as the link to irrigated fields, discharges and percolation ($C_{lin|diff}\ conc[geom_i]$) are assumed to vary in proportion to the simulated irrigation applications for a given diffuse channel polygon from the diffuse channel network map ($area[geom_i] * A_{area}\ net\ irrigation[geom_i]$, m^3) whenever these are greater than zero (irrigation season). Along this downstream route, water losses occur, and it is reasonable to expect that greater irrigation demand across the served area will result in correspondingly higher flow rates. Outside the irrigation season, when no irrigation is applied, these values are instead proportional solely to the geometry area ($area[geom_i]$).

3.4 Results

The simulation years used for the modelling exercise regarding the San Giorgio di Lomellina irrigation district covers the period from 2018 to 2020. Input data and model parameters for the district are those obtained after the calibration of the framework for the entire Lomellina region (over 125,000 hectares, mostly cultivated with rice) illustrated in Chapter 5 of this manuscript.

Regarding the agricultural area, the input vector maps were the same throughout the whole simulation period, and a 20 m resolution was used to define the simulation units. Channel network discharge data for the whole Lomellina area are available from 2018 to 2020. Also in the San Giorgio irrigation district case study presented here, only measured discharges from the 2018 - 2020 period were taken into account.

The overall efficiency of the channel network (linear and diffuse) was set be around 60% during the irrigation season ($\alpha max_{lin|diff} = 0.225$, $GWDc_{lin|diff} = -1.6$) and 20% outside the irrigation season ($\alpha min_{lin|diff} = 0.125$). The simulation area contains 15 channel traits defining the primary irrigation network, or linear channel network, extending for a total length of around 14 km. The linear channel *types* remained unchanged throughout all months and simulation years. The diffuse channel network was configured to extend within the actual simulation units characterized by irrigated crops, which are: poplar (young), rice (wet seeding and continuous flooding - WFL), maize, and rice (dry seeding and intermittent flooding - FTI) soil uses.

3.4.1 Agro-Hydrological Simulations (Agricultural Area)

Alongside the incremental water balance output file (.inc), the framework combines the soil profile output file (.vap) and the crop growth output file (.crp) into a single daily core model outputs table (*comb_key_eff_attr_sim_table_inc*, Figure 44). In more detail, the framework uses the minimum and maximum VAP_node (see Section Soil Use Map, Crop Parameters and Irrigation Management) to filter data from the soil profile output file for each day of the simulation year. The average soil water content (cm^3/cm^3, wcontent), soil water potential (cm, phead), and soil water flux (cm/d, waterflux) are calculated between the provided VAP_nodes. From the crop growth output file, the framework retrieves the columns DVS (-), LAI (-), CrpFac (-), and Rootd (cm). Net irrigation (cm) is calculated as reported in Section Soil Use Map, Crop Parameters and Irrigation Management. In addition to the standard SWAP output files, the daily core model outputs table retains the actual simulation units agricultural area description (*gis_cod_domain*, *comb_index*, *swap3236_soilunit*, *swap3236_soiluse*, *swap3236_inlet_daily*,

swap3236_gwd_daily, *swap3236_meteo_daily*, *comb_area*) and use them as the basis for the subsequent processing of the results. The daily core model outputs table has a number of rows that correspond to the multiplication of the count of all the features contained in the actual simulation units map and the count of the days in the simulation year.

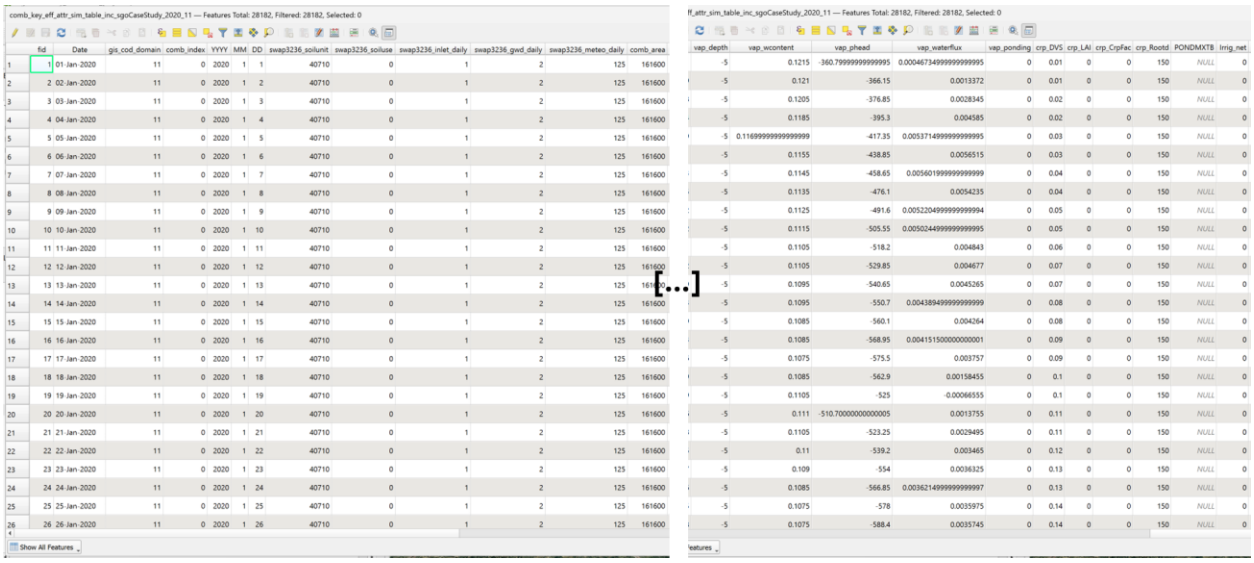

fid	Date	gis_cod_domain	comb_index	YYYY	MM	DD	swap3236_soilunit	swap3236_soiluse	swap3236_inlet_daily	swap3236_gwd_daily	swap3236_meteo_daily	comb_area
1	01-Jan-2020	11	0	2020	1	1	40710	0	1	2	125	161600
2	02-Jan-2020	11	0	2020	1	2	40710	0	1	2	125	161600
3	03-Jan-2020	11	0	2020	1	3	40710	0	1	2	125	161600
4	04-Jan-2020	11	0	2020	1	4	40710	0	1	2	125	161600
5	05-Jan-2020	11	0	2020	1	5	40710	0	1	2	125	161600
6	06-Jan-2020	11	0	2020	1	6	40710	0	1	2	125	161600
7	07-Jan-2020	11	0	2020	1	7	40710	0	1	2	125	161600
8	08-Jan-2020	11	0	2020	1	8	40710	0	1	2	125	161600
9	09-Jan-2020	11	0	2020	1	9	40710	0	1	2	125	161600
10	10-Jan-2020	11	0	2020	1	10	40710	0	1	2	125	161600
11	11-Jan-2020	11	0	2020	1	11	40710	0	1	2	125	161600
12	12-Jan-2020	11	0	2020	1	12	40710	0	1	2	125	161600
13	13-Jan-2020	11	0	2020	1	13	40710	0	1	2	125	161600
14	14-Jan-2020	11	0	2020	1	14	40710	0	1	2	125	161600
15	15-Jan-2020	11	0	2020	1	15	40710	0	1	2	125	161600
16	16-Jan-2020	11	0	2020	1	16	40710	0	1	2	125	161600
17	17-Jan-2020	11	0	2020	1	17	40710	0	1	2	125	161600
18	18-Jan-2020	11	0	2020	1	18	40710	0	1	2	125	161600
19	19-Jan-2020	11	0	2020	1	19	40710	0	1	2	125	161600
20	20-Jan-2020	11	0	2020	1	20	40710	0	1	2	125	161600
21	21-Jan-2020	11	0	2020	1	21	40710	0	1	2	125	161600
22	22-Jan-2020	11	0	2020	1	22	40710	0	1	2	125	161600
23	23-Jan-2020	11	0	2020	1	23	40710	0	1	2	125	161600
24	24-Jan-2020	11	0	2020	1	24	40710	0	1	2	125	161600
25	25-Jan-2020	11	0	2020	1	25	40710	0	1	2	125	161600
26	26-Jan-2020	11	0	2020	1	26	40710	0	1	2	125	161600

[...]

vap_depth	vap_wcontent	vap_phead	vap_waterflux	vap_ponding	crp_DVS	crp_LAI	crp_CrpFac	crp_Rootd	PONDMXTB	Irrig_net
-5	0.1215	-360.79999999999995	0.0004674999999999995	0	0.01	0	0	150	NULL	0
-5	0.121	-366.15	0.0013372	0	0.01	0	0	150	NULL	0
-5	0.1205	-376.85	0.0028345	0	0.02	0	0	150	NULL	0
-5	0.1185	-395.3	0.004585	0	0.02	0	0	150	NULL	0
-5	0.11699999999999999	-417.35	0.005371499999999995	0	0.03	0	0	150	NULL	0
-5	0.1155	-438.85	0.0056515	0	0.03	0	0	150	NULL	0
-5	0.1145	-458.65	0.005601999999999999	0	0.04	0	0	150	NULL	0
-5	0.1135	-476.1	0.0054235	0	0.04	0	0	150	NULL	0
-5	0.1125	-491.6	0.005220499999999994	0	0.05	0	0	150	NULL	0
-5	0.1115	-505.55	0.005024499999999995	0	0.05	0	0	150	NULL	0
-5	0.1105	-518.2	0.004843	0	0.06	0	0	150	NULL	0
-5	0.1105	-529.85	0.004677	0	0.07	0	0	150	NULL	0
-5	0.1095	-540.65	0.0045265	0	0.07	0	0	150	NULL	0
-5	0.1095	-550.7	0.004389499999999999	0	0.08	0	0	150	NULL	0
-5	0.1085	-560.1	0.004264	0	0.08	0	0	150	NULL	0
-5	0.1085	-568.95	0.004151500000000001	0	0.09	0	0	150	NULL	0
-5	0.1075	-575.5	0.003757	0	0.09	0	0	150	NULL	0
-5	0.1085	-562.9	0.00158455	0	0.1	0	0	150	NULL	0
-5	0.1105	-525	-0.00066555	0	0.1	0	0	150	NULL	0
-5	0.111	-510.70000000000005	0.0013755	0	0.11	0	0	150	NULL	0
-5	0.1105	-523.25	0.0029495	0	0.11	0	0	150	NULL	0
-5	0.11	-539.2	0.003465	0	0.12	0	0	150	NULL	0
-5	0.109	-554	0.0036325	0	0.13	0	0	150	NULL	0
-5	0.1085	-566.85	0.003621499999999997	0	0.13	0	0	150	NULL	0
-5	0.1075	-578	0.0035975	0	0.14	0	0	150	NULL	0
-5	0.1075	-588.4	0.0035745	0	0.14	0	0	150	NULL	0

Figure 44. Example of comb_key_eff_attr_sim_table_inc table showing daily core model outputs for the agricultural area of a simulation domain (San Giorgio di Lomellina; gis_cod_domain = 11).

Starting from the daily core model outputs table, field-level hydrological simulation results can be explored for specific simulation units (Figure 45), as depicted in Figure 46 and Figure 47. The following figures show four examples of rice simulation units characterized by two groundwater depth conditions (shallow and deep), one soil type (soil unit 41310, Table 3) and with two irrigation management (WFL and FTI) during the year 2020. For the period from April to October, each graph includes: SWAP input irrigation (Irrigation, cm), runoff (Runoff, cm), estimated net irrigation (Irrigation net, cm), target ponding water level (Pond target, cm), simulated ponding water on the field (Pond actual, cm), soil water potential at -5 cm (P. head, < 0, dm), crop development stage (DVS * 10, -), groundwater table depth (GWD, dm), and rainfall (Rain, cm).

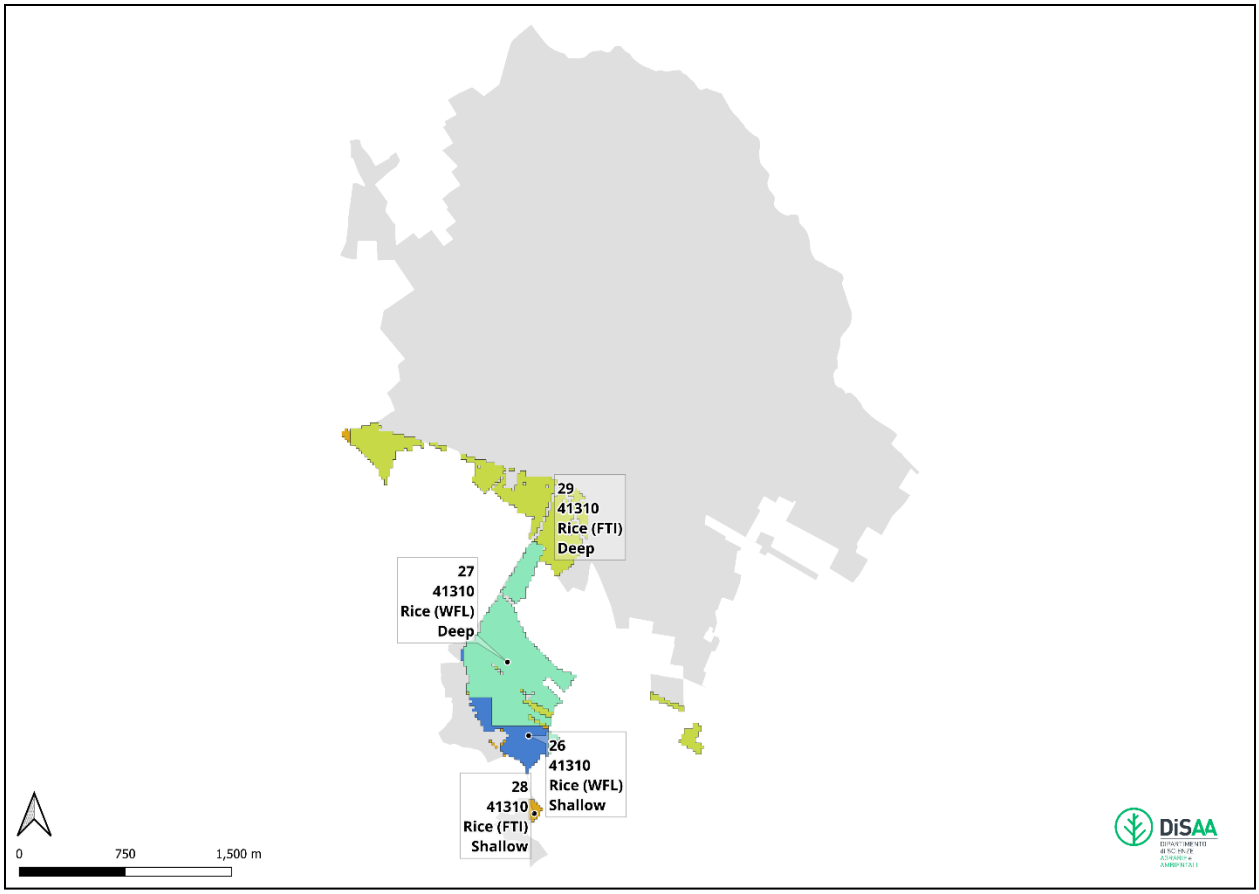

Figure 45. Four simulation units in the agricultural area of the San Giorgio rice district taken as examples (geometries come from the comb_key_eff_table, see Section Potential and Actual Simulation Units for the Agricultural Area).

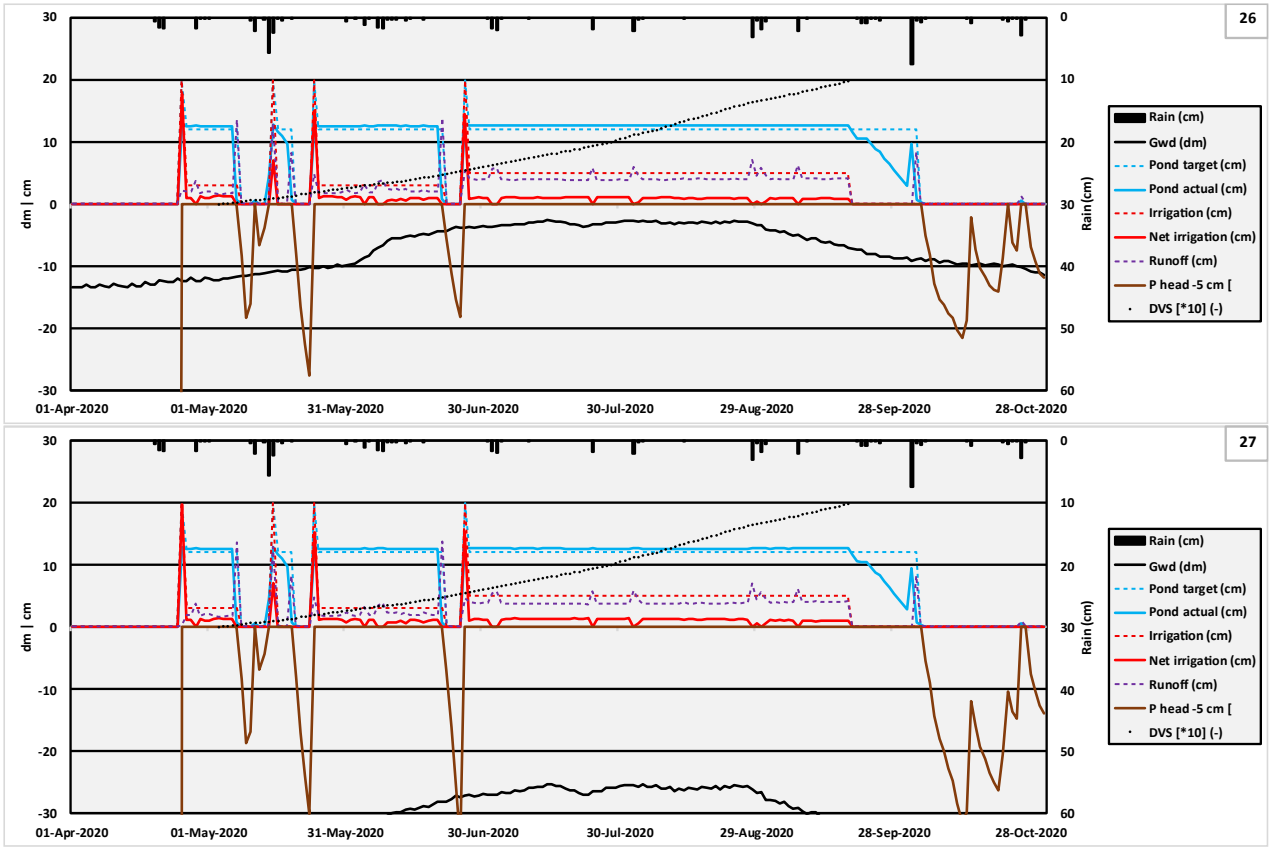

Figure 46. Daily agro-hydrological simulations outputs for two specific simulation units (26 - shallow groundwater depth, and 27 - deep groundwater depth) with WFL management and on soil unit 41310 (Table 3) during 2020.

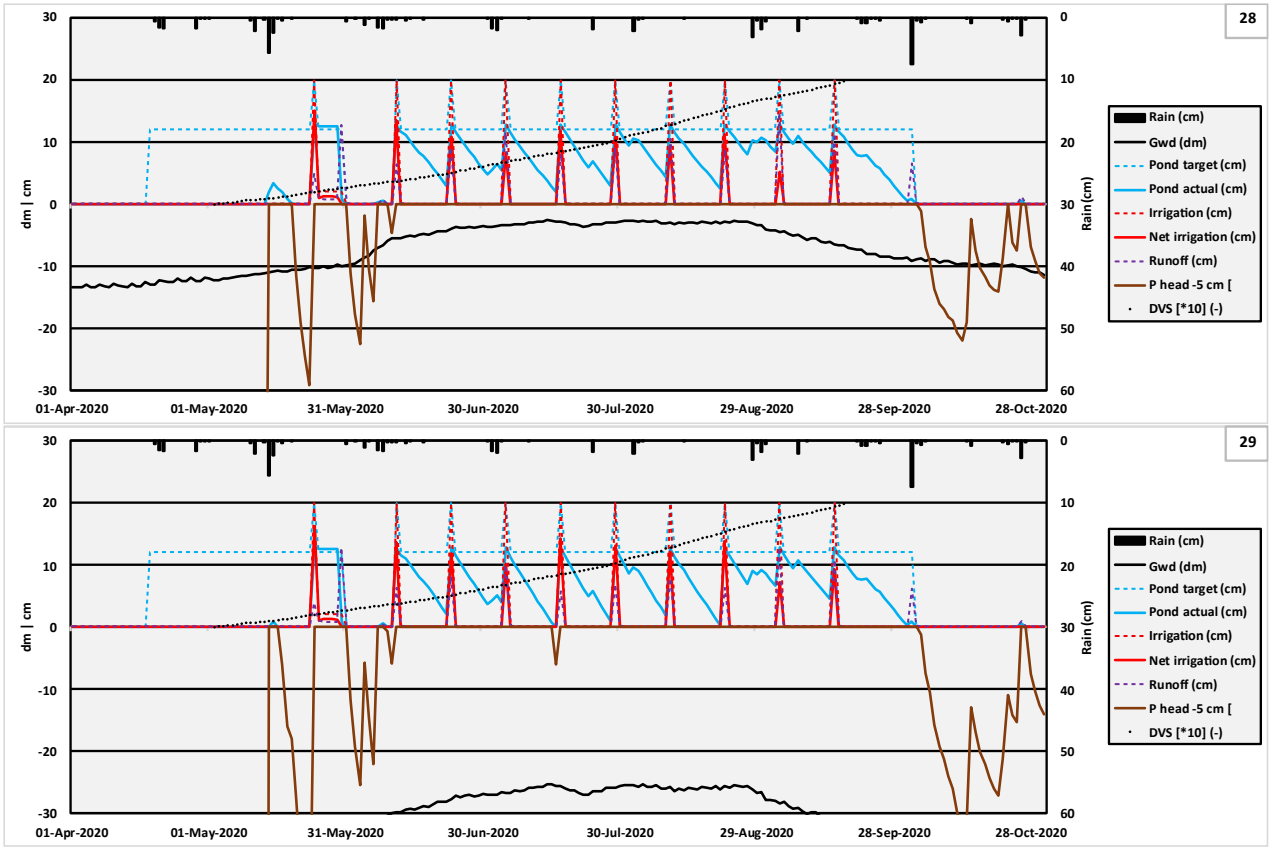

Figure 47. Daily agro-hydrological simulations outputs for two specific simulation units (28 - shallow groundwater depth, and 29 - deep groundwater depth) with FTI management and on soil unit 41310 (Table 3) during 2020.

Table 3. Soil 41310 layers discretization and hydraulic parameters; muddy and hardpan layers within the soil profile are marked in bold.

ISOILLAY	ISUBLAY	HSUBLAY	HCOMP	NCOMP	ISOILLAY1	ORES	OSAT	ALFA	NPAR	KSAT	LEXP	ALFAW	H_ENPR
1	**1**	**22**	**1**	**22**	**1**	**0.000**	**0.398**	**0.003**	**1.235**	**50.000**	**0.500**	**0.003**	**0.000**
2	2	7	1	7	2	0.000	0.341	0.002	1.269	20.320	0.500	0.002	0.000
3	**3**	**10**	**1**	**10**	**3**	**0.000**	**0.286**	**0.002**	**1.294**	**0.100**	**0.500**	**0.002**	**0.000**
4	4	21	1	21	4	0.000	0.380	0.030	1.194	29.893	0.500	0.030	0.000
5	5	141	1	141	5	0.007	0.424	0.038	1.372	188.458	0.500	0.038	0.000

3.4.2 Spatialized Model Calculations (Channel Network)

The effect of channel order (Primary (1), Secondary/no percolation (-2), Secondary (2), Tertiary (3), and No flow/no percolation (4/-4)) and channel length (*comb_length*, km) on the spatial distribution of irrigation discharge (C lin discharge, m^3/s) and percolation (C lin percolation, m^3/s) from the overall linear concentrated model to the single network traits or geometries, is shown in Figure 48. The annual average values of the linear net discharge (0.51 m^3/s) and percolation (-0.11 m^3/s) calculated for the whole channel network of the district

(concentrated model) in 2020 is subdivided into each channel order; discharges values are likewise mapped in Figure 49.

In a similar way, Figure 50 and Figure 51 show the influence of soil uses (Rice (WFL), Rice (FTI), Maize, Poplar (young) and Poplar (mature); a proxy of irrigation application) and areas (*comb_area*, ha) used by the model to spatialize diffuse annual average discharge (C diff discharge, 0.39 m^3/s) and percolation (C diff percolation, -0.09 m^3/s).

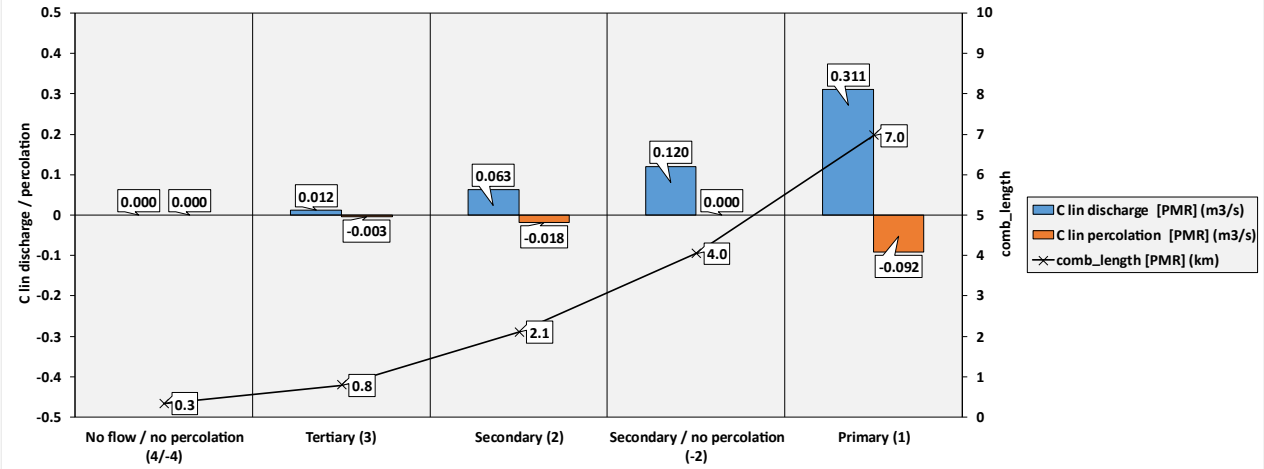

Figure 48. Effect of channel order and length (comb_ length, m) on annual average linear discharge (C lin discharge, m^3/s) and percolation (C lin percolation, m^3/s) values.

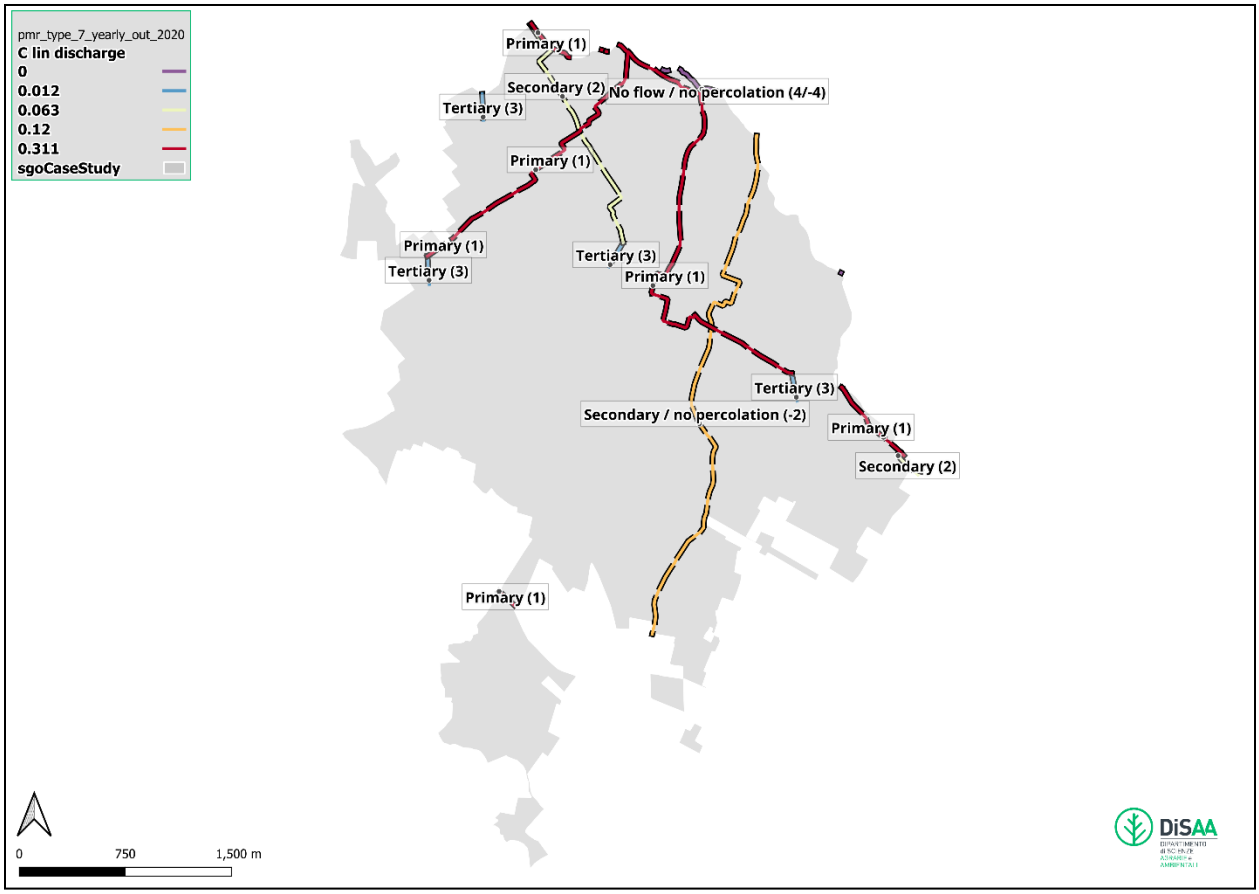

Figure 49. Annual average linear discharge (C lin discharge, m^3/s) and percolation (C lin percolation, m^3/s) maps.

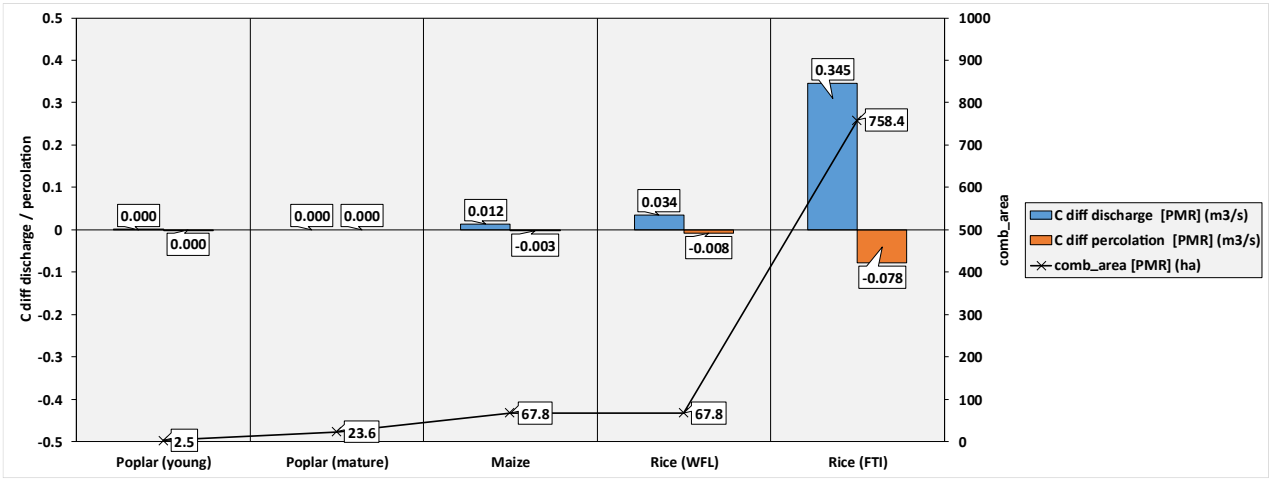

Figure 50. Effect of channel soil use and area (comb_ area, ha) on annual average diffuse discharge (C diff discharge, m^3/s) and percolation (C diff percolation, m^3/s) values.

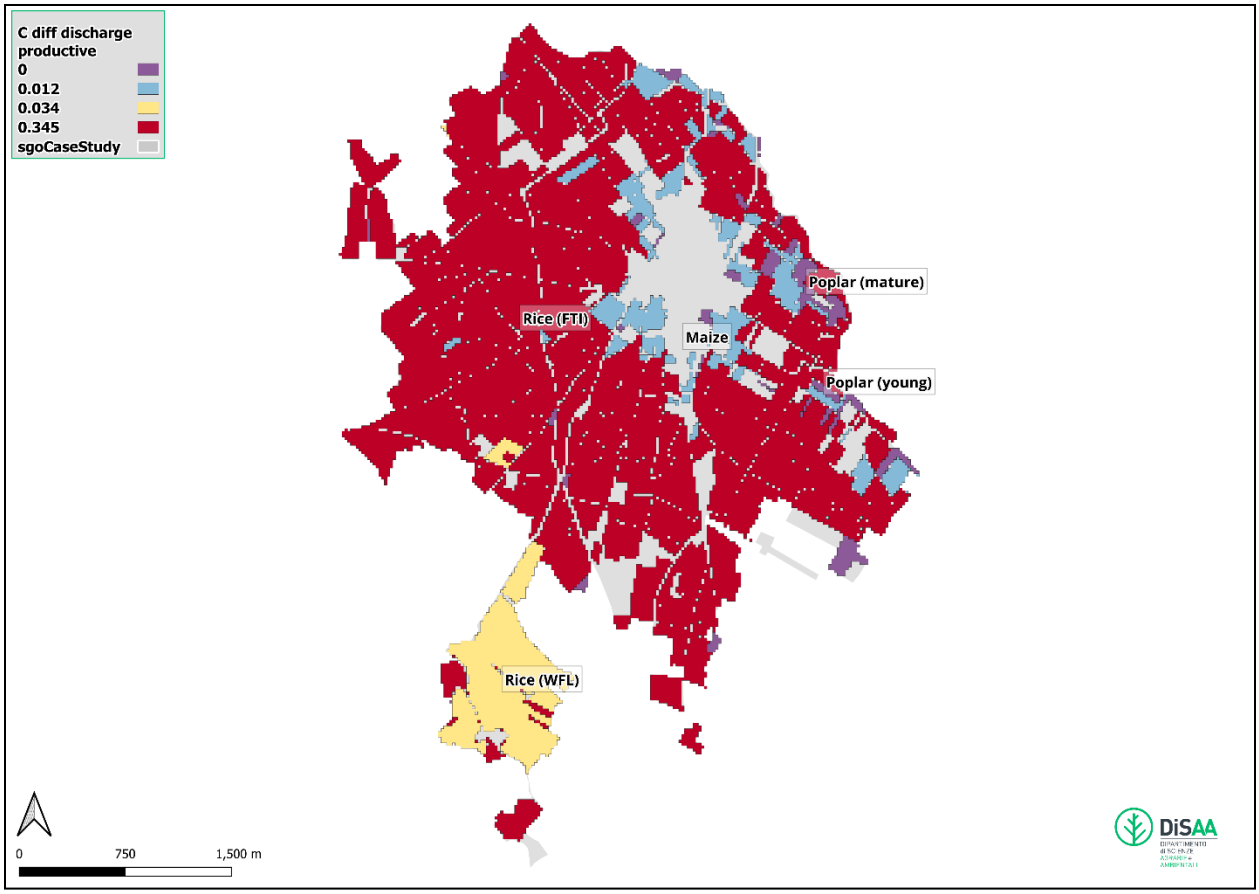

Figure 51. Annual average diffuse discharge (C diff discharge, m^3/s) and percolation (C diff percolation, m^3/s) maps.

3.4.3 Results at the Simulation Domain Level (Agricultural Area and Channel Network)

Starting from the daily core model outputs table, the framework generates a table storing the agricultural area outputs aggregated on a monthly time step on the whole simulation domain or sub-domain (*res_domain_month_table*, Figure 52), with a number of rows corresponding to the months in the simulation year. This operation is repeated for each year of the simulation.

In the generated table, the output variables produced by the core agro-hydrological simulations are aggregated into:

- I) average values (e.g. Groundwater depth - Gwd) II) or accumulated average values (e.g. Net irrigation) weighted over the actual simulation units area (*comb_area*, m^2). Average and accumlated values are reported in meters (m);
- volumes, obtained by multiplying core model outputs (m) by the *comb_area* (m^2). Volumes values are reported in cubic meters (m^3);
- discharges, obtained by dividing volumes (m^3) by the number of seconds (s) in the aggregation period (month). Discharges values are reported in cubic meters per second (m^3/s);
- counts (e.g. number of irrigation events or days of flooding).

Channel concentrated model directly works on a monthly basis, producing an output table for the whole simulation domain or sub-domain (*res_channel_month_table*, Figure 53), with a number of rows corresponding to the months in the simulation year and for each year of the simulation. All the variables stored in this table are in m^3/s.

All the output generated by the two models could be used for producing graphs helpful to evaluate temporal trends of the main output variables over time (Figure 54). This graph provides a monthly comparison between simulated net irrigation requirements (A area net irrigation, m^3/s) and estimated channel network net discharge (C network net discharge, m^3/s), aggregated over the entire simulation domain. It also includes percolation from the agricultural area (A area percolation, m^3/s), percolation from the canal network (C network percolation, m^3/s), district total percolation (District total percolation, m^3/s - A area percolation plus C network percolation), measured/estimated gross irrigation availability (C network gross discharge, m^3/s), average groundwater depth within the domain (GWD, m), the critical groundwater depth threshold (C network GWDc, m) above which channel network losses are zero, and rainfall (Rain, cm).

res_domain_month_table_sgoCaseStudy_2020_11 — Features Total: 12, Filtered: 12, Selected: 0

fid	Date	gis_cod_domain	comb_index	YYYY	MM	DD	swap3236_soilunit	swap3236_soiluse	swap3236_inlet_daily	swap3236_gwd_daily	swap3236_meteo_daily	comb_area	Rain_wl	Snow_wl	Irrig_wl	Interc_wl
1	Jan-2020	11	77	2020	1	31	12	8	1	2	1	11265200	0.0026	0	0	7.925185527110038e-05
2	Feb-2020	11	77	2020	2	29	12	8	1	2	1	11265200	0.0044	0	0	8.169513191066293e-05
3	Mar-2020	11	77	2020	3	31	12	8	1	2	1	11265200	0.05260000000000001	0	0	0.0002646969427972872
4	Apr-2020	11	77	2020	4	30	12	8	1	2	1	11265200	0.0534	0	0.021064872350246778	0.0003703657280829456
5	May-2020	11	77	2020	5	31	12	8	1	2	1	11265200	0.1198	0	0.26479494372048434	0.0013111252352377232
6	Jun-2020	11	77	2020	6	30	12	8	1	2	1	11265200	0.056999999999999995	0	0.3437648687994887	0.002059274935198665
7	Jul-2020	11	77	2020	7	31	12	8	1	2	1	11265200	0.054200000000000005	0	0.5092728047438129	0.0017814941590029475
8	Aug-2020	11	77	2020	8	31	12	8	1	2	1	11265200	0.0826	0	0.3687551042147499	0.0063622415935802295
9	Sep-2020	11	77	2020	9	30	12	8	1	2	1	11265200	0.0432	0	0.32347051095408874	0.001552948194439513
10	Oct-2020	11	77	2020	10	31	12	8	1	2	1	11265200	0.13380000000000003	0	0	0.0012447228633313213
11	Nov-2020	11	77	2020	11	30	12	8	1	2	1	11265200	0.005	0	0	0.00014339274935198666
12	Dec-2020	11	77	2020	12	31	12	8	1	2	1	11265200	0.0952	0	0	0.0009483474771863795

Figure 52. Example of res_domain_month table outputs for the agricultural area of a simulation domain (San Giorgio di Lomellina; gis_cod_domain = 11) in 2020.

res_channel_month_table_sgoCaseStudy_2020_11 — Features Total: 12, Filtered: 12, Selected: 0

fid	Date	gis_cod_domain	YYYY	MM	DD	Irrig_net_q	Runoff_net_q	Gwd_wl	DISCHARGE_IN	DISCHARGE_OUT	Discharge_linear_in_q	Discharge_linear_out_q	Discharge_linear_in_perc_q	iarge_linea
1	Jan-2020	11	2020	1	31	0	0	-3.5756020390514665	0	0	0	0	0	
2	Feb-2020	11	2020	2	29	0	0	-3.757747112560256	0	0	0	0	0	
3	Mar-2020	11	2020	3	31	0	0.0002777777777777778	-3.78333562567221	0	0	0	0	0	
4	Apr-2020	11	2020	4	30	0.061708219135802454	0.009265442901234568	-3.742643896838642	0	0	0	0	0	
5	May-2020	11	2020	5	31	0.7991315008960573	0.3855163993428912	-3.529648961746881	0.931290323	0	0.931290323	0	-0.209540322675	
6	Jun-2020	11	2020	6	30	1.010433862654321	0.07588593518518519	-2.8510764845127777	1.688583333	0	1.688583333	0	-0.379931249925	
7	Jul-2020	11	2020	7	31	1.393866082735962	0.05801205197132616	-2.502247845205274	1.758225806	0	1.758225806	0	-0.39560080635	
8	Aug-2020	11	2020	8	31	0.9658129017323775	0.05682082287933094	-2.4756265461547007	1.643548387	0	1.643548387	0	-0.369798387075	
9	Sep-2020	11	2020	9	30	0.7152081141975308	0.028548089506172835	-2.9903337546899595	0.001	0	0.001	0	-0.00022500000000000002	
10	Oct-2020	11	2020	10	31	0	0.1501168787335723	-3.384676955465476	0	0	0	0	0	
11	Nov-2020	11	2020	11	30	0	0	-3.7063551953508744	0	0	0	0	0	
12	Dec-2020	11	2020	12	31	0	0.003222906212664277	-3.7236800171352713	0	0	0	0	0	

Figure 53. Example of res_channel_month table outputs for the channel network of a simulation domain (San Giorgio di Lomellina; gis_cod_domain = 11) in 2020.

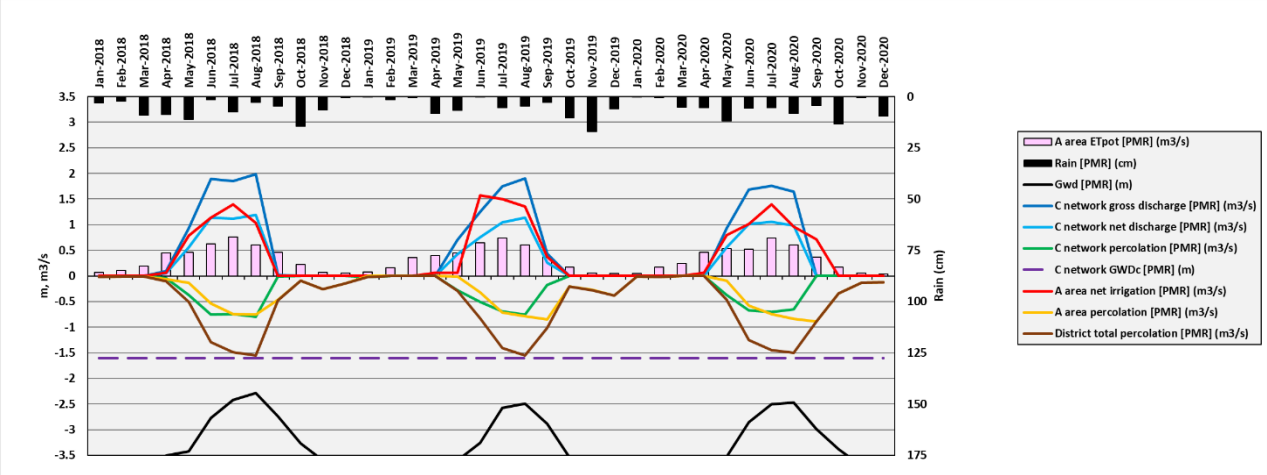

Figure 54. Example of monthly aggregated data weighted by simulation units area within the entire simulation domain (San Giorgio di Lomellina; gis_cod_domain = 11) for the period 2018 - 2020.

3.5 Conclusions

The developed framework is an integrated, modular, and scalable system for physically based simulation of the agro-hydrological balance in lowland agricultural areas, with a focus on rice-growing regions characterized by unlined canal networks. Implemented in Python and coupled with QGIS, the system organizes spatial inputs (soils, land uses, irrigation techniques, groundwater depths, and agro-meteorological conditions) into simulation units, defined as spatial entities with uniform characteristics derived from the intersection of thematic maps within a chosen domain. A relational database underpins this structure, ensuring full traceability and reusability of data for updates or alternative scenarios.

Mapped inputs and parameters are then translated into semi-distributed SWAP simulations, yielding hydrological outputs such as daily values of net irrigation requirements and deep percolations for each unit, later aggregated at the domain scale. The irrigation network is represented through linear and diffuse components, with a dedicated algorithm estimating percolation losses and computing gross and net discharges under both historical and 'what if' scenario conditions. These balance terms are then spatialized onto mapped geometries using a system of weights, preserving domain-scale channel efficiency.

The result is an operational, flexible tool specifically designed for irrigation scenario analysis, supporting both research and decision-making in water management.

4 Validation of hydro-pedotransfer functions for the main Italian paddy district

4.1 Abstract

PedoTransfer functions (PTFs), fed with easily measurable soil properties, are widely adopted for estimating soil hydraulic parameters such as bulk density (BD), soil water retention parameters, and saturated hydraulic conductivity (Ks). These parameters are essential for hydrological modelling. Paddy soils exhibit unique characteristics resulting from prolonged flooding and specific agronomic practices. Commonly, they are inadequately represented in the datasets employed to develop PTFs, raising concerns regarding the applicability of existing PTFs to such soils. This study evaluates the performance of PTFs found in the literature for predicting BD (21 PTFs), soil water retention parameters (20 PTFs), and Ks of the hardpan horizon (55 PTFs) using an observational dataset comprising common and hydraulic soil properties of 170 soil horizons collected in Italy's main rice-growing region. Performance analyses were conducted considering the entire database and dividing the horizons into topsoil, hardpan and subsoil. The results showed that BD can be accurately estimated using a modified version of the PTF of Kaur et al. (2002). Rajkai and Varallyay (1992) PTFs provide an excellent estimation of soil water retention parameters. However, most existing PTFs fail to reliably predict even the magnitude of the hardpan Ks, including those originally developed for rice soils. Therefore, this study developed a novel PTF that outperforms existing alternatives; however, its reliability needs to be further tested using a larger observational sample. These findings support the use of existing PTFs for BD and soil water retention parameters, while emphasis on the need to improve Ks estimation to enhance hydrological modelling of rice systems.

4.2 Motivation and Objectives

The Lomellina territory was shaped during the Quaternary by Pleistocene fluvioglacial activity and Holocene fluvial processes (ERSAF, 2004). Two main Systems are distinguished: the Würmian proglacial plain (L) and the Holocene valleys and terraces (V). Within these, Ente Regionale per i Servizi all'Agricoltura e alle Foreste (ERSAF, https://www.ersaf.lombardia.it/) identified 60 Cartographic Units (UCs), described in the 1:50,000 Lombardy Region Soil Map (https://www.geoportale.regione.lombardia.it/) and in the LOSAN soil database (https://www.losan.ersaflombardia.it/).

Accurate soil water hydraulic parameters (soil water retention curve - $\theta(h)$, and saturated hydraulic conductivity - Ks) are essential for modelling unsaturated flow (Facchi et al., 2018; Raats and Knight, 2018). Because direct measurement is costly (Vereecken et al., 2010), PedoTransfer functions PTFs estimate them from basic soil data (Bouma, 1989; Wösten et al., 2001), often using bulk density (BD) as a key input; when BD is estimated, uncertainty can propagate (Iovino et al., 2009; Szabó et al., 2021). Most PTFs, from simple tables to ML models (Schaap et al., 2001; Zhang and Schaap, 2017), are not calibrated for paddy soils. In rice fields, monoculture and prolonged flooding form a compact hardpan with higher BD and lower Ks (Bouman et al., 2007; Facchi et al., 2018), as also found in the Lomellina paddy soils were the puddling practice is rarely applied, making generic PTFs unreliable (Wösten et al., 2001).

This study presents a dataset containing soil physicochemical and hydraulic parameters measured in the laboratory for 170 soil horizons from 28 profiles sampled in rice-growing areas of Lomellina between 2012 and 2023. This dataset is used to validate PTFs already present in the literature by assessing their estimation accuracy for the paddy soils of this geographical area. The PTFs that guarantee the lowest estimation error are identified for all the soil hydraulic parameters, and calibration coefficients are developed where necessary. In the case of the hardpan Ks specifically, a novel PTF was developed as those in the literature were found to be strongly unsuitable.

4.3 Materials and Methods

4.3.1 Soil Dataset

A dataset of laboratory-measured physicochemical and hydraulic soil properties was compiled to serve as a reference database for evaluating the performance of PTFs derived from literature in estimating the hydraulic properties of paddy soils in the Lomellina district. The dataset comprises 170 soil horizons from 28 profiles sampled in rice-growing areas of the Lomellina between 2012 and 2023 as part of various projects (Figure 55). The resulting dataset encompasses a wide range of variables, including physicochemical parameters such as particle size distribution (percentages of sand, silt and clay), organic matter content (OM) and bulk density (BD).

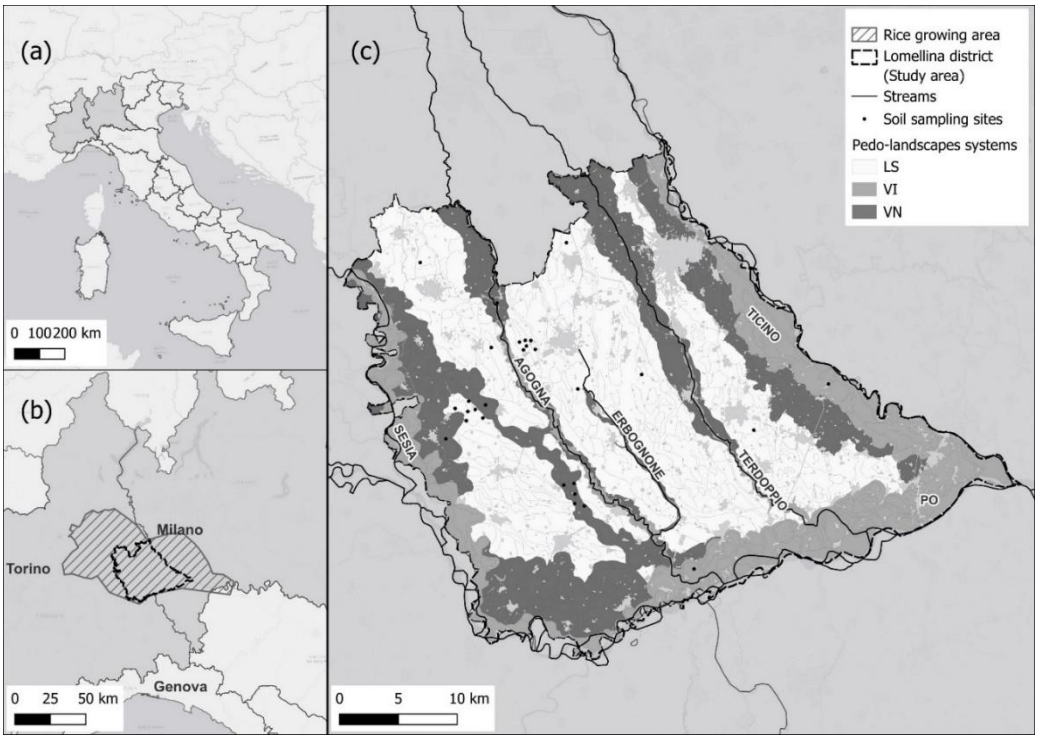

Figure 55. (a) Overview of Italy, with the Lombardy and Piedmont regions highlighted; (b) Focus on the north-western part of Italy showing the rice-growing area (hatched) and the Lomellina district (outlined in black); (c) Study area classified into pedo-landscape sub-systems (LS, VI, VN). Soil sampling sites (black dots) are displayed within the study area and across the different pedo-landscape sub-systems.

To produce the soil water retention curve, the soil water content-pressure head relationship was determined using undisturbed soil samples at pressure heads ranging from 1 to 1,000 kPa, and disturbed soil samples at pressure heads ranging from 1,000 to 1,500 kPa. Specifically, two replicates of small undisturbed soil cores (5 cm in diameter and 3 cm in height) were collected from all horizons, or from the uppermost five horizons where there were more than five, of each soil profile. Bulk density was also measured using the same cores. Furthermore, disturbed soil samples were taken from all horizons, with three replicates used for the analysis. Soil water content at pressure heads up to 5 kPa was determined using a tensiometric box; at higher pressure heads, the pressure plate apparatus was employed. Both methods were carried out in accordance with the official Italian protocol for the physical analysis of soil (D.M. 01/08/1997).

The saturated hydraulic conductivity (Ks) of the hardpans was measured using the core method (Coughlan et al., 2002; Dane and Clarke Topp, 2002). Three large, undisturbed soil cores (14.6 cm in diameter and 15 cm in height) were collected from the hardpan of each soil profile. The hardpan horizon was identified at a depth of around 30 cm in many of the surveyed profiles. This horizon was typically 15 - 20 cm thick, greyish in colour, and exhibited pronounced plasticity. Rather than the usual one or two days required to assess Ks in upland soils, the samples were kept in the Darcy apparatus until the measured Ks value stabilized, replicating the conditions occurring in paddy fields after flooding. Indeed, the measured Ks values typically decrease progressively over time, stabilizing only after several weeks. While this greatly increased the time needed for the measurements, it provided Ks values representative of field conditions during the flooding season instead of the higher values occurring just after flooding. Such a reduction in Ks could be explained by the soil microbiota adapting to increased soil moisture, thereby changing biological activity (Carles Brangarí et al., 2017; Sao et al., 2024). Volk et al., (2016) support this mechanism, having reported a reduction in Ks in soils inoculated with bacteria due to biofilm formation.

The sampling sites were selected to characterize the main rice cultivation conditions in Lomellina based on the following criteria: abundance of the soil unit in the district (i.e., area covered by each UC); possibility of representing the different soil-landscape sub-systems also taking into account the relative area they cover in the district; frequency of rice cultivation in the specific rice field in the period 2010 - 2019.

As shown in Figure 56, the particle size distribution of the 170 soil horizons in the dataset closely matches the overall texture classes of the horizons in Lomellina, as reported in the 1:50,000 Soil Map of Lombardy and in the LOSAN database. In both USDA soil texture triangles, most horizons fall in the lower part of the triangle, indicating a predominance of coarser textures. Soil texture classified according to the USDA textural triangle shows a prevalence of sandy loam soils in both datasets. The datasets differ mainly in that the Lombardy dataset has a higher proportion of sandy textures (i.e. sandy and loamy sand soils), whereas the sample dataset also includes a notable proportion of silty loam soils. This is because, when selecting the profiles to be sampled, attention was paid to identifying also less abundant soils used for rice-growing. It should be noted that sandy loam remains the dominant texture class also among the lower conductivity horizons (indicated by crosses in Figure 56). Overall, it can be concluded that the combined dataset provides a reliable representation of the texture variability observed in the rice-growing soils of Lomellina.

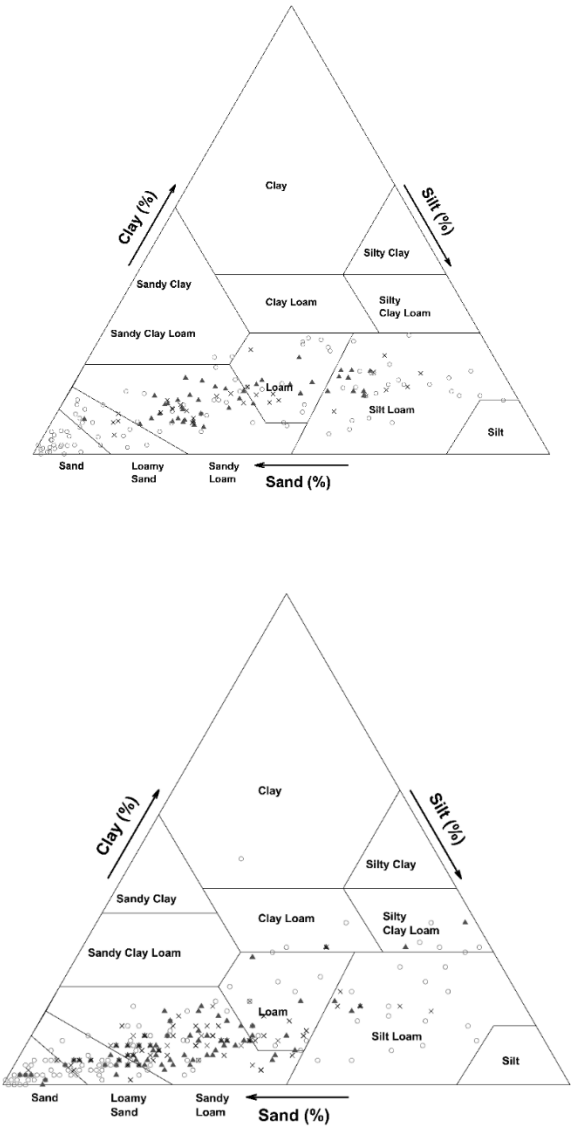

Figure 56. Soil texture classes of the horizons included in the database used in this study (left) and in the whole Lomellina region (right), categorized by soil type: topsoil (triangles), hardpan (crosses) and subsoil (circles).

4.4 PedoTransfer Functions

This Section presents the PTFs selected for the assessment. References for each PTF can be found in Appendices I, II and III which refer to BD, retention curve and Ks, respectively.

4.4.1 PTFs for Estimating Bulk Density

A total of 21 PTFs were selected to estimate BD, covering a wide range of complexity and methodological approaches and including the most widely used models in literature. Many of those

are based on multiple linear regression (MLR) methods, using commonly available inputs such as texture fractions and organic carbon or matter (Rawls, 1983; Tomasella and Hodnett, 1998), making them applicable to a wide range of situations. Others use non-linear regression (NLR) methods (Kaur et al., 2002; Rawls et al., 2004; Wang et al., 2014), which capture complex relationships more effectively, albeit with greater model complexity. Simple linear regressions (LR) models, such as those by Manrique and Jones (1991a,b), are accessible options for large-scale applications where data availability is limited.

Rule-based regression (RBR) approaches (Hollis et al., 2012) incorporate additional categorical horizon descriptors (e.g. top layer, presence of hardpans, initial/final profile depth) to improve accuracy. However, these approaches may be limiting in datasets where such information is not systematically recorded.

The complete list of the PTFs tested, along with the information available on the dataset employed for their development (number of soil samples and sampling location), as well as the inputs required for their application, is reported in Table 4.

Table 4. PTFs selected for estimating the bulk density (BD). Soil's origin and the number of samples (n) on which the PTF development was based are shown. The abbreviated input data are as follows: Sa = sand; Si = silt; Cl = clay; OC = organic carbon; OM = organic matter; Depth_ini, Depth_fin, and Depth_avg: initial, final, and mean depth of the horizon; WP: soil water content at the wilting point.

N	***Reference***	***Source***	***Size***	***Input***
1	Benites et al. (2007)	Brazil	1396	Cl, OC
2	Dexter (2004)	Germany	119	Cl, OM
3	Hollis et al. (1996)	Europe	-	Sa, Li, Cl, OC
4	Hollis et al. (2012)	Europe	67	Sa, Cl, OC
5	Hollis et al. (2012) - b	Europe	67	Sa, Cl, OC, Toplayer, Hardpan, Subsoil, Depth_ini, Depth_fin
6	Kaur et al. (2002)	India	224	OC, Cl, Si
7	Leonaviciute (2000)	Lithuania	140	Si, Cl, OC
8	Manrique-Jones (1991) - a	USA	19651	OC
9	Manrique-Jones (1991) - b	USA	19651	OC
10	Manrique-Jones (1991) - c	USA	19651	Cl, OC, WP
11	Mayer et al. (2019)	Italy	53	Sa, Li, Cl, OC
12	Men et al. (2008)	China	-	Si, Cl, OC
13	Patil-Chaturvedi (2012) - a	India	102	Sa, Si, Cl
14	Patil-Chaturvedi (2012) - b	India	102	Sa, Si, Cl, OC
15	Patil-Chaturvedi (2012) - c	India	102	Sa, Si, OC
16	Rawls (1983)	USA	2721	OM, OM_BD
17	Rawls et al. (2004)	USA	2100	Sa, Cl, OM
18	Tomasella-Hodnett (1998)	Brazil	396	Si, Cl, OC

19	Tranter et al. (2007) - a	Australia	-	Sa, Depth_avg
20	Tranter et al. (2007) - b	Australia	-	Sa, OC, Depth_avg
21	Wang et al. (2014)	China	748	Si, Cl, OC

4.4.2 PTFs for Estimating Soil Water Retention Curve Parameters

A total of 20 PTFs that estimate the parameters of the soil water retention curve were assessed. These PTFs included widely validated models, such as the nine PTFs available in the CalcPTF spreadsheet tool (Guber and Pachepsky, 2010), two models from the Rosetta-3 package (Zhang and Schaap, 2017), Ungaro et al. (2005) model for the Italian soils of the Po Plain, and the European HYPRES function (Wösten et al., 1999). The selected PTFs provide estimates for the van Genuchten and/or Brooks & Corey models using input parameters ranging from basic soil texture and organic carbon content to more specific descriptors, such as bulk density and horizon structure.

These models employ various approaches: most rely on non-linear or multiple linear regressions, whereas more recent models, such as Rosetta-3, utilize machine learning methods (ANN). Some models, including that of Ungaro et al. (2005), combine regression with rule-based classification to explicitly incorporate the structural properties of the soil horizons. Semi-empirical and physically based formulations (NLP) have also been adopted, providing an intermediate level of complexity based on simplified physical relationships (Saxton et al., 1986).

The complete list of the PTFs tested along with the information available on the dataset employed for their development (number of soil samples and sampling location) is reported in Table 5, as are the inputs required for their application.

Table 5. PTFs selected for estimating the parameters of the soil water retention curve according to the van Genuchten and/or Brooks & Corey models. The symbol (C) indicates that a calibration process based on the PTF outcomes is required to obtain the water retention curve (see the Results Section).

N	***Reference***	***Source***	***Size***	***Input***	***Model***
1	Campbell-Shiosawa (1992)[a]		6	Sa, Cl, BD	B&C
2	Gupta-Larson (1979) (C)	USA	43	Sa, Si, Cl, OC, BD	vG
3	Mayr-Jarvice (1999)	England	306	Sa, Si, Cl, OC, BD	B&C
4	Oosterveld-Chang (1980)	Canada	298	Sa, Cl, BD, Prof	B&C
5	Rajkai-Varallyay (1992) (C)	Hungary	270	Sa, Cl, OC, BD	vG
6	Rawls et al. (1982) (C)	USA	5320	Sa, Si, Cl, OC, BD	vG
7	Rawls et al. (1983) (C)	USA	5320	Sa, Si, Cl, OC, BD	vG
8	Rawls-Brakensiek (1985)	USA	5320	Sa, Cl, BD	B&C

9	Saxton et al. (1986)	USA	5320	Sa, Cl, BD	B&C
10	Tomasella-Hodnett (1998) (C)	Brazil	196	Si, Cl, OC	vG
11	Ungaro et al. (2005)	Italia	153	Sa, Si, Cl, ClTes, Str, OC, BD	vG
12	Varallyay et al. (1982)	Hungary	230	Cl, BD	vG
13	Vereecken et al. (1989)	Belgium	182	Sa, Cl, OC, BD	vG
14	Williams et al. (1992) - Eq. 2	Australia	196	Sa, Cl, BD	B&C
15	Williams et al. (1992) - Eq. 1	Australia	196	Sa, Cl, OC, BD	B&C
16	Wösten et al. (1999) - c (Hypress)	Europe	4030	Sa, Si, Cl, OC, BD, Topsoil	vG
17	Wösten et al. (1999)	Europe	4030	Sa, Si, Cl, Prof	vG
18	Wösten et al. (1999) - b	Europe	4030	Si, Cl, OC, BD, Prof	vG
19	Zhang-Schaap (2017) (No BD)	USA, EU	2134	Sa, Si, Cl	vG
20	Zhang-Schaap (2017) (BD)	USA, EU	2134	Sa, Si, Cl, BD	vG

4.4.3 PTFs for Estimating the K_s of the Hardpan

Ks is a key parameter for understanding and modelling water flow in soils. However, its measurement is time-consuming and difficult due to its high variability (typically ranging from 0.01 to 250 cm/d) and to its sensitivity to soil disturbance and measurement methods. This uncertainty also affects the accuracy of estimates provided by PTFs, since Ks shows often a weak correlation with other soil physicochemical and hydraulic parameters. Consequently, PTFs may perform poorly even when applied to soils like those used for their development, and even more so when applied to different soil types. Therefore, issues are expected when applying Ks PTFs to the peculiar soil of paddy field hardpans.

For this reason, the present study has taken great care to search the literature for as many Ks PTFs as possible, without limiting the activity to the most widespread and well-known ones. This resulted in a set of 55 PTFs, which were then used to estimate the Ks values in the Lomellina dataset.

The PTFs collection includes widely used models such as those by Ungaro et al. (2005), Rawls and Brakensiek (1989), and Wösten et al. (1999c), as well as more recent approaches such as Rosetta-3 by Zhang and Schaap (2017), Ottoni et al. (2019), and Patle and Vanlalnunchhani (2020). Notably, the collection also includes two functions developed specifically for paddy soils, Aimrun and Amin (2009) and Zou et al. (2016), even if the sampling locations are in Asia where climate, soils and agricultural practices (e.g., puddling) are very different from those in Lombardy.

Most PTFs are based on multiple linear or non-linear regression, primarily using soil textural properties alongside bulk density and organic matter content. Some models incorporate

porosity (Po) or particle density (PD), while a few use the geometric mean diameter (GMD) and geometric standard deviation (GSD) of the particle size distribution. Several functions also incorporate water content at specific matric potentials (e.g. θ330, θ15000, θs), which improves accuracy but increases complexity due to the need for hydraulic measurements or reliable estimates. Other models estimate Ks from water retention parameters (e.g. Pe, λ), making them suitable for cases where such data is already available.

In addition to these empirical models, artificial neural networks have been used, as in the Rosetta model (Zhang and Schaap, 2017). This approach provides greater flexibility and potentially more accurate predictions.

Table 6 provides a complete list of the PTFs tested, along with the information on the dataset used for their development (number of soil samples and sampling location), and the inputs required for their application.

Table 6. PTFs selected for estimating the saturated soil hydraulic conductivity (Ks) of the hardpans in Lomellina. The table reports soil origin and the number of samples (n) on which the PTF calibration was based.

N	***Reference***	***Location***	***n***	***Input***
1	Ahuja et al. (1989)	USA	473	Theta
2	Aimrun-Amin (2009)	Malaysia	408	Sa, Si, Cl, OC, BD, Theta
3	Arshad et al. (2009)	Iran	175	Sa, Si, Cl, BD
4	Brakensiek et al. (1984)			Sa, Si, Cl, Theta
5	Campbell (1985)[a]			Sa, Si, Cl, BD
6	Campbell (1985)[b]			Sa, Si, Cl, BD
7	Campbell-Shiozawa (1992)	USA	42	Sa, Si, Cl
8	Cosby et al. (1984) (Eq. 1)		1448	Sa, Si, Cl
9	Cosby et al. (1984) (Eq. 2)		1448	Sa, Si, Cl
10	Dane-Puckett (1994)[c]	USA	577	Sa, Si, Cl
11	Jabro (1992)		350	Sa, Si, Cl, BD
12	Julia et al. (2004) (Eq. 1)			Sa, Si, Cl
13	Julia et al. (2004) (Eq. 2)			Sa, Si, Cl, OC
14	Julia et al. (2004) (Tab. 3 - 1 par)			Sa, Si, Cl
15	Julia et al. (2004) (Tab. 3 - 3 par)			Sa, Si, Cl, OC
16	Li et al. (2007) - Tab. 6	China	36	Sa, Si, Cl, OC, BD
17	Mayer et al. (2019)	Italy	5	Sa, Si, Cl, OC, BD

N	*Reference*	*Location*	*n*	*Input*
18	Minasny-McBratney (2000)	Australia		Sa, Si, Cl, Theta
19	Nemes et al. (2005)	USA	886	Sa, Si, Cl, OC, BD
20	Ottoni et al. (2019) - Eq. 1	Brazil, EU	425	Theta
21	Ottoni et al. (2019) - Eq. 2	Brazil, EU	425	Sa, Si, Cl
22	Ottoni et al. (2019) - Eq. 3	Brazil, EU	425	Sa, Si, Cl, BD
23	Ottoni et al. (2019) - Eq. 4	Brazil, EU	425	Sa, Si, Cl, BD
24	Patil et al. (2009) - Eq. 1	India	175	Sa, Si, Cl
25	Patil et al. (2009) - Eq. 2	India	175	Sa, Si, Cl, BD
26	Patil et al. (2009) - Eq. 3	India	175	Sa, Si, Cl, BD, Theta
27	Patil et al. (2009) - Eq. 4	India	175	Sa, Si, Cl, BD, Theta
28	Patle-Vanlalnunchhani (2020) - Eq. 1	India	28	Sa, Si, Cl
29	Patle-Vanlalnunchhani (2020) - Eq. 2	India	28	Sa, Si, Cl, BD
30	Patle-Vanlalnunchhani (2020) - Eq. 3	India	28	Sa, Si, Cl, BD
31	Patle-Vanlalnunchhani (2020) - Eq. 4	India	28	Sa, Si, Cl, OC, BD
32	Patle-Vanlalnunchhani (2020) - Eq. 5	India	28	Sa, Si, Cl, OC, BD, Theta
33	Puckett et al. (1985)		42	Sa, Si, Cl
34	Rawls-Brakensiek (1989)			Sa, Si, Cl, Theta
35	Rawls et al. (1998)			Theta
36	Saxton et al. (1986)[d]		230	Sa, Si, Cl
37	Saxton-Rawls (2006)	Spain	2178	Theta
38	Shwethaa-Prasannab (2013)	India		Sa, Si, Cl
39	Spychalski et al. (2007) - Eq. 9			Theta
40	Spychalski et al. (2007) - Eq. 10			Theta
41	Suleiman-Ritchie (2001) - Eq. from Fig. 4, with h = 100			Theta
42	Suleiman-Ritchie (2001) - Eq. from Fig. 4, with h = 330			Theta
43	Suleiman-Ritchie (2001) - Eq. from Fig. 5			Theta

N	*Reference*	*Location*	*n*	*Input*
44	Timlin et al. (1999)	USA	473	Theta
45	Tomasella-Hodnett (1997)	Brazil	13	Theta
46	Ungaro et al. (2005)	Italy	153	Sa, Si, Cl, OC, BD
47	Vereecken et al. (1990) - Eq. Level 1	Belgium	182	Sa, Si, Cl, OC, BD
48	Weynants et al. (2009)	Belgium	136	Sa, Si, Cl, OC, BD
49	Wösten et al. (2001) - a	Europe	1139	Sa, Si, Cl, OC, BD
50	Wösten et al. (2001)[e] - b	Europe	1139	Sa, Si, Cl, OC, BD
51	Wösten (1999)	Europe	1136	Sa, Si, Cl, OC, BD
52	Yang et al. (2018)	China	86	Sa, Si, Cl, BD
53	Zou et al. (2016)	China	19	Sa, Si, Cl, BD
54	Zhang-Schaap (2017) (no BD)	USA, EU	1306	Sa, Si, Cl
55	Zhang-Schaap (2017) (BD)	USA, EU	1306	Sa, Si, Cl, BD

[a] obtained from Minasny-McBratney (2000)

[b] obtained from Aimrun-Amid (2009)

[c] obtained from Zhang-Schaap (2019)

[d] obtained from Aimun-Amin (2009), Minasny et al. (2000), Soberaj (2001)

[e] obtained from Nemes et al. (2005)

[f] obtained from Ungaro et al. (2005)

4.4.4 Performance Evaluation

The performance of the PTFs was evaluated based on one-to-one correspondence between measured and predicted values of bulk density, soil water content at specific matric potentials, and saturated hydraulic conductivity. Four well-known statistical indices were used to assess model performance: root mean square error (RMSE), median absolute error (MAE), bias, and Nash-Sutcliff model efficiency (ME) (Table 7).

For a satisfactory prediction, the values of the indices should be low for RMSE and MAE, minimal for bias, and high for ME, indicating accurate predictions, limited systematic error, and good reproduction of the variability of the observed data.

Table 7. Statistical indices applied for evaluating PTFs; N is the number of observations, y_i and $\hat{y}_i$, are the observed and predicted values respectively, $\bar{y}$ is the mean of the observed values, and Med denotes the median operator.

Indices	*Formula*
Root mean square error (RMSE)	$RMSE = \sqrt{\frac{\sum_{i=1}^{N}(\hat{y}_i - y_i)^2}{N}}$

Median absolute error (MAE)	$MAE = Med(\lvert\hat{y}_i - y_i\rvert)$
Bias	$Bias = \frac{\sum_{i=1}^{N}(\hat{y}_i - y_i)}{N}$
Model efficiency (ME)	$ME = 1 - \frac{\sum_{i=1}^{N}(y_i - \hat{y}_i)^2}{\sum_{i=1}^{N}(y_i - \bar{y})^2}$

4.5 Results

4.5.1 Bulk Density

For the estimation of the bulk density (BD, g/cm³) of paddy soil horizons, 21 PTFs from the literature were evaluated, also considering possible adaptations. The initial evaluation was carried out using the full dataset of 130 samples, a second evaluation was obtained with the dataset split into three subsets based on the following horizon types: topsoil (40 samples), hardpan (27 samples), and subsoil (63 samples). Table 8 shows the results of the statistical analysis of the performance of the various PTFs that were tested.

Table 8. Results of statistical analysis obtained for the PTFs estimating soil bulk density of paddy horizons in Lomellina.

Reference	***Bias (g/cm³)***	***RMSE (g/cm³)***	***ME (-)***
Benites et al. (2007)	0.077	0.205	-0.27
Dexter (2004)	0.037	0.174	0.31
Kaur et al. (2002)	-0.283	0.324	-1.41
Kaur et al. (2002) mod	-0.003	0.158	0.43
Kaur et al. (2002) mod3	**0.000**	**0.123**	**0.65**
Hollis et al. (1996)	-0.027	0.145	0.43
Hollis et al. (2012)	0.018	0.172	0.02
Hollis et al. (2012) - b	-0.081	0.179	-0.06
Leonaviciute (2000)	0.024	0.160	0.15
Manrique-Jones (1991) - a	-0.101	0.192	-0.23
Manrique-Jones (1991) - b	-0.103	0.207	0.02
Manrique-Jones (1991) - c	0.127	0.214	-0.52
Men et al. (2008)	0.024	0.171	0.03
Patil-Chaturvedi (2012) - a	-0.408	0.445	-5.57
Patil-Chaturvedi (2012) - b	-0.359	0.407	-4.49
Patil-Chaturvedi (2012) - c	-0.433	0.464	-3.93
Rawls (1983)	-0.159	0.230	-0.21
Rawls et al. (2004)	-0.023	0.162	0.13
Tomasella-Hodnett (1998)	-0.239	0.306	-2.11
Tomasella-Hodnett (1998) mod	0.054	0.161	0.14
Tranter et al. (2007) - a	-0.037	0.177	-0.04

Tranter et al. (2007) - b	-0.236	0.296	-1.91
Wang et al. (2014)	0.052	0.176	-0.04

Of the various PTFs examined, the PTF Kaur (mod3) produced the best results for Lomellina paddy soils. This modified model of Kaur et al. (2002) is described and discussed below, along with the original PTF. The Kaur (mod3) has an RMSE of 0.123 and an ME of 0.65. Based on the results of this study, Kaur (mod3) is recommended for estimating BD when the horizon typology (i.e., topsoil, hardpan, subsoil) is known. Where this information is unavailable, another modified version of the model is recommended: Kaur (mod), which includes a single additive constant for all paddy soils.

Some other PTFs showed good performance in estimating bulk density. These include the PTF developed by Hollis (1996) as well as the modified version of the PTF developed by Tomasella and Hodnett (1998) defined in Mayer et al. (2019), which is denoted as Tomasella and Hodnett (mod) in Table 8. The Hollis model, developed using data from European soils, achieved an RMSE of 0.145 and an ME of 0.43. However, it consists of several equations specific to different soil genetic horizons and does not include equations for dense or compact horizons that are typical of paddy fields. Therefore, it would easily result in missing data in the database, requiring the application of other PTFs. The modified Tomasella and Hodnett model performed reasonably well with an RMSE of 0.161 and an ME of 0.14.

4.5.1.1 Modified versions of the PTF Kaur et al. (2002)

The original function Kaur et al. (2002) was developed using a database of 224 samples collected from four experimental sites in India characterized by different land uses including agricultural land, pine and oak forests and barren land. The function is described by the following equation:

$$BD_K = exp(0.313 - 0.191 \cdot OC + 0.02102 \cdot Cl - 0.000476 \cdot Cl^2 - 0.00432 \cdot Si) \quad \text{(Eq. 21)}$$

where OC is the organic carbon content, and Cl and Si represent the weight percentages of clay and silt, respectively.

The original PTF by Kaur et al. (2002) showed poor accuracy, primarily due to a systematic underestimation of the BD. However, there was a good correlation between the estimations and the measured values (Pearson correlation coefficient r = 0.67). To improve the original function for paddy soils, a constant equal in magnitude to the bias (0.28 g/cm³, 128 measured BD values) was added to Eq. 21, resulting in the Kaur (mod) function:

$$BD_{Kmod} = BD_K + 0.28 \quad \text{(Eq. 22)}$$

Further analysis revealed that the estimation bias was related to the type of the soil horizon. This is a reasonable finding, given that different physical, chemical and biological processes affect topsoil, hardpan and subsoil. Based on this finding, the Kaur (mod3) PTF was obtained by applying horizon-specific bias correction parameters to further refine BD estimates:

$$BD_{Kmod3} = BD_K + \beta \quad \text{(Eq. 23)}$$

where the values of β are 0.34, 0.42 and 0.18 for topsoil, hardpan and subsoil, respectively.

In line with the varying degrees of the expected soil clogging, the adjustment is more pronounced for the hardpan horizon, less for the topsoil and minimal for the subsoil.

Figure 57 shows scatter plots comparing the estimated bulk density values obtained using the original function and its modified versions (x-axis) against the measured values (y-axis). The first plot illustrates the overall performance of both the original equation and the modified Kaur (mod) version. The subsequent plots refer to Kaur (mod3) and demonstrate the impact of the additive constant on the estimates produced by the original PTF, shifting them towards those provided by the modified version.

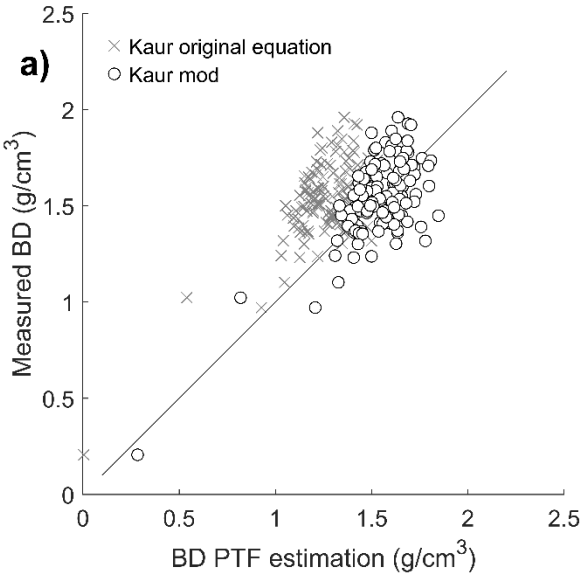
a)
Kaur original equation
Kaur mod
Measured BD (g/cm3)
BD PTF estimation (g/cm3)
0
0.5
1
1.5
2
2.5

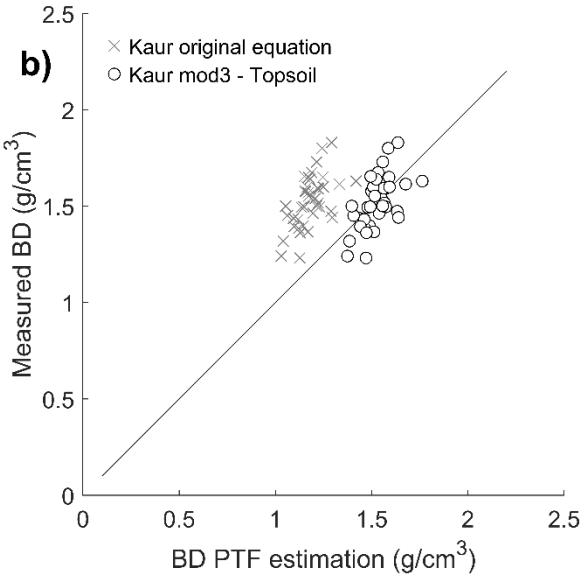
b)
Kaur original equation
Kaur mod3 - Topsoil
Measured BD (g/cm3)
BD PTF estimation (g/cm3)
0
0.5
1
1.5
2
2.5

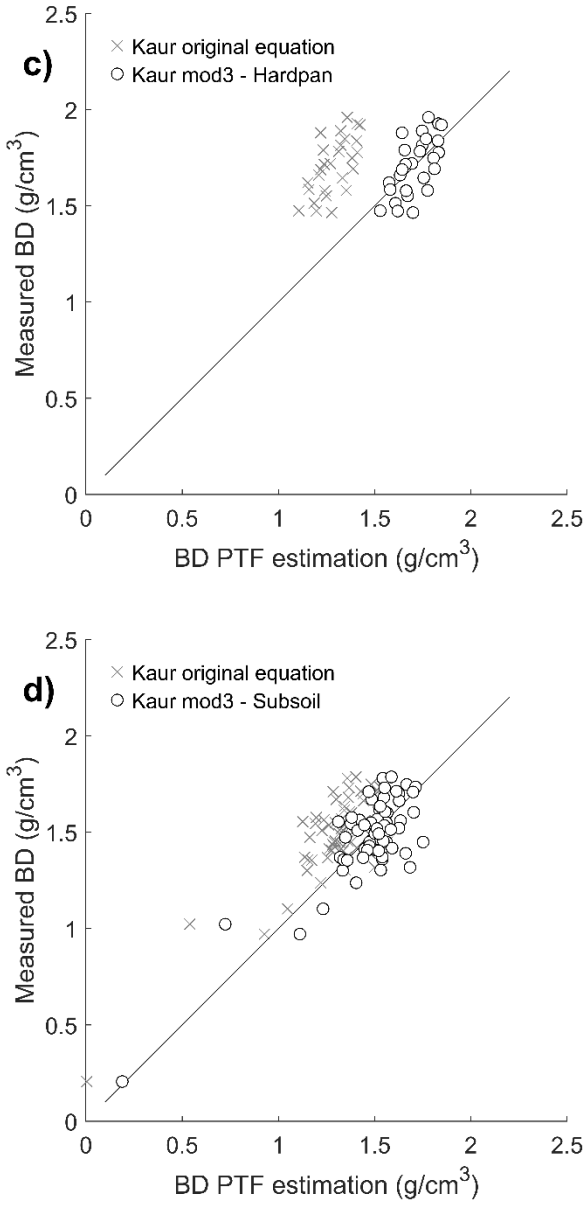

Figure 57. Scatter plots of bulk density (BD) values estimated using the Kaur et al. (2002) equation: (a) Original PTF vs. Kaur (mod); (b) Original PTF vs. Kaur (mod3) - topsoil; (c) Original PTF vs. Kaur (mod3) - hardpan; (d) Original PTF vs. Kaur (mod3) - subsoil.

4.5.2 Water Retention Curve

The performance of 20 PTFs was evaluated in their ability to estimate the soil retention curve parameters of paddy soils. We used 76 soil horizons (27 topsoil, 15 hardpan, and 34 subsoil) from the database for which measured retention curves (i.e., a series of water potential - water content pairs) were available. The analysis was carried out both for all the pressure potentials tested in the laboratory (marked 'All pot.' in the following tables) and for four specific water potential ranges given in Table 9. The analysis of the PTFs performance is discussed for all the soil horizons

and by horizon type. Next, we describe the Rajkai and Varallyay (1992) PTF, as this is usually the one performing the best.

Table 9. List and features of the of the water potential ranges adopted for the analysis. The category 'All pot.' includes all the water potentials listed in the table.

Name of the range	Potential (bar)	Description
Very wet	0.0, 0.01, 0.05	includes saturation and near saturation conditions
Wet	0.1, 0.3, 0.33	includes values around field capacity
Dry	0.7, 1.4, 3.0	includes intermediate potentials
Very dry	6, 12, 15	includes the most negative pressure values, representing very dry soil conditions

The results listed in Table 10 are obtained by considering all the soil horizons in the database.

At the very wet potentials (0 - 0.05 bar), several PTFs performed well: Campbell and Shiosawa (1992), Rawls et al. (1982), Rajkai and Varallyay (1992), Williams et al. (1992) - Eq. 2, and Zhang and Schaap (2017) Rosetta-3 without BD. The PTF of Rajkai and Varallyay (1992) had the lowest RMSE, making it the most accurate for this moisture range.

As the pressure potential decreases (0.1 - 0.33 bar), the estimation error increases for all PTFs except the Rajkai and Varallyay (1992) PTF, which continues to perform well. Furthermore, it is the only PTF that maintains good agreement with laboratory data in the dry range (0.7 - 3 bar), while all the others show significant discrepancies.

At very dry conditions (6 - 15 bar), the performance of several PTFs improves again and the Rajkai and Varallyay (1992) PTF is no longer the best, although it remains reasonably accurate. In this range, the most accurate results come from the PTF Gupta and Larson (1979).

Given the above, it is not surprising that the results for the Rajkai and Varallyay (1992) PTFs are the best PTF when all the pressure heads are considered together (column 'All pot.' of Table 10).

Table 10. RMSE values obtained by comparing the measured water contents at the different potentials with the corresponding estimations of the water retention curve provided by the PTF. The 'Type' column shows the parametric curve obtained from the PTF outputs: B&C stands for Brooks and Corey, vG stands for van Genuchten. Underlined values represent the best performing PTFs, bold ones produce values close to the best one (difference ≤ 0.01).

Reference		RMSE				
	Type	All pot	Very wet	Wet	Dry	Very dry
Campbell-Shiosawa (1992)	B&C	0.081	**0.060**	0.080	0.118	**0.070**
Gupta-Larson (1979)	vG	0.082	0.068	0.094	0.111	**0.061**
Mayr-Jarvice (1999)	B&C	0.213	0.186	0.268	0.256	0.158
Oostervel-Chang (1980)	B&C	0.086	0.075	0.095	0.112	**0.068**
Rajkai-Varallyay (1992)	vG	**0.067**	**0.053**	**0.063**	**0.066**	0.081
Rawls et al. (1982)	vG	0.093	**0.062**	0.095	0.140	0.078
Rawls et al. (1983)	vG	0.102	0.072	0.113	0.147	0.079
Rawls-Brakensiek (1985)	B&C	0.108	0.073	0.122	0.156	0.085

Saxton et al. (1986)	B&C	0.097	0.070	0.101	0.139	0.082
Tomasella-Hodnett (1998)	vG	0.094	0.092	0.094	0.124	**0.070**
Ungaro et al. (2005)	vG	0.111	0.071	0.103	0.147	0.123
Varallyay et al. (1982)	vG	0.123	0.116	0.133	0.155	0.099
Vereecken et al. (1989)	vG	0.114	0.114	0.141	0.132	0.072
Williams et al. (1992) - Eq. 2	B&C	0.084	**0.062**	0.087	0.123	0.069
Williams et al. (1992) - Eq. 1	B&C	0.120	0.100	0.142	0.158	0.090
Wösten et al. (1999)	vG	0.094	0.069	0.102	0.131	0.079
Wösten et al. (1999) - b	vG	0.103	0.077	0.109	0.147	0.085
Wösten et al. (1999) - c (Hypress)	vG	0.094	0.074	0.101	0.133	0.075
Zhang-Schaap (2017) (NoBD)	vG	0.090	**0.063**	0.084	0.137	0.080
Zhang-Schaap (2017) (BD)	vG	0.109	0.097	0.118	0.147	0.084

When the dataset is divided by horizon type (topsoil, hardpan and subsoil), the results are generally consistent with those obtained for the full sample set: the most and least accurate PTFs remain largely unchanged, and performance tends to decrease at intermediate pressure heads. However, there are some notable differences.

Topsoil is a critical layer in paddy soils as it supports the majority of rice root development and plays a vital role in sustaining plant growth, particularly in rice systems during dry periods or when applying water-saving techniques. In such conditions, it is crucial to ensure sufficient soil water content in the topsoil to avoid drought stress and yield loss (Chen et al., 2023). For this reason, accurately estimating the soil water retention curve in this zone is particularly important, especially within the wet range where rice is expected to thrive. Several PTFs performed well at higher water contents (from saturation to field capacity). In addition to the models already identified as accurate for the full dataset, the PTF of Ungaro et al. (2005) also demonstrated good performance in the very wet range. However, as pressure heads decrease and the soil becomes drier, the accuracy of most models decreases. The PTF of Rajkai and Varallyay (1992) remains the only reliable option for drier conditions.

For the hardpan, overall errors are significantly lower compared to other horizons, suggesting that this layer is well represented by most PTFs. The PTFs Zhang and Schaap (2017) (Rosetta-3 with BD) and Oosterveld and Chang (1980) stands out in this case for their consistent accuracy across all pressure ranges, despite their poor performance in other horizons. The PTF model by Rajkai and Varallyay (1992) also remains one of the most accurate, confirming its overall robustness across different soil layers.

Coming to the subsoil, the performance of the PTFs is similar to that observed for the entire dataset. Rajkai and Varallyay (1992) remains the most accurate model, albeit with slightly reduced performance. However, at very dry potentials, PTF of Gupta and Larson (1979) outperforms the others and replaces PTF of Zhang and Schaap (2017) (Rosetta-3 without BD) as one of the best performing models for this horizon.

4.5.2.1 PTFs of Rajkai and Varallyay (1992)

The Rajkai and Varallyay (1992) is the PTF model performing best among those analyzed. It consists of ten equations, shown in Table 11. These equations estimate soil water content at different pressure heads, thus a calibration step is required to derive the retention curve parameters.

This PTF is implemented in the CalcPTF package, published by USDA. The package automatically calibrates the van Genuchten parameters using the following inputs: sand, silt, clay, bulk density (BD) and organic matter (OM).

Table 11. Equations of the Rajkai and Varallyay PTF (1992).

Water potential (cm H_2O)	***Equation***
0	89.75-31.39·BD+0.03·BD·Si
2.5	85.05-27.17·BD-0.024·BD·Si
10	78.58-23.94·BD-0.025·BD·Si
32	69.78-21.74·BD +0.0011· $(Cl+Si)^2$
100	40.39 +0.61·Sa-0.432·Sa·BD-0.0015·Sa^2
200	38.62-0.00479·Sa^2/Si-0.0019·Sa^2 +0.0031·$(Sa/Si)^2$
501	20.87 +0.29·(Cl+Si)-0.83·(Sa/Si) +0.03·(Cl+Si)·(Sa/Si) +0.0051· $(Sa/Si)^2$
2512	2.19 +0.52·(Cl+Si) +3.93·OM-0.07·(Cl+Si)·OM
15849	1.39 +0.36·(Cl+Si) +0.22·OM^2
1258925	0.73 +0.32·OM +0.0018·Cl^2

Figure 58 shows boxplots of the PTFs estimation errors for each matric potential. Only the four PTFs with the best performance are shown, and only for the topsoil samples. This visualisation allows the accuracy of each PTF to be compared directly across different pressure head ranges. It highlights both the average error and the variability of the estimates. Error is typically large for intermediate water potential values, where the PTFs underestimate the measured water content. As shown in Figure 58, the Rajkai and Varallyay (1992) model performs better than the other PTFs tested across the entire range of soil water potentials.

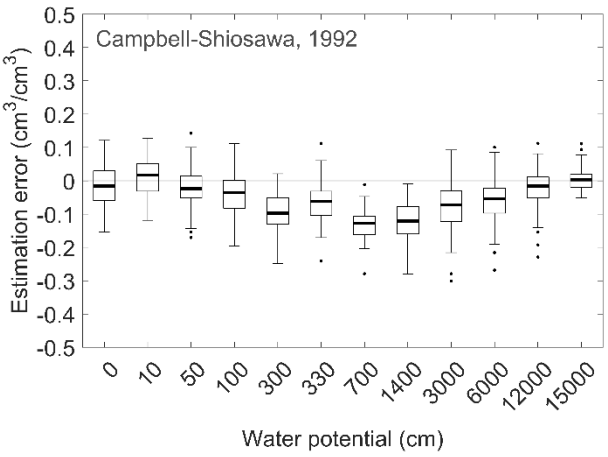
Campbell-Shiosawa, 1992
Estimation error (cm3/cm3)
0.5
0.4
0.3
0.2
0.1
0
-0.1
-0.2
-0.3
-0.4
-0.5
0
10
50
100
300
330
700
1400
3000
6000
12000
15000
Water potential (cm)

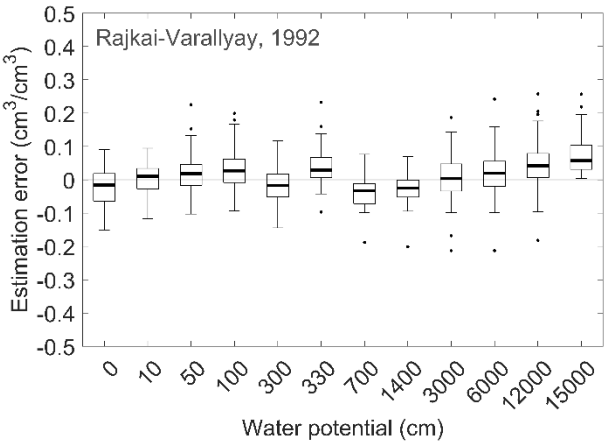
Rajkai-Varallyay, 1992
Estimation error (cm3/cm3)
0.5
0.4
0.3
0.2
0.1
0
-0.1
-0.2
-0.3
-0.4
-0.5
0
10
50
100
300
330
700
1400
3000
6000
12000
15000
Water potential (cm)

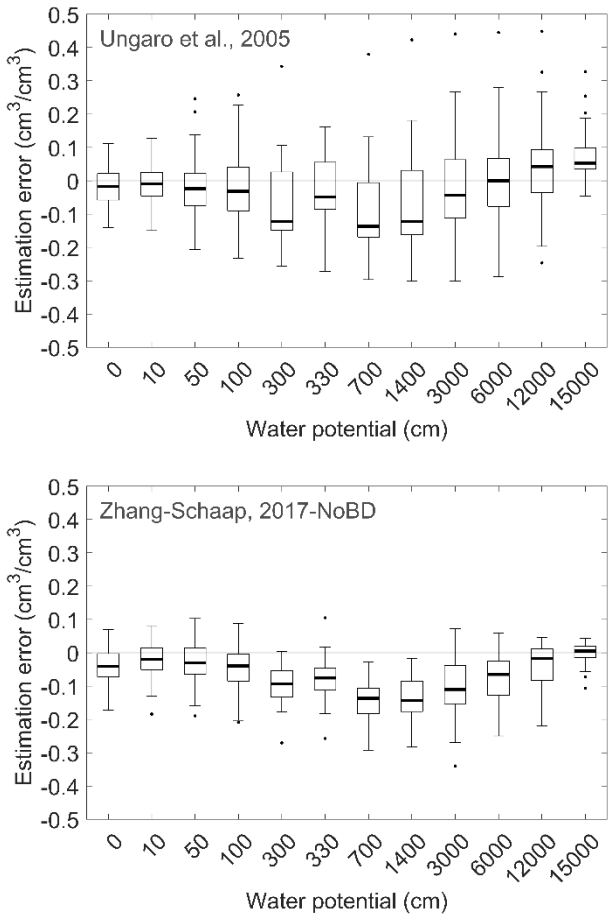

Figure 58. Box plots of the estimation error of soil water potential for all measured values for the better performing PTFs.

4.5.3 Soil Hydraulic Conductivity

Only a subset of the 55 PTFs functions tested for the hardpan Ks is presented in Table 12. As expected, most of the PTFs tested in this study showed very poor predictive performance, so the PTFs presented here were selected for having the following criteria met: only positive estimations of Ks and an RMSE smaller than 10 cm/d (which is quite high having in our database a maximum measured Ks of 1.02 cm/d).

The performance is so poor that all the literature PTFs produced negative model efficiency (ME) values, indicating that the variability of the estimation error was greater than the variability of the measured Ks values. This highlights the general inadequacy of literature PTFs in properly handling the hardpan Ks.

However, a few PTFs performed slightly better, including those by Ottoni et al. (2019, Eq. 4), Nemes et al. (2005), Mayer et al. (2019), Jabro (1992), Wösten et al. (2001-b) and Zou et al. (2016). It is worth highlighting that the scaled version of the PTF by Mayer et al. (2019) is an improvement on the original PTF by Ungaro et al. (2005), which is not included in the table due to a very high RMSE. However, Mayer et al. (2019) only scales the values of the original PTF providing the typical range of Ks values measured in paddy soil hardpans, without increasing the correlation between measured and estimated values.

Notably, the model proposed by Aimrun and Amin (2009) did not outperform the better generic PTFs, despite being developed specifically for Malaysian rice soils, and ranked among the intermediate-performing functions. Conversely, the impressive statistics reported by Ottoni et al. (2019) are only due to a significant and consistent underestimation of the values, resulting in a strong negative bias and low RMSE. The same observation can be made for some other PTFs exhibiting negative bias.

Table 12. Selection of the better performing PTFs for the hardpan Ks estimation. Input data are: sand (Sa), silt (Li), clay (Ar), organic carbon (CO), bulk density (BD) and volumetric water content at given water potentials (Theta). The number of valid estimates (n) differs among PTFs due to limitations in their applicability to certain textural classes or validity ranges, which led to the exclusion of some soil horizons in the case of certain PTFs.

Reference	***Bias***	***RMSE***	***ME***	***n***	***Input***
Ahuja (1989)	-0.221	0.340	-0.726	22	Theta
Aimrun-Amin (2009)	2.458	2.907	< -100	22	Sa, Si, Cl, OC, BD, Theta
Arshad et al. (2009)	2.215	3.040	< -100	22	Sa, Si, Cl, BD
Campbell-Shiozawa (1992)	4.292	6.436	< -100	22	Sa, Si, Cl
Jabro (1992)	**0.440**	**0.809**	**-8.79**	22	Sa, Si, Cl, BD
Julia et al. (2004) - Tab. 3, 1 par	2.588	3.676	< -100	15	Sa, Si, Cl
Li (2007) - Tab. 6	2.104	4.002	< -100	22	Sa, Si, Cl, OC, BD
Mayer et al. (2019)	**0.295**	**0.729**	**-6.94**	22	Sa, Si, Cl, OC, BD
Nemes et al. (2005)	**0.331**	**0.607**	**-4.51**	22	Sa, Si, Cl, OC, BD
Ottoni et al. (2019) - Eq. 1	-0.215	0.336	-0.690	22	Theta
Ottoni et al. (2019) - Eq. 4	**-0.194**	**0.326**	**-0.59**	22	Sa, Si, Cl, BD
Patil et al. (2009) - Eq. 3	4.115	4.359	< -100	22	Sa, Si, Cl, BD, Theta
Patil et al. (2009) - Eq. 4	3.740	3.975	< -100	22	Sa, Si, Cl, BD, Theta
Spychalski et al. (2007) - Eq. 9	2.579	3.350	< -100	11	Theta
Spychalski et al. (2007) - Eq. 10	1.904	2.717	-87.8	10	Theta
Suleiman-Ritchie (2001) - Eq. from Fig. 4, with h = 100	1.178	2.700	< -100	22	Theta
Suleiman-Ritchie (2001) - Eq. from Fig. 5	1.707	4.949	< -100	22	Theta
Timlin et al. (1999)	-0.226	0.344	-0.763	22	Theta
Vereecken et al. (1990) - Eq. Level 1, Tab. 4	4.996	7.941	< -100	22	Sa, Si, Cl, OC, BD
Wösten et al. (2001) - b	**0.492**	**0.818**	**-8.99**	22	Sa, Si, Cl, OC, BD
Wösten (1999)	2.110	2.187	-70.49	22	Sa, Si, Cl, OC, BD
Zou et al. (2016)	**0.900**	**1.960**	**-56.4**	22	Sa, Si, Cl, BD

Figure 59 shows scatter plots comparing the estimated and measured Ks values of some of the best-performing PTFs, alongside the models developed by Zou et al. (2016) and Aimrun and Amin (2009), which were specifically developed for paddy soils.

The graphs generally show an overestimation of Ks, with the x-coordinates generally being larger than the y-coordinates. This is particularly evident in the models by Aimrun and Amin (2009) and Nemes et al. (2005). However, the latter has some estimations quite close to the bisectrix, where the estimated values are close to the measured ones. The estimations of Mayer et

al. (2019) are well centered, with some values close to the bisectrix. Zou et al. (2016) perform comparably to the best models, but with a few overestimated outliers.

On the other hand, it should be noted that none of the presented PTFs show a good correlation between the measured values and the estimations, as this would result in some grouping of the data points around the bisectrix, particularly for higher estimated and measured Ks values. This means that the estimates of the tested PTFs cannot be considered reliable and representative of the true hardpan Ks values.

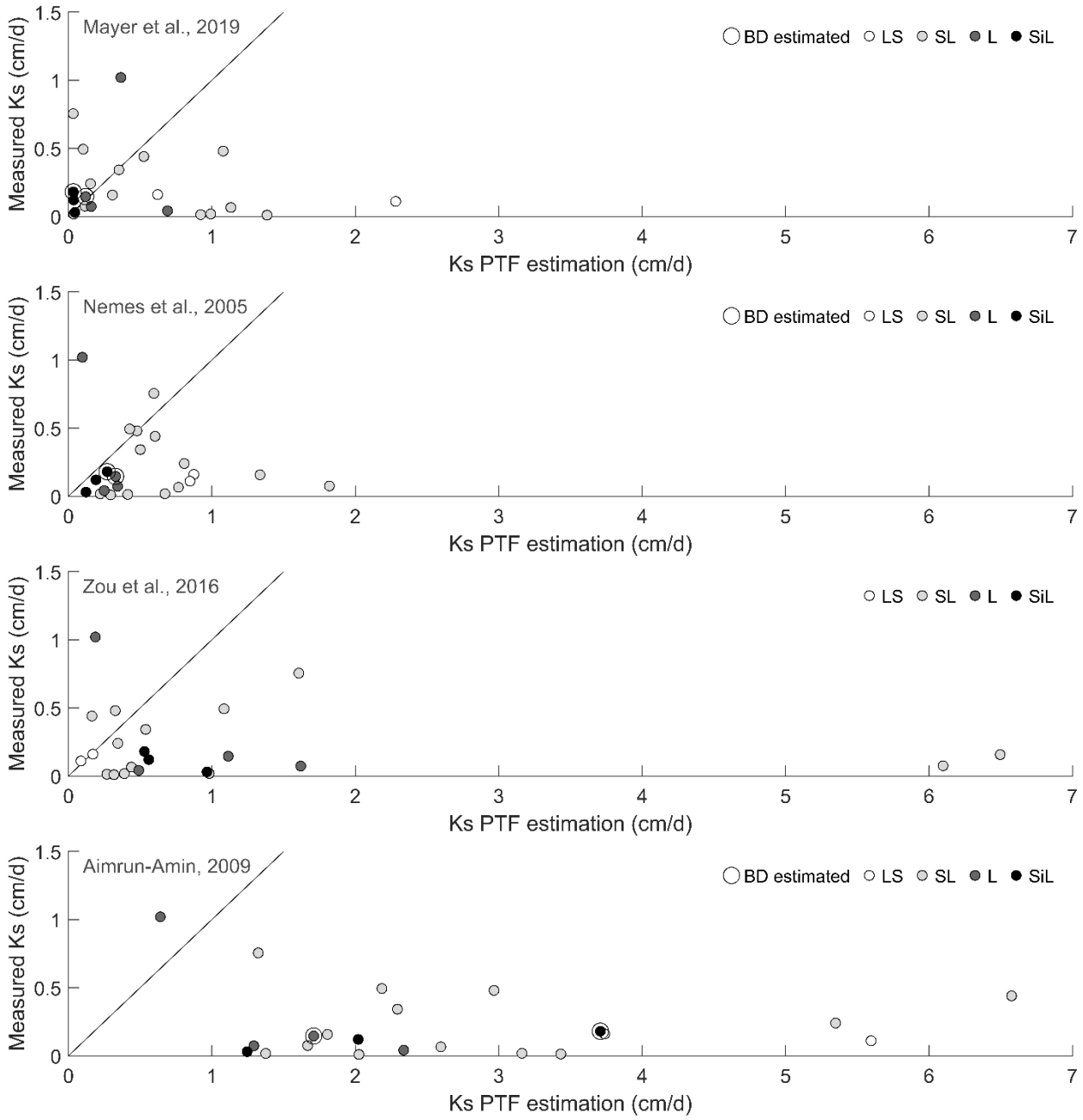

Figure 59. Scatter plots of the measured vs estimated Ks of the hardpan for some of the PTFS that perform well, as well for two specifically developed for paddy soils. The colors of the circles represent the texture classes of the sampled horizons. The large circles show soils for which bulk density was estimated using the modified PTF Kaur method (mod3).

4.5.3.1 Novel PTFs and analysis of log-transformed data

To address the limitations of literature-based PTFs when estimating Ks, we investigated several strategies for improving the accuracy of predictions. These include the application of correction factors, ensemble modelling techniques, the use of averages for specific texture classes and the development of a continuous PTF based on available data.

Among these approaches, we consider the PTF developed here and reported in Eq. 24 (cm/d), to be the most effective and reliable method of estimating Ks for the hardpan of the Lomellina paddy soils.

$$Ks = \exp(0.0571 \cdot \mathrm{Si} - 0.3560 \cdot \mathrm{Cl}) \quad \text{(Eq. 24)}$$

This PTF was calibrated using the MATLAB fitlm function (Statistics and Machine Learning Toolbox applied to log-transformed data) on a dataset comprising 22 measured Ks values of paddy soil hardpans included in the database.

The performance statistics of Eq. 24 are reported in Table 13, alongside the PTFs form the literature that give the best results. A possible outlier in the dataset (a loam soil sample with Ks = 1.02 cm/d; Figure 59) has been removed, in order to obtain a more reliable estimation of the PTFs performance. Additionally, the values of bias, RMSE, ME are reported together with the same statistics computed on the log-transformed Ks values, labelled as '-L'. These last metrics allow multiplicative errors (e.g., an underestimation by a factor of 10) to be assessed in terms of their magnitude, thus improving comparability across a wide range of Ks values. This approach reveals significant differences in PTF behaviour, particularly at lower Ks values.

Table 13. Performance metrics (Bias, RMSE, ME) and their counterparts computed on the log-transformed values of Ks (Bias-L, RMSE-L, ME-L); a possible outlier was excluded.

Riferimento	*Bias*	*RMSE*	*ME*	*Bias-L*	*RMSE-L*	*ME-L*
Aimrun-Amin (2009)	2.59	2.97	< -100	1.90	1.49	-0.42
Eq. 24 (Li, Ar)	**-0.07**	**0.21**	**-0.11**	**-1.31**	**0.49**	**0.85**
Jabro (1992)	0.50	0.81	-15.87	0.34	0.92	0.46
Mayer et al. (2019)	0.34	0.73	-12.86	-0.39	0.98	0.39
Nemes et al. (2005)	0.39	0.59	-7.94	0.25	0.86	0.53
Ottoni et al. (2019) - Eq. 4	-0.16	0.25	-0.64	-2.55	0.78	0.61
Wösten et al. (2001) - b	0.56	0.81	-16.10	0.28	0.94	0.44
Zou et al. (2016)	0.98	2.00	< -100	0.52	1.05	0.30

As expected, the novel PTF based on the dataset as a continuous function of silt and clay contents provide the best statistical values with an ME close to zero (i.e. the variability in the error is no longer overwhelming, but close to the variability of the data). The RMSE is quite small in both natural and log scales, and the ME-L statistic is quite high (0.85).

Compared to PTFs in the literature, the performance of the PTF of Eq. 24 is outstanding and may provide reliable Ks estimations. Because the dataset is currently very small, validation has not been conducted yet; however, this crucial step will be carried out once additional data becomes available. Figure 60 shows the scatter plots of the novel PTF, in both natural and log scales. The datapoints are aligned along the bisectrix, particularly in the log-transformed panel.

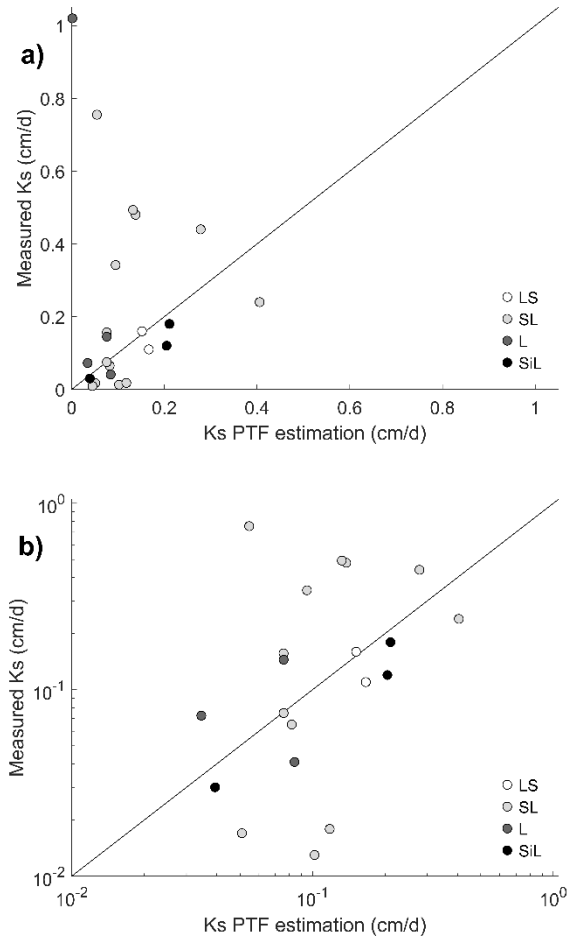

Figure 60. PTF reported in Eq. 24: (a) scatter plot on the natural scale; (b) scatter plot on the logarithmic scale. The colors of the circles represent the texture classes of the sampled horizons. In panel (a) is shown the outlying datapoint discussed in the text (y 1.02 cm/d, on the y axes)

4.5.4 Application of the Selected PTFs to the Lomellina Soil Profiles

A final test on the validity of the chosen PTFs was made by applying the selected functions to the regional dataset of soil profiles available for the Lomellina area, obtained from the regional Soil Map 1:50,000 and the LOSAN soil database. Table 14 shows the descriptive statistics of the main physical and hydraulic soil properties measured in the laboratory, while Table 15 illustrates the descriptive statistics of the main physical and hydraulic soil properties estimated with the selected PTFs for the entire Lomellina regional dataset.

The results are highly comparable, given that the parameters measured and estimated are similar, which is encouraging. For bulk density (BD) and saturated soil water content (θs), the results in Table 14 show strong agreement with those in Table 15, which was somehow expected given the excellent performance of the PTFs in estimating BD and soil water retention parameters. However, in cases where the regional database contains extreme values not adequately represented in the sample database, the accuracy of PTF estimation is difficult to judge (this is the case, for instance, with peat soils, which lead to high maximum values of Ks in Table 15 that have no equivalent in Table 14).

Conversely, agreement on Ks was poorer. Strong discrepancies can also be observed in the maximum and minimum Ks values in the measured and estimated datasets (see Tables 14 and 15). On the one hand, this calls into question the reliability of this PTF that was built using a very small dataset, which, however, represents one third of the total number of hardpans in the soil units in the district. On the other hand, this result could be due to the higher proportion of finer soils in the sample database, which was intended to represent all the main soil types in the Lomellina district, but leading to larger Ks values being computed for the regional database.

Table 14. Descriptive statistics of the main physical and hydraulic soil properties measured in the laboratory for the paddy soils from the Lomellina area. θs is the saturated volumetric water content. For each variable, the number of samples (N), minimum, maximum, mean, and coefficient of variation (CV) are reported.

Variable	***Size***	***Min***	***Mean***	***Max***	***CV (%)***
Sand (%)	170	3	57	99	44
Silt (%)	170	0	32	85	66
Clay (%)	170	0	11	27	56
OC (%)	170	0	1	30	353
BD (g/cm^3)	130	0.21	1.54	1.96	14
θs (cm^3/cm^3)	76	0.30	0.43	0.56	14
Ks (cm/d) $_{hardpan}$	22	**0.009**	**0.23**	**1.02**	117

Table 15. Descriptive statistics of the main physical properties in the regional databases and the hydraulic soil properties estimated by applying the selected PTFs. θs is the saturated volumetric water content. For each variable, the number of samples (N), minimum, maximum, mean, and coefficient of variation (CV) are reported.

Variable	***Size***	***Min***	***Mean***	***Max***	***CV (%)***
Sand (%)	301	2	68	99	35
Silt (%)	301	0	24	79	76
Clay (%)	301	0	8	46	91
OC (%)	301	0	1	32	263
BD (g/cm^3)	301	0.21	1.47	1.93	15
θs (cm^3/cm^3)	301	0.29	0.44	0.82	15
Ks (cm/d) $_{hardpan}$	66	**0.001**	**0.45**	**4.32**	153

In any case, most PTFs found in the literature for the estimation of Ks fail to capture even the correct order of magnitude for Ks (Table 16), with evident outliers produced by the PTFs of Aimrun and Amin (2009), Zou et al. (2016), Jabro (1992), Wösten et al. (2001-b), which also often show rather high median values. Conversely, Ottoni et al. (2019) greatly underestimate the measured values. Instead, the novel PTF suggested in this paper, the PTF Mayer et al. (2019) and, to some extent, the PTF Nemes et al. (2005), closely match the magnitude of the measured Ks data. However, ME values (Table 13) of the PTF of Eq. 24 and those of Mayer et al. (2019) and Nemes et al. (2005) indicate that the estimations of these three PTFs should be treated with caution.

Table 16. Statistics of the Ks values estimated by the PTFs for the Lomellina hardpans (66 values) and those coming from the dataset of measurements (22).

PTF & meas.	*min*	*median*	*mean*	*max*
Measures	**0.009**	**0.13**	**0.23**	**1.02**
Aimrun 2009	1.023	3.54	8075.85	524538.18
Jabro 1992	0.209	1.34	60.78	3867.59
Mayer 2019	0.030	0.09	0.49	5.82
Nemes 2005	0.000	0.84	1.09	4.62
Ottoni 2019	0.012	0.05	0.05	0.28
Eq. 24 (Li, Ar)	**0.001**	**0.30**	**0.45**	**4.32**
Wösten 2001 - b	0.000	0.51	12.06	742.24
Zou 2016	0.000	0.94	348.26	21506.05

4.6 Conclusions

This study evaluates various literature PedoTransfer functions (PTFs) to identify those that are better suited to estimating the bulk density (BD) of paddy soils in the Lomellina district (the largest rice-growing area in northern Italy), as well as the soil water retention curve parameters and the saturated hydraulic conductivity (Ks) of hardpans.

Twenty-one PedoTransfer functions were tested to estimate BD of paddy soils. This was assessed using two different approaches. Firstly, the full dataset of 130 samples was used. Secondly, the dataset was divided according to soil horizon type: topsoil, hardpan, and subsoil. The analysis revealed that the Kaur (mod3) model outperforms the literature PTFs. This model is based on the work of Kaur et al. (2002) and has been modified with an additive constant calibrated on the dataset. The value of this constant depends on the type of soil horizon. This model is recommended for use with Lomellina paddy soils when the position of the soil horizon is known. If this information is unavailable, an alternative is the Kaur (mod) model, which is modified with a general additive constant. Both models require silt, clay and organic carbon content as input variables.

Of the twenty PTFs evaluated for the water retention curve, the Rajkai and Varallyay (1992) function was found to be the most robust and accurate across all soil horizons (topsoil, hardpan, and subsoil) and water potential ranges (from 0 to -15,000 cm). Although its performance decreased slightly under very dry conditions, it remained the most reliable option. The PTF estimates water content at ten predefined pressure heads using sand, silt, clay, bulk density and organic carbon as input. These estimated water contents are then used in a calibration step to derive the van Genuchten model parameters. This process is implemented in the USDA CalcPTF spreadsheet tool (Guber and Pachepsky, 2010), which automates the calibration of the van Genuchten retention curve. This PTF is strongly recommended for Lomellina soils, although its multi-equation structure (i.e., one equation for each pressure head) and the need to operate through the CalcPTF package can make it challenging to use.

The Ks of the hardpan horizon is critical for paddy field hydrology as it controls the rate at which water percolates vertically and helps maintain the ponded water level characteristic of flooded paddies. Of the fifty-five PTFs tested in the literature, nearly all give unreliable and biased estimates, highlighting their general inadequacy in capturing the hydraulic behaviour of clogged

and compacted horizons. This is also true for the two PTFs based on Asian paddy field soils. Even the best models proposed by Nemes et al. (2005) and Mayer et al. (2019) only offered limited improvement, with root mean square error (RMSE) values of 0.61 and 0.73 cm/d, respectively. These values are very large compared to the mean of the measured Ks values (0.23 cm/d). To achieve a better result, this study developed a novel PTF (Eq. 24), which gives an RMSE of 0.21 cm/d and good model efficiency when computed on log-transformed values (ME-L = 0.85). It requires silt and clay percentages as input variables. Despite being developed using a limited dataset (twenty-one data points), we recommend its use to estimate Ks for paddy field hardpans in the Lomellina area, as it substantially outperforms the other available alternatives.

In summary, reliable PTFs have been identified to describe BD and soil water retention curve for the Lomellina paddy fields. Further research on the Ks of their hardpans is essential to validate the proposed PTF or develop a new model. Indeed, the ability to adequately estimate the Ks value of soil profiles is essential for understanding and modelling the hydrological dynamics of paddy fields, especially at large spatial scales.

4.7 Appendices

References of the PTFs applied for bulk density estimation.

N	References
1	Benites, V.M., Machado, P.L.O.A., Fidalgo, E.C.C., Coelho, M.R., Madari, B.E., 2007. Pedotransfer functions for estimating soil bulk density from existing soil survey reports in Brazil. Geoderma 139, 90–97. https://doi.org/10.1016/j.geoderma.2007.01.005
2	Dexter, A.R., 2004. Soil physical quality. Geoderma 120, 201–214. https://doi.org/10.1016/j.geoderma.2003.09.004
3	Hollis 1996: Hannam, J. A., Hollis, J. M., Jones, R. J. A., Bellamy, P. H., Hayes, S. E., Holden, A., Van Liedekerke, M. H., & Montanarella, L. (2009). SPADE-2: The Soil Profile Analytical Database for Europe, Version 2.0 Beta Version March 2009 (Unpublished report, 27 pp.).
4	Hollis, J.M., Hannam, J., Bellamy, P.H., 2012. Empirically-derived pedotransfer functions for predicting bulk density in European soils. European J Soil Science 63, 96–109. https://doi.org/10.1111/j.1365-2389.2011.01412.x Eq. a, Eq. b
5	Kaur, R., Kumar, S., Gurung, H.P., 2002. A pedo-transfer function (PTF) for estimating soil bulk density from basic soil data and its comparison with existing PTFs. Soil Res. 40, 847. https://doi.org/10.1071/SR01023
6	Leonaviciute, N., 2000. Predicting soil bulk and particle densities by pedotransfer functions from existing soil data in Lithuania. Geografijos Metrastis 33, 317-330.
7	Manrique, L.A., Jones, C.A., 1991. Bulk Density of Soils in Relation to Soil Physical and Chemical Properties. Soil Science Society of America Journal 55, 476. https://doi.org/10.2136/sssaj1991.03615995005500020030x
8	Mayer, A., Rienzner, M., Cesari De Maria, S., Romani, M., Lasagna, A., Facchi, A., 2019. A Comprehensive Modelling Approach to Assess Water Use Efficiencies of Different Irrigation Management Options in Rice Irrigation Districts of Northern Italy. Water 11, 1833. https://doi.org/10.3390/w11091833
9	Men, M. X., Peng, Z. P., Hao, X., Yu, Z. R., 2008. Investigation on Pedotransfer function for estimating soil bulk density in Hebei province. Chin. J. Soil Sci., 1, 20.
10	Patil, N.G., Chaturvedi, A., 2012. Estimation of bulk density of waterlogged soils from basic properties. Archives of Agronomy and Soil Science 58, 499–509. https://doi.org/10.1080/03650340.2010.530254 Eq. a, Eq. b, Eq. c
11	Rawls, W.J., 1983. Estimating soil bulk density from particle size analysis and organic matter content. Soil Science 135, 123–125. https://doi.org/10.1097/00010694-198302000-00007
12	Rawls, W.J., Nemes, A., Pachepsky, Ya., 2004. Effect of soil organic carbon on soil hydraulic properties, in: Developments in Soil Science. Elsevier, pp. 95–114. https://doi.org/10.1016/S0166-2481(04)30006-1

13 Tomasella, J., Hodnett, M.G., 1998. ESTIMATING SOIL WATER RETENTION CHARACTERISTICS FROM LIMITED DATA IN BRAZILIAN AMAZONIA. Soil Science 163, 190–202. https://doi.org/10.1097/00010694-199803000-00003

14 Tranter, G., Minasny, B., Mcbratney, A.B., Murphy, B., Mckenzie, N.J., Grundy, M., Brough, D., 2007. Building and testing conceptual and empirical models for predicting soil bulk density. Soil Use and Management 23, 437–443. https://doi.org/10.1111/j.1475-2743.2007.00092.x Eq. a, Eq. b

15 Wang, Y., Shao, M., Liu, Z., Zhang, C., 2014. Prediction of Bulk Density of Soils in the Loess Plateau Region of China. Surv Geophys 35, 395–413. https://doi.org/10.1007/s10712-013-9249-8

References of the PTFs applied for the estimation of water retention curve parameters.

N	References
1	Campbell, G.S., Shiozawa, S., 1992. Prediction of hydraulic properties of soils using particle size distribution and bulk density data. p. 317–328. In M.Th. van Genuchten et al (ed.) Proc. Int.Workshop on Indirect Methods for Estimating the Hydraulic Properties of Unsaturated Soils. University of California, Riverside
2	Gupta, S.C., Larson, W.E., 1979. Estimating soil water retention characteristics from particle size distribution, organic matter percent, and bulk density. Water Resources Research 15, 1633–1635. https://doi.org/10.1029/WR015i006p01633
3	Mayr, T., Jarvis, N.J., 1999. Pedotransfer functions to estimate soil water retention parameters for a modified Brooks–Corey type model. Geoderma 91, 1–9. https://doi.org/10.1016/S0016-7061(98)00129-3
4	Oosterveld, M., Chang, C., 1980. EMPIRICAL RELATIONS BETWEEN LABORATORY DETERMINATIONS OF SOIL TEXTURE AND MOISTURE RETENTION. Can. Agric. Eng. 22:149–151.
5	Rajkai, K., Varallyay G., 1992. Estimating soil water retention from simpler properties by regression techniques. p. 417–426. In M.Th. van Genuchten et al. (ed.) Proc. Int. Workshop on Indirect Methods for Estimating the Hydraulic Properties of Unsaturated Soils. University of California, Riverside.
6	Rawls, W. J., Brakensiek, D. L., Saxton, K. E., 1982. Estimation of Soil Water Properties. Transactions of the ASAE 25, 1316–1320. https://doi.org/10.13031/2013.33720
7	Rawls, W.J., D. L. Brakensiek, B. Soni, 1983. Agricultural Management Effects on Soil Water Processes Part I: Soil Water Retention and Green and Ampt Infiltration Parameters. Transactions of the ASAE 26, 1747–1752. https://doi.org/10.13031/2013.33837
8	Rawls, W.J., Brakensiek, D.L., 1985. Prediction of soil water properties for hydrologic modeling. p. 293–299. In E.B. Jones and T.J.Ward (ed.) Proc. Symp.Watershed Management in the Eighties, Denver, CO. 30 Apr.–1 May 1985. Am. Soc. Civil Eng., New York.
9	Saxton, K.E., Rawls, W.J., Romberger, J.S., Papendick, R.I., 1986. Estimating Generalized Soil-water Characteristics from Texture. Soil Science Soc of Amer J 50, 1031–1036. https://doi.org/10.2136/sssaj1986.03615995005000040039x
10	Tomasella, J., Hodnett, M.G., 1998. ESTIMATING UNSATURATED HYDRAULIC CONDUCTIVITY OF BRAZILIAN SOILS USING SOIL-WATER RETENTION DATA. Soil Science 163, 190–202. https://doi.org/10.1097/00010694-199803000-00003
11	Ungaro, F., Calzolari, C., Busoni, E., 2005. Development of pedotransfer functions using a group method of data handling for the soil of the Pianura Padano–Veneta region of North Italy: water retention properties. Geoderma 124, 293–317. https://doi.org/10.1016/j.geoderma.2004.05.007
12	Varallyay, G., Rajkai K., Pachepsky, Yaa., Shcherbakov, R.A., 1982. Mathematical description of soil water retention curve. (In Russian.) Pochvovedenie 4:77–89.
13	Vereecken, H., Maes, J., Feyen, J., Darius, P., 1989. ESTIMATING THE SOIL MOISTURE RETENTION CHARACTERISTIC FROM TEXTURE, BULK DENSITY, AND CARBON CONTENT. Soil Science 148, 389–403. https://doi.org/10.1097/00010694-198912000-00001
14	Williams, J., Ross, P., Bristow, K., 1992. Prediction of the Campbell water retention function from texture, structure, and organic matter.p. 427–442. In M.Th. van Genuchten et al (ed.) Proc. Int.Workshop on Indirect methods for Estimating the Hydraulic Properties of Unsaturated Soils. University of California, Riverside. Eq. 1, Eq. 2
15	Wösten, J.H.M., Lilly, A., Nemes, A., Le Bas, C., 1999. Development and use of a database of hydraulic properties of European soils. Geoderma 90, 169–185. https://doi.org/10.1016/S0016-7061(98)00132-3 Eq. b, Eq. c

16 Zhang, Y., Schaap, M.G., 2017. Weighted recalibration of the Rosetta pedotransfer model with improved estimates of hydraulic parameter distributions and summary statistics (Rosetta3). Journal of Hydrology 547, 39–53. https://doi.org/10.1016/j.jhydrol.2017.01.004

References of the PTFs applied for saturated hydraulic conductivity estimation.

N	References
1	Ahuja, L.R., Cassel, D.K., Bruce, R.R., Barnes, B.B., 1989. Evaluation of spatial distribution of hydraulic conductivity using effective porosity data. Soil Sci. 148, 404–411.
2	Aimrun, W., Amin, M.S.M., 2009. Pedo-transfer function for saturated hydraulic conductivity of lowland paddy soils. Paddy Water Environ 7, 217–225. https://doi.org/10.1007/s10333-009-0165-y
3	Arshad, R.R., Sayyad, Gh., Mosaddeghi, M., Gharabaghi, B., 2013. Predicting Saturated Hydraulic Conductivity by Artificial Intelligence and Regression Models. ISRN Soil Science 2013, 1–8. https://doi.org/10.1155/2013/308159
4	Brakensiek, D.L., Rawls, W.J., Stephenson, G.R., 1984. Modifying SCS Hydrologic Soil Groups and Curve Numbers for Rangeland Soils, ASAE Paper No. PNR-84-203, St. Joseph.
5	Campbell, G.S., 1985. Soil physics with BASIC: Transport models for soil-plant systems. Development in Soil Science 14, Elsevier Science Publishers B. V., Amsterdam Netherlands, p 150.
6	Campbell, G.S., 1985. Soil physics with basic: transport models for soil-plant systems. Development in Soil Science 14, Elsevier Science Publishers B. V., Amsterdam Netherlands, p 150.
7	Campbell, G. S., Shiozawa, S., 1992. Prediction of hydraulic properties of soils using particle-size distribution and bulk density data. In van Genuchten M T, Leij F J, Lund L J (eds.) Proceedings of International Workshop on Indirect Methods for Estimating the Hydraulic Properties of Unsaturated Soils. University of California, Riverside. pp. 317–328
8	Cosby, B.J., Hornberger, G.M., Clapp, R.B., Ginn, T.R., 1984. A Statistical Exploration of the Relationships of Soil Moisture Characteristics to the Physical Properties of Soils. Water Resources Research 20, 682–690. https://doi.org/10.1029/WR020i006p00682 Eq. 1, Eq. 2
9	Dane, J.H., Puckett, W., 1994. Field soil hydraulic properties based on physical and mineralogical information. Proc. Int. Work. Indirect methods Estim. Hydraul. Prop. unsaturated soils. Univ. California, Riverside, p. 389–403.
10	Jabro, J. D., 1992. Estimation of Saturated Hydraulic Conductivity of Soils From Particle Size Distribution and Bulk Density Data. Transactions of the ASAE 35, 557–560. https://doi.org/10.13031/2013.28633
11	Julià, M.F., Estrela Monreal, T., Sánchez Del Corral Jiménez, A., García Meléndez, E., 2004. Constructing a saturated hydraulic conductivity map of Spain using pedotransfer functions and spatial prediction. Geoderma 123, 257–277. https://doi.org/10.1016/j.geoderma.2004.02.011 Eq. 1, Eq. 2, Tab. 3 - 1 par, Tab. 3 - 3 par
12	Li, Y., Chen, D., White, R.E., Zhu, A., Zhang, J., 2007. Estimating soil hydraulic properties of Fengqiu County soils in the North China Plain using pedo-transfer functions. Geoderma 138, 261–271. https://doi.org/10.1016/j.geoderma.2006.11.018
13	Minasny, B., McBratney, A.B., 2000. Evaluation and development of hydraulic conductivity pedotransfer functions for Australian soil. SoilRes. 38:905–26.
14	Nemes, A., Rawls, W.J., Pachepsky, Y.A., 2005. Influence of Organic Matter on the Estimation of Saturated Hydraulic Conductivity. Soil Science Soc of Amer J 69, 1330–1337. https://doi.org/10.2136/sssaj2004.0055
15	Ottoni, M.V., Ottoni Filho, T.B., Lopes-Assad, M.L.R.C., Rotunno Filho, O.C., 2019. Pedotransfer functions for saturated hydraulic conductivity using a database with temperate and tropical climate soils. Journal of Hydrology 575, 1345–1358. https://doi.org/10.1016/j.jhydrol.2019.05.050 Eq. 1, Eq. 2, Eq. 3, Eq. 4
16	Patil, N.G., Rajput, G.S., Singh, R.B., Singh, S.R., 2009. Development and evaluation of pedotransfer functions for saturated hydraulic conductivity of seasonally impounded clay soils. Eq. 1, Eq. 2, Eq. 3, Eq. 4
17	Patle, G.T., Vanlalnunchhani, P.C., 2020. Pedo-Transfer Functions for Saturated Hydraulic Conductivity of Cultivated Soils in the Mid Hills of Sikkim. Current Science 118, 771. https://doi.org/10.18520/cs/v118/i5/771-777 Eq. 1, Eq. 2, Eq. 3, Eq. 4, Eq. 5

18 Puckett, W.E., Dane, J.H., Hajek, B.F., 1985. Physical and Mineralogical Data to Determine Soil Hydraulic Properties. Soil Science Soc of Amer J 49, 831–836. https://doi.org/10.2136/sssaj1985.03615995004900040008x

19 Rawls, W.J., Brakensiek, D.L., 1989. Estimation of soil water retention and hydraulic properties. USDA-ARS Hydrology Laboratory, Bldg. 007, BARC-West Beltsville, MD 20705 USA; University of Maryland, Department of Agricultural Engineering colleg Park, MD 20472 USA

20 Rawls, W.J., Gimenez, D., Grossman, R., 1998. Use of soil texture, bulk density, and slope of the water retention curve to predict saturated hydraulic conductivity. Trans. ASAE 41, 983.

21 Saxton, K.E., Rawls, W.J., Romberger, J.S., Papendick, R.I., 1986. Estimating generalized soil-water characteristics from texture. Soil Sci Soc Am J. 50: 1031–103

22 Saxton, K.E., Rawls, W.J., 2006. Soil Water Characteristic Estimates by Texture and Organic Matter for Hydrologic Solutions. Soil Science Soc of Amer J 70, 1569–1578. https://doi.org/10.2136/sssaj2005.0117

23 Shwetha, P., Prasanna, K., 2018. Pedotransfer Functions for the Estimation of Saturated Hydraulic Conductivity for Some Indian Sandy Soils. Eurasian Soil Sc. 51, 1042–1049. https://doi.org/10.1134/S1064229318090119

24 Spychalski, M., Kaźmierowski, C., Kaczmarek, Z., 2007. Estimation of saturated hydraulic conductivity on the basis of drainage porosity. Electron. J. Polish Agric. Univ. 10. Eq. 9, Eq. 10

25 Suleiman, A.A., Ritchie, J.T., 2001. Estimating saturated hydraulic conductivity from soil porosity. Trans. ASAE 44, 235. Eq. in fig.4, con h=100, Eq di fig.4, con h=330, Eq. in fig.5

26 Timlin, D.J., Ahuja, L.R., Pachepsky, Ya., Williams, R.D., Gimenez, D., Rawls, W., 1999. Use of Brooks-Corey Parameters to Improve Estimates of Saturated Conductivity from Effective Porosity. Soil Science Soc of Amer J 63, 1086–1092. https://doi.org/10.2136/sssaj1999.6351086x

27 Tomasella, J., Hodnett, M.G., 1997. Estimating unsaturated hydraulic conductivity of Brazilian soils using soil-water retention data. Soil Sci. 162, 703–712.

28 Ungaro, F., Calzolari, C., Busoni, E., 2005. Development of pedotransfer functions using a group method of data handling for the soil of the Pianura Padano–Veneta region of North Italy: water retention properties. Geoderma 124, 293–317. https://doi.org/10.1016/j.geoderma.2004.05.007

29 Vereecken, H., Maes, J., Feyen, J., 1990. ESTIMATING UNSATURATED HYDRAULIC CONDUCTIVITY FROM EASILY MEASURED SOIL PROPERTIES: Soil Science 149, 1–12. https://doi.org/10.1097/00010694-199001000-00001

30 Weynants, M., Vereecken, H., Javaux, M., 2009. Revisiting Vereecken Pedotransfer Functions: Introducing a Closed-Form Hydraulic Model. Vadose Zone Journal 8, 86–95. https://doi.org/10.2136/vzj2008.0062

31 Wösten, J.H.M., Pachepsky, Ya.A., Rawls, W.J., 2001. Pedotransfer functions: bridging the gap between available basic soil data and missing soil hydraulic characteristics. Journal of Hydrology 251, 123–150. https://doi.org/10.1016/S0022-1694(01)00464-4 Eq. a, Eq. b

32 Wösten, J.H.M., Lilly, A., Nemes, A., Le Bas, C., 1999. Development and use of a database of hydraulic properties of European soils. Geoderma 90, 169–185. https://doi.org/10.1016/S0016-7061(98)00132-3 Eq. b, Eq. c

33 Yang, Y., Jia, X., Wendroth, O., Liu, B., 2018. Estimating Saturated Hydraulic Conductivity along a South-North Transect in the Loess Plateau of China. Soil Science Soc of Amer J 82, 1033–1045. https://doi.org/10.2136/sssaj2018.03.0126

34 Zou, G., Li, Yong, Wang, Y., Liu, D.L., Liu, X., Li, Yuyuan, Wu, J., 2016. Pedo-transfer functions for estimating the hydraulic properties of paddy soils in subtropical central China. Archives of Agronomy and Soil Science 62, 982–993. https://doi.org/10.1080/03650340.2015.1109078

35 Zhang, Y., Schaap, M.G., 2017. Weighted recalibration of the Rosetta pedotransfer model with improved estimates of hydraulic parameter distributions and summary statistics (Rosetta3). Journal of Hydrology 547, 39–53. https://doi.org/10.1016/j.jhydrol.2017.01.004 Eq. with BD, Eq. without BD

5 Application of QGIS-SWAP-Paddy to the Lomellina Region to Evaluate the Effects of AWD and Other Irrigation Strategies on the Irrigation System Water Balance

5.1 Abstract

Rice cultivation in the Lomellina area has long relied on wet seeding with continuous flooding (WFL). Increasing water scarcity has encouraged farmers to adopt raw water-saving practices such as dry seeding followed by delayed flooding (DFL) or intermittent flooding (FTI), and has encouraged the exploration of alternative practices such as Alternate Wetting and Drying (AWD). This study uses the newly developed QGIS-SWAP-Paddy framework, which couples a semi-distributed SWAP module with a channel network model within a QGIS context, to the simulation of irrigation requirements, conveyance losses, and vertical percolation across the entire Lomellina area (127,033 ha, 62,615 ha under rice). The framework was calibrated against the 2020 irrigation daily discharges delivered to the area and monitored by the Irrigation Consortium (AIES), and validated using the irrigation discharge data series for the years 2018 and 2019. These operations were carried out considering the 'current irrigation' situation (PMR, including two rice irrigation management - WFL and FTI). Finally, the framework was used to assess the effects of four scenarios over the period 2013 - 2023: PMR (the 'current situation'), WFL, DFL, and AWD. At the field level, results show that average annual irrigation amount in the area decreases from 2.9 m under WFL to 2.4 m under DFL (-17.2%), 2.1 m under AWD (-27.6%), and 1.5 m under FTI (-48.3%). At the domain-scale, water demand is reduced by 18% under DFL, 29.6% under AWD, and 31.7% under PMR compared to WFL (1,52.5 m^3/s). AWD achieves a Water Application Efficiency (WAE) of 54.1%, comparable to PMR (55.3%) and higher than DFL (42.6%) and WFL (41.8%). Similarly, it attains a Relative Water Supply (RWS) of 2.8, comparable to PMR (2.9) and lower than both DFL (3.9) and WFL (3.8), indicating a closer balance between supply and demand. By enabling early-season groundwater recharge while reducing peak consumption in June, AWD once again proves to be a promising adaptation technique for addressing initial low aquifer levels in April and May, as well as inter-crop competition for water in June and July. These are challenges that are becoming increasingly problematic for rice-growing areas in northern Italy.

5.2 Motivation and Objectives

Historically, rice cultivation in Lomellina (Figure 61) has taken place through wet seeding followed by continuous flooding until two to three weeks prior to harvest (WFL). However, due to an increase in the frequency of water scarcity events, farmers are converting to water-saving methods, such as dry seeding with either delayed flooding (DFL) or intermittent flooding (FTI), both of which beginning at the third to fourth leaf stage. In Mayer et al. (2019) and in Gilardi et al. (2023) a modelling tool was developed and employed to estimate irrigation and groundwater recharge in a 1,000 hectares rice district in Lomellina. Simulations carried out in the San Giorgio irrigation district and evidence reported by farmers and irrigation managers, indicate that dry seeding with DFL or FTI leads to deeper phreatic groundwater table depths in April and May and

reduced irrigation efficiency in June and partially in July. Conversely, the simulation results showed that wet seeding and alternate wetting and drying (AWD) decreases the need for irrigation from June onwards, while also supporting early groundwater recharge.

The newly developed modelling framework QGIS-SWAP-Paddy (see Chapter 3) uses the open-source QGIS (https://qgis.org/) software environment to convert spatial data from a GeoPackage (https://www.geopackage.org/) database into physically based field-level simulations performed with the well-known SWAP (https://www.swap.alterra.nl/) agro-hydrological model. The framework streamlines the physical description of a simulation domain and the implementation of alternative irrigation management strategies providing an integrated tool that functions like a relational database. The framework also provides an ad hoc irrigation channel network model, enabling the assessment of irrigation water requirements at the inlet of complex lowland irrigation districts.

In this thesis, the framework has been parameterized for the entire Lomellina area (127,033 ha, of which 62,615 are occupied by rice) and used to conduct a scenario analysis to estimate irrigation requirements and groundwater recharge under four different rice irrigation management strategies, which are: I) WFL, II) FTI, III) DFL, IV) AWD. The simulation period covered 11 years (from 2013 to 2023) including very wet years (i.e., 2014) and very dry years (i.e., 2022). Scenarios are: PMR (the 'current situation', including two rice irrigation management - WFL and FTI), WFL, DFL, and AWD. Apart from the PMR scenario, the remaining scenarios are based on the same irrigation technique being used for all the rice fields in the region.

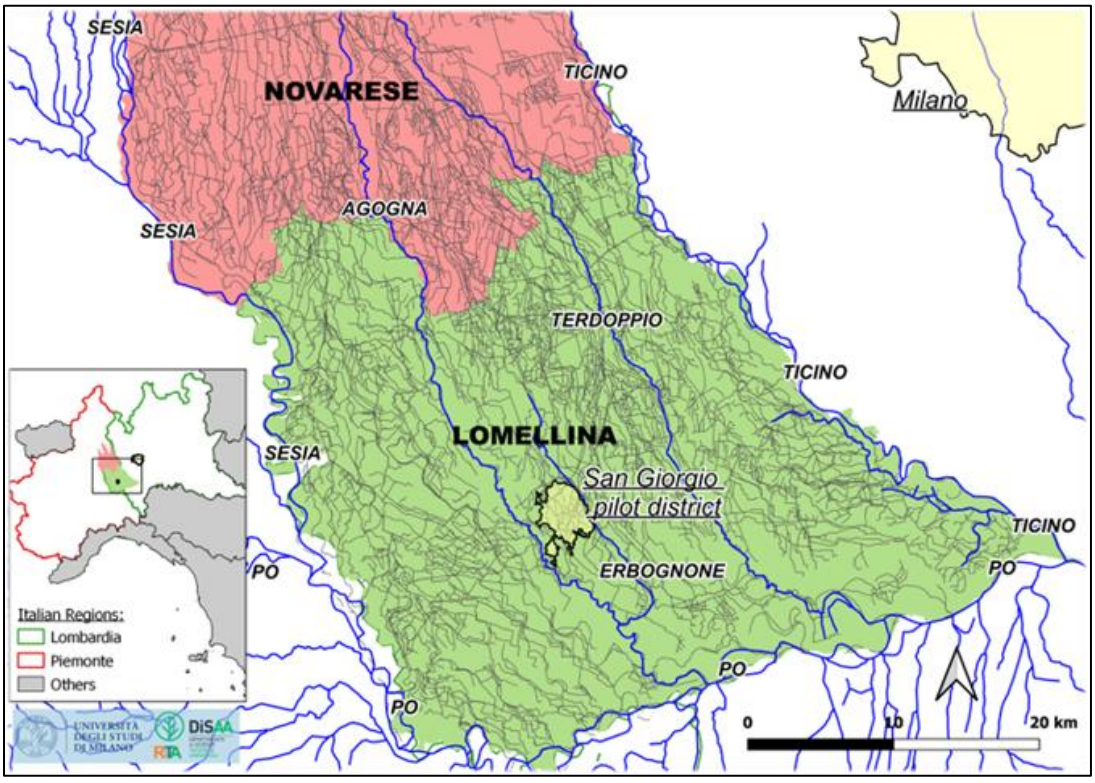

Figure 61. Territorial framework of the Lomellina area (Northern Italy), with the location of the San Giorgio irrigation district highlighted.

5.3 Materials and Methods

5.3.1 Modelling Framework

The QGIS-SWAP-Paddy modelling framework enables two distinct groups of processes to be simulated within a given domain (see Figure 62). (i) the former takes place in the agricultural area and (ii) the latter regards the channel network. The first sub-model applies a semi-distributed version of SWAP to estimate net irrigation requirements and deep percolation from the agricultural area. The second sub-model contains an algorithm designed specifically to describe complex channel networks that are so often found in low-land rice areas.

Whether historical input data are used or not (in the case of scenario simulation), the channel network percolation estimated by the model can be used to calculate the net discharge (measured discharge minus channel network losses, representing the irrigation water availability for the agricultural area) or the gross discharge (net irrigation coming from the agricultural area plus channel network losses, representing the total district water requirements) of a simulation domain.

The agricultural area model runs daily, identifying individual simulation units (fields or larger areas defined by unique crops and irrigation management practices or physical characteristics) within a simulation domain. Designed to accurately simulate continuously or intermittently flooded rice fields alongside other crops, it takes the maximum ponding water level allowed in the simulation into account as a core element of rice irrigation management. SWAP removes surplus water from paddies when this threshold is met, enabling controlled drying periods when no ponding is set. To accurately regulate ponding levels within SWAP simulations, excess input water must be supplied: net irrigation requirements are determined by subtracting daily simulated runoff from the total amount of water supplied to the fields. This methodology assumes predominantly one-dimensional vertical fluxes in the vadose zone and minimal connectivity between adjacent simulation units in lowland agricultural areas. Once the simulations have been completed, the outcomes can be observed on a daily basis for individual simulation units and aggregated monthly at the simulation domain level.

By contrast, the channel network model operates exclusively at the monthly scale. This methodological approach assumes that the cumulative simulated values of net irrigation requirement from the agricultural area can be effectively compared with the estimated net discharge of the channel network across the simulation domain at the monthly time step. The spatial implementation of the channel network model is not addressed for the Lomellina in this thesis. This aspect will be considered in a further development of the simulation activities for the Lomellina area, when QGIS-SWAP-Paddy will be coupled with a distributed groundwater flow model for the Lomellina region. This means that, although the implemented equations can provide an estimate of the net or gross discharge for the two interconnected portions of the channel system (the main linear network and the diffuse secondary network, which is fed by the former to serve each field in the agricultural area), in the current Lomellina configuration these two portions have been implemented to provide an overall water balance for the irrigation network similar to that presented in Chapter 2. The equations used in the framework can be simplified as follows:

$$\begin{cases} C_{network}\ \boldsymbol{net\ discharge}_t = C_{network}\ \boldsymbol{gross\ discharge}_t + C_{network}\ \boldsymbol{percolation}_t, & \text{historical} \\ C_{network}\ \boldsymbol{gross\ discharge}_t = C_{network}\ \boldsymbol{net\ discharge}_t - C_{network}\ \boldsymbol{percolation}_t, & \text{scenario} \end{cases} \quad \text{(Eq. 25)}$$

$$\boldsymbol{C_{network}\ percolation_t} = -\begin{cases} \boldsymbol{C_{network}\ gross\ discharge_t} * \alpha_{network_t}, & \text{historical} \\ \dfrac{\left(\alpha_{network_t} * \boldsymbol{C_{network}\ net\ discharge_t}\right)}{\left(1 - \alpha_{network_t}\right)}, & \text{scenario} \end{cases} \quad \text{(Eq. 26)}$$

$$\alpha_{network_t} = \begin{cases} \alpha min_{network_t}, & mod_1 \\ min\left(\alpha max_{network_t},\ \ max\left(0,\ \ GWDc_{network_t} - GWD_t\right)\right), & mod_2 \end{cases} \quad \text{(Eq. 27)}$$

where:

- $C_{network}\ net\ discharge$ (m^3/s) equals the irrigation water availability for the agricutural area (set to match the net irrigation coming from the agricoltural area in a scenario simulation, when measured data are not available),
- $C_{network}\ gross\ discharge$ (m^3/s) equals the irrigation water entering the simulation domain (tabulated in historical scenario, when measured data are available),

- $C_{network}\ percolation$ (m^3/s, negative) equals the percolation losses for the channel network,
- $\alpha_{network}$ (-, between 0 and 1) equals the estimated loss factor for the channel network,
- $\alpha max_{network}$ (-, between 0 and 1) equals the maximum value of $\alpha_{network}$ for the channel network (user defined),
- $\alpha min_{network}$ (-, between 0 and 1) equals the minimum value of $\alpha_{network}$ for the channel network (user defined),
- GWD (m, negative) equals the aggregated monthly average groundwater depth within the agricultural area,
- $GWDc_{network}$ (m, negative) equals the critical groundwater depth above which losses from the channel network should be equal to zero (user defined),

  - t (-) is the month of the simulation year.

To calculate the loss factor $\alpha_{network}$, the user can select one of three modes for each month within the same simulation year. In the first two, the user can specify: mod1) where $\alpha_{network}$ is equal to the fixed value $\alpha min_{network}$ (e.g., 0.2), or mod2) where $\alpha_{network}$ varies from a minimum value of zero ($GWD \geq GWDc_{network}$) to a maximum value $\alpha max_{network}$ (e.g., 0.4, $GWD < GWDc_{network}$). The former is useful for imposing fixed loss rates, which could be preferable in months outside the irrigation season, while the latter is useful in months when the depth of the groundwater table reduces percolation from the channel network, as is often the case during the irrigation season.

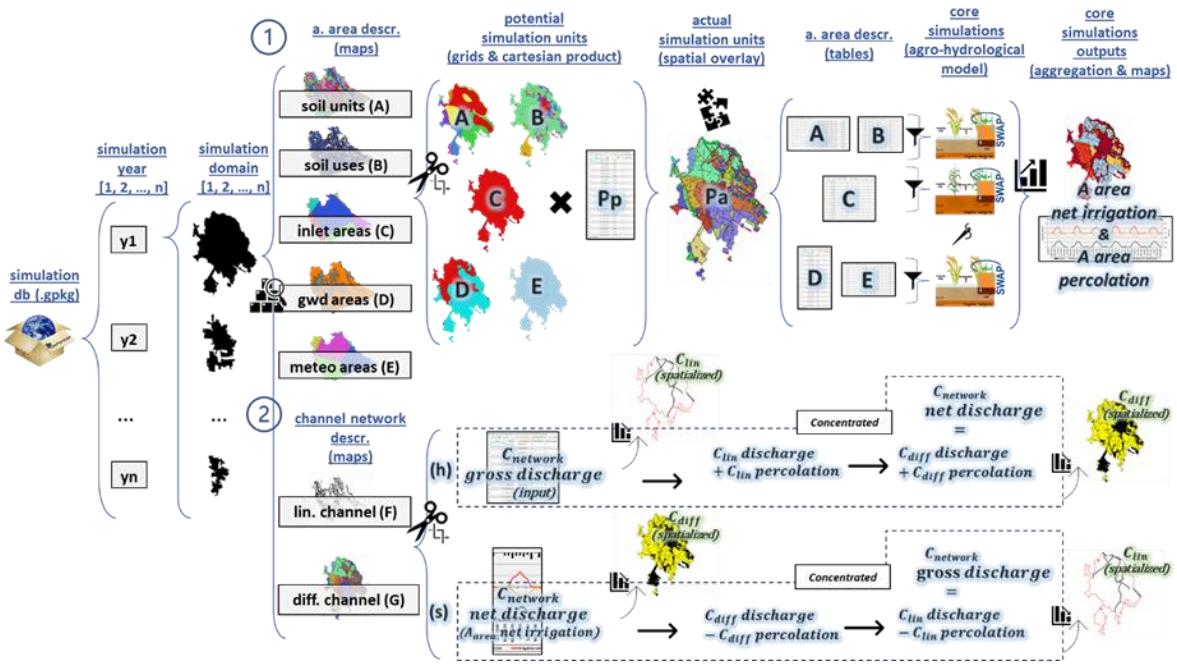

Figure 62. A schematic overview of the steps followed by the framework to: (1) semi-distribute the SWAP model within the agricultural area, and (2) describe the channel network of a simulation domain; both for a user defined simulation year.

5.3.2 Input Data Description for the PMR Scenario

All the data presented in this Section describe the Lomellina's 'current status', referred to as the PMR scenario. This scenario considers the two rice irrigation techniques currently applied by the farmers to the rice crops: I) WFL, II) and FTI.

The semi-distributed simulation approach used to model the agricultural area relies on two main data sources. Firstly, spatial maps show the spatial distribution of key factors (soil units, soil uses and irrigation techniques, groundwater depth zones, and agro-meteorological areas) across the simulation domain. Secondly, tabular parameters and time series provide a quantitative description of these factors for the field-scale simulations run by SWAP.

In the present study, the input spatial maps remained constant throughout the entire simulation period (2013 - 2023) and in all the simulated scenarios. What changed between scenarios are some parameters (crop parameters and irrigation techniques) and time series (groundwater depth series).

The channel network model, applied solely in its concentrated component, required defining a table of monthly gross discharges recorded for the entire simulation domain. In particular, daily discharges measured by AIES for the Lomellina region were only available for the period 2018 - 2020.

5.3.2.1 Agricultural Area Description

The agricultural area simulation resulted in 848 simulation units covering around 127,033 ha. Simulations included 60 soil types, 8 soil uses (5 productive and 3 non-productive), and 2 groundwater depth areas (shallow and deep). The following Sections present spatial maps, along with parameters and data series that describe the agricultural area of the Lomellina region, as provided to the framework.

5.3.2.1.1 Agrometeorological Data

The reference agro-meteorological station for the case study (located in Castello d'Agogna, Pavia - 45°14'49.2"N, 8°42'03.6"E) is managed by ARPA Lombardia (https://www.arpalombardia.it/). From 1993 to 2024 (April - September), average records include: cumulative rainfall of 322 mm, air temperature of 20.6°C, wind speed at 2 meters of 1.5 m/s, and daily solar radiation at 233.3 W/m2. Figure 63 presents the distributions of monthly rainfall (RAIN, cm), as well as minimum (Tmin, °C) and maximum (Tmax, °C) temperatures for the years 2018-2020. The map showing the area of influence of the selected agro-meteorological station (not shown here) consisted of a single polygon covering the entire simulation domain.

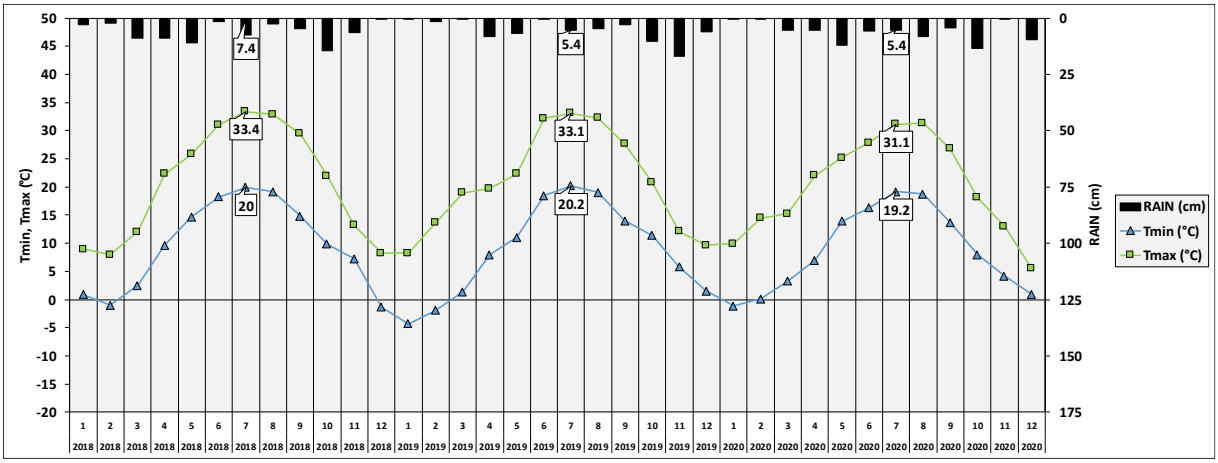

Figure 63. Monthly rainfall (cm) and Tmin - Tmax (°C) temporal patterns for the Castello d'Agogna (Pavia) meteo station in 2018 - 2020. Labels show values for each July in the data series.

5.3.2.1.2 Soil Units and Soil Hydraulic Parameters

The study area comprises a total of 60 different Cartographic Units (UCs) as delineated by ERSAF 1:50,000 Lombardy Region Soil Map (https://www.geoportale.regione.lombardia.it/) and detailed within the LOSAN soils database (https://www.losan.ersaflombardia.it/).

Soil hydraulic parameters for rice soils were estimated using PedoTransfer Functions (PTFs) identified in a recent UNIMI-DiSAA investigation (see Chapter 4).

Conceptually, the typical soil profile of a paddy field consists of three layers: I) a submerged unstructured 'muddy' top layer, which is in the rooted soil (usually 20 - 30 cm thick), II) a compacted and dense 'low conductivity' hardpan layer, that greatly reduces the vertical movement of water, and III) a subsoil, which generally hosts the upper limit of the first aquifer. During submersion, the vertical percolation process is primarily influenced by the properties of the hardpan layer, particularly its hydraulic conductivity, thickness and depth within the profile. The estimated saturated hydraulic conductivity (KSAT, cm/d) and thickness (cm) of the hardpan layer were adjusted through the calibration process, maintaining the original positioning of this layer as described by ERSAF.

By way of example, among the rice UCs described (i.e. only those that intersect with land uses cultivated with rice), Figure 64 shows only those occupying areas above the 90th percentile (2,368 ha) of the total rice soil unit area considered (which includes 58 units, 62,615 ha). Similarly,

Table 17 shows a rice paddy example (soil 40710). The Calibration and validation Section explains the criteria used to parameterize muddy and hardpan layers within rice soil profiles in Lomellina.

For non-paddy soils, hydraulic parameters were determined using the PTFs developed by Rawls and Brakensiek (1989), which are extensively recognized for use in agricultural soils in Lombardy, particularly in various implementations of the IdrAgra modelling system developed by the UNIMI-DiSAA research group (https://idragra.unimi.it/).

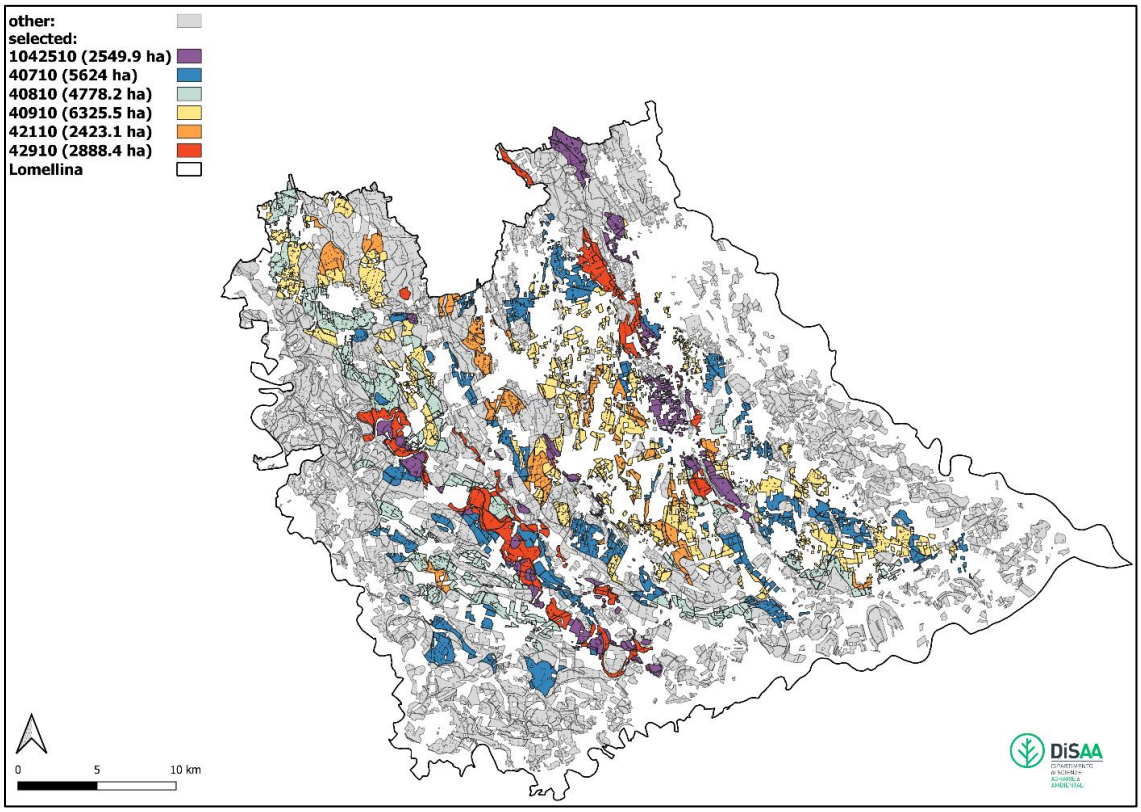

Figure 64. Spatial distribution of rice soil units (58 units, 62,615 ha) within the Lomellina region. The selected soil units (areas above the 90th percentile of the total rice soil unit area) are listed in the legend (soil unit code and area covered in hectares). All the remaining soil units are shown in grey.

Table 17. Soil 40710 layers discretization and hydraulic parameters (SWAP Mualem - van Genuchten parameters); muddy and hardpan layers within the soil profile are marked in bold. ISOILLAY is the horizon index; ISUBLAY the sub-layer index; HSUBLAY the sub-layer thickness (cm); HCOMP the numerical compartment thickness (cm); NCOMP the number of compartments per sub-layer; ORES the residual volumetric water content (cm³/cm³); OSAT the saturated volumetric water content (cm³/cm³); ALFA the shape parameter alfa of the main drying curve (1/cm); NPAR the shape parameter n; KSAT the saturated hydraulic conductivity (cm/d); LEXP the exponent in the hydraulic conductivity function (-); ALFAW the secondary α parameter for the wetting curve, used only in case of hysteresis (1/cm); and H_ENPR the air entry pressure head (cm).

ISOILLAY	ISUBLAY	HSUBLAY	HCOMP	NCOMP	ORES	OSAT	ALFA	NPAR	KSAT	LEXP	ALFAW	H_ENPR
1	**1**	**35**	**1**	**35**	**0.000**	**0.437**	**0.051**	**1.228**	**50.000**	**0.500**	**0.051**	**0.000**
2	**2**	**10**	**1**	**10**	**0.000**	**0.324**	**0.002**	**1.256**	**0.100**	**0.500**	**0.002**	**0.000**
3	3	5	1	5	0.000	0.403	0.016	1.193	61.321	0.500	0.016	0.000
4	4	25	1	25	0.000	0.415	0.045	1.272	311.280	0.500	0.045	0.000
5	5	126	1	126	0.000	0.429	0.042	1.302	390.574	0.500	0.042	0.000

5.3.2.1.3 Soil Uses and Irrigation Strategies

The Lombardy Region Geoportal (https://www.geoportale.regione.lombardia.it/) offers different databases describing soil uses in the study area, including DBGT (Database Geo-Topografico), Dusaf 7.0 (Uso e Copertura del Suolo), and the SIARL (Carta uso agricolo) agricultural land use map (here used for the year 2020). For this study, data were spatially overlaid and used to create a synthetic map that remained valid throughout the whole simulation period.

The FTI rice and maize were located where the land designated as arable in the DBGT had a majority of rice or maize cells in the SIARL layer. Ente Nazionale Risi (ENR, https://www.enterisi.it/) data on rice fields cultivated using wet seeding in 2020 was added to the previous maps to locate areas associated with WFL management. This is because the regional databases do not report this information (i.e. the rice class is not split according to different irrigation management strategies). Poplar locations were retrieved from Dusaf (all the arboriculture practiced in the area has been associated with poplar cultivation, as is indeed plausible) and their distribution was divided into young (irrigated) and mature (non-irrigated) based on a 40 - 60% ratio, following the same strategy described in Mayer et al. (2019). Productive soil uses are shown in Figure 65.

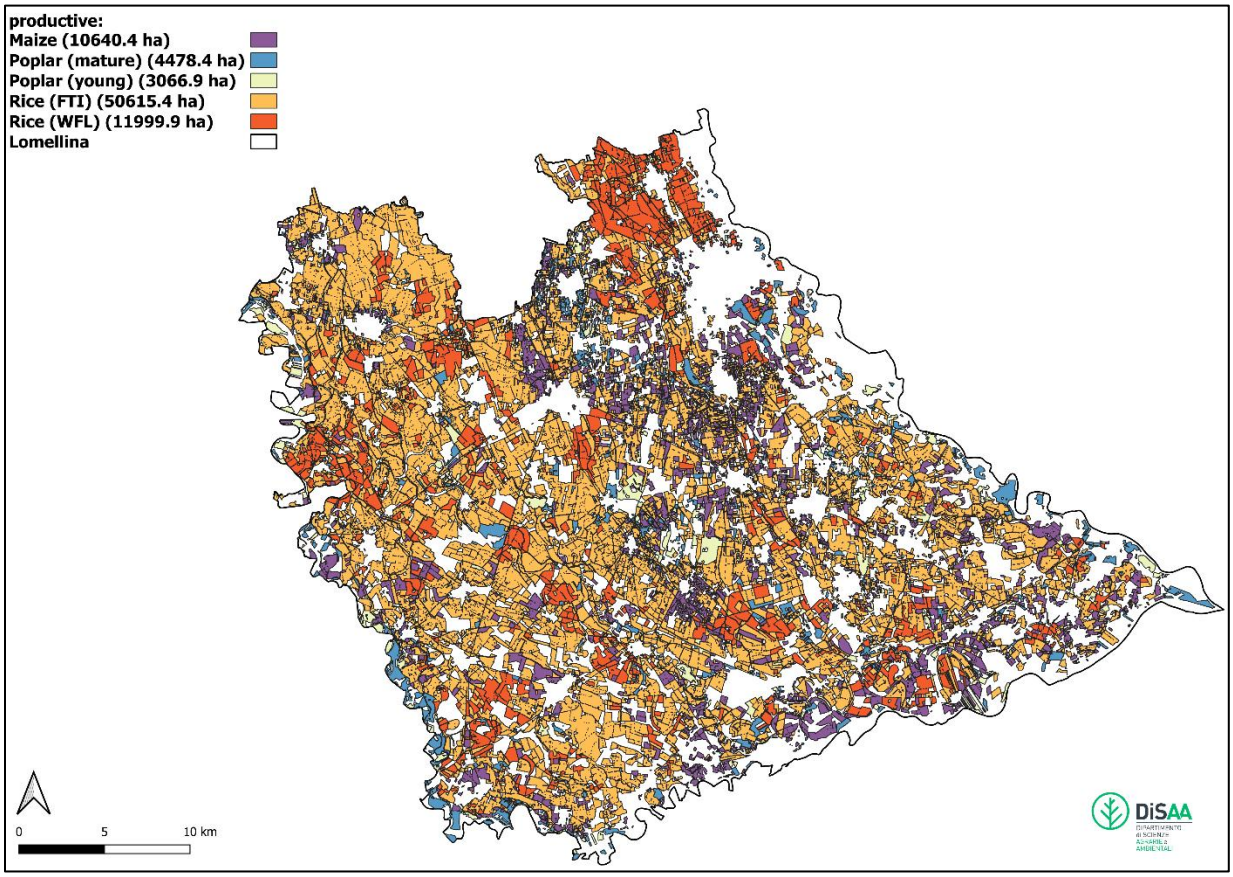

Figure 65. Spatial distribution of productive soil uses within the Lomellina region (PMR scenario). Selected soil uses (WFL, FTI, maize, young and mature poplar) are listed in the legend (soil use name and area covered in hectares).

Non-productive soil uses (Figure 66) include fallows (those arable lands from DBGT that were not rice or maize in the SIARL map), riparian vegetation (classified as deciduous forest in the Dusaf map), and urban or unclassifiable areas (bare soils). Urban and unclassifiable areas were grouped together into the so-called 'bare soil' category since they mainly represent urban surfaces of the region (small towns, roads, etc.) that cannot be simulated in any other way in SWAP except by treating them as areas without any vegetation cover.

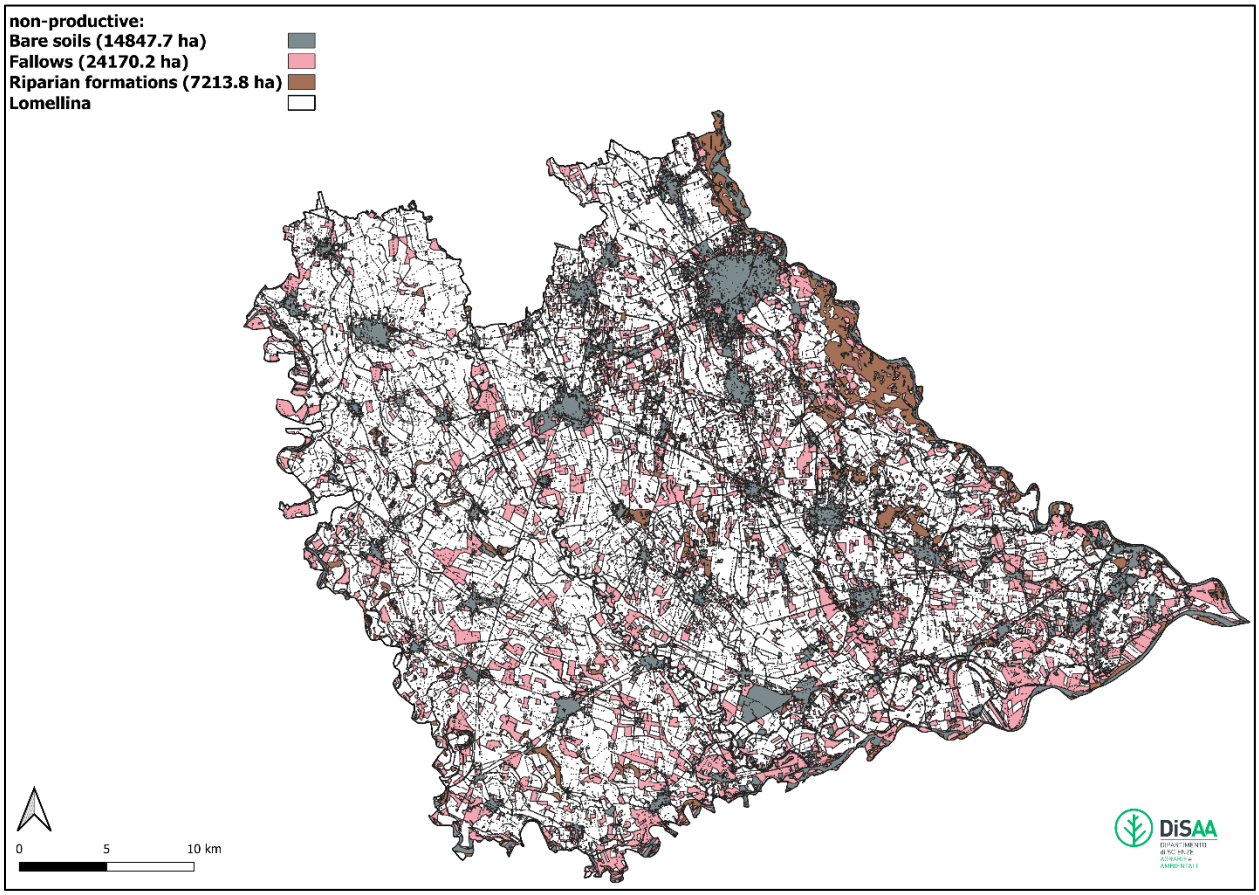

Figure 66. Spatial distribution of non-productive soil uses within the Lomellina region. Selected soil uses (fallows, riparian formations, and bare soils) are listed in the legend (soil use name and area covered in hectares).

In Gilardi et al. (2023), a crop development model was developed and calibrated for both wet (WFL and AWD) and dry seeded (FTI and DFL) rice considering observative data of the year 2020, with the help of ENR. The model uses a degree days approach to estimate: I) a likely seeding date, not featured in SWAP, and II) phenological stages from emergence to harvest, in a similar way to what is implemented in SWAP. In this study, the development model has been further enhanced in its irrigation scheduling component. This improvement leverages the new modelling framework's ability to set time-dependent ponding thresholds and to enable a rational integration of fixed and crop-specific irrigation management at the field scale. Basically, the model adjusts SWAP inputs related to fixed irrigation applications based on changes in crop Development Stage (DVS), allowing highly customized irrigation management to be created for the different types of rice simulated in this study. The irrigation distributed during the season by the development model

represents the gross irrigation input to the SWAP model, from which the runoff generated during the field-level simulations will be subtracted daily to calculate the net irrigation requirement of the crop.

The seeding date is identified verifying the achievement of a minimum temperature threshold ($T_{seeding}$, ◦C) in a forward moving window ($D_i + n$; with n equals to 4 in the current case study) built from a minimum seeding date ($D_{\min}$) up to a maximum seeding date (D_{max}), when, even if the temperature criterion is not satisfied, seeding is forced to occur:

$$\frac{\sum_{i=D_{min}}^{D_{min}+n} T_{mean}}{n+1} \geq T_{seeding} \quad \text{(Eq. 28)}$$

where

- T_{mean}(◦C) is the daily mean air temperature,
- i (−) is the day index.

Three different growing stages are used to describe the development of rice: I) seeding-emergence, II) emergence-flowering (DVS from 0 to 1), III) flowering-harvest (DVS from 1 to 2). DVS values in a specific day is calculated using the equation:

$$DVS^{i+1} = DVS^{i} + \frac{T_{eff}}{T_{sum}} \quad \text{(Eq. 29)}$$

$$T_{eff} = \begin{cases} 0, & T_{mean} < T_{base} \\ T_{mean} - T_{base}, & T_{base} \leq T_{mean} \leq T_{cutoff} \\ T_{cutoff} - T_{base}, & T_{mean} > T_{cutoff} \end{cases} \quad \text{(Eq. 30)}$$

where

- T_{eff} (◦C) is the thermal contribution of the day,
- T_{sum} (◦C) is the thermal amount defined to satisfy the achievement of a growing stage (emergence, flowering harvest),
- T_{base} and T_{cutoff} (◦C) are the minimum and the maximum temperatures for crop development for each specific growing stage range, if different.

This model was used to calculate rice phenologies and schedule irrigation also in the current study, using the following parameters: D_{min} was set to 30 April for wet seeding and 23 April for dry seeding, D_{max} corresponded to D_{min} plus 30 days, $T_{seeding}$ was 10 °C, T_{base} was also 10 °C, T_{cutoff} was 40 °C, T_{sum} was 23 for wet seeding and 67 for dry seeding, T_{sum} - DVS from 0 to 1 was 1051 °C, and T_{sum} - DVS from 1 to 2 was 752 °C. Figure 67 shows the simulated rice seeding/emergence (CROPSEEDING; CROPSTART) and harvest (CROPEND), along with the irrigation depth gross input (IRGDEPTH) provided to SWAP for both simulated rice types in the PMR scenario during 2018 to 2020.

With respect to the irrigation management, WFL fields are kept with ponded water from about a week before seeding until the final drying, except for brief dry periods needed for plant

emergence and agronomic tasks (typically two before and one after tillering). FTI reflects the common practices nowadays used in northern Italy: rice is dry seeded, initially flooded for about a week, then irrigated using rotation from the tillering phase onwards. Dry and wet seeded rice leaf area index (LAI, -), crop factor (CF. -) and rooting depth (RD, cm) as function of DVS are listed in Table 18. In both dry and wet seeded rice, the leaf area index (LAI) typically follows a sigmoidal trajectory, with a rapid increase after canopy establishment and a maximum reached around flowering (DVS ≈ 1.0 - 1.1). This pattern is consistent with observations for high-yielding Oryza sativa cultivars under optimal management (Bouman et al., 2005; Yoshida, 1981). The slightly higher initial LAI and CF in the dry seeded scenario are consistent with the earlier canopy closure typically reported for direct seeding on dry soil, which promotes faster early leaf expansion compared to wet seeding (Farooq et al., 2011). Rooting depth stabilising at ~35 cm is typical for flooded rice systems, where anaerobic conditions limit deep root penetration (Yoshida, 1981). The CF values exceeding 1.0 in mid-season aligns with FAO-56 guidelines for peak evapotranspiration stages (Allen et al., 1998).

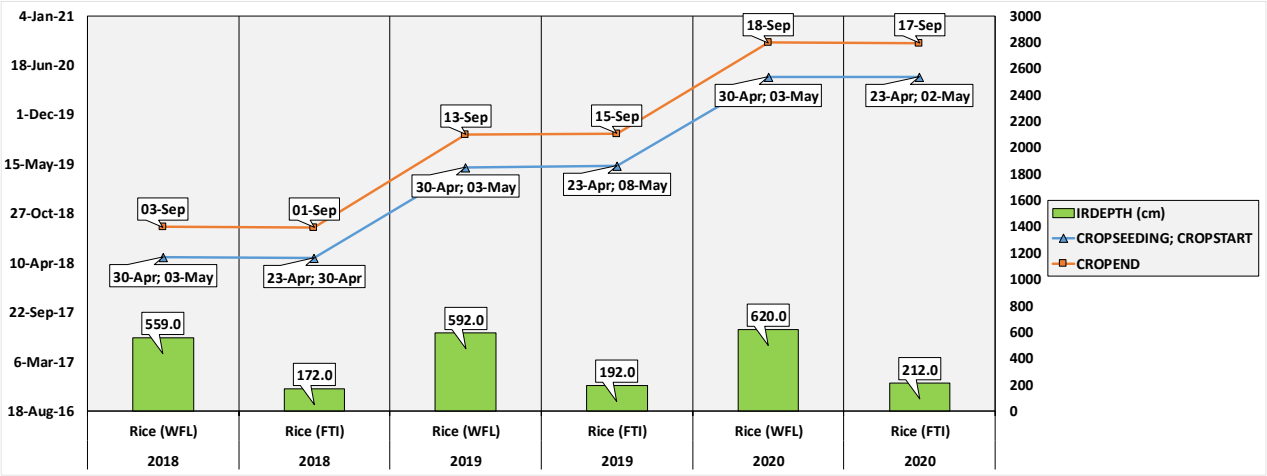

Figure 67. Simulated rice seeding/emergence (CROPSEEDING; CROPSTART), harvest (CROPEND), and irrigation depth (IRGDEPTH, cm) used in SWAP for the rice irrigation management strategies WFL and FTI under the PMR scenario from 2018 to 2020.

Table 18. Dry and wet seeded rice leaf area index (LAI, -), crop factor (CF. -) and rooting depth (RD, cm) as function of DVS.

DVS	LAI dry	CF dry	RD dry (cm)	LAI wet	CF wet	RD wet (cm)
0.00	0.10	0.35	5.00	0.00	0.00	0.00
0.40	0.70	0.70	20.00	0.70	0.70	20.00
0.90	1.50	1.10	35.00	1.50	1.10	35.00
1.10	5.00	1.10	35.00	5.00	1.10	35.00
1.65	4.70	1.10	35.00	4.70	1.10	35.00
2.00	4.00	0.60	35.00	4.00	0.60	35.00

Maize and Poplar description (Table 19 and Table 20) are largely derived from Mayer et al. (2019). Maize followed a fixed growth cycle (20 April - 3 September) and received border irrigation of 200 mm after 70% of the Readily Available Water (RAW) depletion. The simulated

LAI trajectory for maize exhibited a steep rise between DVS 0.34 and 0.94, peaking at 5.2, which is consistent with the maximum values (≈ 4.5 - 6.0) reported for modern Zea mays hybrids under non-limiting conditions; the CF reaching 1.0 during mid-season indicates full canopy closure, consistent with the near-complete radiation interception and peak evapotranspiration reported for maize under optimal conditions (Elli et al., 2025; Maddonni and Otegui, 1996; Muchow et al., 1990). Rooting depth reaching 80 cm by DVS 0.94 is consistent with literature, although conservative, since maize roots are known to extend well beyond 1 m in well-drained soils (Dardanelli et al., 1997; Hammer et al., 2009). For poplar, a generic deciduous forest model was employed: young trees received two 200 mm border irrigations (late June and early August) while mature trees relied solely on rainfall.

Table 19. Maize leaf area index (LAI, -), crop factor (CF. -) and rooting depth (RD, cm) as function of DVS.

DVS	LAI	CF	RD (cm)
0.00	0.10	0.33	5.00
0.34	0.50	0.33	50.00
0.94	5.20	1.00	80.00
1.60	4.70	1.00	80.00
2.00	3.70	0.45	80.00

Table 20. Young and mature poplar leaf area index (LAI, -), crop factor (CF. -) and rooting depth (RD, cm) as function of DVS.

DVS	LAI young	CF young	RD young (cm)	LAI mature	CF mature	RD mature (cm)
0.00	1.40	0.14	150.00	2.00	0.20	250
0.57	1.75	0.32	150.00	2.50	0.45	250
0.91	2.80	0.70	150.00	4.00	1.00	250
1.07	2.80	0.70	150.00	4.00	1.00	250
1.41	1.75	0.35	150.00	2.50	0.50	250
2.00	1.40	0.14	150.00	2.00	0.20	250

Fallows (NatureGrass.crp), riparian vegetation (NatureForestDecid.crp), and bare soils (BareSoil.crp) description were retrieved from demo crop data published together with the version 3.2.36 of SWAP (Kroes et al., 2008).

5.3.2.1.4 Groundwater Depth Areas and Series

The most recent spatially distributed groundwater piezometry data for the phreatic acquifer of the study area is available via the Lombardy Region Geoportal (https://www.geoportale.regione.lombardia.it/, ARPA Lombardia - Piezometrie 2014 degli acquiferi superficiali e profondi). The data presented on the regional portal are based on surveys conducted during two intensive campaigns led in May and September 2014. The Digital Terrain Model (DTM), which is also accessible via the Lombardy Region Geoportal (https://www.geoportale.regione.lombardia.it/, DTM 5X5 - Modello digitale del terreno), provides elevation data.

Groundwater piezometry combined with DTM was used to determine groundwater depths for describing phreatic water table conditions in the simulated domain. Based on the classification of areas as shallow (≥ -1 m) or deep (< -1 m) by Mayer et al. (2019) using data from the peak of

the irrigation season, in this study data from the September 2014 campaign were selected to represent groundwater levels affected by summer irrigation practices, as this was the most suitable available. Figure 68 shows the distribution of groundwater depth zones. Compared to the entire simulated territory, areas with shallow groundwater cover 24.9%, while those with deep groundwater cover 75.1%.

Figure 69 shows the monthly data series from 2018 to 2020 for the two groundwater depth classes (GW - shallow and deep) used in this study. The groundwater level data series measured twice a month in various piezometers installed in Lomellina by the Associazione Irrigazione Est Sesia (AIES, https://www.estsesia.it/) are currently being analyzed. In the meantime, for this study, the existing data series measured in the district of San Giorgio di Lomellina are being used under the assumption that they are also sufficiently representative for the entire Lomellina region.

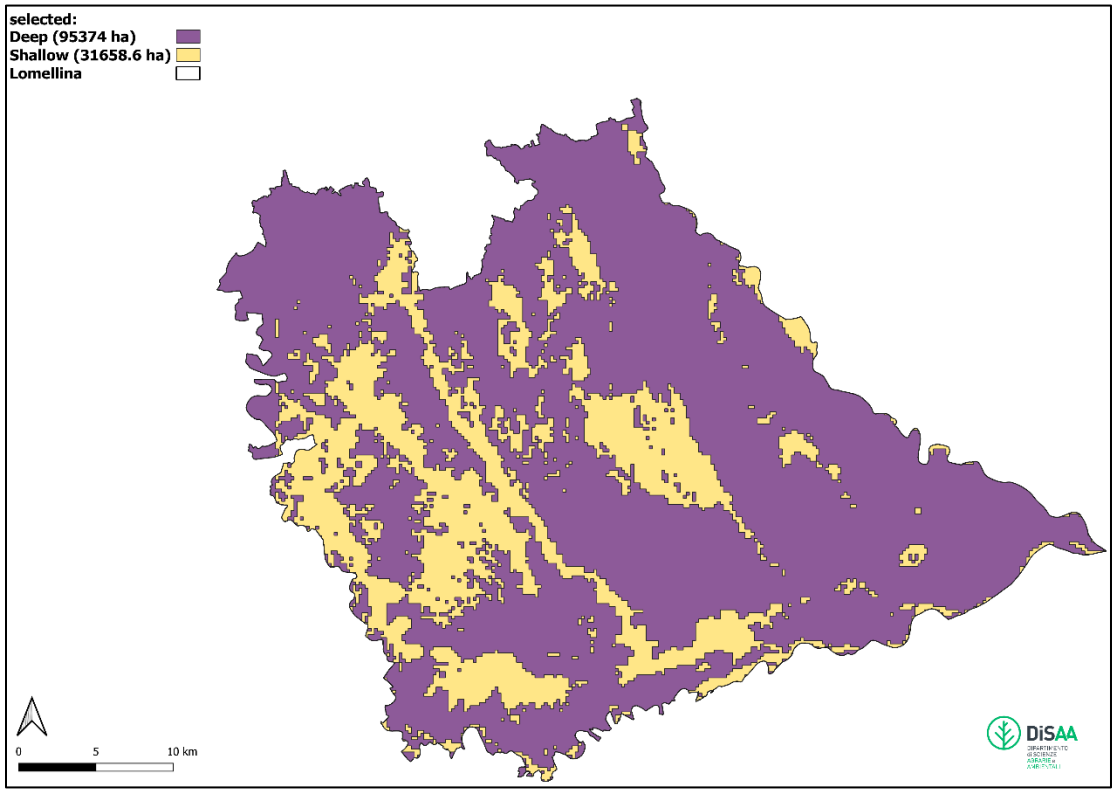

Figure 68. Spatial distribution of groundwater depth zones (shallow and deep) within the Lomellina region. Legend shows groundwater depth zones and areas covered in hectares.

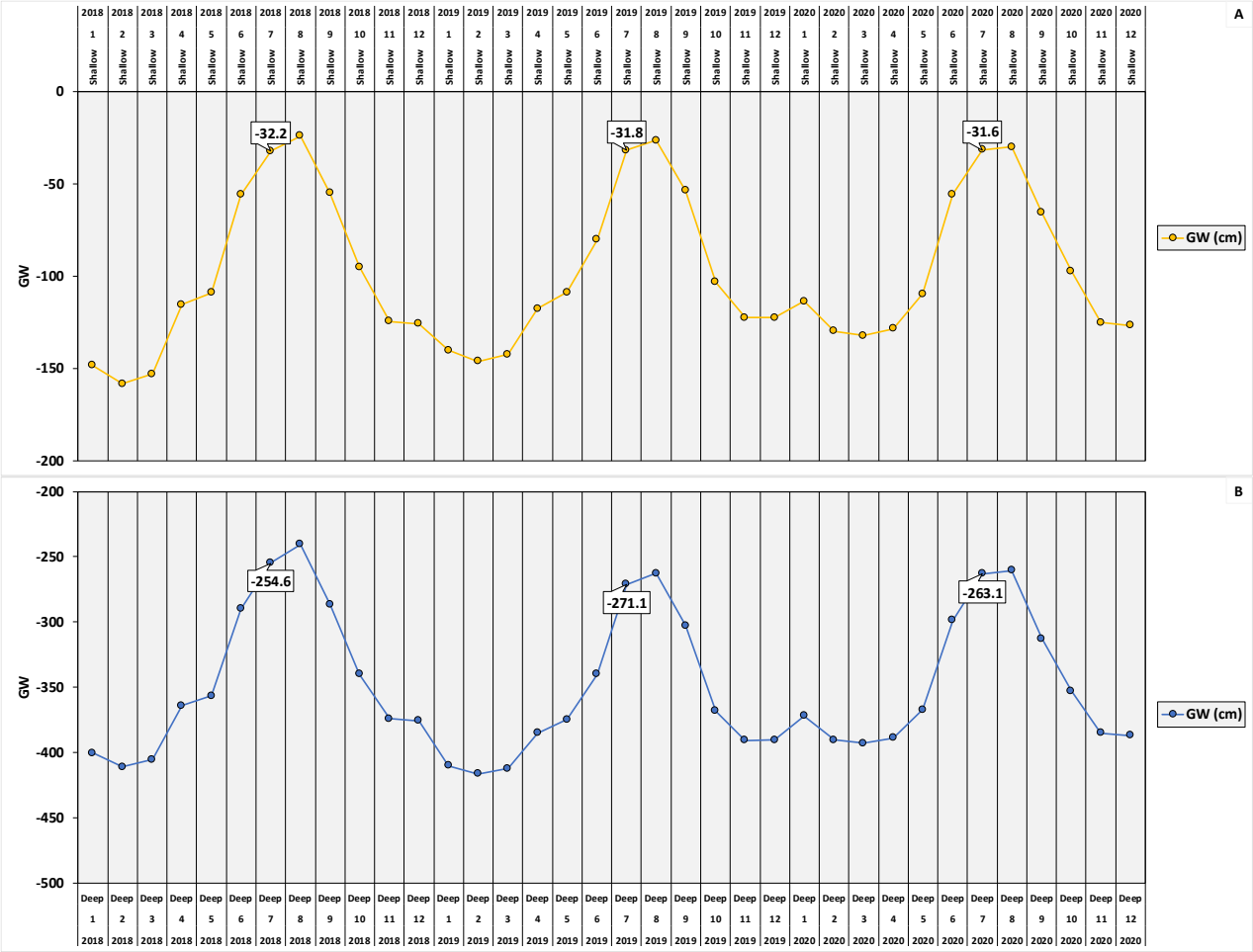

Figure 69. Monthly groundwater depth series (A - shallow, B - deep; GW - m) used for 2018 - 2020 to describe groundwater table conditions within the Lomellina region (PMR scenario). Labels show values for each July in the data series.

5.3.2.2 Channel Network Measured Discharges

Data on measured irrigation discharges for the Lomellina region was only available for the years 2018 - 2020. The dataset needed by the modelling framework was compiled using daily irrigation discharges data directly managed by AIES together with the information coming from the regional database 'Catasto Utenze Idriche di Regione Lombardia' (CUI), which includes irrigation supplies from surface water bodies not managed by AIES and from depression springs and private wells. Both databases were provided by the AIES consortium for this study.

For the data coming from CUI, ad hoc procedures were developed in collaboration with AIES and employed to derive the most representative values for each existing irrigation water source (i.e. some fields relating to individual users in the database were no data, so they were estimated based on the fields that were complete). Also, the monthly patterns of the CUI irrigation sources were reconstructed, since only annual data were provided by the CUI database. Figure 70 depicts the final monthly irrigation discharges (DISCHARGE_IN, m^3/s) available for the Lomellina simulation domain; the highest discharge value was observed in July. Considering that month, the average (2018 - 2023) unit water allocation for the irrigated agricultural area (76,322.56 ha; sum of Rice (WFL), Rice (FTI), Maize, and Poplar (young) soil uses) was of 2.56 l/s ha^{-1}.

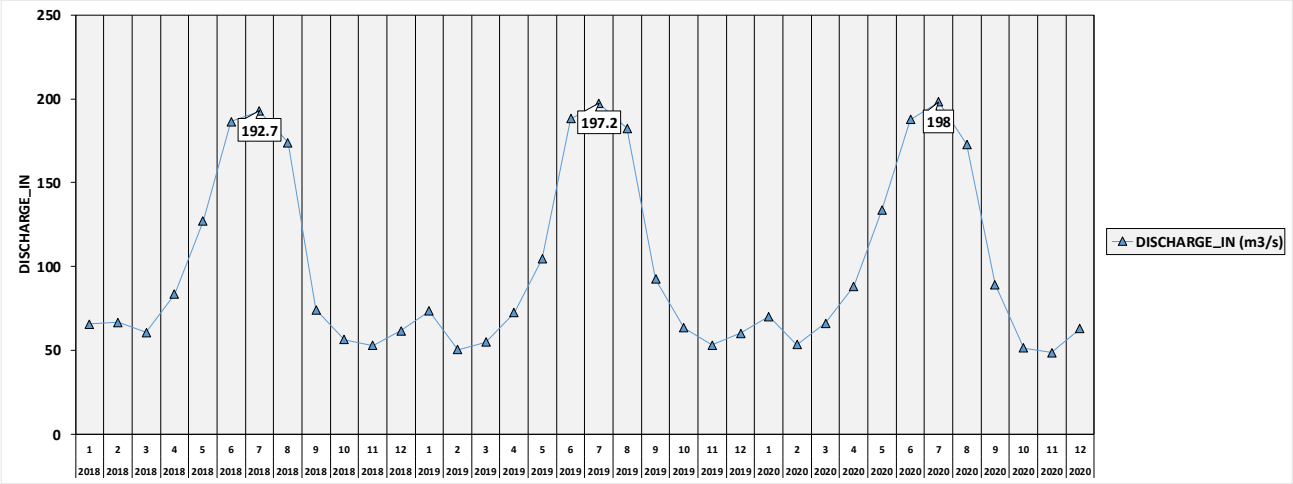

Figure 70. Monthly irrigation discharges (DISCHARGE_IN, m^3/s) for the Lomellina area in 2018 - 2020. The highest discharge value was observed in July for all years.

5.3.3 Calibration and Validation

The calibration of the semi-distributed agricultural area sub-model was carried out considering the PMR scenario (two rice irrigation strategies: WFL and FTI), and it was performed through the manual adjustment of parameters associated with the rice irrigation management (ponding water level in the case of WFL and application amounts and scheduling in the case of FTI; these parameters were included within the crop development model described in the Section 5.3.2.1.3), as well as of some hydraulic properties of rice soils (in particular: thickness of the hardpan layer - cm, and maximum and minimum values of its saturated hydraulic conductivity - KSAT, cm/d).

Calibration was performed for the year 2020, with the final objective of minimizing discrepancies between simulated net irrigation ($A_{area}\ net\ irrigation$, m^3/s) and estimated net irrigation availability, this latter corresponding to the channel network net discharge ($C_{network}\ net\ discharge$, m^3/s), for the agricultural area on a monthly scale. The year 2020 was chosen for the calibration because the soil use map and the crop development model used throughout the simulation period were both primarily based on data from that year. Furthermore, AIES stated that 2020 was a year in which there was sufficient water to meet the Lomellina area's irrigation needs.

The years 2018 and 2019 were used for validation purposes since the spatial distribution of soil uses can be considered similar to that of 2020 and measured irrigation discharges have been provided by AIES also for these two years. According to the information provided by AIES, FTI irrigation scheduling in San Giorgio di Lomellina district in 2018 was broadly consistent with that adopted in Mayer et al. (2019) and Gilardi et al. (2023). Rotations averaged 10 days during the first month (until early June), followed by 12-day intervals for the rest of the season. In 2019, however, conditions were exceptionally severe. In fact, a very dry winter was followed by a spring with little rainfall. This, combined with changes in irrigation methods, led to very low groundwater levels at the start of the irrigation season. While May was saved by rainfall, June was again very dry compared to the average. Thus, while May 2019 was favorable, with no or very few irrigations

required, from that point onward, available water was insufficient. Irrigation rotations for rice were extended to 20 days for the entire season, with peaks of 25 days, and in the southern part of the district irrigation intervals reached 30 days. This critical situation also occurred throughout the wider Lomellina area.

During the calibration and validation phases, only the discharges occurring within the Lomellina channel network between May and September were taken into account, as these can be directly associated with the region's irrigation water requirements (i.e. in April and October more water is available in the canal network than is used for irrigation).

The parameterization of the channel network model for the whole Lomellina was informed by insights from the San Giorgio case study and conducted in collaboration with AIES. The aim was to accurately represent network losses as observed by the association's experts. During the irrigation season (April - October), the channel network operated with an overall efficiency of around 60% (corresponding to a loss factor of 0.4, or 0.225 for the linear and diffuse components). Outside the irrigation season, efficiency was set at around 80% (a loss factor of 0.2, corresponding to 0.125 for the linear and diffuse components). The critical groundwater depth threshold of -1.6 m, above which channel network losses are assumed to be zero, was applied in the same way as in the San Giorgio di Lomellina district.

Within the calibration process, KSAT and thickness of hardpan layers of the rice soil profiles were, respectively, set to 10 cm and limited to the range 0.1 - 1.0 cm/d (Figure 71). This was done after a series of tests, in order to ensure that, on average, soils of Lomellina guarantee a simulated ponding water of 12 cm, in the case of WFL, and a maximum irrigation rotation of 12 days, in the case of FTI. The optimal target value for the ponding water level was defined based on works already carried out in San Giorgio di Lomellina, while the maximum irrigation rotation of 12 days is, as already mentioned, indicated by AIES as a reference for years with satisfactory irrigation allocations for the same district.

A fixed hardpan thickness for all the rice soils in Lomellina was set based on field observations of a fairly constant hardpan thickness averaging between 5 and 15 - 20 cm, and for practical reasons since calibrating thickness across 60 soils would have been operationally burdensome. To impose a uniform thickness of 10 cm for the hardpan horizon in simulated rice profiles, each profile was first checked for the presence of such a horizon (see Chapter 4). Since in a paddy soil the presence of a hardpan is generally expected, even when it was not originally detected (i.e. in cases where the ERSAF soil reference profile for the UC was for instance located in fields with other crops), a new layer was inserted by replicating the characteristics of either the overlying or the underlying horizon, selected on a case-by-case basis. Where the original ERSAF description locates a horizon with hardpan characteristics, this layer was split into two twin horizons if thicker than 10 cm. Different hardpan thicknesses were tested during preliminary simulations, but 10 cm was identified as the most suitable value. Once the hardpan was defined in every profile, its thickness was set to exactly 10 cm, ensuring that the lower boundary of the hardpan horizon did not extend beyond the upper limit of the subsequent layer, and that the muddy layer retained a minimum thickness of 5 cm.

Moreover, to reproduce the typical de-structured muddy surface horizon of rice soils, the top layer was set to a KSAT of 50 cm/d when the value obtained by the PTF application was lower, for all the simulated rice soils.

Regarding non-rice simulation units, irrigation management (in the case of maize and irrigated poplar) and soil discretization and parameters have not been modified.

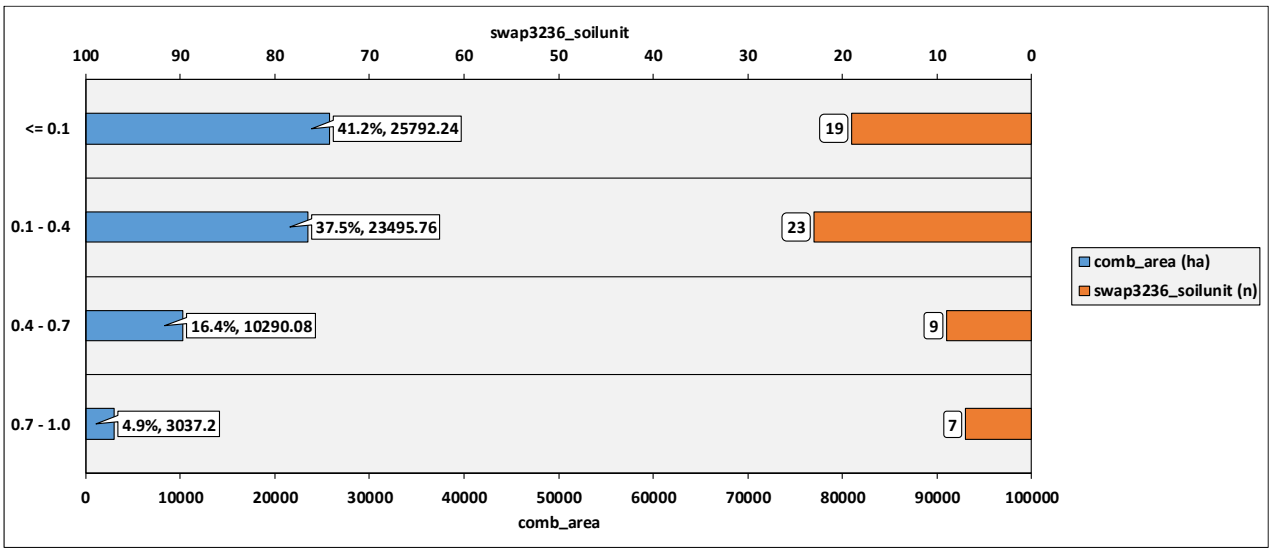

Figure 71. Rice soils areas (comb_area, ha) and simulated soil combinations count (swap3236_soilunit, n) for different classes of hardpan KSAT (cm/d) values within the calibration range adopted. The percentages in the area bars are calculated using the total simulated rice soils area (62,615 ha) as a reference.

Model evaluation for calibration and validation was conducted using recommended indices in Moriasi et al. (2007), specifically the Nash-Sutcliffe Efficiency (NSE, -), the RMSE-observations standard deviation ratio (RSR, -), and Percent Bias (PBIAS, %).

$$\mathrm{NSE} = 1 - \frac{\sum_{t=1}^{n}\left(y_t^{obs} - y_t^{sim}\right)^2}{\sum_{t=1}^{n}\left(y_t^{obs} - \overline{y_{obs}}\right)^2} \quad \text{(Eq. 31)}$$

$$RSR = \frac{\sqrt{\sum_{t=1}^{n}\left(y_t^{obs} - y_t^{sim}\right)^2}}{\sqrt{\sum_{t=1}^{n}\left(y_t^{obs} - \overline{y_{obs}}\right)^2}} \quad \text{(Eq. 32)}$$

$$PBIAS = \frac{\sum_{t=1}^{n}\left(y_t^{obs} - y_t^{sim}\right) \cdot 100}{\sum_{t=1}^{n} y_t^{obs}} \quad \text{(Eq. 33)}$$

where

- y_t^{obs} are the estimated monthly $C_{network}\ net\ discharge$ (m^3/s),
- y_t^{sim} are the simulated monthly $A_{area}\ net\ irrigation$ (m^3/s),
- $\overline{y_{obs}}$ is the average of the estimated monthly $C_{network}\ net\ discharge$ (m^3/s),
  - t (-) is the month of the simulation year.

NSE ranges from negative infinity to 1 (optimal value). Values between 0 and 1 are generally considered acceptable levels of performance, while negative values indicate unacceptable performance. RSR varies from 0 (optimal value) to a large positive number. The lower the RSR, the better the model's performance. PBIAS has an optimal value of 0, with low

absolute values indicating accurate model simulation. Positive values point to an underestimation bias, whereas negative values indicate an overestimation bias. Monthly performance rates from Moriasi et al. (2007) are reported in Table 21. As introduced above, the evaluation indices were calculated only for the months within the irrigation season (May - September).

Table 21. Monthly performances rating from Moriasi et al. (2007).

Performance Rating	NSE	RSR	PBIAS (%) - Streamflow
Very Good	0.75 - 1.00	0.00 - 0.50	< ±10
Good	0.65 - 0.75	0.50 - 0.60	±10 - ±15
Satisfactory	0.50 - 0.65	0.60 - 0.70	±15 - ±25
Unsatisfactory	< 0.50	> 0.70	> ±25

5.3.4 Irrigation Scenarios

Except for the PMR scenario, the other scenarios are named considering the irrigation management imposed to all the rice fields within the simulation domain (107 simulation units, 62,615 ha): I) wet seeding and continuous flooding (WFL), II) dry seeding and delayed flooding (DFL), III) wet seeding and Alternated Wetting and Drying (AWD).

Each irrigation practice follows a crop pattern based on the seeding type (wet for AWD and dry for DFL) and has a specific irrigation schedule, detailed later. Scenarios also differ in lower boundary conditions (Figure 72). Due to the lack of a comprehensive groundwater model for the Lomellina, groundwater data series for each scenario were retrieved from those simulated for San Giorgio di Lomellina. Outside the paddy fields, land use follows the PMR scenario, and the channel network characteristics are assumed to be unchanged across all scenarios.

The WFL scenario uses the same irrigation scheduling as described in Section 5.3.2.1.3, but for the bottom boundary condition it uses simulated groundwater level data series coming from the San Giorgio district under that specific irrigation management. Among the simulated scenario, WFL has the highest aquifer levels throughout the entire irrigation season, like those traditionally observed in the area before the introduction of dry seeding and water-saving techniques, like DFL and FTI.

For DFL, dry seeding is used, and the fields are flooded from the tillering stage until final drying. The lower boundary conditions for this scenario were obtained from simulations conducted in San Giorgio, where dry seeding was found to cause a rather significant drop in groundwater levels in the first part of the irrigation season. This was the practice adopted when DFL was introduced by the ENR as an innovative technique about 15 - 20 years ago, but it is now often replaced by FTI because, under conditions of water scarcity, the AIES irrigation consortium enforces a rotation of water supplies.

For the implementation of AWD, data were taken from previous experimentations (MEDWATERICE, and RISWAGEST projects) conducted with ENR at CRR-ENR (Centro Ricerche sul Riso; Castello D'Agogna, Pavia, Italy), already discussed in Gilardi et al. (2023), and from a new protocol developed specifically for the Lomellina region within the RISOSOST project. Within this framework, after wet seeding, AWD cycles are set to start at the tillering stage when the soil water potential reaches -10 kPa (-100 cm) at a depth of -5 cm, corresponding to the safe AWD category as defined by Carrijo et al. (2017). Additionally, AWD involves continuous flooding for approximately 20 - 30 days after panicle initiation to reduce cadmium accumulation

in the grain. This approach is consistent with findings in scientific literature (Vitali et al., 2024), which indicate that water management practices can significantly influence heavy metal uptake in rice, with AWD generally reducing arsenic concentrations but potentially increasing cadmium and nickel levels compared to continuous flooding. This is particularly relevant considering the current EU legislation (Regulation (EU) 2023/915), which sets maximum levels for milled rice of 0.20 mg/kg for inorganic As and 0.15 mg/kg for Cd. After this period, AWD resumes until the rice field undergoes final drying.

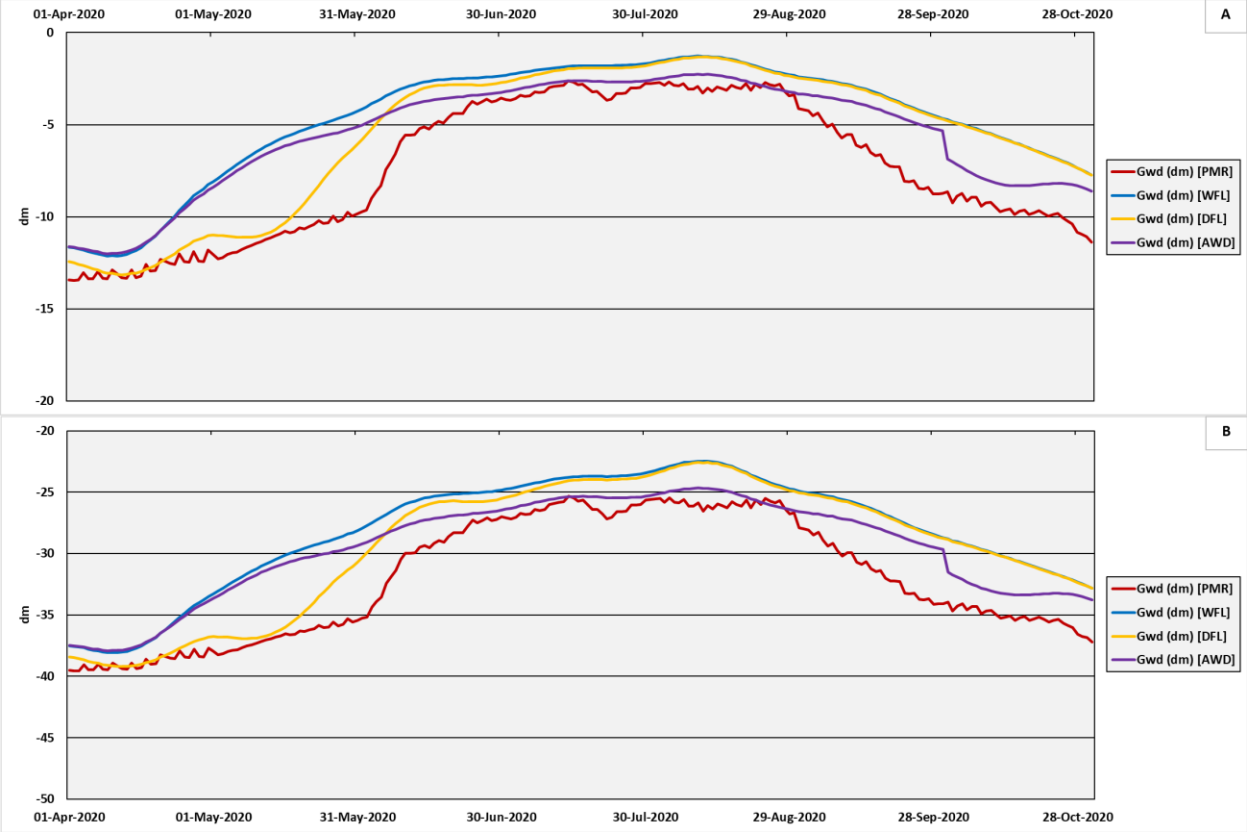

Figure 72. Simulated groundwater depth data series (A - shallow, and B - deep: GWD, dm) for PMR, WFL, DFL, and AWD scenarios; data reported are for the period April - October 2020.

5.3.5 Irrigation System Performance

Three indicators were employed to facilitate the analysis of the results: Water Application Efficiency (WAE, %), Distribution Efficiency of the channel network (DE, %), and Relative Water Supply (RWS, -). These three indicators, among the most commonly used to assess the performance of agricultural irrigation systems (Ahmad et al., 2024), are here formulated as:

$$WAE = \frac{A_{area}\, ETpot_t}{(\boldsymbol{A_{area}\, net\ irrigation_t} + Rain_t)} \qquad \text{(Eq. 34)}$$

$$DE = \frac{\boldsymbol{C_{network}\ net\ discharge_t}}{\boldsymbol{C_{network}\ gross\ discharge_t}} \quad \text{(Eq. 35)}$$

$$RWS = \frac{(\boldsymbol{A_{area}\ net\ irrigation_t} + Rain_t - \boldsymbol{C_{network}\ percolation_t})}{A_{area}\ ETpot_t} \quad \text{(Eq. 36)}$$

where

- $A_{area}\ ETpot$ (m, m^3/s) is the potential evapotranspiration,
- $A_{area}\ net\ irrigation$ (m, m^3/s) is the net irrigation needs simulated for the agricultural area,
- $Rain$ (m, m^3/s) is the rainfall,

- $C_{network}\ net\ discharge$ (m^3/s) is the irrigation water availability for the agricultural area,
- $C_{network}\ gross\ discharge$ (m^3/s) is the irrigation water entering at the inlet of a simulation domain,
- $C_{network}\ percolation$ (m^3/s, negative) is the estimated percolation coming from the channel network of a simulation domain,

- t (-) is the month of the simulation year.

WAE is the ratio of net crop water requirements to the total water delivered to the field (irrigation plus rainfall). An ideal value of 100% means supply exactly meets demand. As a field-level indicator, it excludes conveyance losses. Typical values are about 60% for surface irrigation, 75% for sprinkler, and up to 90% for drip systems (Bos et al., 1994; Burt et al., 1997; Molden, 1998; Pereira et al., 2012).

DE is the fraction of water entering a system's headworks that reaches the fields, i.e. the inverse of conveyance losses. While 100% is theoretical, observed values vary with lining, soil, and reach length: 60 - 80% in long unlined canals, 70 - 85% in medium reaches, 80 - 90% in short reaches, and about 95% in well-maintained lined canals (Burt et al., 1997; Molden, 1998; Pereira et al., 2012).

RWS compares total water supplied at the system inlet (including rainfall) with crop water requirements, indicating adequacy at system or district scale. Values near 1.0 denote balance; 0.8 - 1.0 slight deficit; 1.2 oversupply (Bos et al., 2005; Molden, 1998).

Indicators were calculated during the irrigation season (April - October) when the net irrigation was greater than 0 and WAE was at or below 100%. This was done to avoid non-representative results from months with low irrigation and minimal crop water requirement (generally, in April and October).

5.4 Results and discussion

5.4.1 Calibration and Validation

Figure 73 provides a monthly comparison between simulated net irrigation requirements ($A_{area}\ net\ irrigation$, m³/s) and estimated channel network net discharge ($C_{network}\ net\ discharge$, m³/s), aggregated over the entire simulation domain (values from the

agricultural area are weighted by simulation units area) for the years 2020 (calibration) and 2018 and 2019 (validation). It also includes percolation from the agricultural area (A area percolation, m³/s), percolation from the channel network ($C_{network}\ percolation$, m³/s), district total percolation (District total percolation, m³/s - A area percolation plus $C_{network}\ percolation$), gross irrigation availability ($C_{network}\ gross\ discharge$, m³/s), average groundwater depth within the domain (GWD, cm), the critical groundwater depth threshold ($GWDc_{network}$, cm) above which channel network losses are zero, potential evapotranspiration ($A_{area}\ ETpot$, m³/s) and rainfall ($Rain$, cm).

A visual analysis shows that during the central months of the irrigation season (June - August), the modelled agricultural water demand closely matched measured discharges, except for June 2019. In the early irrigation period (May), requirements appeared to be underestimated only in 2019, whereas in 2018 and 2020 the simulations successfully tracked the observed discharges. This supports the assumption of late-April rice seeding dates and confirms that in April, discharges circulating in the channel network are not yet applied to rice fields. In the late irrigation period (September), a clear underestimation of irrigation requirements was observed only in 2018. No irrigation diversions were recorded in October in any of the three reference years (2018 - 2020). To avoid discrepancies in the initial and final months of the irrigation season, April and October were excluded from the calculation of performance indices.

The calibration and validation efficiency indices are reported in Table 22. For the calibration year 2020, all performance metrics indicated very good agreement between estimates and observations (NSE = 0.766, RSR = 0.483, PBIAS = 5.31%, all rated very good according to Moriasi et al., 2007). In the validation phase, results for 2018 showed unsatisfactory NSE and RSR values (NSE = 0.439, RSR = 0.749) but good PBIAS (12.74%), whereas 2019 recorded unsatisfactory NSE and RSR (NSE = 0.008, RSR = 0.996) alongside very good PBIAS (4.83%).

In 2019, estimated agricultural irrigation water requirements diverged notably from measured irrigation availability values in May and June. AIES reported that while May 2019 was favorable (low irrigation demand), from June onwards irrigation water availability was reported as critically insufficient. The mismatch between simulated crop water needs and measured flow rates in 2019 is therefore not unexpected.

Performance in 2018 was mainly compromised by September, when the crop had already reached maturity and irrigation demand was minimal. Mean maximum temperatures during the core growing season (May - September) were highest in 2018, averaging 30.53 °C, compared with 29.46 °C in 2019 and 28.47 °C in 2020. Mean minimum temperatures followed a similar pattern (17.37 °C in 2018, 16.53 °C in 2019, and 16.36 °C in 2020). The warmer conditions in 2018 accelerated phenological development, resulting in a shorter crop cycle and harvest in early September. In contrast, the cooler conditions in 2019 and 2020 delayed maturation, with harvest occurring in mid-September.

When considering the entire 2018 - 2020 period, the aggregated performance indices show unsatisfactory NSE (0.380) and RSR (0.787) but very good PBIAS (7.59%). However, the 'clean' version of the dataset, obtained by excluding the identified critical months (September 2018 and May - June 2019), yields markedly improved results (NSE = 0.771, RSR = 0.479, PBIAS = 3.68%, all rated very good), numerically demonstrating that, once these anomalous periods are removed, the model parametrization is valid. Considering the large spatial extent of the study area and the inherent complexity of the modelling task, the calibration is considered satisfactory.

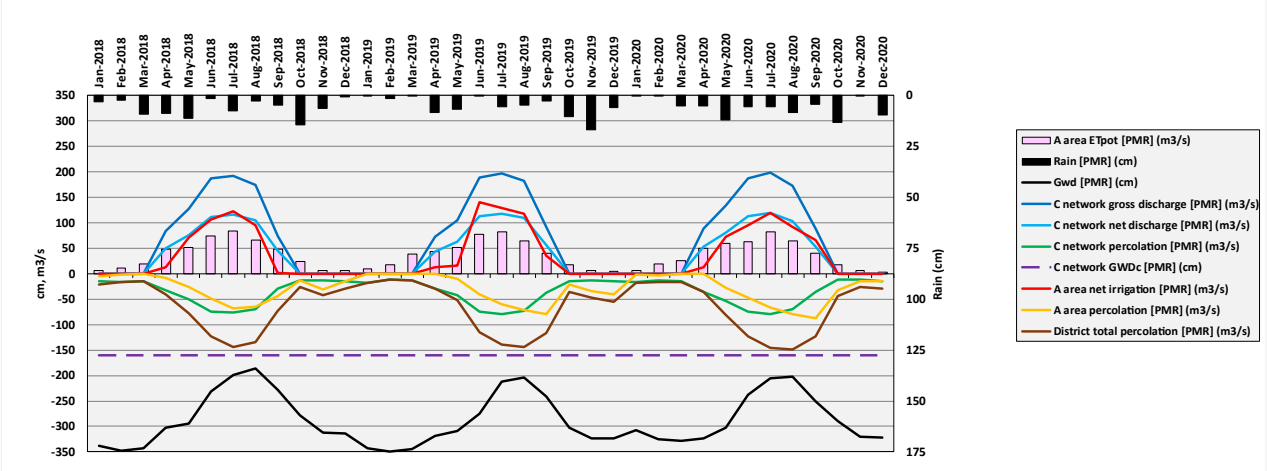

Figure 73. Calibration results for the Lomellina region (2018 - 2020). Values reported for the agricultural area are monthly aggregated data for the entire simulation domain (i.e. weighted for the areas of the corresponding simulation units).

Table 22. Model evaluation for the years 2020 (calibration) and 2018/2019 (validation). The 'clean' version of the dataset is obtained by excluding the critical months September 2018 and May - June 2019.

Index	Value	Moriasi et al. (2007)
2018		
NSE (-)	0.439	Unsatisfactory
RSR (-)	0.749	Unsatisfactory
PBIAS (%)	12.736	Good
2019		
NSE (-)	0.008	Unsatisfactory
RSR (-)	0.996	Unsatisfactory
PBIAS (%)	4.831	Very good
2020		
NSE (-)	0.766	Very good
RSR (-)	0.483	Very good
PBIAS (%)	5.312	Very good
2018 - 2020		
NSE (-)	0.380	Unsatisfactory
RSR (-)	0.787	Unsatisfactory
PBIAS (%)	7.586	Very good
2018 - 2020 (clean)		
NSE (-)	0.771	Very good
RSR (-)	0.479	Very good
PBIAS (%)	3.681	Very good

5.4.2 Field-level Simulations

Figure 74 and Figure 75 depict the WFL and FTI irrigation management simulated by QGIS-SWAP-Paddy in 2020 (PMR scenario) on soil unit 40710 (see Section 5.3.2.1.2) under two

groundwater depth conditions (shallow and deep). An example of the simulated DFL and AWD management scenarios on the same soil unit and under two groundwater table conditions are shown in Figure 76 and Figure 77, respectively. All the figures shows: SWAP input irrigation (Irrigation, cm), runoff (Runoff, cm), estimated net irrigation (= Irrigation - Runoff), target ponding water level (Pond target, cm), simulated ponding water on the field (Pond actual, cm), soil water potential at -5 cm (P. head, dm), crop development stage (DVS, -), groundwater table depth (GWD, cm), and rainfall (Rain, cm). These figures present daily water balance results generated by SWAP at the field scale. The soil water potential at -5 cm is shown to visually track the activation of AWD irrigation when the soil water potential reaches -10 kPa (AWD, -10 dm) at a depth of -5 cm.

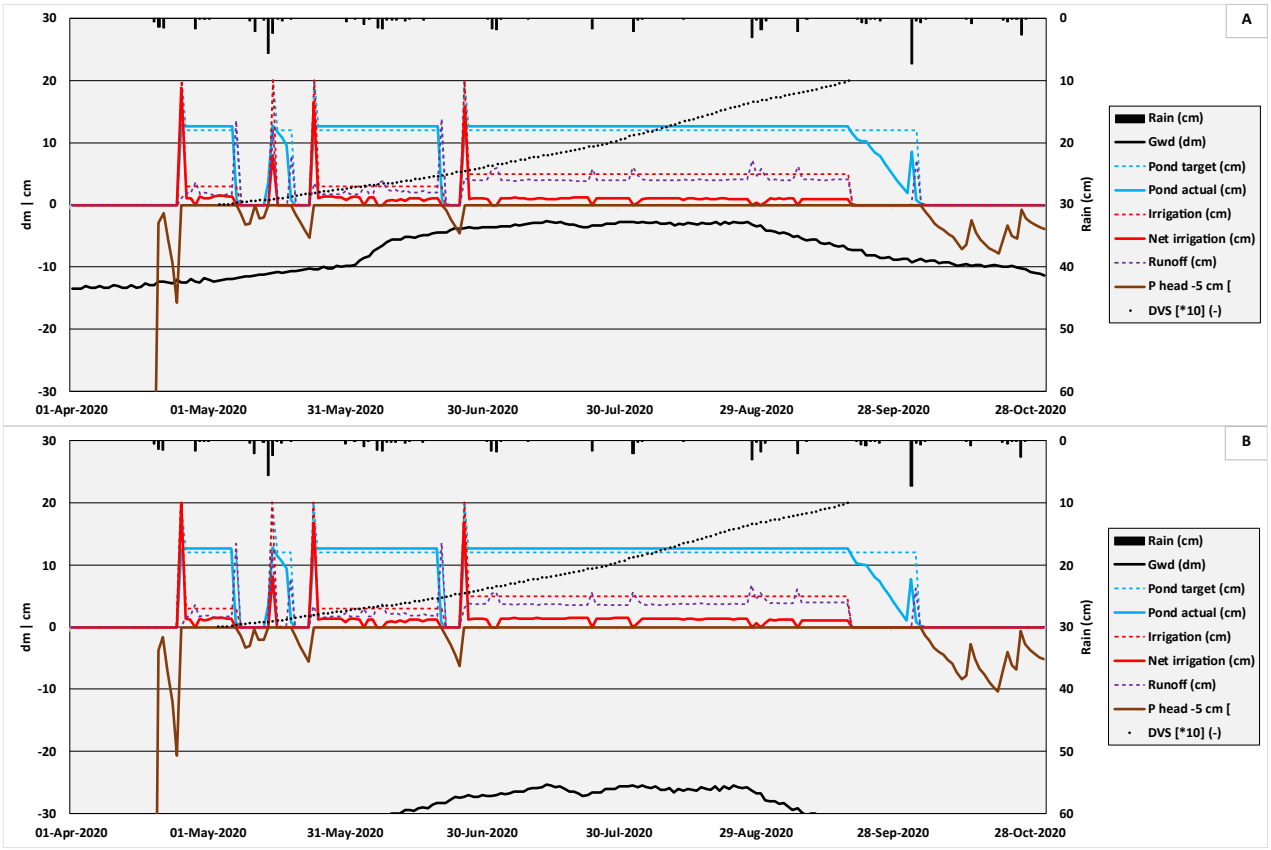

Figure 74. WFL irrigation management on soil 40710 (Table 17) with two groundwater depth conditions: A - shallow, B- deep (PMR scenario; 2020).

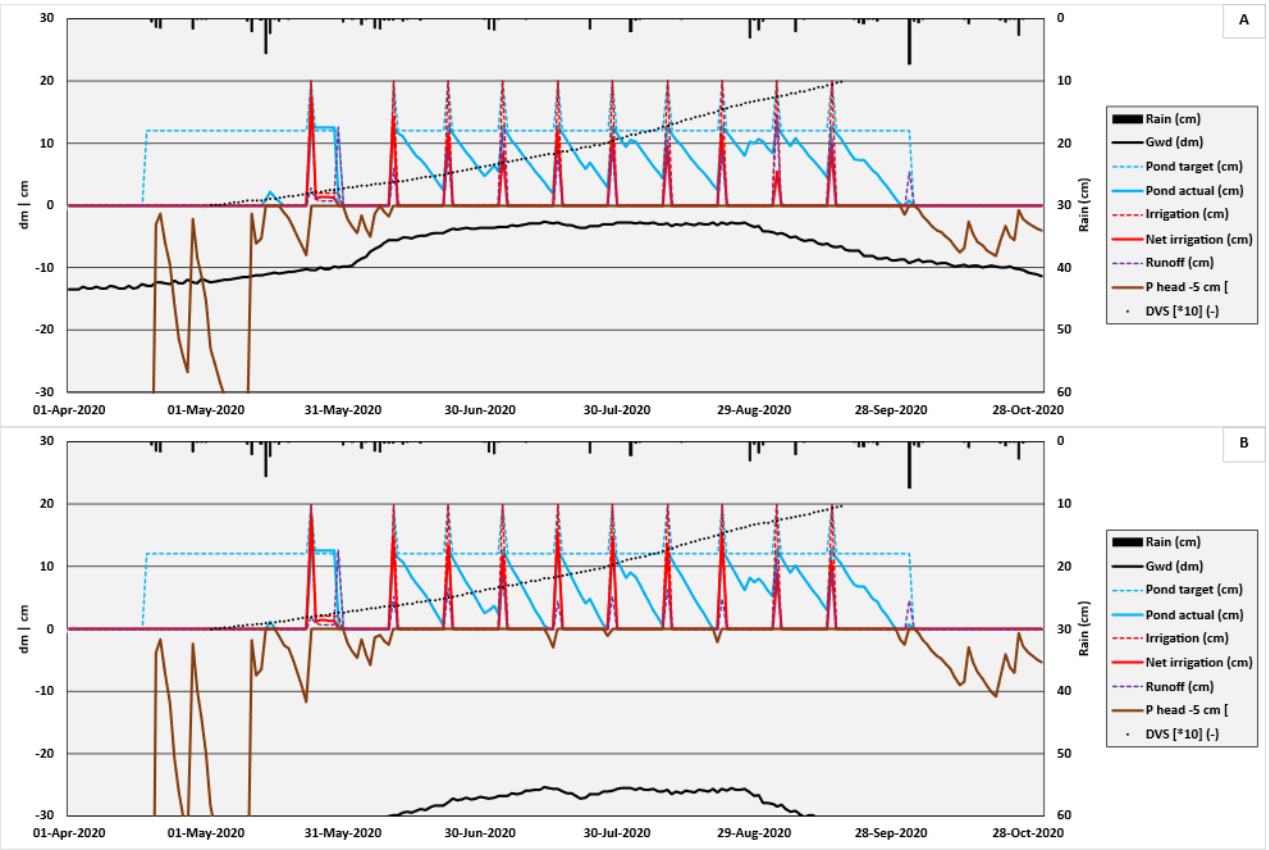

Figure 75. FTI irrigation management on soil 40710 (Table 17) with two groundwater depth conditions: A - shallow, B- deep (PMR scenario; 2020).

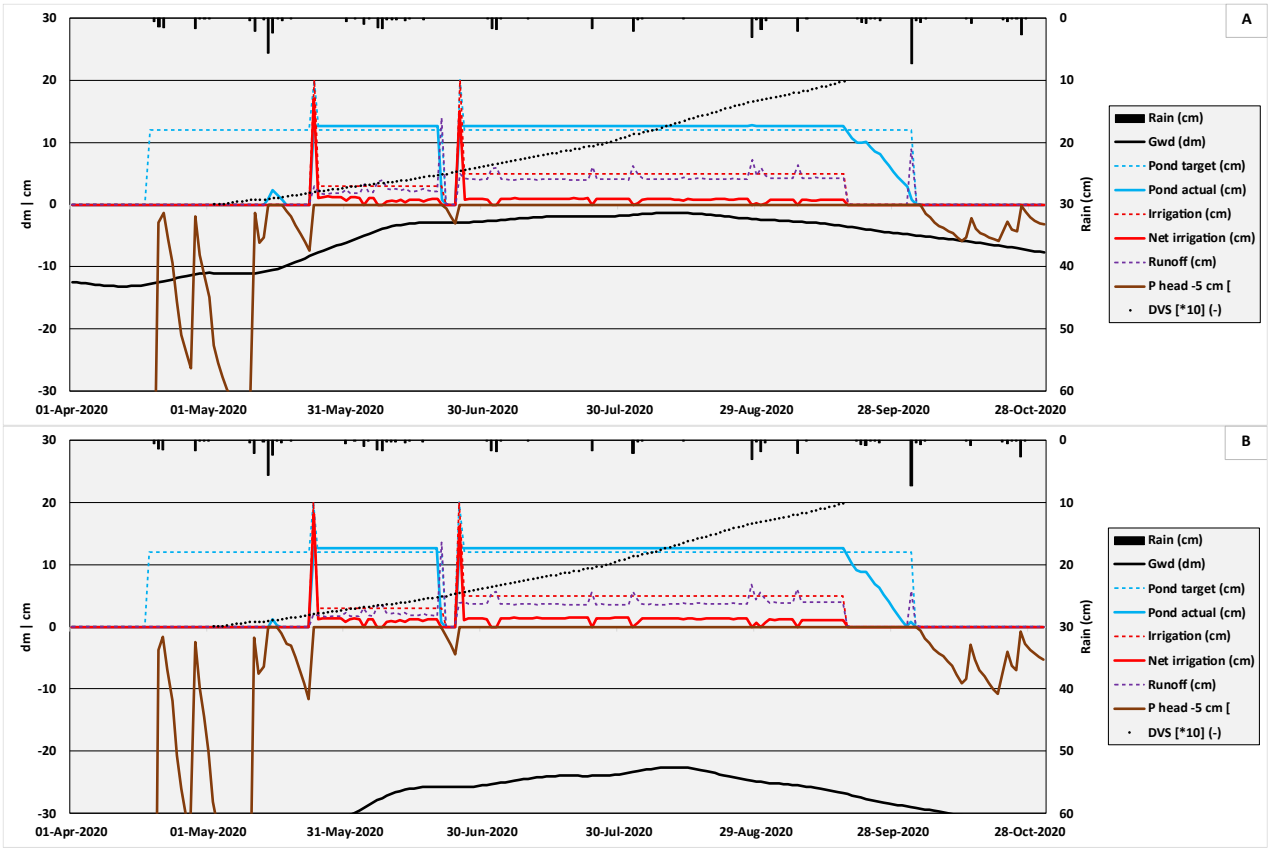

Figure 76. DFL irrigation management on soil 40710 (Table 17) with two groundwater depth conditions: A - shallow, B- deep (DFL scenario; 2020).

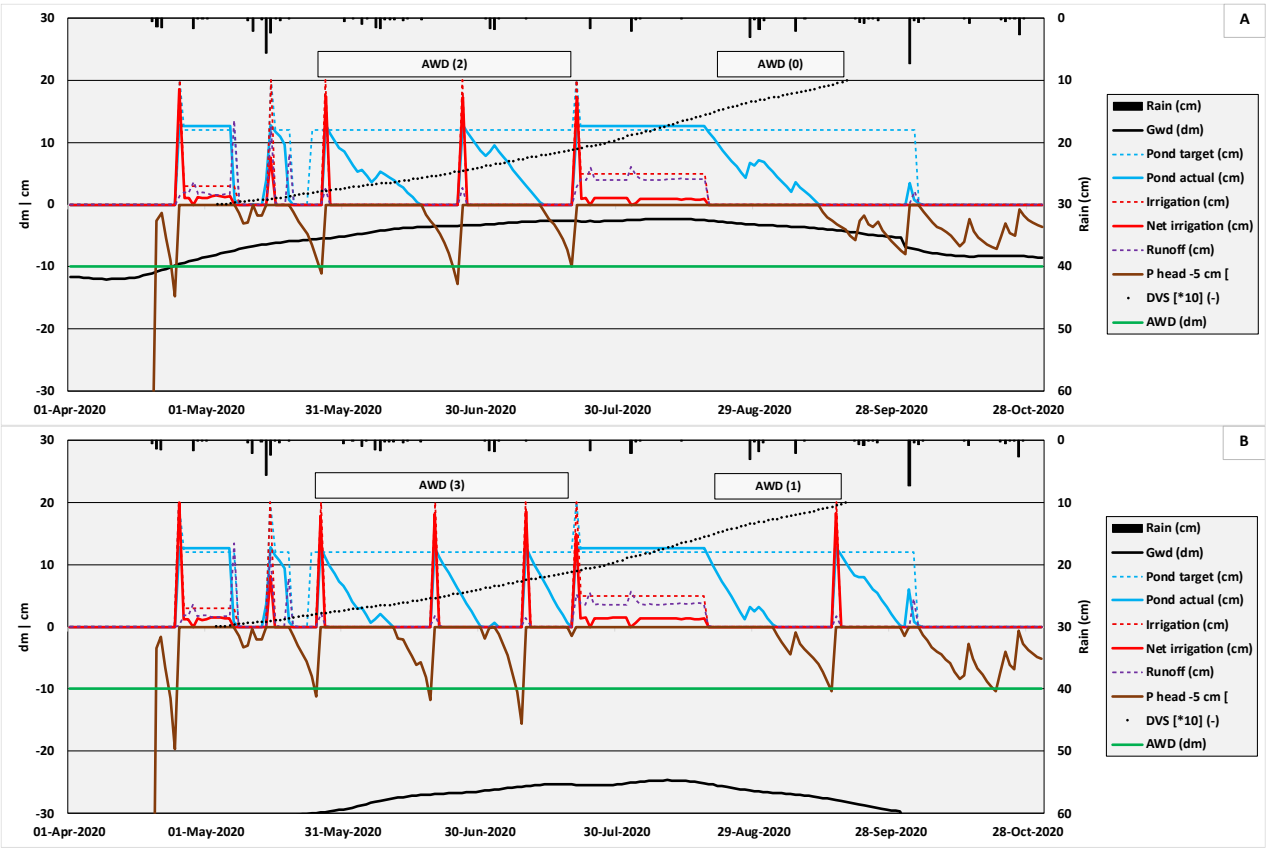

Figure 77. AWD irrigation management on soil 40710 (Table 17) with two groundwater depth conditions: A - shallow, B- deep (AWD scenario; 2020).

The following results summarize the behavior at field-level for the different simulated scenarios (PMR - Figure 78, WFL - Figure 79, AWD - Figure 80, and DFL - Figure 81). Results include data on both net irrigation requirements (A_{area} $net\ irrigation$, m), deep percolation (A area percolation, m), number of days of submersion (A area s irrigation, n), and number of irrigation events (A area n irrigation). The days of submersion refer to the total number of days in which the field simulations record a net irrigation value greater than zero, corresponding to periods when the fields are flooded under WFL, DFL, and AWD management, whereas the number of irrigation events refers only to the count of individual applications not followed by days of flooding. In the case of FTI, these represent simply the number of turned irrigation applications, while in the case of AWD they correspond to irrigation events resulting from the alternating irrigation cycles. Apart from PMR, WFL, DFL and AWD scenarios results are reported for each groundwater depth condition simulated (shallow and deep). Discussion of the results is mainly done based on average values (irrigation heights or number of applications) calculated for the period 2013 - 2023 including both shallow and deep groundwater conditions for each soil use.

WFL rice cultivated under the PMR scenario recorded the highest irrigation applications (3.1 m). The difference between this and the same type of management applied to rice in the WFL scenario, which recorded slightly lower average consumption (2.9 m, -6.45% compared to WFL under the PMR scenario), lies solely in the lower boundary condition used. The PMR scenario has lower groundwater levels throughout the irrigation season compared to the WFL scenario; clearly,

higher groundwater levels lead to lower irrigation needs for the simulated rice units. In terms of water use, the WFL management scenario is followed by DFL (2.4 m, -22.6% compared to WFL under the PMR scenario and -17.2% compared to WFL in the WFL scenario), which, despite the delayed flooding of the fields, benefits, in terms of the total amount of water applied, from the dry seeding technique adopted at the beginning of the season (April - May). Both WFL and DFL show higher water uses when under deep groundwater conditions (WFL shallow: 2.4 m, WFL deep: 3.4 m, +41.7% from shallow to deep; DFL shallow: 1.9 m, DFL deep: 2.8 m, +47.4% from shallow to deep).

AWD scenario resulted in a seasonal water use of 2.1 m (-32.3% compared to WFL under the PMR scenario and -27.6% compared to WFL in the WFL scenario), with an average of 4.9 irrigation applications. During the 2019 - 2020 agricultural season, a safe AWD strategy (WLD ≥ -10/15 cm; SWP at -5 cm ≈ -5 kPa) was tested alongside WFL in a field experiment conducted within the MEDWATERICE project at CRR-ENR (Gharsallah et al., 2023). In that trial, AWD reduced water use by about 20% compared to WFL, without any loss in rice yield. In the RISWAGEST project (Vitali et al., 2024), carried out during the 2021 - 2022 agricultural seasons at CRR ENR, wet seeding was combined with two AWD strategies: a safe version and a strong version (WLD ≥ -20/25 cm; SWP at -5 cm ≈ -20 kPa). Over the two years of trials, safe AWD achieved water savings of around 25%, and strong AWD about 31%, both without yield reduction (even in 2022, when irrigation water availability was limited). The AWD implementation adopted in this study, with irrigation starting when the soil water potential at -5 cm depth reaches -10 kPa (≈ -100 cm), lies between the safe and strong versions tested in MEDWATERICE and RISWAGEST. Therefore, results obtained are consistent with the experimental evidence gathered at CRR ENR. AWD water savings versus WFL aligns with earlier findings (10 - 25%) by Bouman & Tuong (2001), Belder et al. (2004), and Carrijo et al. (2017). The higher water savings observed in this study are likely related to the lighter soil textures (loam/sandy loam) of the case study, which have higher percolation rates than the predominantly clayey soils of many Asian, thus increasing the potential water savings achievable through AWD. Figure 82 shows the spatial distribution of AWD irrigation events in 2020 for all the rice simulation units (107 units, 62,615 ha) considered in the scenario. The class that collects the most simulation units ranges between 3 and 6 interventions (69 units, 45,323.52 ha, more than 70% of the total rice area). In the figure the average $A_{area}\ net\ irrigation$ (m) and average agricultural area deep percolation (m) for each class is also reported. On average, the difference in the number of applications between shallow and deep groundwater conditions is 3 events. Here, the groundwater depth condition heavily influences the number of AWD irrigation events simulated (3.2 under shallow condition and 6.3 under deep condition). Between the average irrigation applications for shallow groundwater conditions (1.7 m) and for deep groundwater conditions (2.5 m), there is a percentage increase of about 47.1%.

FTI recorded the lowest consumption (1.5 m), corresponding to -51.6% compared to WFL under the PMR scenario and -48.3% compared to WFL in the WFL scenario. Despite the lower number of applications relative to AWD (FTI: 8.4 vs AWD: 4.9), in terms of mere water use, FTI benefits from the dry seeding technique applied and the absence of submersion during the flowering phase.

As regards percolation, values are essentially consistent with net irrigation applications.

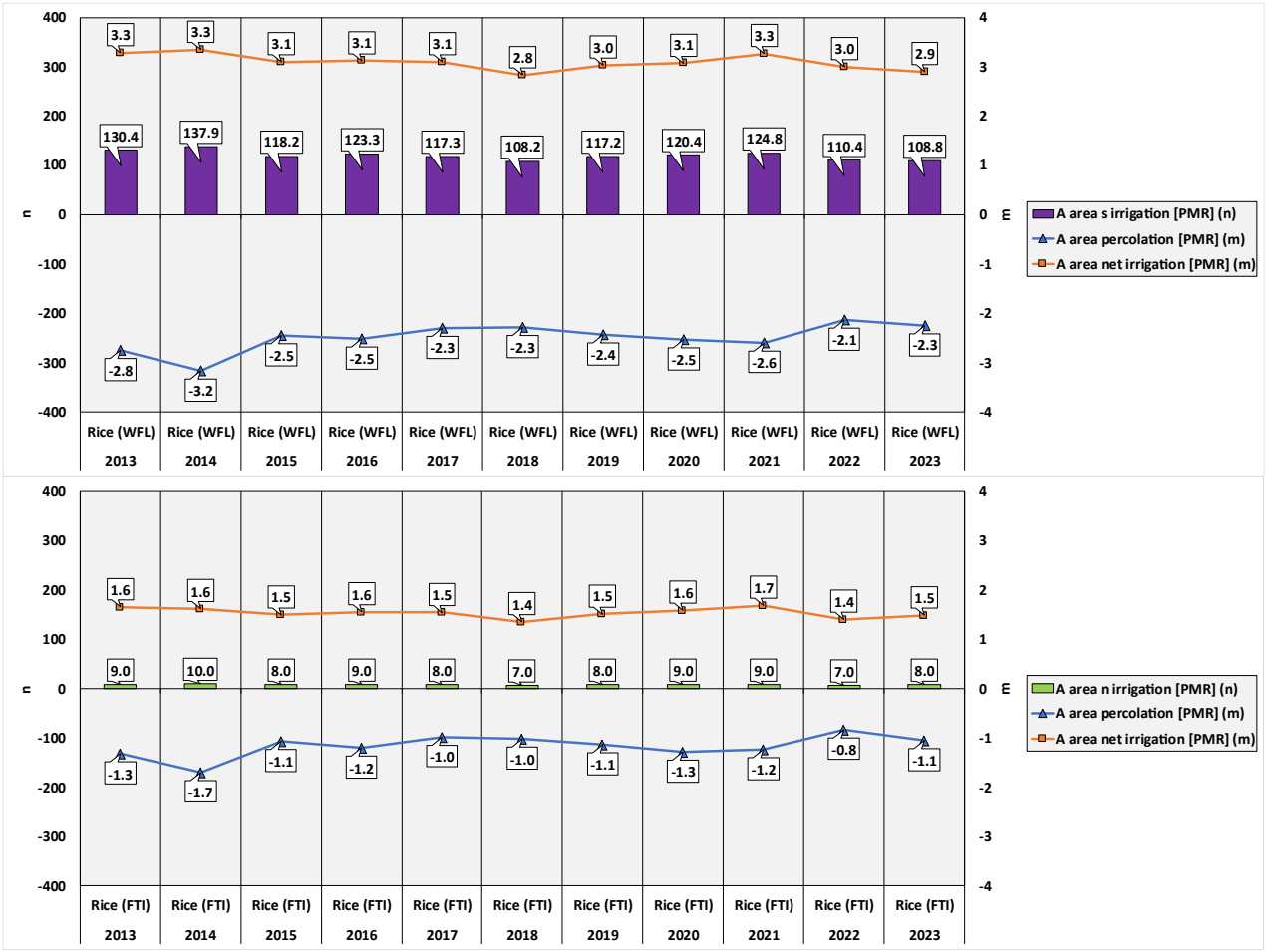

Figure 78. Yearly field-level simulation results (WFL and FTI; PMR scenario, 2013 - 2023). Results include net irrigation requirements (A_{area} net irrigation, m), deep percolation (A area percolation, m), number of days of submersion (A area s irrigation, n), and number of irrigation events (A area n irrigation).

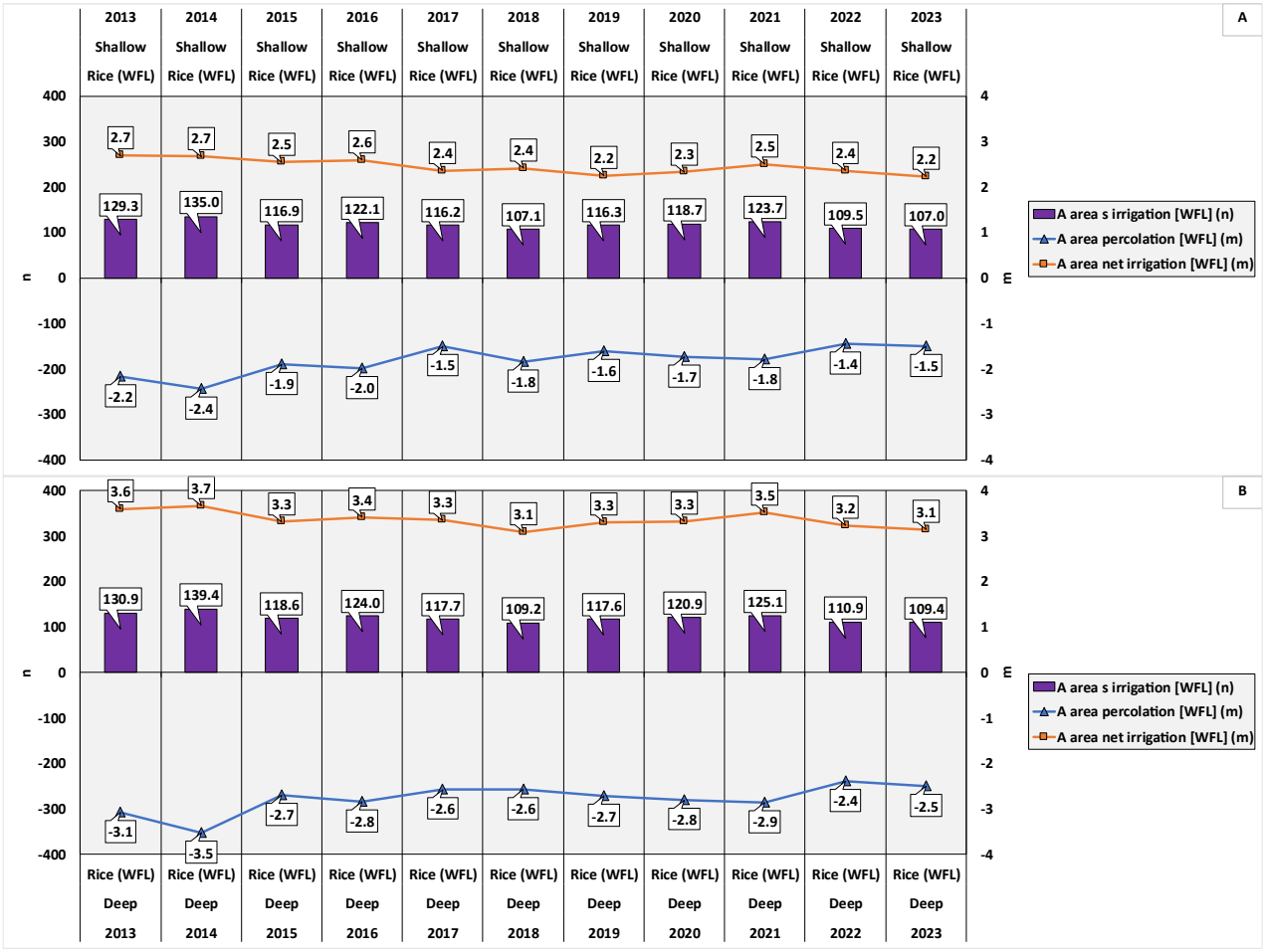

Figure 79. Yearly field-level simulation results (WFL shallow groundwater, and WFL deep groundwater; WFL scenario, 2013 - 2023). Results include net irrigation requirements (A_{area} net irrigation, m), deep percolation (A area percolation, m), and number of days of submersion (A area s irrigation, n).

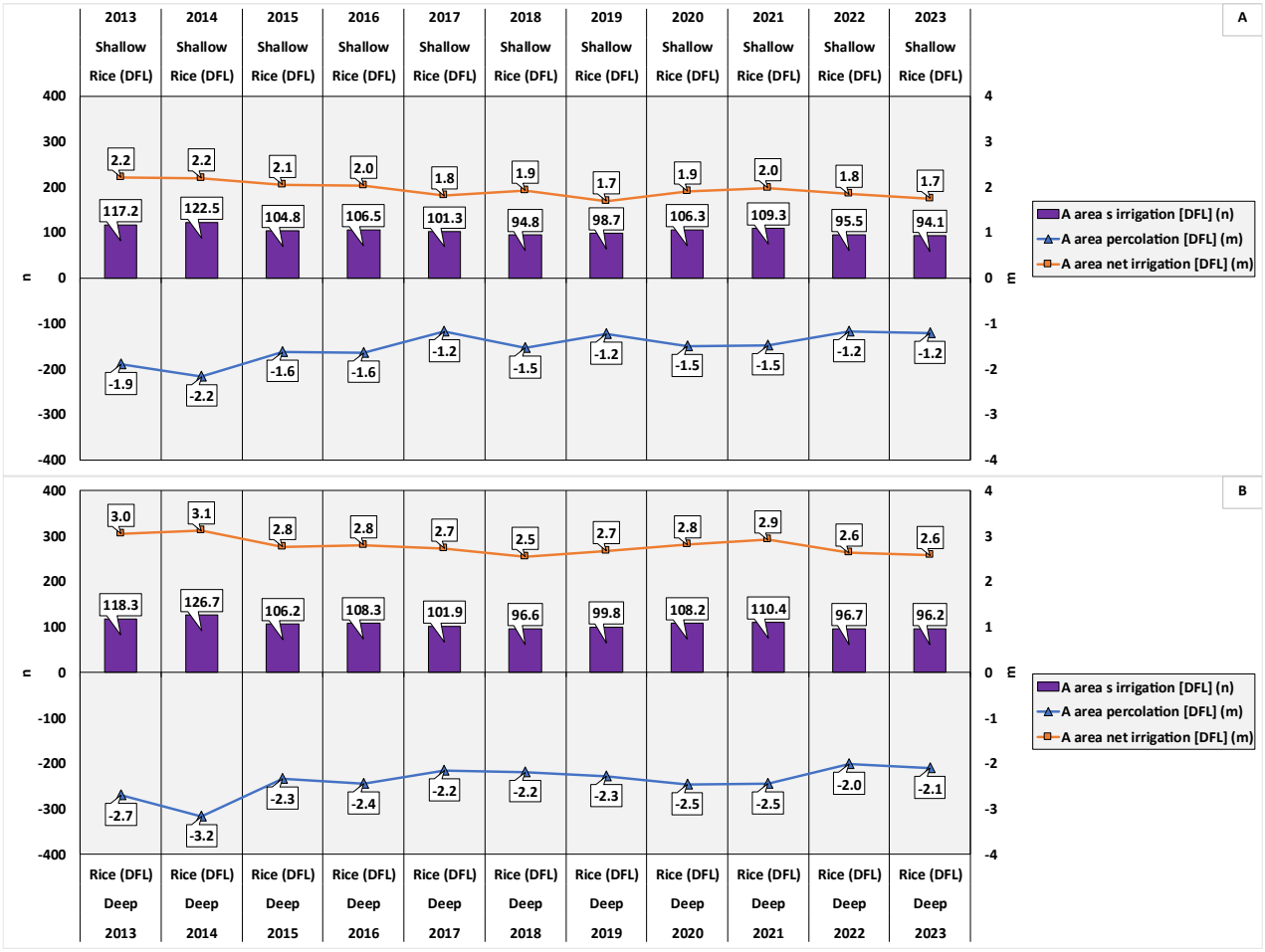

Figure 80. Yearly field-level simulation results (DFL shallow groundwater, and DFL deep groundwater; DFL scenario, 2013 - 2023). Results include net irrigation requirements (A_{area} net irrigation, m), deep percolation (A area percolation, m), and number of days of submersion (A area s irrigation, n).

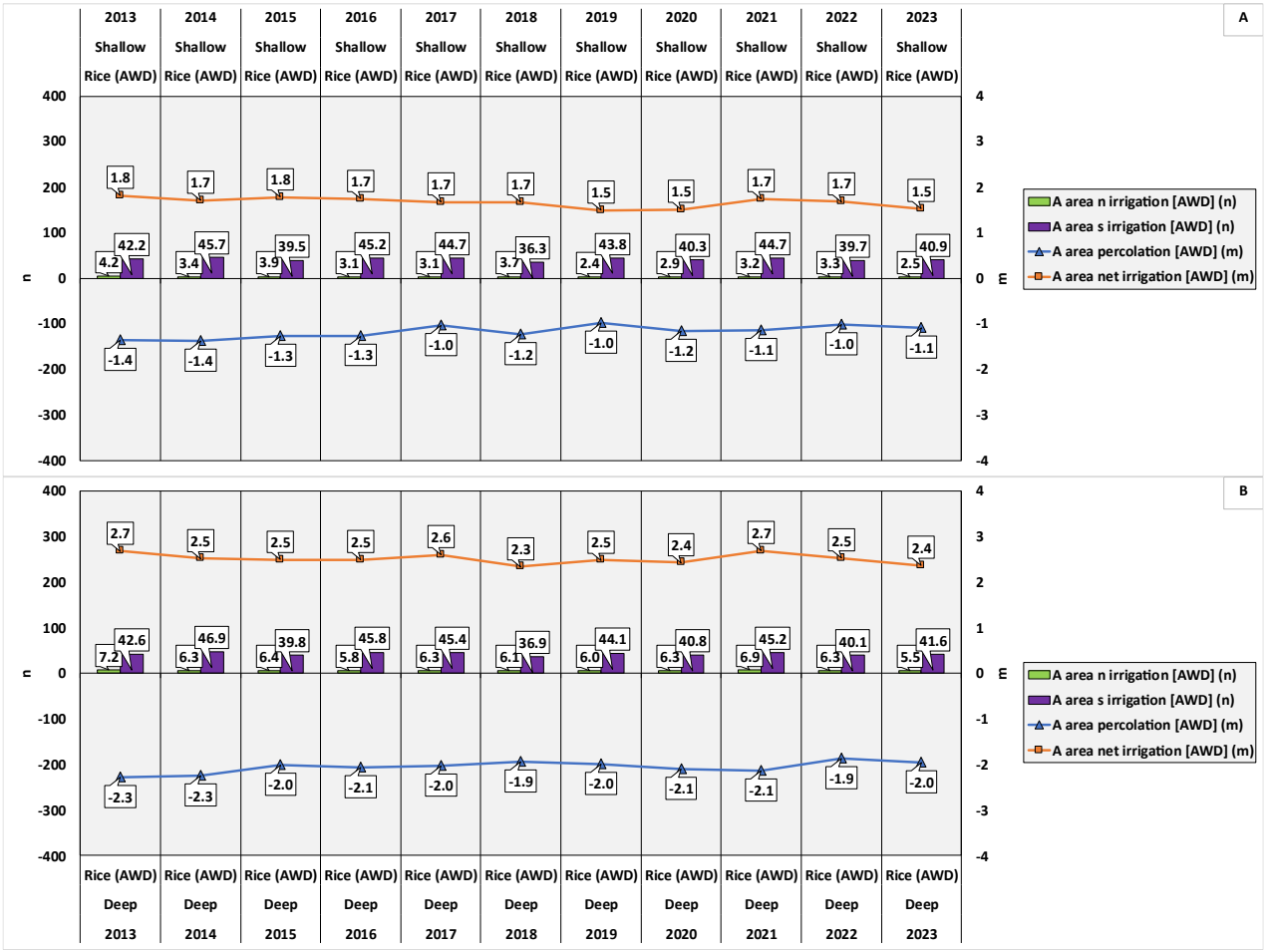

Figure 81. Yearly field-level simulation results (AWD shallow groundwater, and AWD deep groundwater; AWD scenario, 2013 - 2023). Results include net irrigation requirements (A_{area} net irrigation, m), deep percolation (A area percolation, m), number of days of submersion (A area s irrigation, n), and number of irrigation events (A area n irrigation).

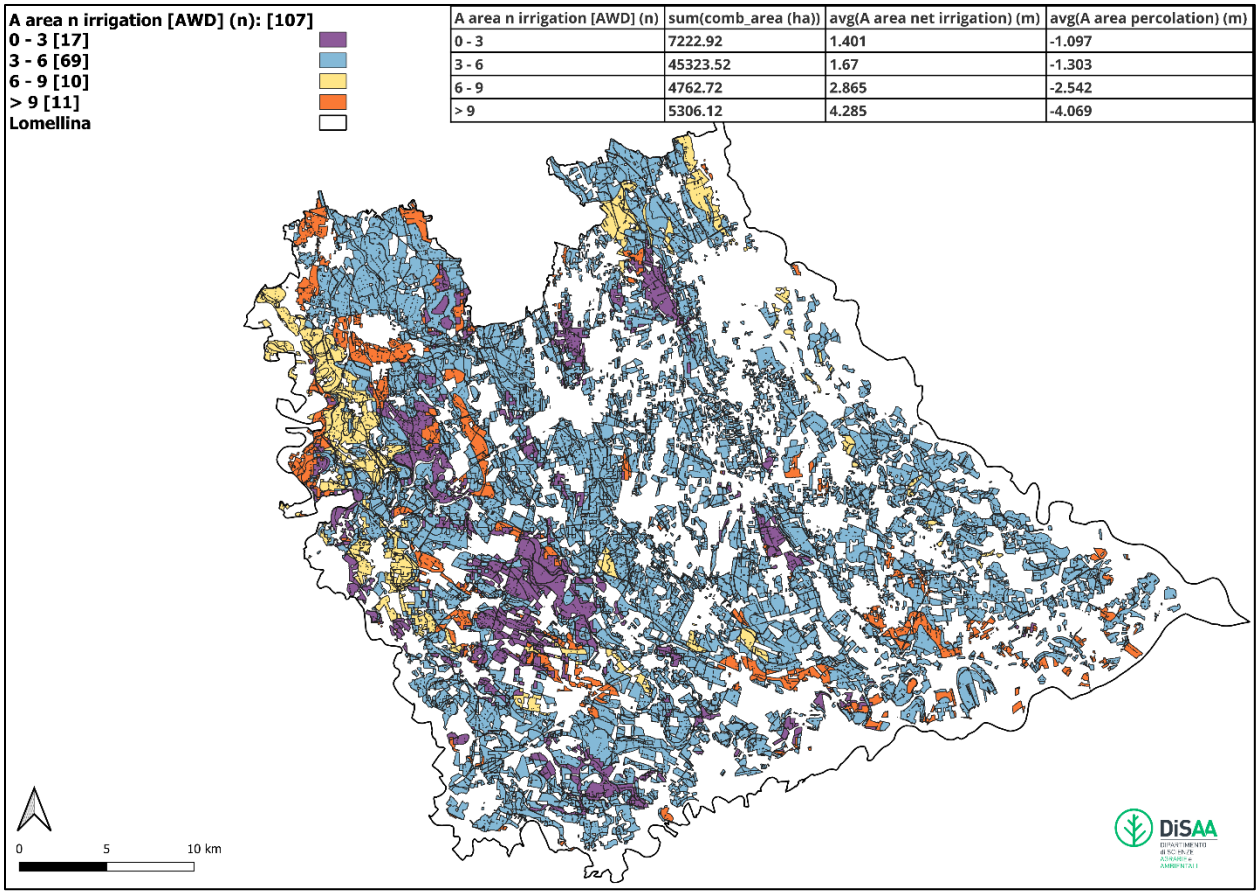

A area n irrigation [AWD] (n)	sum(comb_area (ha))	avg(A area net irrigation) (m)	avg(A area percolation) (m)
0 - 3	7222.92	1.401	-1.097
3 - 6	45323.52	1.67	-1.303
6 - 9	4762.72	2.865	-2.542
> 9	5306.12	4.285	-4.069

Figure 82. Spatial distribution of AWD irrigation events (n) for the year 2020. Simulation units count is reported in the legend on the left; average A_{area} net irrigation (m) and average agricultural area deep percolation (m) for each irrigation event class is reported in the table on the right.

5.4.3 Domain-level Simulations

Figure 83 shows monthly results aggregated over the entire simulation domain from 2013 to 2023, and for all the simulated scenarios (PMR, WFL, DFL, and AWD). Values (A_{area} $ETpot$, A_{area} $net\ irrigation$, A area percolation) coming from the agricultural area semi-distributed sub-model (m) are weighted by simulation units area (m^2) within the entire simulation domain (m^3) and, then, reported in m^3/s. Channel network gross discharges ($C_{network}$ $gross\ discharge$ - i.e. the district total requirement, that is agricultural A_{area} $net\ irrigation$ plus $C_{network}$ $percolation$) and $C_{network}$ $percolation$, are produced by the channel network sub-model directly in m^3/s. $Rain$, average groundwater depth within agricultural area of the simulated domain (GWD), and the critical groundwater depth above which percolation losses from the channel network should be equal to zero ($GWDc_{network}$) are in cm. District total percolation (m^3/s) is the sum of agricultural area percolation and channel network percolation. Moreover, Figure 84 reports average (2013 - 2023) monthly channel network gross discharges and district total percolations.

With respect to the annual district irrigation requirements (sum of monthly values reported in Figure 84), the WFL scenario shows the highest overall usage (1,152.5 m^3/s), followed by DFL

(945.5 m³/s, -18.0%), AWD (812.0 m³/s, -29.6%), and PMR (787.1 m³/s, -31.7%). In San Giorgio di Lomellina, AWD returned a water use slightly higher (+2.4%) than DFL. The different parameterization of the AWD compared to the previous study could explain these differences. In facts, the development model studied together with ENR has been further refined in its irrigation scheduling component, given the potential of the new modelling framework to define time dependent ponding thresholds and allow a rational integration between fixed and crop-related irrigation management at field level (AWD uses a mix of the two, fixed irrigation scheduling for seeding and re-flooding during flowering and crop-related during the actual AWD management). Moreover, these differences could be also attributable to values of the saturated hydraulic conductivity of the hardpan horizons in rice soils, which are higher in the pilot district than in the entire Lomellina area. One Ks value was in the 0.7 - 1.0 range, one in 0.4 - 0.7, three in 0.1 - 0.4, and, most notably, none below 0.1. This probably penalized management with wet seeding at the time of first flooding of fields in the first part of the season (end of April - May). AWD re-flooding during flowering in July, instead, requires less water since fields are already alternatively irrigated in the preceding months (end of May - June).

In terms of average monthly values, the analysis highlights June as the most critical month for both the WFL and DFL scenarios (with DFL surpassing WFL, and both notably exceeding PMR and AWD), while July emerges as the most significant for AWD and PMR, wherein AWD water use exceeds PMR but remains below DFL and WFL. This seems in line with farmers and irrigation managers perception that, since the introduction of DFL in Northern Italy, competition for irrigation water is increasing in June and partially in July. It should be noted that in previous simulations conducted in San Giorgio di Lomellina, DFL showed 25% higher water use than WFL (for the entire Lomellina area, however, this was just 3.8%). This happened in a simulation setup that dynamically adapts groundwater level within the simulation domain based on district total percolations. Incorporating a dynamically responsive aquifer, even for the Lomellina region, would likely accentuate differences between delayed-flood and continuous-flood approaches. Notably, AWD exhibits a marked reduction in usage during June compared to all other scenarios. Scenarios involving wet seeding (WFL, and AWD) clearly indicate higher irrigation demand during the early season months (April - May), contrasted with those involving dry seeding (PMR, and FTI).

District annual and monthly total percolations largely follow the same relative order as irrigation usage. Annual values are as follows: WFL, with -1 007.7 m³/s, followed by DFL, with -857.3 m³/s (-14.9%), AWD, with -731.7 m³/s (-27.4%), and PMR, with -696.4 m³/s (-30.9%).

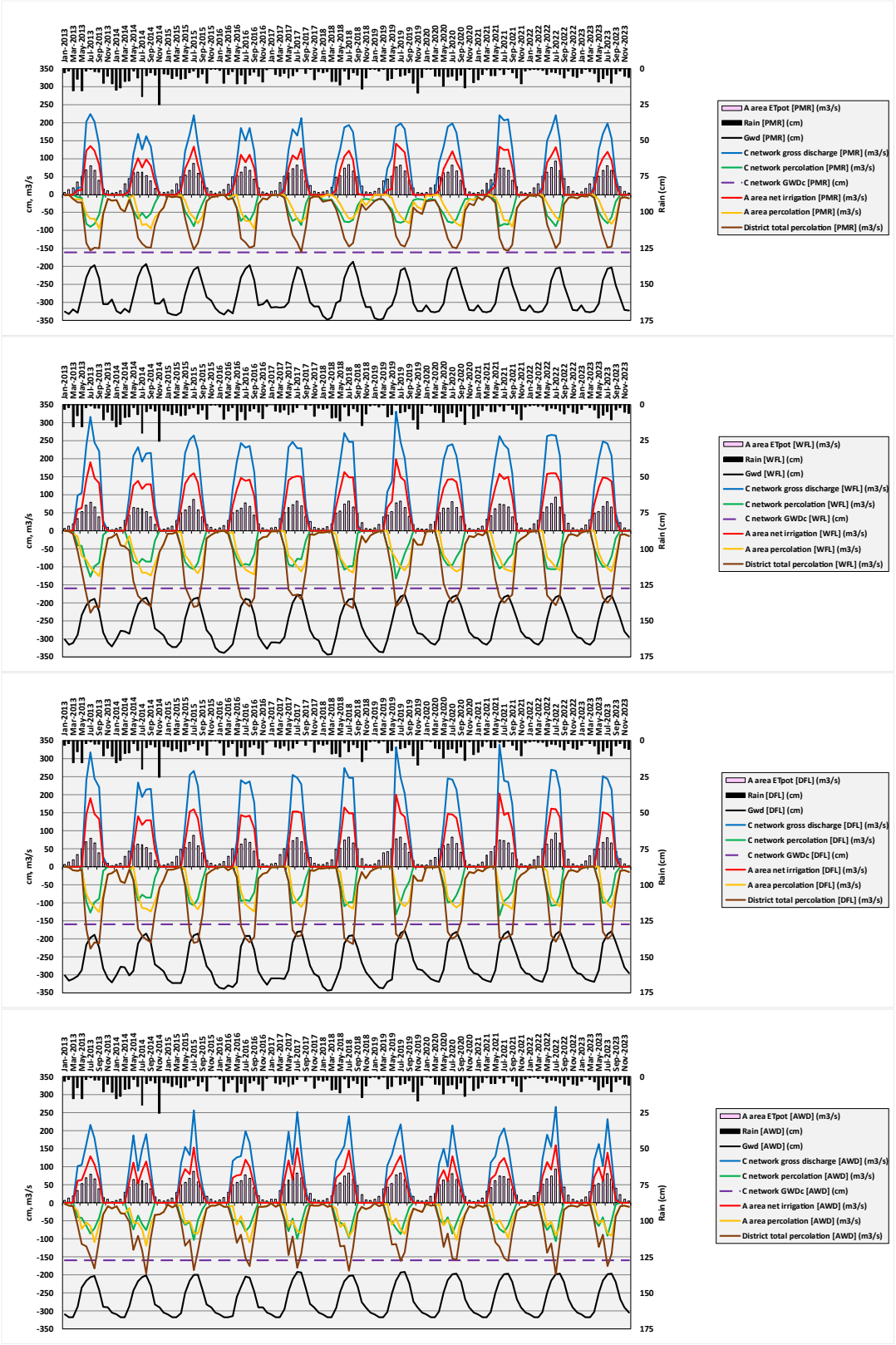

Figure 83. Monthly simulation results (2013 - 2023) aggregated over the entire simulation domain from 2013 to 2023, and for all the simulated scenarios (PMR, WFL, DFL, and AWD).

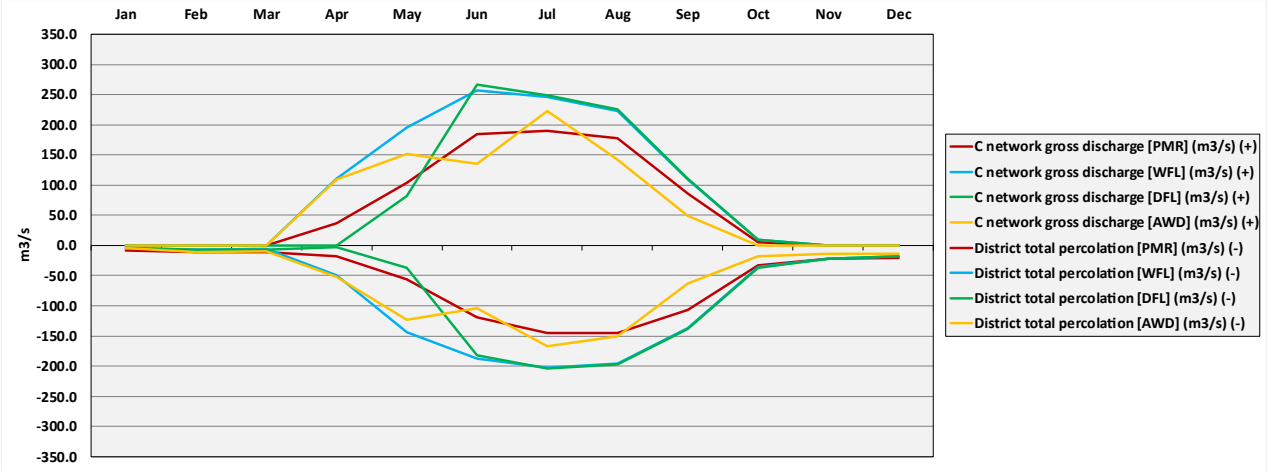

Figure 84. Average (2013 - 2023) monthly $C_{network}$ gross discharge and district total percolation (both in m³/s) for all the simulated scenarios (PMR, WFL, DFL, and AWD).

5.4.4 Irrigation System Performance

With the current parameterization of the channel network model, variations in $C_{network}$ *gross discharge* are primarily attributed to rice irrigation management practices within the agricultural area, rather than to changes in the channel network's efficiency (DE, Figure 85 - average monthly values calculated for DE in 2013 - 2023). Average district groundwater depth series (GWD) has rarely reached the threshold ($GWDc_{network}$) that would prevent percolation from the channel network across all the simulated scenarios. Consequently, the overall channel network losses amount to approximately 0.4% for the whole irrigation season, except for July and August for the WFL and DFL scenarios. Although the simulated aquifer series are identical to those in San Giorgio, the failure to meet the critical $GWDc_{network}$ threshold is primarily due to the spatial distribution of aquifer depth zones. Across the entire Lomellina area, the shallow aquifer accounts for about 25% of the surface and the deep aquifer for about 75%, whereas in San Giorgio these proportions were approximately 40% and 60%, respectively. This difference matters because, to obtain the average groundwater depth for the territory, the model weights the values from each aquifer series by the corresponding area of its depth zone.

This configuration is further illustrated by the average (2013 - 2023) monthly values of WAE (Figure 86) and RWS (Figure 87), whose rankings are consistent with the simulated district total requirements under the different scenarios. PMR records the highest yearly WAE (based on the average of the monthly values reported in Figure 86) at 55.3%, followed by AWD (54.1%), DFL (42.6%), and WFL (41.8%). AWD achieves the lowest yearly RWS (average of monthly values reported in Figure 87) at 2.8, with PMR next (2.9), followed by WFL (3.8) and DFL (3.9). Performance for WFL, DFL and AWD are higher than those simulate for San Giorgio. Again, this can be explained by better use of irrigation resources at field level in the simulated scenarios (crop development and irrigation management model) and by the different nature of the simulated soils (saturated hydraulic conductivity of the hardpan).

In terms of annual performance, AWD is very close to the PMR scenario despite requiring greater total irrigation volumes (812.0 m³/s vs 787.1 m³/s). This advantage is largely driven by

AWD exceptional performance in the critical month of June (WAE: 70.5% vs 53.9%; RWS: 2.2 vs 3.0) a result of the alternating water management strategy applied in this scenario. Additional gains are observed in the latter part of the season (August - October). However, AWD underperforms relative to PMR in the early season (April - May), due to wet seeding practices applied across all the rice-growing area, and again in July, when re-flooding is undertaken during the flowering stage.

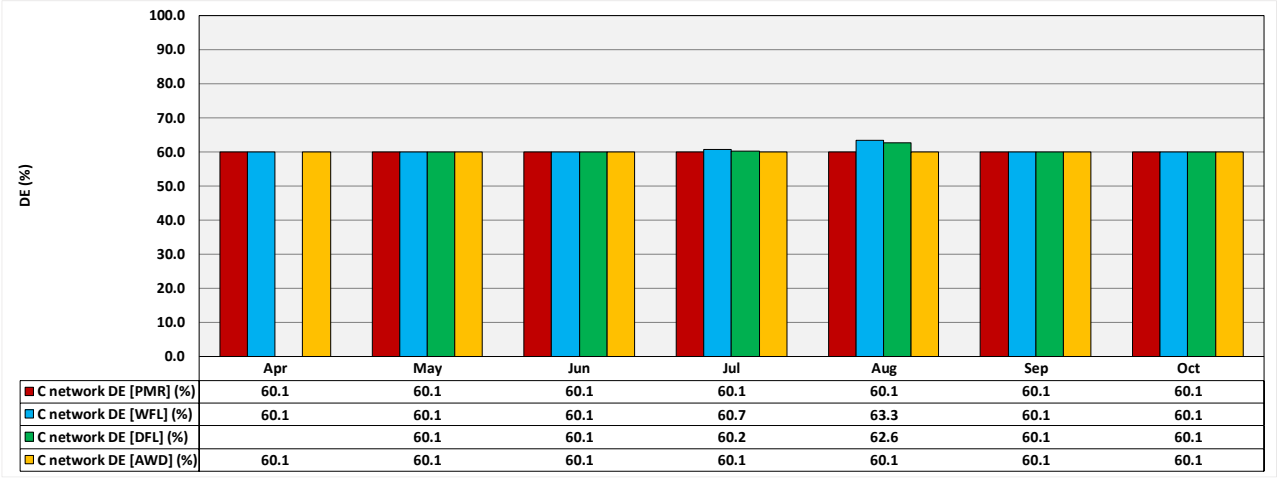

	Apr	May	Jun	Jul	Aug	Sep	Oct
C network DE [PMR] (%)	60.1	60.1	60.1	60.1	60.1	60.1	60.1
C network DE [WFL] (%)	60.1	60.1	60.1	60.7	63.3	60.1	60.1
C network DE [DFL] (%)		60.1	60.1	60.2	62.6	60.1	60.1
C network DE [AWD] (%)	60.1	60.1	60.1	60.1	60.1	60.1	60.1

Figure 85. Average (2013 - 2023) monthly values of Distribution Efficiency of the channel network - DE (%).

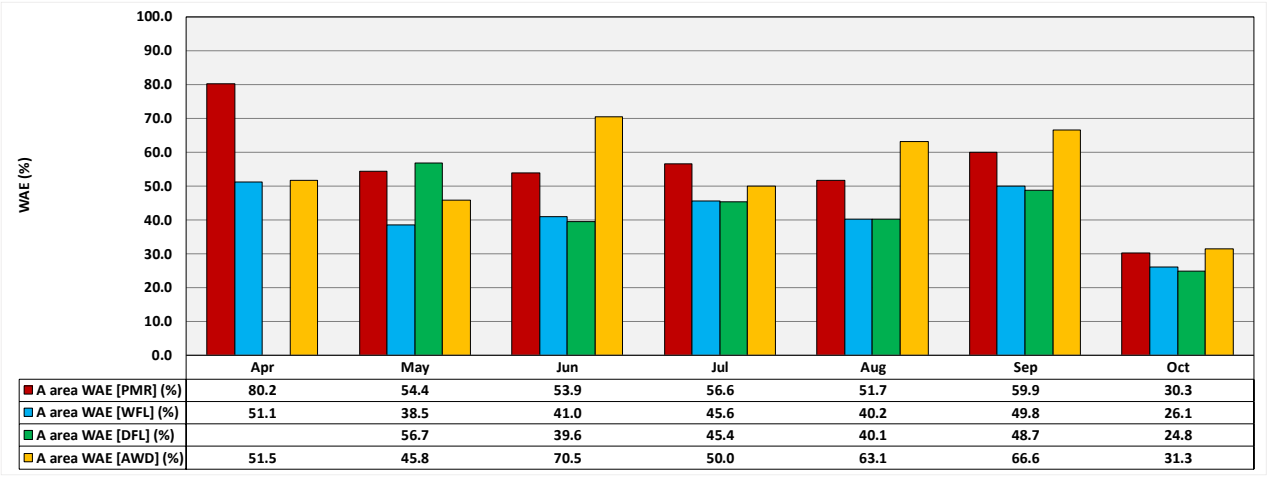

	Apr	May	Jun	Jul	Aug	Sep	Oct
A area WAE [PMR] (%)	80.2	54.4	53.9	56.6	51.7	59.9	30.3
A area WAE [WFL] (%)	51.1	38.5	41.0	45.6	40.2	49.8	26.1
A area WAE [DFL] (%)		56.7	39.6	45.4	40.1	48.7	24.8
A area WAE [AWD] (%)	51.5	45.8	70.5	50.0	63.1	66.6	31.3

Figure 86. Average (2013 - 2023) monthly values of Water Application Efficiency - WAE (%).

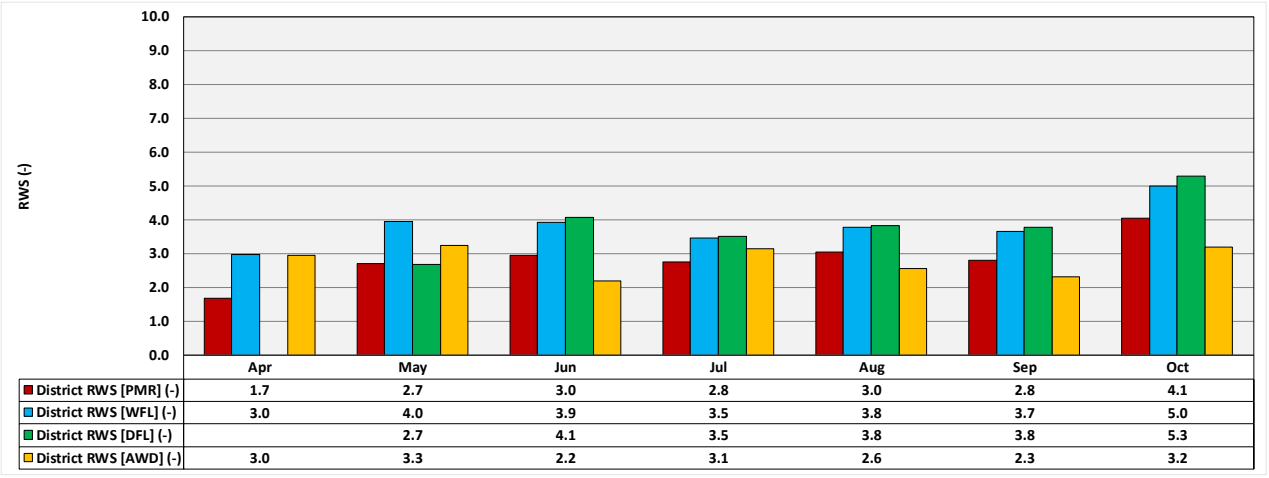

	Apr	May	Jun	Jul	Aug	Sep	Oct
District RWS [PMR] (-)	1.7	2.7	3.0	2.8	3.0	2.8	4.1
District RWS [WFL] (-)	3.0	4.0	3.9	3.5	3.8	3.7	5.0
District RWS [DFL] (-)		2.7	4.1	3.5	3.8	3.8	5.3
District RWS [AWD] (-)	3.0	3.3	2.2	3.1	2.6	2.3	3.2

Figure 87. Average (2013 - 2023) monthly values of Relative Water Supply - RWS (-).

5.5 Conclusions

This study advances the state of district-scale rice irrigation modelling in northern Italy by extending the baselines of Mayer et al. (2019) and Gilardi et al. (2023) through the newly developed QGIS-SWAP-Paddy framework. By coupling a semi-distributed SWAP module with a channel network sub-model, the framework delivers spatially detailed estimates of irrigation demand in agricultural areas, channel network conveyance losses and groundwater recharge across the entire Lomellina district (127,033 hectares, 62,615 of which are under rice cultivation) between 2013 and 2023.

Simulations consider four irrigation management scenarios. The first one (PMR) reflects the current state combining wet seeding and continuous flooding (WFL, ≈ 20%) and dry seeding and intermittent flooding (FTI, ≈ 80%). The second method applies wet seeding with continuous flooding (WFL) across all rice areas, while the third method imposes dry seeding with delayed flooding (DFL), and the fourth method applies Alternate Wetting and Drying (AWD).

Calibration against 2020 channel discharge measurements for Lomellina yielded a very good performance according to Moriasi et al. (2007). During the main irrigation period (June - August) from 2018 to 2020, simulated agricultural water demand generally matched measured discharges, with the notable exception of 2019. In that year, divergences in May and June reflected actual conditions: AIES records for San Giorgio di Lomellina indicate low irrigation demand in May but critically insufficient water availability from June onwards, consistent with the mismatch observed in the simulations. Excluding the critical months (September 2018 and May - June 2019) produces a cleaner dataset and markedly improves performance (NSE = 0.771, RSR = 0.479, PBIAS = 3.68%, all rated very good), confirming that the model parametrization is valid once anomalous periods are removed. Considering the size of the study area and the complexity of the modelling task, the results confirm that the model reliably reproduced water balances at both field and simulation domain scale, across 60 soil types and under varying shallow and deep groundwater conditions.

At the field level, results show that average annual irrigation depths decrease from 2.9 m under WFL to 2.4 m under DFL (-17.2%), 2.1 m under AWD (-27.6%), and 1.5 m under FTI (-48.3%). AWD water savings relative to WFL are consistent with earlier findings by Bouman &

Tuong (2001), Belder et al. (2004), and Carrijo et al. (2017), as well as with previous field experiments conducted in the study area by UNIMI-DiSAA research group (MEDWATERICE, RISWAGEST). While FTI achieves the greatest water savings, it fails to maintain submergence during the flowering stage, a critical period for preventing heavy-metal accumulation in rice grains (Vitali et al., 2024). This is particularly relevant considering Regulation (EU) 2023/915, which establishes strict maximum levels for inorganic arsenic and cadmium in rice. AWD, by contrast, incorporates a 20 - 30 days phase of continuous flooding after panicle initiation to limit cadmium uptake, before resuming intermittent drying until final field drainage. Moreover, FTI has been associated with significant yield reductions, averaging 21% across major Italian rice varieties, due to lower tillering and reduced nitrogen uptake under non-flooded conditions (Miniotti et al., 2016).

Domain-level annual water requirements rank the strategies unambiguously. WFL demands 1,52.5 m^3/s, DFL reduces demand by 18%, AWD by 29.6%, and the PMR by 31.7% with respect to WFL. Monthly patterns show WFL remaining the most water-intensive throughout the season, DFL peaking in June due to dry seeding and delayed flooding, and AWD concentrating flooding around July flowering to secure grain quality and limit cadmium uptake. In the AWD scenario, water-rationing measures in June significantly reduce consumption following initial wet seeding months. Scenarios with wet seeding (WFL, and AWD) show higher irrigation demand in the early season (April - May) compared to dry seeding (PMR, and FTI); a critical aspect to consider under future climate change conditions or reduced water availability during these months.

Performance metrics further underscore AWD's advantages. Its Water Application Efficiency (WAE) of 54.1% nearly matches PMR's 55.3%, while outperforms DFL (42.6%) and WFL (41.8%). The Relative Water Supply (RWS) falls from 3.8 - 3.9 under continuous regimes (WFL, and DFL) to 2.9 under PMR and 2.8 under AWD, reflecting a closer supply-demand balance in AWD.

By enabling early-season groundwater recharge while reducing peak consumption, AWD offers a promising response to initial low aquifer levels and inter-crop competition for water in June; a challenge increasingly faced by northern Italian rice-growing areas. AWD averaged 4.9 field applications (3.2 under shallow groundwater, and 6.3 under deep), showing AWD's sensitivity to groundwater table depth condition (irrigation requirements drop by up to 47% from shallow to deep groundwater table depth). Lomellina's lighter and more permeable soils than those found in other rice-growing areas of the world (Gassman et al., 2022), coupled with a responsive shallow aquifer and dense canal-field connectivity, could amplify AWD's dual benefits of water savings and groundwater recharge. Its district-scale adoption hinges on irrigation consortia governance shifts toward demand-driven scheduling, farmer incentives, and return to wet seeding in spring (Gharsallah et al., 2023; Lampayan et al., 2015). Future work under the PROMEDRICE project will link QGIS-SWAP-Paddy to a distributed MODFLOW model, refining surface-groundwater feedback and trying to answer the question of how maximize wet seeding and AWD regional gains. Beyond this, the coupling would also enable the evaluation of other Agricultural Managed Aquifer Recharge (AgMAR) strategies (Patnaik et al., 2024), including winter flooding of rice fields (Negri et al., 2020).

6 Conclusions and Future Research

Rice is a cornerstone of global food security, with the majority of its production occurring in irrigated systems (Chauhan et al., 2017; Gassman et al., 2022). These systems are increasingly under pressure from water scarcity, climate variability, and competition among different users (Bouman et al., 2007; Liu et al., 2022; Silalertruksa et al., 2017). The Lomellina region, situated in the north-western Po Valley, encompasses one of the largest rice-growing areas in Europe (Giuliana et al., 2024), with nearly 65,000 hectares of paddies distributed within a dense network of unlined irrigation canals and underlain by one of the continent's most extensive phreatic aquifers. Lomellina's territory reflects not only the natural presence of coarse-textured soils with relatively high percolation rates compared to most rice-growing regions worldwide (Gassman et al., 2022), but also centuries of human intervention. A long-standing tradition of wet seeding and continuous flooding (WFL) has progressively sculpted the territory into a functional, semi-artificial water landscape, where agronomic practices and hydraulic infrastructure co-evolve (Miniotti et al., 2016; Monaco et al., 2021). Over the past two decades, however, water scarcity has driven a progressive shift toward dry seeding with delayed flooding (DFL) or fixed-turn irrigation (FTI). While these techniques reduce seasonal water volumes, they can also depress early-season groundwater levels and exasperate competition for the irrigation resource in June - July. The exceptional drought of 2022 (AIT, 2024) exposed, once more, the fragility of rice-growing areas in Northern Italy and reinforced the need for strategies that save water without dismantling the virtuous semi-natural reuse cycle sustained by the canal-field-aquifer system (Cesari De Maria et al., 2017; Mayer et al., 2019; Zampieri et al., 2019).

This Thesis provided tools and useful answers to the problems highlighted, which are summarized below in the text.

The tool presented in Chapter 2 functioned as a proof-of-concept, being a prototype agro-hydrological framework developed and applied to the San Giorgio di Lomellina irrigation district (about 1,000 hectares) to test the effects of alternative irrigation strategies and quantify their hydrological impacts on the water resource system within the district. The modelling system is composed by three sub-models developed within a MATLAB framework: a physically based, semi-distributed agro-hydrological model and two empirical models, the former for the channel network percolation and the latter for the groundwater levels. Five irrigation management strategies, relevant to the area, were compared, including Alternate Wetting and Drying (AWD). This first application yielded a key insight: in shallow-aquifer rice systems, irrigation efficiency cannot be meaningfully evaluated without explicitly accounting for groundwater level and its contribution to crop water supply. This work also highlighted the value of using irrigation performance indicators into model-based scenario analysis for supporting decision-making at the irrigation-district scale. Among the simulated scenarios, safe AWD emerged as a promising compromise, reducing seasonal irrigation demand by 16% compared to WFL. This reduction, slightly lower but consistent with the CRR-ENR field trials (20 - 25% savings) and the meta-analysis by Carrijo et al. (2017) (23.4%), demonstrates that AWD can reduce the total irrigation use in the agricultural season, but mainly in the central and most critical months of the season. In June, AWD achieved a Relative Water Supply (RWS) of 3.57, compared with 6.02 for DFL and 5.13 for FTI. This value is well above the oversupply threshold of 1.2 reported in the literature (Bos et al., 2005; Molden, 1998), but represents an important improvement in supply

adequacy and resource balance in the specific context of this study. Over the irrigation season, AWD recorded a Water Application Efficiency (WAE) of 0.37 (37%), markedly below the ~ 60% field-level efficiency typically reported as an average for all the surface irrigation methods (Burt et al., 1997; Pereira et al., 2012), reflecting the high percolation losses characteristic of Lomellina's coarse-textured soils. The Distribution Efficiency (DE) was found to be 0.70 (70%), aligning with the lower bound of the 70 - 85% range for medium-length unlined canals (Molden, 1998).

Chapter 3 delivered a tool able to generalize the modelling concepts developed in the prototype agro-hydrological framework described in Chapter 2. The QGIS-SWAP-Paddy framework was developed to operationalize the prototype's logic at full district scale, integrating spatial data harmonization, semi-distributed SWAP simulations, and a more flexible channel-network sub-model. Its architecture directly address the need for a multi-scale, physically based agro-hydrological model identified in the background (Siad et al., 2019; Uniyal and Dietrich, 2021). However, its accuracy would inevitably depend on the quality of the parameters, particularly the soil hydraulic parameters, which are the most difficult to estimate in rice-growing areas. This dependency is the reason for the work presented in Chapter 4.
Nex steps to consolidate and extend the framework's applicability will be:

1. *Operational manual and QGIS plugin release*: drafting a comprehensive user manual to standardize workflows and facilitate adoption, with the long-term goal of packaging the framework as an open-source plugin for publication in the official QGIS repository.
2. *Application to other case studies*: extending the framework to other irrigation districts to test its transferability across contrasting hydrological, agronomic, and infrastructural contexts. A priority target is the Baix Ter irrigation district in north-eastern Catalonia (Spain), an alluvial plain with 841 ha of rice embedded in a 3,000 hectares mixed-crop irrigation network. The area is characterized by a Mediterranean maritime climate (~ 600 mm annual rainfall), poorly drained and variably saline soils, and from a change that has taken place in recent years from WFL to DFL. This activity has already begun as part of a doctoral thesis at the University of Girona: the PhD student was hosted by the Agricultural Hydraulics Research Group at DiSAA-UNIMI for three months and began working on the implementation of QGIS-SWAP-Paddy for the Baix Ter.
3. *Coupling with a groundwater model*: in the San Giorgio prototype, a district-specific groundwater level model (m a.s.l.) was used to consider the effects of the irrigation strategies on the groundwater levels, as well as the bottom boundary conditions for the SWAP simulations. This coupling mechanism is currently absent in the QGIS-SWAP-Paddy framework. Future developments would couple a groundwater flow model such as MODFLOW to the framework.

These planned developments aim to transform the QGIS-SWAP-Paddy framework from a research-grade modelling into a shareable, and extensible decision-support tool for irrigation district management under diverse environmental and operational conditions.

Chapter 4 provided reliable hydrological parameters for rice paddy soils in the Lomellina area. Recognizing that most PedoTransfer functions (PTFs) are unsuited to long-cultivated paddy soils with compacted, biologically clogged hardpans (Bouman et al., 2007; Facchi et al., 2018), the study evaluated 21 PTFs for bulk density - BD), 20 for the soil water retention curve - $\theta(h)$, and 55 for hardpan saturated hydraulic conductivity - Ks. It identified Kaur (mod3)

(Kaur et al., 2002) and Rajkai and Varallyay (1992) as the most reliable for BD and θ(h) and developed a new Ks PTF with root mean square error (RMSE) = 0.21 cm d^{-1} and Nash-Sutcliff model efficiency calculated on log-transformed values ME-L = 0.85, far outperforming the best literature models (Nemes et al., 2005; Mayer et al., 2019). These locally validated parameters became the essential input for the application of the QGIS-SWAP-Paddy to the Lomellina area (Chapter 5). In this application, soil hydraulic parameters are derived from the ERSAF 1:50,000 soil database. This resolution is well suited to representing spatial variability at the Lomellina district scale. However, when moving to local or field-scale applications, the coarse resolution and generalised nature of ERSAF-based parameters may not fully capture fine-scale heterogeneity in soil texture, structure, and hardpan properties. A future activity will be therefore assessing these PTFs at field scale, using measured paddy field water balances monitored in MEDWATERICE, RISWAGEST and PROMEDRICE projects, to test whether their performance remains consistent across scales. Such validation should not focus solely on whether the estimated parameter values match the measured soil profiles in the case studies, but also on whether, even when parameterized at a different spatial scale, they reproduce a simulated water balance sufficiently compatible with that observed in the field. This assessment will be carried out directly within the framework, which is inherently applicable at multiple scales, thereby enabling an evaluation of parameter transferability from district- to field-level modelling.

Chapter 5 closed the methodological loop by applying QGIS-SWAP-Paddy, parameterized with the identified soil PTFs, to the entire Lomellina district (127,033 ha; 62,615 ha rice). The framework was calibrated for the year 2020 and validated in 2018 and 2019 using 'current status' data (PMR: WFL + FTI) and then applied for 'scenario analysis' over the period 2013 - 2023. Four scenarios (PMR, WFL, DFL, and safe AWD) were simulated. At the field scale, AWD reduced annual irrigation depths by 27.6% compared to WFL, while FTI achieved a reduction of 48.3%, but at the cost of agronomic risks, notably the potential for cadmium and nickel accumulation in soils under sustained aerobic conditions due to the absence of flooding (Vitali et al., 2024) and significant yield reduction (Miniotti et al., 2016). At district scale, AWD cut annual water requirements by 29.6% compared to WFL, with a WAE of 54.1%, slightly below the ~ 60% typical for well-managed surface irrigation systems reported by Burt et al. (1997) and Pereira et al. (2012), but markedly higher than WFL (41.8%) and DFL (42.6%), and close to PMR (55.3%). The RWS for AWD was 2.8, substantially lower than the 3.8 - 3.9 of WFL/DFL, indicating a significant reduction in oversupply (Bos et al., 2005; Molden, 1998), yet still reflecting the high percolation and conveyance losses characteristic of the Lomellina area. In the critical month of June, AWD achieved a WAE of 70.5% and an RWS of 2.2, outperforming all other scenarios in application efficiency and in moderating oversupply during peak irrigation demand.

Building on the results and methodological advances presented in this Thesis, several targeted research developments can be identified to further enhance the framework's predictive capacity, operational relevance, and strategic value for irrigation-district management in Lomellina. These opportunities can be grouped into three main strands:

1. *Coupling with a groundwater model, AWD and Managed Aquifer Recharge (MAR) zoning*
   Coupling QGIS-SWAP-Paddy with a groundwater model such as MODFLOW would enable two-way feedback between percolation, canal seepage, and groundwater-table dynamics, refining district-scale requirement estimates and improving the evaluation of groundwater storage-oriented strategies. The integrated modelling approach could be employed to determine the optimal geographic adoption of AWD for maximizing recharge

benefits. For instance, AWD could be concentrated in the northern part of the Lomellina to raise groundwater levels through wet seeding, which would sustain irrigation in the southern part of the region that is also the least abundant in surface water sources.
Winter flooding (WF) of rice fields, when implemented as an Agricultural Managed Aquifer Recharge (Ag-MAR) strategy (Patnaik et al., 2024), can under suitable conditions achieve very high percolation efficiencies of 92 - 97%, thereby potentially improving water availability for the following cropping season (Negri et al., 2020). Moreover, this technique proved to deliver many agronomic benefits such as accelerating straw decomposition and suppressing winter weed germination, limiting erosion through soil surface protection, alongside different environmental and socio-economic co-benefits (Brogi et al., 2015; Fogliatto et al., 2010; Niang et al., 2016). However, WF effectiveness at district scale would depend on timing, location, flooded area extent and coordination with irrigation managers. Its potential could be further assessed through integrated modelling approaches such as coupling QGIS-SWAP-Paddy with MODFLOW.
These research activities would therefore pave the way for strategic WF and AWD zoning.

2. *Climate change scenarios*
Future work could test the paddy irrigation scenarios identified under projected mid-century climate conditions (IPCC, https://www.ipcc.ch/), in order to assess the robustness of management strategies in the face of greater climate variability and more frequent extreme weather events. This would provide operational guidance to irrigation consortia and decision makers. Evidence from Cambodia and Thailand suggests that irrigation techniques and scheduling choices can significantly impact outcomes such as rice yield, water productivity, farmer income and greenhouse gas emissions under climate change. These choices can sometimes offset or amplify the direct effects of projected climatic shifts. In Cambodia, AWD combined with short-cycle varieties increased yield by up to +18% and WUE by +19% compared to continuous flooding. In contrast, under continuous flooding long-cycle varieties lost up to -53% yield in the same climate scenarios (Phoeurn et al., 2024). In Thailand, simulations projected that climate change alone would reduce crop yields by up to 11.4% and farmer income by 34.4% compared to the current situation. When continuous flooding was replaced with alternate wetting and drying (AWD), methane emissions fell by 45% and water productivity improved under several climate-change scenarios (Meemungkung and Chotpantarat, 2025).

Although this dissertation's research is based on the specific agro-hydrological context of Lomellina, the author believes it introduces a replicable approach to lowland irrigation systems facing similar challenges worldwide.

References

Ahmad, M.T., Haie, N., Gonçalves, J.M., Pinho, J., Yen, H., Yakubu, M.L., Mohammed, M.U., Suleimana, A., 2024. Performance assessment and indicators for agricultural water management - A review. Water & Environment J 38, 192–211. https://doi.org/10.1111/wej.12913

Ahuja, L.R., Cassel, D.K., Bruce, R.R., Barnes, B.B., 1989. EVALUATION OF SPATIAL DISTRIBUTION OF HYDRAULIC CONDUCTIVITY USING EFFECTIVE POROSITY DATA: Soil Science 148, 404–411. https://doi.org/10.1097/00010694-198912000-00002

Aimrun, W., Amin, M.S.M., 2009. Pedo-transfer function for saturated hydraulic conductivity of lowland paddy soils. Paddy Water Environ 7, 217–225. https://doi.org/10.1007/s10333-009-0165-y

AIT, 2024. Earth observation: current challenges and opportunities for environmental monitoring, AIT Series: Trends in earth observation. Italian Society of Remote Sensing (AIT); ISSN: 2612-7148, ISBN: 978-88-944687-2-4, DOI: 10.978.88944687/24, Firenze, Italy.

Allen, R.G., Pereira, L.S., Raes, D., Smith, M., 1998. Crop evapotranspiration: guidelines for computing crop water requirements, FAO irrigation and drainage paper, M-56, ISBN: 978-92-5-104219-9. Food and Agriculture Organization of the United Nations, Rome.

Belder, P., Bouman, B.A.M., Cabangon, R., Guoan, L., Quilang, E.J.P., Yuanhua, L., Spiertz, J.H.J., Tuong, T.P., 2004. Effect of water-saving irrigation on rice yield and water use in typical lowland conditions in Asia. Agricultural Water Management 65, 193–210. https://doi.org/10.1016/j.agwat.2003.09.002

Bos, M.G., Burton, M.A., Molden, D.J. (Eds.), 2005. Irrigation and drainage performance assessment: practical guidelines, 1st ed. CABI Publishing, UK. https://doi.org/10.1079/9780851999678.0000

Bos, M.G., Murray-Rust, D.H., Merrey, D.J., Johnson, H.G., Snellen, W.B., 1994. Methodologies for assessing performance of irrigation and drainage management. Irrig Drainage Syst 7, 231–261. https://doi.org/10.1007/BF00881553

Bouma, J., 1989. Using Soil Survey Data for Quantitative Land Evaluation, in: Stewart, B.A. (Ed.), Advances in Soil Science, Advances in Soil Science. Springer US, New York, NY, pp. 177–213. https://doi.org/10.1007/978-1-4612-3532-3_4

Bouman, B.A.M., Lampayan, R.M., Tuong, T.P., 2007. Water management in irrigated rice: coping with water scarcity. International Rice Research Institute, Los Baños, Philippines.

Bouman, B.A.M., Peng, S., Castañeda, A.R., Visperas, R.M., 2005. Yield and water use of irrigated tropical aerobic rice systems. Agricultural Water Management 74, 87–105. https://doi.org/10.1016/j.agwat.2004.11.007

Bouman, B.A.M., Tuong, T.P., 2001. Field water management to save water and increase its productivity in irrigated lowland rice. Agricultural Water Management 49, 11–30. https://doi.org/10.1016/S0378-3774(00)00128-1

Brogi, A., Pernollet, C.A., Gauthier-Clerc, M., Guillemain, M., 2015. Waterfowl foraging in winter-flooded ricefields: Any agronomic benefits for farmers? Ambio 44, 793–802. https://doi.org/10.1007/s13280-015-0678-0

Burt, C.M., Clemmens, A.J., Solomon, K.H., Howell, T.A., Strelkoff, T.S., 1997. Irrigation Performance Measures: Efficiency and Uniformity. J. Irrig. Drain Eng. 125, 97–99. https://doi.org/10.1061/(ASCE)0733-9437(1999)125:2(97)

Campbell, G.S., Shiozawa, S., n.d. Prediction of hydraulic properties of soils using particle size distribution and bulk density data, in: M.Th. van Genuchten et al (Ed.) Proc. Int. Workshop on Indirect Methods for Estimating the Hydraulic Properties of Unsaturated Soils. University of California, Riverside.

Carles Brangarí, A., Sanchez-Vila, X., Freixa, A., M. Romaní, A., Rubol, S., Fernàndez-Garcia, D., 2017. A mechanistic model (BCC-PSSICO) to predict changes in the hydraulic properties for bio-amended variably saturated soils. Water Resources Research 53, 93–109. https://doi.org/10.1002/2015WR018517

Carrijo, D.R., Lundy, M.E., Linquist, B.A., 2017. Rice yields and water use under alternate wetting and drying irrigation: A meta-analysis. Field Crops Research 203, 173–180. https://doi.org/10.1016/j.fcr.2016.12.002

Cesari De Maria, S., Bischetti, G.B., Chiaradia, E.A., Facchi, A., Miniotti, E.F., Rienzner, M., Romani, M., Tenni, D., Gandolfi, C., 2017. The role of water management and environmental factors on field irrigation requirements and water productivity of rice. Irrig Sci 35, 11–26. https://doi.org/10.1007/s00271-016-0519-3

Chauhan, B.S., Jabran, K., Mahajan, G., 2017. Rice Production Worldwide. Springer International Publishing AG, Cham.

Chen, G., Peng, L., Gong, J., Wang, J., Wu, C., Sui, X., Tian, Y., Hu, M., Li, C., He, X., Yang, H., Zhang, Q., Ouyang, Y., Lan, Y., Li, T., 2023. Effects of water stress on starch synthesis and accumulation of two rice cultivars at different growth stages. Front. Plant Sci. 14, 1133524. https://doi.org/10.3389/fpls.2023.1133524

Coughlan et al., 2002. Soil Physical Measurement and Interpretation for Land Evaluation. CSIRO Publishing. https://doi.org/10.1071/9780643069879

Dane, J.H., Clarke Topp, G. (Eds.), 2002. Methods of Soil Analysis: Part 4 Physical Methods, SSSA Book Series. Soil Science Society of America, Madison, WI, USA. https://doi.org/10.2136/sssabookser5.4

Dardanelli, J.L., Bachmeier, O.A., Sereno, R., Gil, R., 1997. Rooting depth and soil water extraction patterns of different crops in a silty loam Haplustoll. Field Crops Research 54, 29–38. https://doi.org/10.1016/S0378-4290(97)00017-8

Elli, E.F., Kalogeropoulos, G., Trifunovic, S., Kosola, K.R., Archontoulis, S.V., 2025. Historical changes in maize light extinction coefficient and light capture due to breeding and plant density. Agronomy Journal 117, e70170. https://doi.org/10.1002/agj2.70170

ENR, 2024. Superfici investite a riso 2024 - dati espressi in ettari. URL https://www.enterisi.it/upload/enterisi/bilanci/St1bis-2024_15916_2951.pdf (accessed 9.27.25).

ERSAF, 2004. Suoli e paesaggi della provincia di Pavia.

Facchi, A., Rienzner, M., Cesari De Maria, S., Mayer, A., Chiaradia, E.A., Masseroni, D., Silvestri, S., Romani, M., 2018. Exploring scale-effects on water balance components and water use efficiency of toposequence rice fields in Northern Italy. Hydrology Research 49, 1711–1723. https://doi.org/10.2166/nh.2018.125

Farooq, M., Siddique, K.H.M., Rehman, H., Aziz, T., Lee, D.-J., Wahid, A., 2011. Rice direct seeding: Experiences, challenges and opportunities. Soil and Tillage Research 111, 87–98. https://doi.org/10.1016/j.still.2010.10.008

Fasola, M., Ruiz, X., 1996. The Value of Rice Fields as Substitutes for Natural Wetlands for Waterbirds in the Mediterranean Region. Colonial Waterbirds 19, 122. https://doi.org/10.2307/1521955

Fogliatto, S., Vidotto, F., Ferrero, A., 2010. Effects of winter flooding on weedy rice (Oryza sativa L.). Crop Protection 29, 1232–1240. https://doi.org/10.1016/j.cropro.2010.07.007

Gassman, P.W., Jeong, J., Boulange, J., Narasimhan, B., Kato, T., Somura, H., Watanabe, H., Eguchi, S., Cui, Y., Sakaguchi, A., Hoang Tu, L., Jiang, R., Kim&Jeffrey G. Arnold, M.-K., Ouyang, W., 2022. Simulation of rice paddy systems in SWAT: A review of previous applications and proposed SWAT+ rice paddy module. International Journal of Agricultural and Biological Engineering 15, 1–24. https://doi.org/10.25165/j.ijabe.20221501.7147

Gharsallah, O., Rienzner, M., Mayer, A., Tkachenko, D., Corsi, S., Vuciterna, R., Romani, M., Ricciardelli, A., Cadei, E., Trevisan, M., Lamastra, L., Tediosi, A., Voccia, D., Facchi, A., 2023. Economic, environmental, and social sustainability of Alternate Wetting and Drying irrigation for rice in northern Italy. Front. Water 5, 1213047. https://doi.org/10.3389/frwa.2023.1213047

Gilardi, G.L.C., Mayer, A., Rienzner, M., Romani, M., Facchi, A., 2023. Effect of Alternate Wetting and Drying (AWD) and Other Irrigation Management Strategies on Water Resources in Rice-Producing Areas of Northern Italy. Water 15, 2150. https://doi.org/10.3390/w15122150

Giuliana, V., Lucia, M., Marco, R., Simone, V., 2024. Environmental life cycle assessment of rice production in northern Italy: a case study from Vercelli. Int J Life Cycle Assess 29, 1523–1540. https://doi.org/10.1007/s11367-022-02109-x

Gonçalves, J.M., Nunes, M., Ferreira, S., Jordão, A., Paixão, J., Eugénio, R., Russo, A., Damásio, H., Duarte, I.M., Bahcevandziev, K., 2022. Alternate Wetting and Drying in the Center of Portugal: Effects on Water and Rice Productivity and Contribution to Development. Sensors 22, 3632. https://doi.org/10.3390/s22103632

Guber, A.K., Pachepsky, Y.A., 2010. Multimodeling with Pedotransfer Functions. Documentation and User Manual for PTF Calculator (CalcPTF) Version 3.0.

Gupta, S.C., Larson, W.E., 1979. Estimating soil water retention characteristics from particle size distribution, organic matter percent, and bulk density. Water Resources Research 15, 1633–1635. https://doi.org/10.1029/WR015i006p01633

Hammer, G.L., Dong, Z., McLean, G., Doherty, A., Messina, C., Schussler, J., Zinselmeier, C., Paszkiewicz, S., Cooper, M., 2009. Can Changes in Canopy and/or Root System Architecture Explain Historical Maize Yield Trends in the U.S. Corn Belt? Crop Science 49, 299–312. https://doi.org/10.2135/cropsci2008.03.0152

Heinen, M., Mulder, M., Van Dam, J., Bartholomeus, R., De Jong Van Lier, Q., De Wit, J., De Wit, A., Hack - Ten Broeke, M., 2024. SWAP 50 years: Advances in modelling soil-water-atmosphere-plant interactions. Agricultural Water Management 298, 108883. https://doi.org/10.1016/j.agwat.2024.108883

Hollis, J.M., Hannam, J., Bellamy, P.H., 2012. Empirically-derived pedotransfer functions for predicting bulk density in European soils. European J Soil Science 63, 96–109. https://doi.org/10.1111/j.1365-2389.2011.01412.x

Iovino, M., Bagarello, V., Castellini, M., Giordano, G., Sgroi, A., 2009. FUNZIONI DI PEDOTRASFERIMENTO PER LA DETERMINAZIONE DELLA CURVA DI RITENZIONE IDRICA DEI SUOLI SICILIANI.

https://www.researchgate.net/publication/258831599_FUNZIONI_DI_PEDOTRASFERIMENTO_PER_LA_DETERMINAZIONE_DELLA_CURVA_DI_RITENZIONE_IDRICA_DEI_SUOLI_SICILIANI
J. D. Jabro, 1992. Estimation of Saturated Hydraulic Conductivity of Soils From Particle Size Distribution and Bulk Density Data. Transactions of the ASAE 35, 557–560. https://doi.org/10.13031/2013.28633
Johnson, J.M., Clarke, K.C., 2021. An area preserving method for improved categorical raster resampling. Cartography and Geographic Information Science 48, 292–304. https://doi.org/10.1080/15230406.2021.1892531
Kaur, R., Kumar, S., Gurung, H.P., 2002. A pedo-transfer function (PTF) for estimating soil bulk density from basic soil data and its comparison with existing PTFs. Soil Res. 40, 847. https://doi.org/10.1071/SR01023
Köppen, W., 1936. Das geographische System der Klimate (1936).
Kroes, J.G., Groenendijk, P., Hendriks, R.F.A., Jacobs, C.M.J., 2008. Alterra Report1649 - Swap32 Theory description and user manual.
Lampayan, R.M., Rejesus, R.M., Singleton, G.R., Bouman, B.A.M., 2015. Adoption and economics of alternate wetting and drying water management for irrigated lowland rice. Field Crops Research 170, 95–108. https://doi.org/10.1016/j.fcr.2014.10.013
Li, P., Ren, L., 2019a. Evaluating the effects of limited irrigation on crop water productivity and reducing deep groundwater exploitation in the North China Plain using an agro-hydrological model: I. Parameter sensitivity analysis, calibration and model validation. Journal of Hydrology 574, 497–516. https://doi.org/10.1016/j.jhydrol.2019.04.053
Li, P., Ren, L., 2019b. Evaluating the effects of limited irrigation on crop water productivity and reducing deep groundwater exploitation in the North China Plain using an agro-hydrological model: II. Scenario simulation and analysis. Journal of Hydrology 574, 715–732. https://doi.org/10.1016/j.jhydrol.2019.03.034
Li, Y., Chen, D., White, R.E., Zhu, A., Zhang, J., 2007. Estimating soil hydraulic properties of Fengqiu County soils in the North China Plain using pedo-transfer functions. Geoderma 138, 261–271. https://doi.org/10.1016/j.geoderma.2006.11.018
Liang, K., Zhong, X., Huang, N., Lampayan, R.M., Pan, J., Tian, K., Liu, Y., 2016. Grain yield, water productivity and CH 4 emission of irrigated rice in response to water management in south China. Agricultural Water Management 163, 319–331. https://doi.org/10.1016/j.agwat.2015.10.015
Linquist, B.A., Anders, M.M., Adviento-Borbe, M.A.A., Chaney, R.L., Nalley, L.L., Da Rosa, E.F.F., Van Kessel, C., 2015. Reducing greenhouse gas emissions, water use, and grain arsenic levels in rice systems. Global Change Biology 21, 407–417. https://doi.org/10.1111/gcb.12701
Liu, X., Liu, W., Tang, Q., Liu, B., Wada, Y., Yang, H., 2022. Global Agricultural Water Scarcity Assessment Incorporating Blue and Green Water Availability Under Future Climate Change. Earth's Future 10, e2021EF002567. https://doi.org/10.1029/2021EF002567
Maddonni, G.A., Otegui, M.E., 1996. Leaf area, light interception, and crop development in maize. Field Crops Research 48, 81–87. https://doi.org/10.1016/0378-4290(96)00035-4
Manrique, L.A., Jones, C.A., 1991. Bulk Density of Soils in Relation to Soil Physical and Chemical Properties. Soil Science Society of America Journal 55, 476. https://doi.org/10.2136/sssaj1991.03615995005500020030x

Mascherpa, P., Rienzner, M., Tkachenko, D., Gandolfi, C., Facchi, A., 2025. SmartWT: an IoT device for the remote monitoring of water levels in rice paddies. Presented at the AIIA 2025 International Conference 'BIOSYSTEMS ENGINEERING FOR THE GREEN TRANSITION,' Reggio Calabria, September 21-24, 2025.

Mayer, A., Rienzner, M., Cesari De Maria, S., Romani, M., Lasagna, A., Facchi, A., 2019. A Comprehensive Modelling Approach to Assess Water Use Efficiencies of Different Irrigation Management Options in Rice Irrigation Districts of Northern Italy. Water 11, 1833. https://doi.org/10.3390/w11091833

Meemungkung, A., Chotpantarat, S., 2025. Climate Change Impacts on Rice Farming in Thailand's Bang Pakong River Basin: an analysis Using Cropwat and DSSAT Models. Earth Syst Environ 9, 1983–2000. https://doi.org/10.1007/s41748-025-00723-x

Miniotti, E.F., Romani, M., Said-Pullicino, D., Facchi, A., Bertora, C., Peyron, M., Sacco, D., Bischetti, G.B., Lerda, C., Tenni, D., Gandolfi, C., Celi, L., 2016. Agro-environmental sustainability of different water management practices in temperate rice agro-ecosystems. Agriculture, Ecosystems & Environment 222, 235–248. https://doi.org/10.1016/j.agee.2016.02.010

Molden, D.J., 1998. Indicators for comparing performance of irrigated agricultural systems. International Water Management Institute, Colombo, Sri Lanka.

Monaco, S., Volante, A., Orasen, G., Cochrane, N., Oliver, V., Price, A.H., Teh, Y.A., Martínez-Eixarch, M., Thomas, C., Courtois, B., Valé, G., 2021. Effects of the application of a moderate alternate wetting and drying technique on the performance of different European varieties in Northern Italy rice system. Field Crops Research 270, 108220. https://doi.org/10.1016/j.fcr.2021.108220

Moriasi, J. G. Arnold, M. W. Van Liew, R. L. Bingner, R. D. Harmel, T. L. Veith, 2007. Model Evaluation Guidelines for Systematic Quantification of Accuracy in Watershed Simulations. Transactions of the ASABE 50, 885–900. https://doi.org/10.13031/2013.23153

Muchow, R.C., Sinclair, T.R., Bennett, J.M., 1990. Temperature and Solar Radiation Effects on Potential Maize Yield across Locations. Agronomy Journal 82, 338–343. https://doi.org/10.2134/agronj1990.00021962008200020033x

Nayar, N.M., 2014. Origins and phylogeny of rices. Academic Press, Amsterdam Boston.

Negri, C., Chiaradia, E., Rienzner, M., Mayer, A., Gandolfi, C., Romani, M., Facchi, A., 2020. On the effects of winter flooding on the hydrological balance of rice areas in northern Italy. Journal of Hydrology 590, 125401. https://doi.org/10.1016/j.jhydrol.2020.125401

Nemes, A., Rawls, W.J., Pachepsky, Y.A., 2005. Influence of Organic Matter on the Estimation of Saturated Hydraulic Conductivity. Soil Science Soc of Amer J 69, 1330–1337. https://doi.org/10.2136/sssaj2004.0055

Niang, A., Pernollet, C.A., Gauthier-Clerc, M., Guillemain, M., 2016. A cost-benefit analysis of rice field winter flooding for conservation purposes in Camargue, Southern France. Agriculture, Ecosystems & Environment 231, 193–205. https://doi.org/10.1016/j.agee.2016.06.018

Oosterveld, M., Chang, C., 1980. EMPIRICAL RELATIONS BETWEEN LABORATORY DETERMINATIONS. CANADIAN AGRICULTURAL ENGINEERING 22.

Ottoni, M.V., Ottoni Filho, T.B., Lopes-Assad, M.L.R.C., Rotunno Filho, O.C., 2019. Pedotransfer functions for saturated hydraulic conductivity using a database with

temperate and tropical climate soils. Journal of Hydrology 575, 1345–1358. https://doi.org/10.1016/j.jhydrol.2019.05.050
Patil, N.G., Rajput, G.S., Singh, R.B., Singh, S.R., 2009. Development and evaluation of pedotransfer functions for saturated hydraulic conductivity of seasonally impounded clay soils.
Patle, G.T., Vanlalnunchhani, P.C., 2020. Pedo-Transfer Functions for Saturated Hydraulic Conductivity of Cultivated Soils in the Mid Hills of Sikkim. Current Science 118, 771. https://doi.org/10.18520/cs/v118/i5/771-777
Patnaik, G.P., Mishra, A.K., Sharma, S., Das, T.P., 2024. Efficient Water Management Strategies and Recharge Potential Under Rice-Based Cropping Systems, in: Mishra, A.K., Sharma, S., Mishra, A. (Eds.), Key Drivers and Indicators of Soil Health Management. Springer Nature Singapore, Singapore, pp. 153–171. https://doi.org/10.1007/978-981-97-7564-4_9
Pedretti, D., Cavalca, L., Masetti, M., Signorini, S., Zecchin, S., 2024. Spatially variable organic-matter-driven clogging in a stormwater infiltration pond: Isotopic, microbiological and hydrogeological evidence. Science of The Total Environment 955, 177111. https://doi.org/10.1016/j.scitotenv.2024.177111
Pereira, L.S., Cordery, I., Iacovides, I., 2012. Improved indicators of water use performance and productivity for sustainable water conservation and saving. Agricultural Water Management 108, 39–51. https://doi.org/10.1016/j.agwat.2011.08.022
Phoeurn, C.A., Degré, A., Oeurng, C., Ket, P., 2024. Evaluating the impact of climate change on yield and water use efficiency of different dry-season rice varieties cultivated under conventional and alternate wetting and drying conditions. Environ Monit Assess 196, 1190. https://doi.org/10.1007/s10661-024-13363-x
Raats, P.A.C., Knight, J.H., 2018. The Contributions of Lewis Fry Richardson to Drainage Theory, Soil Physics, and the Soil-Plant-Atmosphere Continuum. Front. Environ. Sci. 6, 13. https://doi.org/10.3389/fenvs.2018.00013
Rajkai, K., Varallyay, G., 1989. Estimating soil water retention from simpler properties by regression techniques, in: M.Th. van Genuchten et al. (Ed.) Proc. Int. Workshop on Indirect Methods for Estimating the Hydraulic Properties of Unsaturated Soils. University of California, Riverside. pp. 417–426.
Rawls, W.J., 1983. ESTIMATING SOIL BULK DENSITY FROM PARTICLE SIZE ANALYSIS AND ORGANIC MATTER CONTENT1: Soil Science 135, 123–125. https://doi.org/10.1097/00010694-198302000-00007
Rawls, W.J., Brakensiek, D.L., 1989. Estimation of Soil Water Retention and Hydraulic Properties, in: Morel-Seytoux, H.J. (Ed.), Unsaturated Flow in Hydrologic Modeling. Springer Netherlands, Dordrecht, pp. 275–300. https://doi.org/10.1007/978-94-009-2352-2_10
Rawls, W.J., D. L. Brakensiek, K. E. Saxtonn, 1982. Estimation of Soil Water Properties. Transactions of the ASAE 25, 1316–1320. https://doi.org/10.13031/2013.33720
Rawls, W.J., Nemes, A., Pachepsky, Ya., 2004. Effect of soil organic carbon on soil hydraulic properties, in: Developments in Soil Science. Elsevier, pp. 95–114. https://doi.org/10.1016/S0166-2481(04)30006-1
Richards, L.A., 1931. CAPILLARY CONDUCTION OF LIQUIDS THROUGH POROUS MEDIUMS. Physics 1, 318–333. https://doi.org/10.1063/1.1745010

Sao, S., Praise, S., Nishiyama, M., Ann, V., Phung, L.D., Watanabe, T., 2024. Response of bacterial communities and soil chemistry to flood durations and recovery phases. Environ Sci Pollut Res 32, 9429–9442. https://doi.org/10.1007/s11356-024-35001-2

Saxton, K.E., Rawls, W.J., 2006. Soil Water Characteristic Estimates by Texture and Organic Matter for Hydrologic Solutions. Soil Science Soc of Amer J 70, 1569–1578. https://doi.org/10.2136/sssaj2005.0117

Saxton, K.E., Rawls, W.J., Romberger, J.S., Papendick, R.I., 1986. Estimating Generalized Soil-water Characteristics from Texture. Soil Science Soc of Amer J 50, 1031–1036. https://doi.org/10.2136/sssaj1986.03615995005000040039x

Schaap, M.G., Leij, F.J., Van Genuchten, M.Th., 2001. rosetta : a computer program for estimating soil hydraulic parameters with hierarchical pedotransfer functions. Journal of Hydrology 251, 163–176. https://doi.org/10.1016/S0022-1694(01)00466-8

Schaap, M.G., Van Genuchten, M.Th., 2006. A Modified Mualem–van Genuchten Formulation for Improved Description of the Hydraulic Conductivity Near Saturation. Vadose Zone Journal 5, 27–34. https://doi.org/10.2136/vzj2005.0005

Siad, S.M., Iacobellis, V., Zdruli, P., Gioia, A., Stavi, I., Hoogenboom, G., 2019. A review of coupled hydrologic and crop growth models. Agricultural Water Management 224, 105746. https://doi.org/10.1016/j.agwat.2019.105746

Silalertruksa, T., Gheewala, S., Mungkung, R., Nilsalab, P., Lecksiwilai, N., Sawaengsak, W., 2017. Implications of Water Use and Water Scarcity Footprint for Sustainable Rice Cultivation. Sustainability 9, 2283. https://doi.org/10.3390/su9122283

Singh, R., Jhorar, R.K., Van Dam, J.C., Feddes, R.A., 2006a. Distributed ecohydrological modelling to evaluate irrigation system performance in Sirsa district, India II: Impact of viable water management scenarios. Journal of Hydrology 329, 714–723. https://doi.org/10.1016/j.jhydrol.2006.03.016

Singh, R., Kroes, J.G., Van Dam, J.C., Feddes, R.A., 2006b. Distributed ecohydrological modelling to evaluate the performance of irrigation system in Sirsa district, India: I. Current water management and its productivity. Journal of Hydrology 329, 692–713. https://doi.org/10.1016/j.jhydrol.2006.03.037

Szabó, B., Weynants, M., Weber, T.K.D., 2021. Updated European hydraulic pedotransfer functions with communicated uncertainties in the predicted variables (euptfv2). Geosci. Model Dev. 14, 151–175. https://doi.org/10.5194/gmd-14-151-2021

Tomasella, J., Hodnett, M.G., 1998. ESTIMATING SOIL WATER RETENTION CHARACTERISTICS FROM LIMITED DATA IN BRAZILIAN AMAZONIA: Soil Science 163, 190–202. https://doi.org/10.1097/00010694-199803000-00003

Tuong, P., Bouman, B.A.M., Mortimer, M., 2005. More Rice, Less Water—Integrated Approaches for Increasing Water Productivity in Irrigated Rice-Based Systems in Asia. Plant Production Science 8, 231–241. https://doi.org/10.1626/pps.8.231

Ungaro, F., Calzolari, C., Busoni, E., 2005. Development of pedotransfer functions using a group method of data handling for the soil of the Pianura Padano–Veneta region of North Italy: water retention properties. Geoderma 124, 293–317. https://doi.org/10.1016/j.geoderma.2004.05.007

Uniyal, B., Dietrich, J., 2021. Simulation of Irrigation Demand and Control in Catchments – A Review of Methods and Case Studies. Water Resources Research 57, e2020WR029263. https://doi.org/10.1029/2020WR029263

Vereecken, H., Maes, J., Feyen, J., Darius, P., 1989. ESTIMATING THE SOIL MOISTURE RETENTION CHARACTERISTIC FROM TEXTURE, BULK DENSITY, AND CARBON CONTENT: Soil Science 148, 389–403. https://doi.org/10.1097/00010694-198912000-00001

Vereecken, H., Weynants, M., Javaux, M., Pachepsky, Y., Schaap, M.G., Van Genuchten, M.Th., 2010. Using Pedotransfer Functions to Estimate the van Genuchten–Mualem Soil Hydraulic Properties: A Review. Vadose Zone Journal 9, 795–820. https://doi.org/10.2136/vzj2010.0045

Vitali, A., Moretti, B., Bertora, C., Miniotti, E.F., Tenni, D., Romani, M., Facchi, A., Martin, M., Fogliatto, S., Vidotto, F., Celi, L., Said-Pullicino, D., 2024. The environmental and agronomic benefits and trade-offs linked with the adoption alternate wetting and drying in temperate rice paddies. Field Crops Research 317, 109550. https://doi.org/10.1016/j.fcr.2024.109550

Volk, E., Iden, S.C., Furman, A., Durner, W., Rosenzweig, R., 2016. Biofilm effect on soil hydraulic properties: Experimental investigation using soil-grown real biofilm. Water Resources Research 52, 5813–5828. https://doi.org/10.1002/2016WR018866

Wang, Y., Shao, M., Liu, Z., Zhang, C., 2014. Prediction of Bulk Density of Soils in the Loess Plateau Region of China. Surv Geophys 35, 395–413. https://doi.org/10.1007/s10712-013-9249-8

Williams, J., Ross, P., Bristow, K., 1992. Prediction of the Campbell water retention function from texture, structure, and organic matter, in: M.Th. van Genuchten et al (Ed.) Proc. Int. Workshop on Indirect Methods for Estimating the Hydraulic Properties of Unsaturated Soils. University of California, Riverside.

Wopereis, M.C.S., Bouman, B.A.M., Kropff, M.J., Ten Berge, H.F.M., Maligaya, A.R., 1994. Water use efficiency of flooded rice fields I. Validation of the soil-water balance model SAWAH. Agricultural Water Management 26, 277–289. https://doi.org/10.1016/0378-3774(94)90014-0

Wösten, J.H.M., Lilly, A., Nemes, A., Le Bas, C., 1999. Development and use of a database of hydraulic properties of European soils. Geoderma 90, 169–185. https://doi.org/10.1016/S0016-7061(98)00132-3

Wösten, J.H.M., Pachepsky, Ya.A., Rawls, W.J., 2001. Pedotransfer functions: bridging the gap between available basic soil data and missing soil hydraulic characteristics. Journal of Hydrology 251, 123–150. https://doi.org/10.1016/S0022-1694(01)00464-4

Xu, H., 2006. Modification of normalised difference water index (NDWI) to enhance open water features in remotely sensed imagery. International Journal of Remote Sensing 27, 3025–3033. https://doi.org/10.1080/01431160600589179

Yoshida, S., 1981. Fundamentals Of Rice Crop Science.

Zampieri, M., Ceglar, A., Manfron, G., Toreti, A., Duveiller, G., Romani, M., Rocca, C., Scoccimarro, E., Podrascanin, Z., Djurdjevic, V., 2019. Adaptation and sustainability of water management for rice agriculture in temperate regions: The Italian case-study. Land Degrad Dev 30, 2033–2047. https://doi.org/10.1002/ldr.3402

Zhang, Y., Schaap, M.G., 2017. Weighted recalibration of the Rosetta pedotransfer model with improved estimates of hydraulic parameter distributions and summary statistics (Rosetta3). Journal of Hydrology 547, 39–53. https://doi.org/10.1016/j.jhydrol.2017.01.004

Zoffoli, G., Gangi, F., Ferretti, G., Masseroni, D., 2023. The potential of a coordinated system of gates for flood irrigation management in paddy rice farm. Agricultural Water Management 289, 108536. https://doi.org/10.1016/j.agwat.2023.108536

Zou, G., Li, Yong, Wang, Y., Liu, D.L., Liu, X., Li, Yuyuan, Wu, J., 2016. Pedo-transfer functions for estimating the hydraulic properties of paddy soils in subtropical central China. Archives of Agronomy and Soil Science 62, 982–993. https://doi.org/10.1080/03650340.2015.1109078

Annex 1

Herbicide and Nutrient Monitoring in Surface Waters and Groundwater of a Paddy District in Northern Italy

This chapter is based on the Author's Accepted Manuscript of: Tediosi A, Ferrari F, Voccia D et al (2024) Herbicide and nutrient monitoring in surface waters and groundwater of a paddy district in northern Italy. Environ Sci Pollut Res 31:52963–52979. https://doi.org/10.1007/s11356-024-34692-x. The final published version is available at the above DOI.

Authors

Alice Tediosi[1], Federico Ferrari[1], Diego Voccia[2], Olfa Gharsallah[3], Lucrezia Lamastra[2], Lucio Botteri[1], Riccardo Rossi[1], Tommaso Ferrari[1], Nicola Ballerini[1], Giulio Luca Cristian Gilardi[3], Arianna Facchi[3]

[1]Aeiforia Srl, Strada Faggiola 12/16, Gariga Di Podenzano, PC, Italy
[2]Dipartimento Di Scienze E Tecnologie Alimentari Per Una Filiera Agro-Alimentare Sostenibile (DiSTAS), Università Cattolica del Sacro Cuore, Via Emilia Parmense 84, Piacenza, Italy
[3]Dipartimento Di Scienze Agrarie E Ambientali - Produzione, Università Degli Studi Di Milano, Territorio, Agroenergia, Via Celoria 2, Milan, Italy
Corresponding autor: Alice Tediosi, alice.tediosi@aeiforia.eu

Abstract

Italy is the leading rice producer in Europe and the second in the Mediterranean basin (after Egypt), with most of the production concentrated in a large paddy area between the Lombardy and Piedmont regions (northern Italy). In this area, irrigation of rice was traditionally carried out by wet seeding and continuous flooding; in the last fifteen years, this technique has been gradually replaced by dry seeding followed by a delayed flooding (DFL) or by an alternation of flooding and dry periods (FTI), which are economically more advantageous. This study presents the results of an extensive monitoring campaign designed and carried out in 2021 in a representative paddy district of the Lomellina area (Pavia, northern Italy) to assess the impact of the actual rice cropping strategies on surface water and groundwater quality, with particular attention to two widely used herbicides (MCPA and clomazone) and to nutrient losses (e.g., N, P, K). Results show that MCPA and clomazone concentrations detected in surface water and groundwater are always below the RAC (Regulatory Acceptable Concentration) values. As to nutrients, they do not show significant trends along the season in surface water and groundwater: this may be due to the fact that nutrient sources are many. Concerning concentrations, nitrates may pose a problem for the area, especially for groundwater. However, further studies are needed to understand to which extent rice cropping can be considered the major source of contamination for water resources.

Keywords Rice paddy; Herbicides; Nutrient losses; Environmental monitoring; Surface water quality; Groundwater quality

Introduction

Rice is one of the most important grain crops around the world, serving as a staple food for 50% of the world population (Weng et al. 2019; Muthayya et al. 2015). Therefore, it is considered to be a high-value crop (Gosetti et al. 2019). In Europe and Northern Africa, it is cultivated on a total area of about 1.2 million hectares (FAO, FAOSTAT 2020). In this area, the most important rice-producing countries are Egypt (554,205 ha), Italy (227,320 ha), and Spain (102,060 ha). Apart from a few dry periods needed for agronomic reasons, rice is traditionally grown in fields that are flooded from crop establishment to a few weeks before harvest. Northern Italy has a very long tradition of flooded rice, because of the high availability of water from spring precipitations and mountain runoff (Monaco et al. 2021). However, in recent years, especially during the last 10–15 years, the traditional water seeding and continuous flooding (WFL) has been gradually replaced by dry seeding, followed by a delayed flooding at the 3rd - 4th leaf (DFL) or even by a turn-based irrigation (FTI) when water for a continuous flooding after the dry seeding is not available (Gilardi et al. 2023). This shift was triggered by the fact that the dry seeding is economically more advantageous than the wet seeding, given the lower production costs due to the reduced amount of labour and energy inputs needed. In particular, there are benefits in the type of machinery used. In fact, with the wet seeding, farmers need dedicated tractors with metal wheels adapted to the rice paddies. This aggravates the overall farm management, including the movement of metal-wheeled tractors across roads. Especially in the case of fragmented farms where the movement of tractors and machinery is very burdensome, dry seeding guarantees a more efficient and inexpensive seeding management. In loam/sandy-loam soils (like those in the study area), dry seeding improves the effectiveness of seeding. Furthermore, dry seeding avoids the spread of algae and specific weeds (Gharsallah et al. 2023). Despite the advantages that dry seeding has brought to farmers and the water saving achievable (e.g., 14% of water saving in the whole irrigation season for DFL (Gilardi et al. 2023), this change is leading to different unexpected problems. The main ones are: (i) that the study area is facing a lowering of groundwater levels in the first months of the agricultural season. This lowering reduces the contribution of groundwater to water discharges in the irrigation network, and a shifting to June of the maximum irrigation requirement of the district, that is currently leading to a more exasperated competition between rice and the other crops cultivated in the area (Gilardi et al. 2023; Zampieri et al. 2015, 2019); (ii) increase in surface and groundwater nitrogen losses: high soil solution nitrate concentrations and leaching from the root zone as a result of nitrification under oxic soil conditions represents the greatest environmental constraint of dry seeding cropping system (Miniotti et al. 2016; Pittelkow et al. 2015; Belder et al. 2005), threatening river and groundwater quality (Zampieri et al. 2019); (iii) considering ecosystems, dry seeding can bring some serious disadvantages as traditionally flooded rice fields provide habitat for spring migrants and locally breeding birds (Imperio et al. 2017).

Rice production is affected by weed proliferation that may significantly reduce rice yields. To protect their crops, farmers widely use combinations of herbicides. Moreover, in order to improve yields, nutrients are also used as fertilisers. Despite that the industry makes efforts to design formulations characterised by high efficiency at low doses and low persistence in order to minimise the environmental impact, the intrinsic features of these chemicals make them able to spread in water and soil, as well as in the atmosphere. Therefore, the assessment of their environmental impact is of great importance. According to Gosetti et al. (2019), the contamination of water bodies is one of the major problems related to the sustainability of the areas cultivated with rice.

From a legislative viewpoint, the protection of water resources from contamination due to pesticide use is one of the main goals of the European policy (e.g., 2000/60/EC, 2008/105/EC, 2009/128/EC) (EU, 2000; EU, 2008; EU, 2009), as well as the environmental quality of freshwater with respect to eutrophication and nutrient concentrations (e.g., 91/676/EEC, 91/271/EEC, 2010/75/EU, 2020/2184/EU for drinking water, and the before-mentioned 2000/60/EC) (EEC, 1991a, 1991b; EU, 2010; EU, 2020). Different criteria have been established to reduce pesticide transfers from sites of application to water resources (Vidotto et al. 2021). Moreover, agri-environmental measures have been developed and applied to reduce nutrient pollution of the aquatic environment (e.g., Common Agricultural Policy, European Green Deal, 'Farm to Fork' Strategy). Different studies showed that herbicides and their metabolites are the Plant Protection Products (PPPs) mostly detected in surface waters, while fungicides were the substances mainly found in groundwater (Parisse et al. 2020). The intensive use of PPPs may pose a risk to the environment and this risk is enhanced when they are applied on rice, due to the strict connection with the water compartment (Resgalla et al. 2007; Ueji and Inao 2008). The 2020 report made by the Italian National Institute for Environment Protection and Research (ISPRA) showed PPP residues on 77.3% and 35.9% of the monitored points in surface waters and groundwater, respectively (Parisse et al. 2020; Vidotto et al. 2021).

While the impact of rice cropping on the water resource in Asia is relatively well-studied (Liu et al. 2018; Cui et al. 2020; Weng et al. 2019; Harlina et al. 2014), there is less research devoted to this topic in Europe and, in particular, in Italy (Gosetti et al. 2019; and Miniotti et al. 2016, only for nitrogen). The present study was developed in the context of the MEDWATERICE project (www.medwaterice.org), an international project that aimed to explore sustainability of innovative irrigation options, to reduce rice water consumption and rice environmental impacts, and to extend rice cultivation outside of the traditional paddy areas. The project included a number of case studies in different Mediterranean countries. The Italian case study was focussed on enhancing the understanding of water quantity and environmental issues in the rice cropping systems of the largest rice area in Europe, facing these problems both at the farm scale and at the district scale. In particular, the irrigation district scale (10^3–10^4 ha) is crucial when the goal is to support decisions of authorities that deal with water resource planning and management at the regional scale, since rice fields are often not isolated units but part of large areas where strong intra-field interactions may occur. The pilot district for the study is located in San Giorgio di Lomellina (Pavia, Italy) and the research aims to evaluate the impact on surface water and groundwater quality of rice cropping in northern Italy, of which the study district is considered to be a representative area. Rice being the crop with the largest impact in terms of fertilisers and pesticide use (Bechini and Castoldi 2009; Zampieri et al. 2019), this study has the purpose of illustrating the results of a monitoring campaign conducted in 2021 to assess the impact on surface water and groundwater of MCPA and clomazone, two active ingredients widely used on rice, and of nutrients (i.e., N, P, K) in the San Giorgio di Lomellina district. In recent years, the usage of MCPA and clomazone in the cultivation of rice in northern Italy has increased, and therefore these herbicides are gaining attention as far as their environmental fate is concerned. However, to our knowledge some research is available (Fernández et al. 2019; López-Piñeiro et al. 2019; McManus et al. 2014; Galhano et al. 2011; Alister et al. 2010; Marchesan et al. 2007), but not for Italy nor specifically for the district-scale. MCPA (2-methyl-4-chlorophenoxyacetic acid) is a systemic post-emergence phenoxy herbicide used to control broadleaf annual and perennial weeds (including thistle and dock) in rice, cereals, vines, peas, potatoes, flax, grasslands, forestry applications, and on rights-of-way (Richard and Pohanish 2015). Due to its high solubility and

poor adsorption to the soil matrix, MCPA is susceptible to transport into surface and groundwater bodies. For this reason, it can be responsible of compromised water quality and breaches of legislative standards (Morton et al. 2020). In the study area, MCPA is used during sprouting on rice, approximately 35 to 45 days after seeding. However, products based on MCPA exist, which are also registered for other uses, for example maize, other cereals (e.g., barley, sorghum, oats, wheat), canal/ditch banks, railways, industrial areas. Clomazone selectively controls many annual broadleaved and grass weeds in different crops (e.g., rice, sugarcane, tobacco, soybean, cotton, peppers, and pumpkin). It can be applied pre-emergence or pre-planting with incorporation but has limited post-emergence activity (Zimdahl 2018). It is highly soluble in water and quite volatile, so may be prone to drift. It is not persistent in the soil system, but may be persistent under certain conditions in waterbodies. It tends to be moderately toxic to most fauna and flora. It is moderately toxic to mammals and is considered to be a reproduction/developmental toxin (PPDB: Pesticide Properties DataBase; http://sitem.herts.ac.uk/aeru/ppdb/en/Reports/168.htm). In the study area, it is applied on rice on dry soil, at the stage of 2–3 leaves, 20 to 30 days after seeding. Rice is seeded in the area between the end of April and the end of May.

As to nutrients, this study focused on N, P, and K losses. N, P, and K are essential nutrients for plant growing and an excess can stimulate nuisance growths of aquatic plants in water bodies. The most common forms of N available for plant growth in water are the inorganic forms, namely, nitrate (NO_3), nitrite (NO_2) and ammonia (NH_3/NH_4) and organic forms such as urea (the breakdown product of proteins). Nitrate is the most commonly available and ammonia the most readily assimilated by plants.

Materials and Methods

Case Study Area

The study area presented in this paper is located in the most important rice-growing area of Italy, that is the portion of the Padana plain on the left bank of the Po River and along the Ticino River, straddling the regions of Lombardy and Piedmont (more than 200,000 ha; about 92% of the Italian rice-growing area). The pilot irrigation district for the MEDWATERICE project is within the administrative boundary of San Giorgio di Lomellina (Pavia), located about 45 km southwest of the city of Milan and extending over an area of 990 ha. It is bounded to the West by the river Agogna and to the East by the river Erbognone (or Arbogna) (Fig. 1). This district is considered to be representative of a large part of Italy's main rice-growing area.

Over the last decade, the rice area within the district remained stable at 90% of the agricultural land. The remaining 10% is mainly cropped with maize and poplar. Soils are generally sandy-loam or loamy-sand. Because of the texture, soil organic matter content is low as well as nitrogen content. The climate is humid subtropical. From a geomorphological point of view, the district area belongs to the lower part of the alluvial plain that originated during the Würm glaciation (Mayer et al. 2019). The surface area is mainly flat, except for some sand deposits of fluvial origin and the valleys where the main rivers flow nowadays. The phreatic groundwater surface varies and can be very shallow in some areas due to the topography and the summer flooding of paddies (Mayer et al. 2019; Gilardi et al. 2023). Associazione Irrigazione Est Sesia (AIES) is responsible of the management of the irrigation and drainage network in the district. Irrigation water comes almost exclusively from surface water bodies (Arbogna and Po rivers through the Cavour canal). The main irrigation channels for the district are: 'Canalino', 'Cavo

Isimbardi' and 'Roggia Comunale di San Giorgio'. As well as in the other Italian rice areas, Ente Nazionale Risi (ENR) is informed of the agronomic practices adopted by farmers.

In recent years, the San Giorgio di Lomellina irrigation district has witnessed a massive adoption of the dry seeding technique, followed by a DFL or by a FTI, instead of the traditional WFL. Table 1 illustrates the transition from the wet to the dry seeding practices in the San Giorgio di Lomellina district during the period 2013–2019, in which DFL reached 100% of the total rice area.

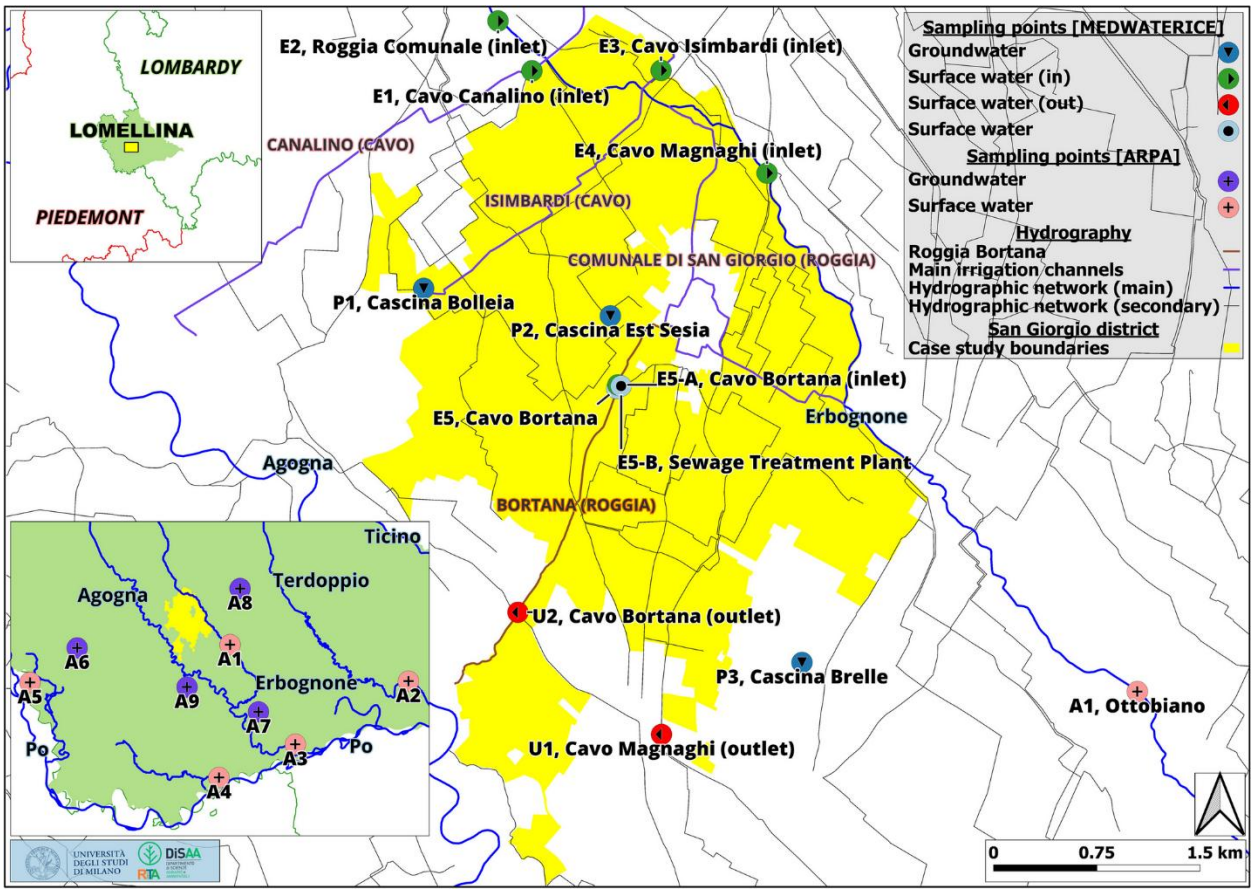

Fig. 1. General overview of the San Giorgio irrigation district (Pavia, Italy). Case study area in yellow. Adapted from Tediosi A, Ferrari F, Voccia D et al (2024) Herbicide and nutrient monitoring in surface waters and groundwater of a paddy district in northern Italy. Environ Sci Pollut Res 31:52963–52979. https://doi.org/10.1007/s11356-024-34692-x under exclusive licence to Springer-Verlag GmbH Germany, part of Springer Nature 2024.

Table 1. Transition from the wet to the dry seeding practices in the San Giorgio di Lomellina district during the period 2013–2019 (ENR data, 2020). Adapted from Tediosi A, Ferrari F, Voccia D et al (2024) Herbicide and nutrient monitoring in surface waters and groundwater of a paddy district in northern Italy. Environ Sci Pollut Res 31:52963–52979. https://doi.org/10.1007/s11356-024-34692-x under exclusive licence to Springer-Verlag GmbH Germany, part of Springer Nature 2024.

Agricultural season	Dry seeding (%)	Wet seeding (%)
2013	40.1	59.9
2016	92.5	7.5

2019	100	0

Monitoring Campaign

As to groundwater, three piezometers were identified. The selection was based on groundwater flow direction and on groundwater level (Fig. 2), with two piezometers located in the shallow and one in the deep groundwater areas (Fig. 2). Piezometric wells were positioned in the district at the beginning of 2015, and are made by PVC pipes (from 3 to 4.5 m long, 1.5 m windowed in the lower part, with an internal diameter of about 4 cm) installed into holes drilled with a hand auger. During this study, they were sampled approximately on a monthly basis.

For surface water, water was sampled at the inlet and at the outlet of the district in order to see whether herbicide usage and fertilisation within the district had an impact on water quality. Hence, a choice was made to sample the main canals entering the district and draining the district, and the following were selected: Roggia Comunale, Cavo Canalino, Cavo Isimbardi, Roggia Bortana, and Cavo Magnaghi. In particular: five irrigation inlet points, two irrigation outlet points, and one point in a channel collecting also water from a civil sewage treatment plant (STP) were identified (Fig. 1). The latter was selected in order to assess the impact of nonagricultural sources, especially in relation to N. Figure 3 reports details relative to the sampling points in the confluence of the ditch from the STP and Roggia Bortana. Roggia Bortana was sampled upstream (E5-A) and downstream (E5) the ditch from the STP. The ditch from the STP was sampled from a bridge located approximately 20 m from the confluence with Roggia Bortana (E5-B).

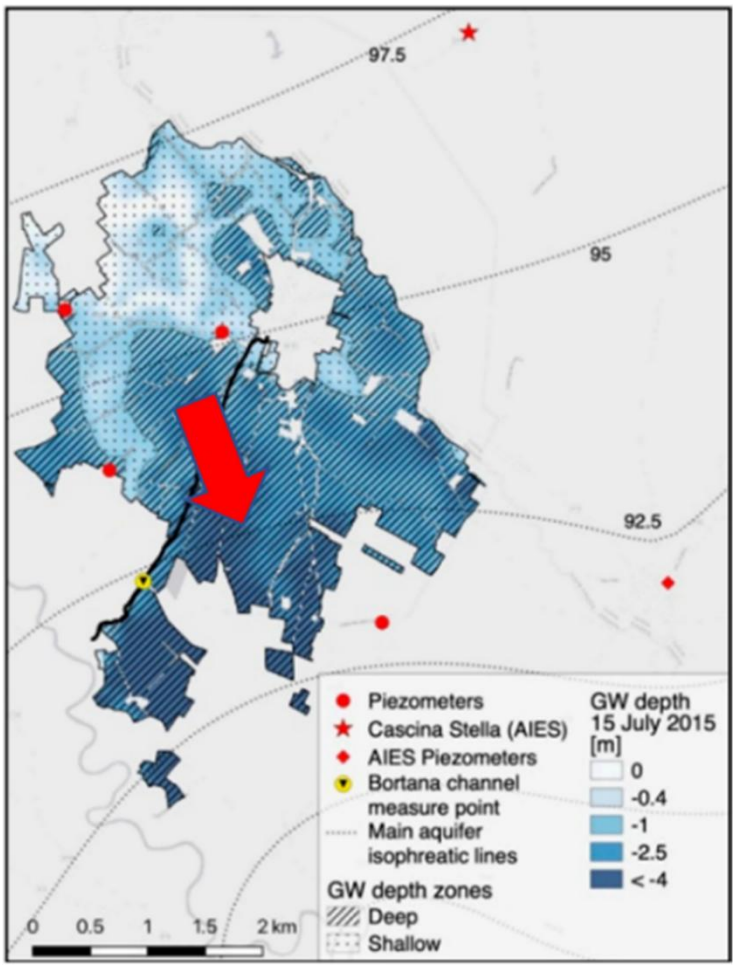

Fig. 2. Groundwater depth zones in San Giorgio (2015) and main groundwater flux direction (red arrow). Adapted from Tediosi A, Ferrari F, Voccia D et al (2024) Herbicide and nutrient monitoring in surface waters and groundwater of a paddy district in northern Italy. Environ Sci Pollut Res 31:52963–52979. https://doi.org/10.1007/s11356-024-34692-x under exclusive licence to Springer-Verlag GmbH Germany, part of Springer Nature 2024.

A number of criteria were used to choose the surface water sampling points: importance in the irrigation network, accessibility for sampling, presence of water discharge, location at the inlet/outlet of the district (to compare quality of water entering and going out of the district).

The sampling campaign started on 26th May 2021 and continued until the end of the agricultural season (3rd September 2021), including eleven sampling events (Table 2). In addition, a sampling event was performed on 20th April to assess water quality prior to pesticide and fertiliser treatments on rice (t0 sampling event). Piezometric wells were often dry out of the flooding periods, which is consistent with the irrigation management strategies (i.e., dry seeding and delayed flooding or dry seeding and fixed turned flooding) adopted in the area in the last fifteen years, which triggered a decrease in groundwater levels until June.

Sampling Procedure

Water sampling was carried out in the best possible way to preserve test compounds from photodegradation and from surface adsorption on sample containers (e.g., use of fluorinated HDPE flasks, samples protection from sunlight).

Surface water sampling consisted of a series of grab samples. In each sampling point, three samples of 250 mL each were taken at one-hour intervals. A composite sample of 750 mL was then created, merging the three samples. The composite sample was used to prepare three Nalgene flasks of 200 mL and a 50-mL Falcone tube for the different analyses.

As to groundwater, all sampling procedures were taken from existing guidelines (CropLife International 2001, and Gimsing et al. 2019) to ensure a contamination-free and representative sample of the local groundwater. In particular, the piezometer head was cleaned with water/acetone before opening the seals and a plastic film was laid on the soil to avoid contamination of the equipment. A sampling pipe connected to a 12V vacuum peristaltic pump was inserted and lowered to the bottom of the piezometer. All components used were made from inert materials. This ensured that the samples taken are neither influenced nor altered by the sampling procedure. Before collecting samples, piezometer was purged. Purging involves the removal of three times the water volume inside the piezometer in order to minimize a potential risk of contamination/alteration of the samples. Two sample replicates were collected in labelled 250-mL fluorinated HDPE-bottles and an additional sample was collected in labelled 60-mL plastic container. After collecting the samples, the tube and the glassware were rinsed with water and acetone in order to prevent cross contamination between piezometers. Immediately after collection, both surface water and groundwater samples were stored in a cool dark box or portable freezer. The temperature was kept below -8 °C until transferred to frozen storage (-20°C +/-5 °C). During transport, the samples were kept at a low temperature using portable freezers (at least -8 °C +/-2 °C) and then stored in the freezer.

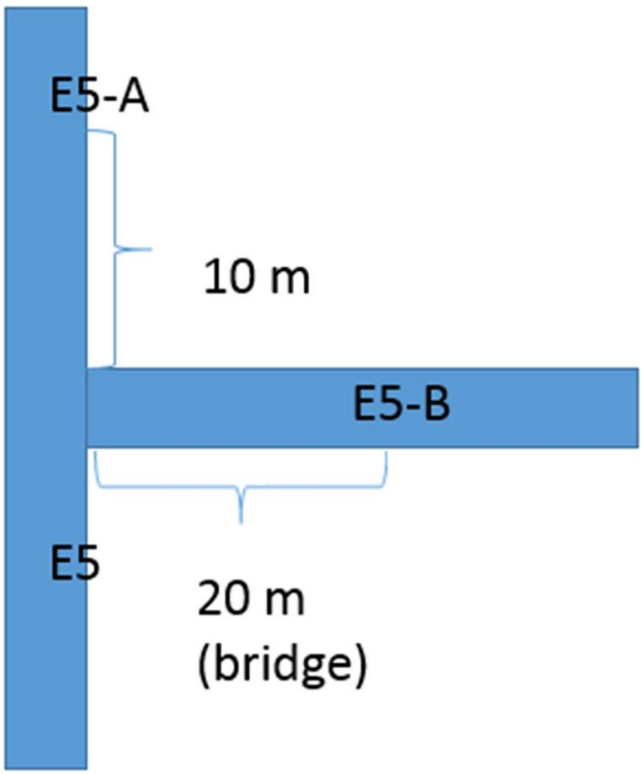

Fig. 3. Sketch of the E5 sampling points. E5-A is Roggia Bortana upstream the ditch from the sewage treatment plant (STP). E5 is Roggia Bortana downstream the ditch from the STP and E5-B is the ditch from the STP. E5-B was sampled from a bridge located approxi mately 20 m from the confluence with Roggia Bortana. Adapted from Tediosi A, Ferrari F, Voccia D et al (2024) Herbicide and nutrient monitoring in surface waters and groundwater of a paddy district in northern Italy. Environ Sci Pollut Res 31:52963–52979. https://doi.org/10.1007/s11356-024-34692-x under exclusive licence to Springer-Verlag GmbH Germany, part of Springer Nature 2024.

Analytical Methods

Nutrients from the water samples were all analysed via a spectrophotometric method with a Hach kit associated with a Hach Lange DR6000 spectrophotometer: K (LCK228, 5–50 mg/L, Hach), NO3 (LCK339, 0.23–13.5 mg/L, Hach), NH3/NH4 (LCK304, 0.015–2.0 mg/L, Hach) and P (LCK349, 0.05–1.5 mg/L, Hach). Differently, NO2 (N-NO2 0.09–0.5 mg/L) was analysed using a modified version of the colorimetric method known as Griess method. The method is based on the reaction of nitrite with sulphanilamide (Sigma Aldrich) in the presence of hydrochloric acid (36%, Carlo Erba) to form a diazonium cation, which is subsequently coupled with N-(1-naphthyl)ethylenediamine dihydrochloride (Sigma-Aldrich) in acidic medium to form a stable bluish violet azo dye that absorbs at 530 nm. Urea was analysed with a Urea Assay Kit from Sigma-Aldrich (N-Ureic 0.56–2.8 mg/L). Total nitrogen was estimated as the sum of inorganic nitrogen forms (i.e., nitrates, nitrites, ammonia) and organic nitrogen form (i.e., urea). Urea was used as main component of organic nitrogen due to the fact that urea-based fertilisers account as one of the main sources of organic nitrogen in paddy fields (Han et al. 2021).

*Table 2. Details about the monitoring campaign (OK = sample collected; X = sample not collected). * Sample collected in the Agogna river (just upstream the diversion of Roggia Comunale); **sample partially collected (only 1 Nalgene flask and 1 Falcon tube). Adapted from Tediosi A, Ferrari F, Voccia D et al (2024) Herbicide and nutrient monitoring in surface waters and*

	Event 1	Event 2	Event 3	Event 4	Event 5	Event 6	Event 7	Event 8	Event 9	Event 10	Event 11	Event 12
Date	20/4/21	26/5/21	3/6/21	10/6/21	17/6/21	23/6/21	1/7/21	8/7/21	15/7/21	29/7/21	19/8/21	3/9/21
E1	X	OK	OK	OK	OK	OK	OK	OK	OK	OK	OK	OK
E2	OK*	OK	OK	OK	OK	OK	OK	OK	OK	OK	OK	OK
E3	OK	OK	OK	OK	OK	OK	OK	OK	OK	OK	OK	OK
E4	OK	OK	OK	OK	OK	OK	OK	OK	OK	OK	OK	OK
E5	X	OK	OK	OK	OK	OK	OK	OK	OK	OK	OK	OK
E5-A	X	X	OK	OK	OK	OK	OK	OK	OK	OK	OK	OK
E5-B	X	X	OK	OK	OK	OK	OK	OK	OK	OK	OK	OK
U2	OK	OK	OK	OK	OK	OK	OK	OK	OK	OK	OK	OK
U1	OK	OK	OK	OK	OK	OK	OK	OK	OK	OK	OK	OK
P1	X	X	X	X	OK	X	X	X	OK	X	OK	X
P2	X	X	OK	X	OK	X	X	X	OK	X	OK	X
P3	X	X	X	X	OK**	X	X	X	OK	X	OK	X

As to herbicides, Clomazone (Supelco, PESTANAL®, analytical standard) and MCPA (Honeywell Riedel-de Haën) were separated with a RP-18 column (150 × 2.1 mm, Kinetex 5 um Phenomenex) and quantified by high performance liquid chromatography (HPLC) with triple quadrupole mass detector. The mobile phase consisted of methanol:water acidified with 0.2% formic acid and with a gradient programme applied from 25:75% v/v to 65:35% v/v in 6 min and isocratic for 8 min. Flow rate was 0.2 mL/min and the injection volume was 20 µL. The ionization was carried out with an ESI interface (Thermo-Fisher) in positive mode for clomazone and negative mode for MCPA. Parameters were: spray capillary voltage 4200 V for clomazone and 3500 for MCPA, sheath gas and auxiliary gas 35 and 14 psi, respectively; temperature of the heated capillary 350° C, source collision induced dissociation (CID) 10 V. The mass spectrometric analysis was performed in selected reaction monitoring (SRM) mode. For the fragmentation of clomazone, [M] + = 240 m/z, the argon collision pressure was 1.2 mTorr and the detected and quantified ions were 89, 99 m/z (collision energy 45 V) and 125 m/z (20 V). For the detected and quantified ions of MCPA, [M] − = 199 m/z, the argon collision pressure was 1.2 mTorr and the fragment ions were 106 m/z (collision energy 30 V) and 141 m/z (15 V).

Oasis HLB cartridges (Supelco, Supel™-Select HLB SPE Tube) were considered suitable SPE devices for pre-concentration of the herbicides in this study due to their hydrophilic and lipophilic characteristics as reported in Tran et al. (2007). Briefly, samples pH was decreased to 3 with formic acid (Sigma-Aldrich) and NaCl (Sigma-Aldrich, 10 g/L) was added to aid in the recoveries. Before pre-concentration, all samples were filtered through Glass microfiber filters (Gf/A, Whatman). The water samples were then loaded onto the cartridges via a vacuum manifold and after completion the cartridges were washed with deionized water. The excess water was removed by opening the valves and letting air to pass through the cartridge for 30 min. The herbicides absorbed on the cartridges were eluted with methanol (Carlo Erba) and after reducing to near dryness under a nitrogen stream, the samples were reconstituted in a mixture of the HPLC mobile phase (Methanol/HPLC grade Water 1:1) and an aliquot of 20 µL was then injected into the HPLC system. Overall, this extraction procedure resulted in a 1:1000 preconcentration of water samples prior to HPLC–MS analysis.

Calibration curves were constructed from the analy sis of solutions containing the range of 0.1–1000 µg/L of each analyte, showing a good linearity and a LOQ (Limit of Quantification) (based upon a signal to noise ratio of 10:1) of 4 µg/L for both herbicides (0.004 µg/L considering not preconcentrated samples). Recoveries from spiked herbicides in both tap and distilled water varied from 80 to 100% for clomazone and 85 to 100% for MCPA.

Statistical analysis of nutrient and herbicide concentrations in surface water and groundwater samples was evaluated using a Kruskal–Wallis coupled with Dunn-Bonferroni test with RStudio 4.4.0 software. Herbicide and nutrient concentration mean values were calculated by replacing '< LOQ' with a value equal to 'LOQ/2'.

Results and Discussion

Herbicides in Surface Water

The monitored clomazone and MCPA concentrations show that water quality at the inlet of the district is affected by treatments occurring outside the district. Concentrations detected are always below the RAC values for both herbicides. In general, the average concentrations monitored at the inlet and at the outlet of the district are comparable, so we can infer that the herbicide treatments occurred within the district do not worsen water quality.

In the case of MCPA, the minimum concentration detected in the inlet sampling points is < LOQ, the maximum is 13.56 µg/L and the mean value is 1.13 µg/L. Excluding the highest peak dated 15th July, concentrations tend to be higher in June (10th and 17th June) than in the rest of the period monitored. If the seeding occurred in the district around the end of April or the beginning of May, this would be consistent with the timing of treatment on rice. The highest peak was monitored in the E5-B sampling point. This point is located in the ditch coming from the STP, so we can hypothesise that it is not triggered by MCPA treatment on rice (Fig. 3). It can be noted that this high peak does not affect the concentration monitored in the E5 sampling point, downstream the STP. Discharge from the STP was estimated lower (0.18 m3/s) than the discharge at E5 (0.28 m3/s); however, MCPA concentration downstream the STP is even lower than upstream. We hypothesise that this is an outlier, maybe due to human error in the sampling or in the labelling.

For clomazone (Fig. 4b), the minimum concentration monitored is < LOQ, the maximum is 3.11 µg/L and the mean value is 0.17 µg/L. Also in this case, there is a trend with higher concentrations in June, consistently with the seeding and treatment timing in the study area.

At the outlet of the district (Fig. 5), MCPA minimum concentration detected is < LOQ, the maximum is 3.31 µg/L, and the mean value is 0.48 µg/L. Especially in U2, it is possible to note a trend with higher concentrations in June, which then decrease, and then slightly increase again at the end of August (Fig. 5a). A similar trend can be observed for clomazone (Fig. 5b). Clomazone minimum concentration monitored is < LOQ, the maximum is 0.36 µg/L, and the mean value is 0.04 µg/L.

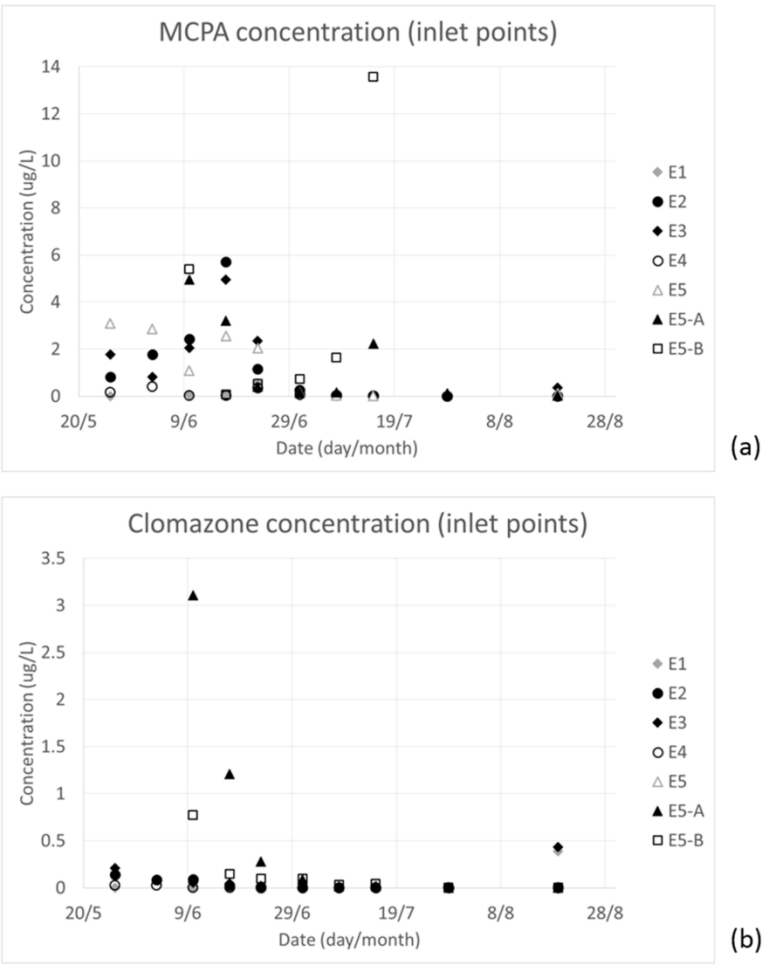

Fig. 4. MCPA (a) and clomazone (b) concentrations in the inlet sampling points. Adapted from Tediosi A, Ferrari F, Voccia D et al (2024) Herbicide and nutrient monitoring in surface waters and groundwater of a paddy district in northern Italy. Environ Sci Pollut Res 31:52963–52979. https://doi.org/10.1007/s11356-024-34692-x under exclusive licence to Springer-Verlag GmbH Germany, part of Springer Nature 2024.

The monitored clomazone and MCPA concentrations show that the water quality at the inlet of the district is affected by treatments occurring outside (i.e., upstream) the district. In some cases, concentrations are below 1 µg/L (e.g., E1, E4); in other cases, concentrations are higher (e.g., E2, E3, E5). However, MCPA and clomazone concentrations detected are always below the RAC values, which are 5.3 µg/L for clomazone (chronic risk for aquatic invertebrates) (EC 2017), and 15.2 µg/L for MCPA (acute risk for aquatic plants) (CTGB 2017). At the outlet, herbicide concentrations tend to be higher in U2 than in U1, for both MCPA and clomazone. However, they are always below the RAC values. Therefore, it is believed that there is little impact on water quality and that the agronomic practices are suitable and well applied to minimise the environmental risk related to these two herbicides. In general, the average concentrations monitored at the inlet and at the outlet of the district are comparable: in fact, the statistical analysis performed did not show a significant difference among the sampling points. So, we can infer that the herbicide treatments that occurred within the district do not worsen water quality.

When looking at other studies, MCPA was detected in Swiss surface waters to a maximum concentration of 1.6 µg/L in five agricultural catchments (Spycher et al. 2018). In the present study,

concentrations may be higher due to a more widespread application and to the specificities of rice cropping. In Ireland, data collected during the period 2013 - 2015 show MCPA maximum concentration of 18 µg/L, recorded in 2013 in the Banoge River (Co. Wexford) (EPA 2017; Morton et al. 2020). For clomazone, Marchesan et al. (2007) reported average concentrations ranging between 1.34 and 4.97 µg/L and maximum concentrations of 4.82–8.85 µg/L in two Brazilian rivers during the rice growing season.

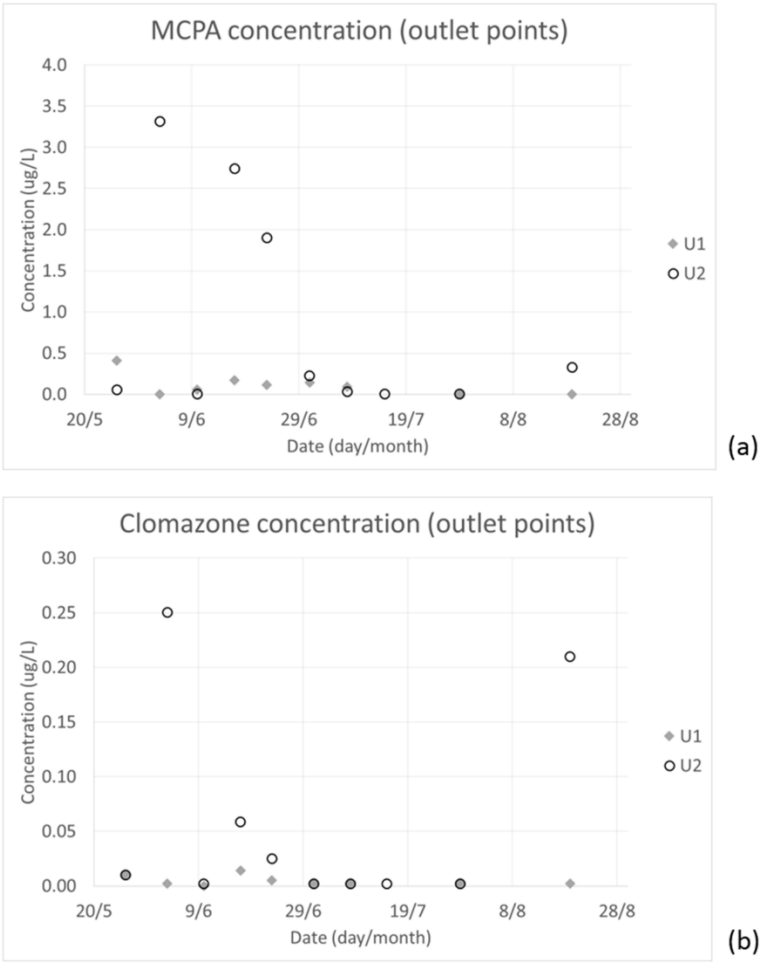

Fig. 5. MCPA (a) and clomazone (b) concentrations in the outlet sampling points. Adapted from Tediosi A, Ferrari F, Voccia D et al (2024) Herbicide and nutrient monitoring in surface waters and groundwater of a paddy district in northern Italy. Environ Sci Pollut Res 31:52963–52979. https://doi.org/10.1007/s11356-024-34692-x under exclusive licence to Springer-Verlag GmbH Germany, part of Springer Nature 2024.

The regional agency for environmental protection (ARPA, Agenzia Regionale per la Protezione dell'Ambiente) of the Lombardy Region regularly monitors water quality in the regional territory. For surface water, in the period 2016–2021 data were monitored with different frequency and timing, depending on year and location. For clomazone, data by ARPA are available only for 2019 to 2021. ARPA data in the period 2016–2021 in the neighbourhood of the study area (i.e., Breme, Pieve del Cairo, Mezzana Bigli, Zinasco and Ottobiano sampling points) show maximum concentrations in surface water that are lower than those found in the present study, which were 5.7 µg/L for MCPA (13.56 µg/L in the ditch from the STP) and 3.1 µg/L for

clomazone. For MCPA, ARPA average concentration is 0.54 µg/L (min < 0.03 µg/L – max 0.74 µg/L) in June, 0.09 µg/L (min < 0.03 µg/L – max 0.14 µg/L) in July, and 0.01 µg/L in August (min < 0.03 µg/L – max 0.03 µg/L). For clomazone, ARPA average concentration is 0.08 µg/L (min < 0.03 µg/L – max 0.25 µg/L) in June, 0.01 µg/L (min < 0.03 µg/L – max 0.06 µg/L) in July, and in August all concentration values in the dataset are < 0.03 µg/L. The differences between ARPA data and the data of this study could be due to the fact that ARPA monitoring was not continuous along the whole agricultural season. In particular, in the agricultural season June–August 2021, ARPA monitored surface water only once (in June or July, depending on the sampling point); however, with a single sampling event, it is difficult to detect herbicide peaks. Moreover, in our sampling, discrepancies in concentrations are observed among monitoring points, suggesting that the sampling location (due to its site-specific conditions) can have an important impact on the levels of pesticides in surface water. Finally, ARPA sampling points are commonly located in larger streams and channels farer from the paddy fields compared to those selected in the present study (which leads to a different role of dilution). Indeed, in the present study, surface water samples are always taken from small water bodies close to rice areas.

Nutrients in Surface Water

In the case of nutrients in surface water, the main highlights are: (i) no trend is observed and nutrient losses are spread along the whole agricultural season; (ii) nitrate concentrations tend to be higher at the outlet than at the inlet; (iii) a K peak of almost 60 mg/L is observed at the outlet and may be linked to a heavy rainfall event.

No specific trends can be observed at the different sampling points, which reasonably means that nutrient losses to surface water tend to be spread along the whole agricultural season (Fig. 6). Note that N losses can be due to both extensive use of N-based fertilisers, livestock (Bijay-Singh and Craswell 2021), but also to civil wastewater discharges and industrial activities. According to Mockler et al. (2017), N contributions from wastewater ranged between ≤ 7% and 33%, while P contributions reached 78% in the most densely populated areas.

In the case of the inlet sampling points, for total N, the minimum concentration detected in the inlet sampling points is 0.32 mg/L, the maximum is 7.82 mg/L and the mean value is 2.10 mg/L. For P-PO4, the minimum concentration monitored is < LOQ mg/L, the maximum is 3.88 mg/L and the mean value is 0.34 mg/L. As shown in Fig. 6b, a single peak was detected on 29th July (3.88 mg/L in E2). This peak may have been triggered by a heavy rainfall event that occurred on the night between 26 and 27th July (21 mm in an hour). In the case of K, the minimum concentration monitored is < LOQ, the maximum is 9.90 mg/L and the mean value is 3.58 mg/L. The ditch from the STP (E5-B; Fig. 3) shows the highest average concentration of total N (3.32 mg/L). However, in terms of minimum and maximum concentrations, values are in line with other sampling points. Pryor et al. (2007) reported higher total N average concentrations from different STPs in Narragansett Bay (USA), ranging between 7.5 mg/L and 69 mg/L. Note that the limit imposed by the Italian legislation (reported by the 'Gazzetta Ufficiale della Repubblica Italiana' – serie generale n.88, Allegato 5 2006) is either a yearly average concentration of 10 mg/L or a daily average concentration of 20 mg/L. The average P-PO4 concentration measured in E5-B (0.63 mg/L) is comparable with the average detected in other points. The maximum concentration in E5-B is 1.43 mg/L and it is in line with the lower limit of the data published by Cabo et al. (2022), who reported a phosphate concentration in the range 1.5–3 mg/L of P-PO4 in the final discharge effluent from a STP in Spain. The limit imposed by the Italian legislation (reported by the 'Gazzetta Ufficiale della Repubblica Italiana' - serie generale n.88, Allegato 5 2006) is 10 mg/L

of total P. For K, E5-B shows the highest mean value (5.49 mg/L). Maximum concentration in E5-B (9.02 mg/L) is comparable with other sampling points. Minimum concentration is < LOQ. K concentration in effluents from domestic wastewater reported by Arienzo et al. (2009) vary between 10 and 30 mg/L. Data collected in the present study tend to be lower, as the maximum value is in line with the lower limit of this range. By comparing concentrations of total N, P-PO4 and K in E5-A (upstream the STP) and in E5 (downstream the STP), we see that concentrations are higher downstream the STP in the 80% and 90% of the samples, for total N and P-PO4, respectively. In the case of K, concentrations are higher downstream only in 40% of the samples.

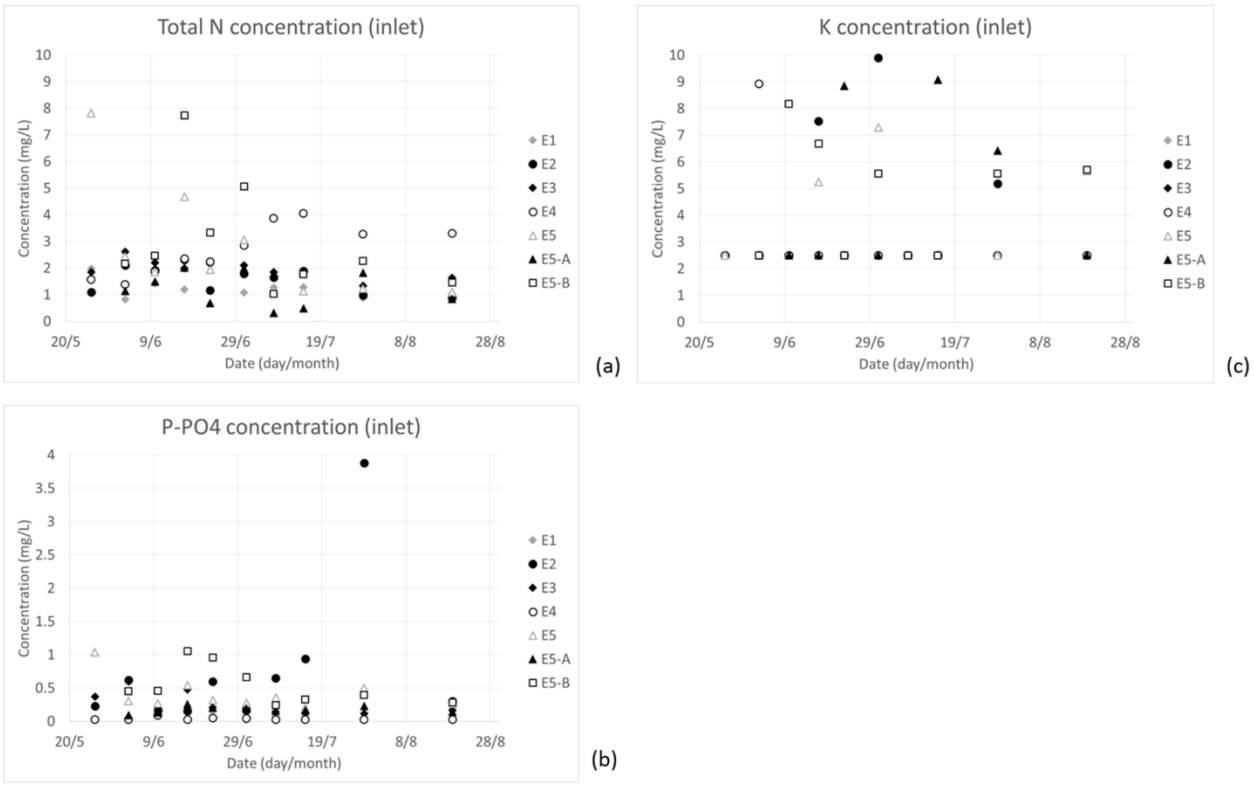

Fig. 6. Nutrient concentrations detected at the inlet sampling points: total N (a), P-PO4 (b), and K (c). Adapted from Tediosi A, Ferrari F, Voccia D et al (2024) Herbicide and nutrient monitoring in surface waters and groundwater of a paddy district in northern Italy. Environ Sci Pollut Res 31:52963–52979. https://doi.org/10.1007/s11356-024-34692-x under exclusive licence to Springer-Verlag GmbH Germany, part of Springer Nature 2024.

At the outlet, total N minimum concentration is 1.25 mg/L, the maximum is 3.59 mg/L and the mean value is 2.33 mg/L. P-PO4 minimum concentration is < LOQ, the maximum is 0.66 mg/L and the mean value is 0.24 mg/L. K minimum concentration detected is < LOQ, the maximum is 57.60 mg/L, and the mean value is 5.30 mg/L. It is important to note that, over 24 samples (12 sampling events times 2 outlet sampling points), in 20 of them, K concentration was < LOQ, in three of them it was 6–7 mg/L and in the remaining sample the concentration detected was 57.60 mg/L (Fig. 7). This high peak can be linked to the heavy rainfall mentioned before, considering that K can be easily lost by the leaching process (Mendes et al. 2016).

By comparing data monitored at the inlet of the district with data monitored at the outlet, it can be seen that total N maximum concentration is 7.82 mg/L at the inlet and 3.59 mg/L at the outlet; while mean concentrations are 2.10 mg/L at the inlet and 2.33 mg/L at the outlet. For P-

PO4, maximum and mean values are higher at the inlet (3.88 and 0.34 mg/L, respectively) than at the outlet (0.66 and 0.24 mg/L, respectively). In the case of K, concentrations at the outlet are higher than at the inlet: maximum concentrations are 9.90 mg/L and 57.60 mg/L at the inlet and outlet, respectively. K mean values are 3.58 mg/L at the inlet and 5.30 mg/L at the outlet.

The statistical analysis performed showed that, when comparing surface water sampling points, the main significant difference in the monitoring period for N concentrations was observed between E1 and both U1 and U2. E1 exhibited significantly lower N concentrations compared to U1 and U2 (data not shown). This difference was not observed for other inlet sampling points, while a statistically significant difference was observed for E1 and both E4 and E5-B. The only significant difference in the monitoring period for K concentrations was observed between E5-B and both E1 and E3, with E5-B having lower K compared to both E1 and E3 (data not shown). P concentrations showed the highest variation. Significant differences were observed between several inlet sampling points (E1 - E2, E2 - E4, E3 - E4, E1 - E5, E4 - E5, E1 - E5-B and E4 - E5-B), and between U1 and various other sampling points (E2, E3, E5, E5-B), with U1 concentrations lower than the inlet sampling points (data not shown). So, there seems to be an increase in N concentrations and a decrease in P concentrations within the district.

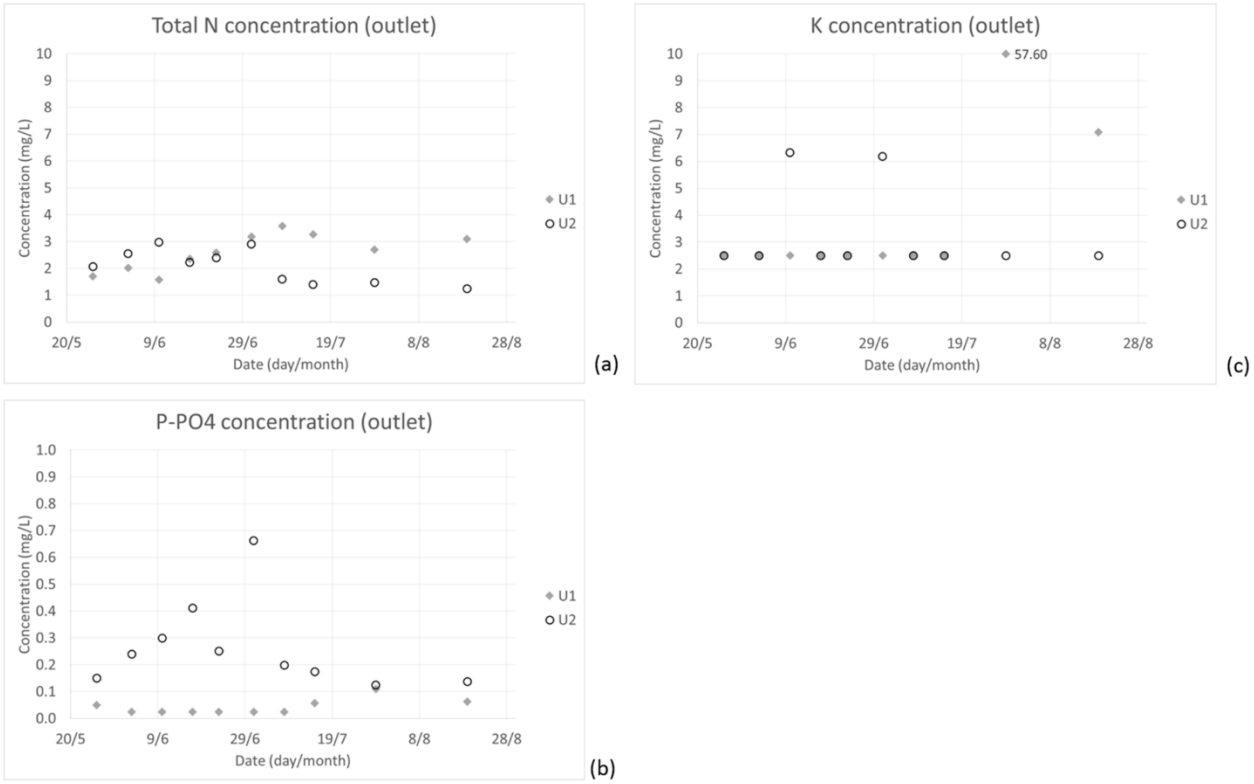

Fig. 7. Nutrient concentrations detected at the outlet sampling points: Total N (a), P-PO4 (b), and K (c). Adapted from Tediosi A, Ferrari F, Voccia D et al (2024) Herbicide and nutrient monitoring in surface waters and groundwater of a paddy district in northern Italy. Environ Sci Pollut Res 31:52963–52979. https://doi.org/10.1007/s11356-024-34692-x under exclusive licence to Springer-Verlag GmbH Germany, part of Springer Nature 2024.

When looking at N-NO3 only, at the inlet, minimum, maximum and average concentrations of N-NO3 are 0.25 mg/L, 3.73 mg/L, and 1.12 mg/L, respectively. At the outlet, minimum concentration is 0.73 mg/L, maximum concentration is 3.32 and the mean value is 1.71 mg/L.

Miniotti et al. (2016) reported field-scale data collected in 2012 - 2013, where N-NO3 concentrations reached a maximum concentration of 5.50 mg/L. Amin et al. (2021) reported N-NO3 concentrations in surface water from a rice field, where a range of 0.6–5.6 mg/L was monitored. N-NO3 concentrations detected in the present study are in line with the values reported by Miniotti et al. (2016) and Amin et al. (2021). According to a synthetic index for NO3 developed by ISPRA, the Italian Institute for Environmental Protection and Research (ISPRA 2023) and based on 91/676/CEE Directive, as far as nitrates are concerned, the following thresholds are established to characterize NO3 status in surface waters:

- 0 - 9.99 mg/L
- 10 - 24.99 mg/L (significance threshold)
- 25 - 39.99 mg/L (high significance threshold)
- 40 - 50 mg/L (attention threshold)
- > 50 mg/L (pollution threshold)

At the inlet of the district, nitrate concentrations fall in the 'significance' (10 - 24.99 mg/L) class in 6.4% of the samples. At the outlet, they fall in the range of 'significance' in 25% of them. At both inlet and outlet, concentrations are never in the higher classes.

Data monitored by ARPA in the period 2016 - 2021 show maximum concentrations that tend to be lower than the data observed in this study, which are 7.82 mg/L for total N, 3.88 mg/L for P-PO4 and 57.60 mg/L for K. For total N, ARPA average concentration is 2.33 mg/L (min 1.2 mg/L - max 3.7 mg/L) in June, 1.94 mg/L (min < 1.3 mg/L - max 2.5 mg/L) in July, and 1.93 mg/L in August (min 1.1 mg/L - max 3.8 mg/L). For total P, ARPA average concentration is 0.06 mg/L (min < 0.05 mg/L - max 0.1 mg/L) in June, 0.05 mg/L (min < 0.05 mg/L - max 0.12 mg/L) in July, and 0.07 mg/L (min 0.05 mg/L - max 0.1 mg/L) in August. For K, ARPA average concentration is 3.26 mg/L (min 2.5 mg/L - max 4.3 mg/L) in June, 3.18 mg/L (min 2.7 mg/L - max 3.8 mg/L) in July, and 3.37 mg/L (min 2.9 mg/L - max 4.1 mg/L) in August. The reasons for the lower values found by ARPA are the same as those already mentioned for herbicides.

Herbicides in Groundwater

In this Section, groundwater quality results are reported and discussed. The main highlight is that herbicide concentrations detected in the samples are always below 0.02 μg/L.

MCPA and clomazone concentrations are found to be always below 0.02 μg/L (Fig. 8). Note that, in general, in the case of groundwater sampled below 1-m depth, according to Directive 2006/118/EC a concentration of 0.1 μg/L should be considered as the end-point, which means that concentrations above this threshold are to be considered high and posing a risk in terms of water quality (Voccia et al. 2024; Dolan et al. 2013). In this study, groundwater is sampled from small piezometers and therefore when sampling more than 1 L of water as in this case, it is difficult to refer it to a specific depth, since a significant portion of piezometer is emptied.

The statistical analysis did not show any significant difference among herbicide concentrations detected in the three piezometers.

These results are consistent with the data monitored by ARPA in the neighbourhood of the district in the period 2019 - 2021, when data are available. For both MCPA and clomazone, concentrations found in 4 different sampling points (i.e., Valle Lomellina, Ferrera Erbognone, Tromello and Lomello) are always < 0.03 μg/L, apart from a single case in which clomazone was detected at a concentration of 0.04 μg/L (Lomello, 27th May 2021). Nevertheless, it must be noted that ARPA samples groundwater in April–May and October–November and not during the agricultural season as it was done in the present study. In addition to that, the ARPA groundwater

monitoring network includes both wells and piezometers with a length which is often > 15 m, even if monitoring the phreatic aquifer. Nevertheless, three out of four ARPA groundwater monitoring points close to the San Giorgio district have a length < 15 m and thus the concentrations detected are expected to be lower but more comparable with those acquired in the piezometers used in this study, which are shallower and intercept the upper part of the phreatic groundwater table during the irrigation season.

A 4-year study performed in Catalonia (Spain), which monitored 18 different groundwater bodies, reported MCPA maximum and average concentrations of 0.20 µg/L and 0.03 µg/L, respectively (Köck-Schulmeyer et al. 2014). These concentrations are approximately tenfold higher than those presented in this study (maximum and average concentrations of 0.019 µg/L and 0.005 µg/L).

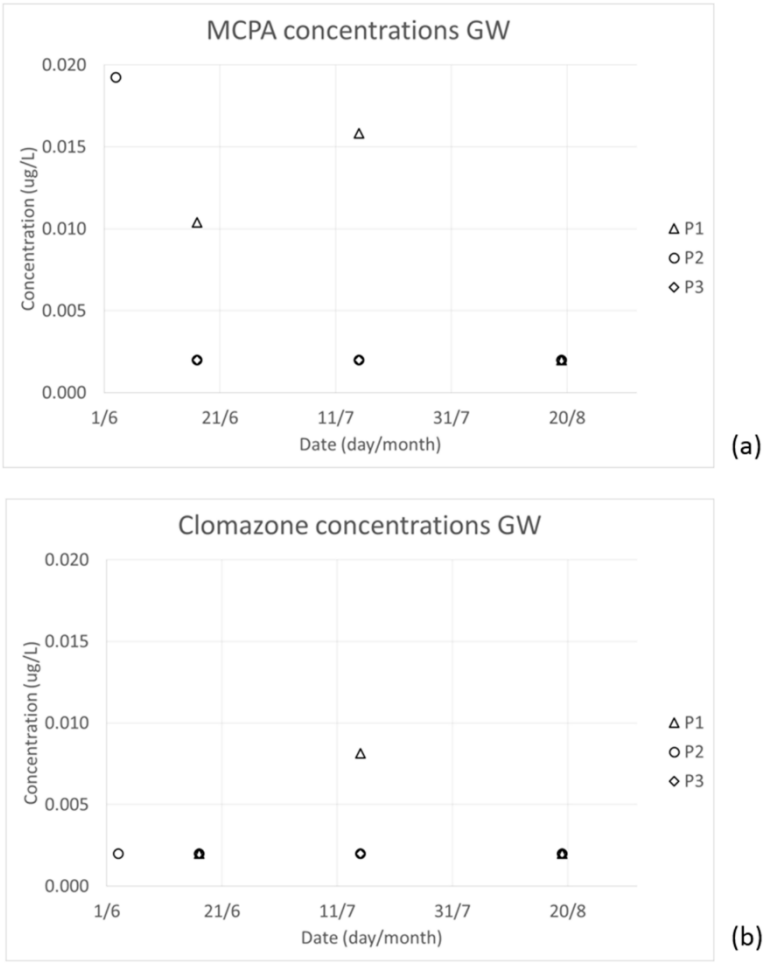

Fig. 8. MCPA (a) and clomazone (b) concentrations (µg/L) monitored in the piezometers sampled (P1, P2, and P3). Adapted from Tediosi A, Ferrari F, Voccia D et al (2024) Herbicide and nutrient monitoring in surface waters and groundwater of a paddy district in northern Italy. Environ Sci Pollut Res 31:52963–52979. https://doi.org/10.1007/s11356-024-34692-x under exclusive licence to Springer-Verlag GmbH Germany, part of Springer Nature 2024.

Nutrients in Groundwater

As to nutrients in groundwater, we highlight that: (i) nitrogen, and nitrates in particular, may pose a problem for the area; and (ii) the three piezometers monitored show different results (average concentrations are higher in P3 than in P1 and P2, with statistically significant differences for total N and K between P1 and P3).

In the piezometers monitored, nutrients showed different behaviours (Fig. 9). The maximum concentration of total N detected in the samples is 24.56 mg/L, the minimum is 0.28 mg/L and the mean value is 8.23 mg/L. In the case of P-PO4, the maximum concentration is 2.02 mg/L, the minimum is 0.19 mg/L and the mean value is 0.68 mg/L. As to K, the maximum is 87.80 mg/L, the minimum is < LOQ and the mean value is 29.36 mg/L. For total N and K, losses resulted to be higher in P3 (average concentration of 20.08 mg/L for total N and 78.90 mg/L for K) than in P2 (4.22 mg/L and 6.06 mg/L for total N and K, respectively) than in P1 (0.38 mg/L of total N and < LOQ for K). In the case of P-PO4, P3 still shows the highest concentrations (average of 0.89 mg/L), followed by P1 (0.84 mg/L), and P2 (0.32 mg/L). The statistical analysis performed shows significant differences only between P1 and P3 for both N and K levels, with higher N and K concentrations in P3 than in P1. No statistically significant differences are observed in P concentrations in the different piezometers. It should be noted that in P3 the legal limit for nitrates of 50 mg/L is always exceeded (detected values of nitrates are: 108 mg/L, 80.8 mg/L, 76.2 mg/L). Being downstream of the district, well P3 (Fig. 1, Cascina Brelle) could indicate a high nitrate contribution to groundwater quality that occurred in the district. However, the high N concentrations found in P3 could be due to generalized groundwater pollution, as values do not show a decreasing trend along the season and possibly other contributions than rice occur. In fact, human contribution to nutrient concentration in surface water and groundwater includes many activities other than rice cropping (e.g., other crops, livestock, civil contribution) (Lerner 2007; Bijay-Singh and Craswell 2021). By the way, sources of contamination near the well may be more important than those further upstream in determining the quality of the sampled water. Nutrients in groundwater might be also due to losses from civil sewage pipes (Wakida and Lerner 2005; Nguyen and Venohr 2021). In this sense, nutrient concentration in P2 could be higher compared to P1 due to the proximity to the urbanized area (town centre).

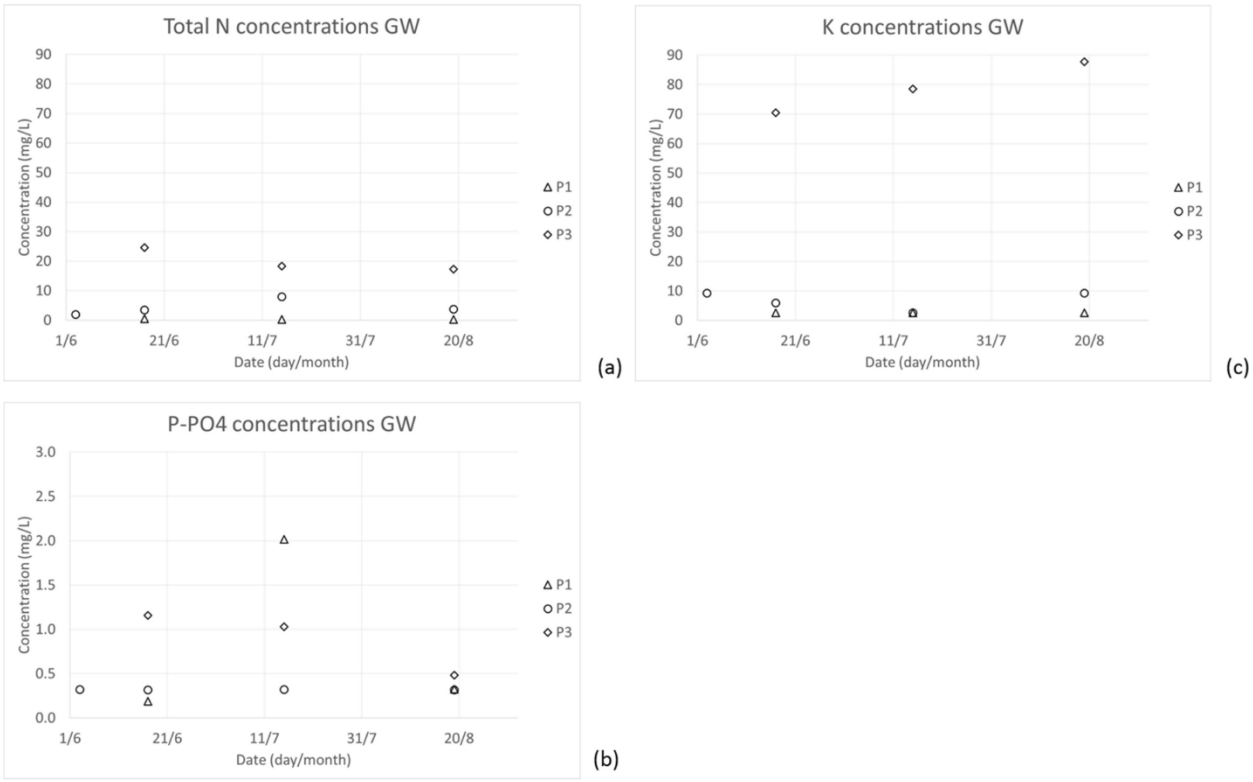

Fig. 9. Nutrient concentrations (mg/L) monitored in the piezometers sampled: total N (a), P-PO4 (b), and K (c). Adapted from Tediosi A, Ferrari F, Voccia D et al (2024) Herbicide and nutrient monitoring in surface waters and groundwater of a paddy district in northern Italy. Environ Sci Pollut Res 31:52963–52979. https://doi.org/10.1007/s11356-024-34692-x under exclusive licence to Springer-Verlag GmbH Germany, part of Springer Nature 2024.

Another study performed in Lomellina (Gosetti et al. 2019) showed maximum concentrations of total N, P-PO4 and K comparable with the present study. Gosetti et al. (2019) recorded the following maximum concentrations in 2015 - 2016: 22.4 mg/L of total N, 0.95 mg/L of P, and 91.3 mg/L of K. It should be noted that Gosetti et al. (2019) sampled the groundwater in piezometers similar to those used in the present study, but installed close to rice paddies, since the study was conducted at the farm scale in a rice farm.

By comparing data collected in the present study with the data monitored in the surrounding area by ARPA in 2021, it is possible to note that the latter values are much lower (total N ranging between < 1 and 8.7 mg/L, total P between 0.17 and < 0.05 mg/L, K between 1.5 and 2.3 mg/L). However, ARPA monitoring skips the whole agricultural season (as samples were taken in May and October); as a consequence, data cannot be directly compared to the dataset collected in this study. As to nutrients in groundwater, limits imposed by the Italian legislation are the following (reported by the 'Gazzetta Ufficiale della Repubblica Italiana' - serie generale n.165 2016): nitrates 50 mg/L, nitrites 0.5 mg/L, ammonium 0.5 mg/L. Instead, K and P have no limits, although the fixed residue values (of the sum of N, P, and K) cannot exceed 1500 mg/L. All samples resulted to be within this limit; however, among all the groundwater samples collected, 30% exceeded law limit for nitrates, but law limits for both ammonia and nitrites are never exceeded. So, concerning N, the main issue for groundwater in the district is related to nitrates. According to 91/676/CEE directive, 4 quality classes can be established for nitrate concentrations in groundwater: 0 - 24 mg/L, 25 - 39 mg/L, 40 - 50 mg/L, and > 50 mg/L. Considering all samples,

60% of them fall in the first class, 10% in the second class, and 30% in the fourth and worst class. In particular, P1 nitrate concentrations are always in the first class, P2 in the first and second classes, and P3 always in the fourth class.

Conclusions

This study investigated the presence of two commonly used herbicides in rice cropping (i.e., MCPA and clomazone) and nutrients in surface water and groundwater of the San Giorgio di Lomellina irrigation district, located in the Lombardy-Piedmont rice area. Sample collection and analysis being very expensive and time-consuming activities, this study was limited in time - one single agricultural season, 2021 - and in space - San Giorgio di Lomellina district, extending for 1000 ha. Although a longer and more widespread monitoring activity would be needed to better assess surface water and groundwater quality in the whole Lombardy-Piedmont rice area, which is the most important in Europe, we consider the district to be well representative of the surrounding agricultural land, both in terms of land use and groundwater table depth. Thus, the findings of this study can give a first insight into the impact of rice farming in the Lombardy-Piedmont regions on water resources.

As to herbicides, data at the inlet and at the outlet of the district are comparable: MCPA average concentration is 1.13 µg/L (min < LOQ - max 5.7 µg/L, excluding the peak of 13.56 µg/L from the STP) at the inlet, and 0.48 µg/L (min < LOQ - max 5.98 µg/L) at the outlet. This means that surface water quality does not seem to degrade due to MCPA and clomazone treatments occurring in the district. As to groundwater, MCPA and clomazone concentrations monitored are always below 0.02 µg/L, showing a little impact on groundwater quality related to these two herbicides. Because of the differences observed between surface waters and groundwater, we can infer that the main pathway for MCPA and clomazone transport occurs along the surface river network (e.g., runoff).

As far as nutrients are concerned, they do not show significant trends in surface waters along the season. This may be due to the fact that nutrient sources can be many and include sources other than rice (e.g., other crops, civil contribution, livestock). Total N average concentration is 2.10 mg/L (min 0.17 mg/L - max 7.82 mg/L) at the inlet and 2.33 mg/L (min 1.25 mg/L - max 3.57 mg/L) at the outlet. P-PO4 average concentration is 0.34 mg/L (min 0.02 mg/L - max 3.88 mg/L) at the inlet and 0.24 mg/L (min < LOQ - max 0.66 mg/L) at the outlet. K average concentration is 3.58 mg/L (min > LOQ – max 9.90 mg/L) at the inlet and 5.30 mg/L (min > LOQ - max 57.60 mg/L) at the outlet. When looking at N-NO3, the average concentration is 1.12 mg/L (min 0.25 mg/L - max 3.73 mg/L) at the inlet, and 1.71 mg/L (min 0.73 mg/L - max 3.32 mg/L) at the outlet. In the case of groundwater, total N average concentration is 8.23 mg/L (min 0.28 mg/L - max 24.56 mg/L). P-PO4 average concentration is 0.68 mg/L (min 0.19 mg/L - max 2.02 mg/L). As to K, the average concentration is 29.36 mg/L (min < LOQ – max 87.80 mg/L). Focusing on nitrates only, in P3 the legal limit of 50 mg/L is always exceeded. So, monitoring results point to the fact that nitrates may be more of a problem for the area than herbicides, and this seem especially true for groundwater. For nitrates, however, the sources of origin may be many and varied, and a further study would be needed to understand if rice cropping could be considered the primary source of contamination for the area.

Acknowledgements This study was carried out thanks to the MEDWATERICE project 'Towards a sustainable water use in Mediterranean rice-based agro-ecosystems'

(https://www.medwaterice.org/), selected in 2018 in the context of the PRIMA Program (https://prima-med.org; PRIMA-Section 2 - 2018).

Author contribution Arianna Facchi, Federico Ferrari, Olfa Gharsallah and Alice Tediosi designed the study. Data collection was performed by Federico Ferrari, Tommaso Ferrari, Lucio Botteri, Riccardo Rossi and Nicola Ballerini. Sample analysis was performed by Diego Voccia and Lucrezia Lamastra. The first draft of the manuscript was written by Alice Tediosi with contributions of Olfa Gharsallah and Diego Voccia. Giulio Gilardi supported the graphic design of images. Arianna Facchi, Giulio Gilardi and Olfa Gharsallah commented on previous versions of the manuscript. All authors read and approved the final manuscript.

Funding Funded, for the Italian partners, by the MUR (Italian Ministry of University and Research).

Data availability statement The data supporting the results reported in this paper can be obtained by contacting alice.tediosi@aeiforia.eu.

Declarations

Ethics approval This is an observational study with no ethical approval required. The MEDWATERICE project, in the frame of which this study was carried out, had no ethical issues. The research did not involve any of the following: human embryos and human foetuses, human participants, human cells or tissues, personal data, animals, third countries, dual use, misuse, nor other ethical issue.

Competing Interests The authors declare no competing interests.

References

Alister CA, Araya MA, Kogan M (2010) Adsorption and desorption variability of four herbicides used in paddy rice production. J Environ Sci Health B 46(1):62–68. https://doi.org/10.1080/03601234.2011.534372

Amin MMG, Akter A, Jahangir MMR, Ahmed T (2021) Leaching and runoff potential of nutrient and water losses in rice field as affected by alternate wetting and drying irrigation. J Environ Manag 297:113402. https://doi.org/10.1016/j.jenvman.2021.113402

Arienzo M, Christen E, Quayle W, Kumar A (2009) A review of the fate of potassium in the soil-plant system after land application of wastewaters. J Hazard Mater 164:415–422. https://doi.org/10.1016/j.jhazmat.2008.08.095

Bechini L, Castoldi N (2009) On-farm monitoring of economic and environmental performances of cropping systems: results of a 2-year study at the field scale in northern Italy. Ecol Indic 9(6):1096–1113. https://doi.org/10.1016/j.ecolind.2008.12.008

Belder P, Bouman BAM, Spiertz JHJ et al (2005) Crop performance, nitrogen and water use in flooded and aerobic rice. Plant Soil 273:167–182. https://doi.org/10.1007/s11104-004-7401-4

Bijay-Singh, Craswell E (2021) Fertilizers and nitrate pollution of surface and ground water: an increasingly pervasive global problem. SN Appl Sci 3:518. https://doi.org/10.1007/s42452-021-04521-8

Cabo A, Gouveia S, Cameselle C, Lee KH (2022) Monitoring of phosphorus discharge in a sewage treatment plant with a phosphate automated analyser. Environ Sci: Adv 1:483–490. https://doi.org/10.1039/D2VA00062H

Council of the European Communities (1991a) Council Directive 91/271/EEC of 21 May 1991 concerning urban waste-water treatment. https://eur-lex.europa.eu/legal-content/EN/TXT/?uri=CELEX%3A31991L0271&qid=1677074491532. Accessed 15 December 2023

Council of the European Communities (1991b) Council Directive 91/676/EEC of 12 December 1991 concerning the protection of waters against pollution caused by nitrates from agricultural sources. https://eur-lex.europa.eu/legal-content/EN/TXT/?uri=CELEX%3A31991L0676&qid=1677074285054. Accessed 15 December 2023

CTGB, Het College voor de toelating van gewasbeschermingsmiddelen en biociden (2017) BIJLAGE IV, Riskmanagement. 7737 N. MCPA. U 46 MCPA, 20170584 NLKUG

Cui N, Cai M, Zhang X, Abdelhafez A, Zhou L, Sun H, Zhou S (2020) Runoff loss of nitrogen and phosphorus from a rice paddy field in the east of China: effects of long-term chemical N fertilizer and organic manure applications. Glob Ecol Conserv 22:e01011. https://doi.org/10.1016/j.gecco.2020.e01011

da Mendes CW, Alves Júnior J, da Cunha PCR, da Silva AR, Evangelista AWP, Casaroli D (2016) Potassium leaching in different soils as a function of irrigation depths. Rev Bras Eng Agríc Ambient 20(11):972–977

Dolan T, Howsam P, Parsons DJ, Whelan MJ (2013) Is the EU drinking water directive standard for pesticides in drinking water consistent with the precautionary principle? Environ Sci Technol 47(10):4999–5006. https://doi.org/10.1021/es304955g

Environmental Protection Agency (2017) EPA water quality in Ireland 2010–2015. Johnstown Castle, Wexford

European Commission (2017) Draft Renewal Assessment Report prepared according to the Commission Regulation (EU) N° 1107/2009. Clomazone, Vol. 3 – B.9 (PPP) – Clomazone 36 g/l CS

European Union (2000) 2000/60/EC. Directive 2000/60/EC of the European Parliament and of the Council of 23 October 2000 establishing a framework for Community action in the field of water policy. https://eur-lex.europa.eu/legal-content/EN/TXT/?uri=CELEX%3A32000L0060&qid=1677075308375. Accessed 15 December 2023

European Union (2008) 2008/105/EC. Directive 2008/105/EC of the European Parliament and of the Council of 16 December 2008 on environmental quality standards in the field of water policy, amending and subsequently repealing Council Directives 82/176/EEC, 83/513/EEC, 84/156/EEC, 84/491/EEC, 86/280/EEC and amending Directive 2000/60/EC of the European Parliament and of the Council. https://eur-lex.europa.eu/legal-content/EN/TXT/?uri=CELEX%3A32008L0105&qid=1677075365169. Accessed 15 December 2023

European Union (2009) 2009/128/CE. Directive 2009/128/EC of the European Parliament and of the Council of 21 October 2009 establishing a framework for Community action to achieve the sustainable use of pesticides. https://eur-lex.europa.eu/legal-content/EN/ALL/?uri=celex%3A32009L0128. Accessed 22 February 2023

European Union (2010) 2010/75/EC. Directive 2010/75/EU of the European Parliament and of the Council of 24 November 2010 on industrial emissions (integrated pollution prevention and control). https://eur-lex.europa.eu/legal-content/EN/TXT/?uri=CELEX%3A32010L0075. Accessed 15 December 2023

European Union (2020) Directive (EU) 2020/2184 of the European Parliament and of the Council of 16 December 2020 on the quality of water intended for human consumption. https://eur-lex.europa.eu/legal-content/en/TXT/?uri=CELEX%3A32020L2184. Accessed 15 December 2023

FAO, FAOSTAT (2020) Data. http://www.fao.org/faostat/en/#data. Accessed 15 December 2023

Fernández D, Gómez S, Albarrán Á, Peña D, Rozas MÁ, Rato-Nunes JM, López-Piñeiro A (2019) How the environmental fate of clomazone in rice fields is influenced by amendment with olive-mill waste under different regimes of irrigation and tillage. Pest Manag Sci 76:1795–1803. https://doi.org/10.1002/ps.5705

Galhano V, Gomes L, Eduardo F, Videira R, Peixoto F (2011) Impact of herbicides on non-target organisms in sustainable irrigated rice production systems: state of knowledge and future prospects. In: Kortekamp A (ed) Herbicides and environment. InTech, Rijeka. ISBN: 978-953-307-476-4. Available from: http://www.intechopen.com/books/herbicides-and-environment/impact-of-herbicides-on-non-target-organisms-in-sustainable-irrigated-rice-production-systems-state. Accessed 17 June 2024

Gazzetta Ufficiale della Repubblica Italiana (2006) Serie Generale n. 88 del 14–4–2006. Supplemento Ordinario alla Gazzetta Ufficiale. Allegato 5

Gazzetta Ufficiale della Repubblica Italiana (2016) Serie Generale n. 165 del 16–7–2016

Gharsallah O, Rienzner M, Mayer A, Tkachenko D, Corsi S, Vuciterna R, Romani M, Ricciardelli A, Cadei E, Trevisan M, Lamastra L, Tediosi A, Voccia D, Facchi A (2023) Economic, environmental, and social sustainability of alternate wetting and drying irrigation for rice in northern Italy. Front Water 5:1213047. https://doi.org/10.3389/frwa.2023.1213047

Gilardi GLC, Mayer A, Rienzner M, Romani M, Facchi A (2023) Effect of alternate wetting and drying (AWD) and other irrigation management strategies on water resources in rice-producing areas of Northern Italy. Water 15:2150. https://doi.org/10.3390/w15122150

Gimsing AL et al (2019) Conducting groundwater monitoring studies in Europe for pesticide active substances and their metabolites in the context of Regulation (EC) 1107/2009. J Consum Prot Food Saf 14:1–93. https://doi.org/10.1007/s00003-019-01211-x

CropLife International (2001) Water quality monitoring: preparation & conduct of studies for the trace analysis of crop protection products in water. Technical monograph no. 20, Dec. 2001. Dépôt Légal: D/1998/2537/3

Gosetti F, Robotti E, Bolfi B, Mazzucco E, Quasso F, Manfredi M, Silvestri S, Facchi A (2019) Monitoring of water quality inflow and outflow of a farm in Italian Padana plain for rice cultivation: a case study of two years. Environ Sci Pollut Res 26. https://doi.org/10.1007/s11356-019-05155-5

Han H, Gao R, Cui Y, Gu S (2021) Transport and transformation of water and nitrogen under different irrigation modes and urea application regimes in paddy fields. Agric Water Manag 255:107024. https://doi.org/10.1016/j.agwat.2021.107024

Harlina A, Mazratul A, Abdul R, Norli I, Noridayu M (2014) Impact of rice paddies plantation activities on surface water quality in Mukim 5, Seberang Perai Utara, Malaysia. Int J Adv Agric Environ Eng 1(1):2349–1523 (EISSN 2349-1531)

Imperio S, Ranghetti L, von Hardenberg J (2017) Effects of protection status, climate, and water management of rice fields on long-term population dynamics of herons and egrets in north-western Italy. In: 6th Symposium for Research in Protected Areas, 2–3 November 2017, Salzburg (Austria), Conference Volume, pp 255–257

ISPRA, Italian Institute for Environmental Protection and Research (2023) https://indicatoriambientali.isprambiente.it/it/acque-interne/indice-sintetico-inquinamento-da-nitrati-delle-acque-superficiali-no3-status. Accessed 19 June 2024 (in Italian)

Köck-Schulmeyer M, Ginebreda A, Postigo C, Garrido T, Fraile J, López de Alda M, Barceló D (2014) Four-year advanced monitoring program of polar pesticides in groundwater of Catalonia (NE-Spain). Sci Total Environ 470–471:1087–1098. https://doi.org/10.1016/j.scitotenv.2013.10.079

Lerner DN (2007) Estimating urban loads of nitrogen to groundwater. Water Environ J 17(4):239–244

Liu J, Liu H, Liu R, Amin MG, Mostofa, Zhai L, Wang H, Zhang X, Zhang Y, Zhao Y, Ding X (2018) Water quality in irrigated paddy systems. https://doi.org/10.5772/intechopen.77339

López-Piñeiro A, Peña D, Albarrán Á, Sánchez-Llerena J, Becerra D, Fernández D, Gómez S (2019) Environmental fate of bensulfuron-methyl and MCPA in aerobic and anaerobic rice-cropping systems. J Environ Manag 237:44–53. https://doi.org/10.1016/j.jenvman.2019.02.058

Marchesan E, Zanella R, de Avila LA, Camargo ER, de Machado SLO, Macedo VRM (2007) Rice herbicide monitoring in two Brazilian rivers during the rice growing season. Sci Agric (Piracicaba, Braz) 64(2):131–137. https://doi.org/10.1590/S0103-90162007000200005

Mayer A, Rienzner M, Cesari de Maria S, Romani M, Lasagna A, Facchi A (2019) A comprehensive modelling approach to assess water use efficiencies of different irrigation management options in rice irrigation districts of Northern Italy. Water 11:1833. https://doi.org/10.3390/w11091833

McManus SL, Richards KG, Grant J, Mannix A, Coxon CE (2014) Pesticide occurrence in groundwater and the physical characteristics in association with these detections in Ireland. Environ Monit Assess 186(11):7819–7836. https://doi.org/10.1007/s10661-014-3970-8

Miniotti EF, Romani M, Said-Pullicino D, Facchi A, Bertora C, Peyron M, Celi L (2016) Agro-environmental sustainability of different water management practices in temperate rice agro-ecosystems. Agric Ecosyst Environ 222:235–248. https://doi.org/10.1016/j.agee.2016.02.010

Mockler EM, Deakin J, Archbold M, Gill L, Daly D, Bruen M (2017) Sources of nitrogen and phosphorus emissions to Irish rivers and coastal waters: estimates from a nutrient load apportionment framework. Sci Total Environ 601–602:326–339. https://doi.org/10.1016/j.scitotenv.2017.05.186

Monaco S, Volante A, Gabriele O, Cochrane N, Oliver V, Price A, Teh YA, Martinez-Eixarch M, Thomas C, Courtois B, Valè G (2021) Effects of the application of a moderate alternate wetting and drying technique on the performance of different European varieties in Northern Italy rice system. Field Crops Res 270:108220. https://doi.org/10.1016/j.fcr.2021.108220

Morton PA, Fennell C, Cassidy R et al (2020) A review of the pesticide MCPA in the land-water environment and emerging research needs. Wires Water 7:e1402. https://doi.org/10.1002/wat2.1402

Muthayya S, Sugimoto JD, Montgomer S, Maberly GF (2015) An overview of global rice production, supply, trade, and consumption. Ann N Y Acad Sci 1324:7–17

Nguyen H, Venohr M (2021) Harmonized assessment of nutrient pollution from urban systems including losses from sewer exfiltration: a case study in Germany. Environ Sci Pollut Res 28. https://doi.org/10.1007/s11356-021-12440-9

Parisse B, Pontrandolfi A, Epifani C, Alilla R, De Natale F (2020) An agrometeorological analysis of weather extremes supporting decisions for the agricultural policies in Italy. IJAm 15–30. https://doi.org/10.13128/ijam-790

Pittelkow C, Liang X, Linquist B et al (2015) Productivity limits and potentials of the principles of conservation agriculture. Nature 517:365–368. https://doi.org/10.1038/nature13809

PPDB (n.d.) Pesticide Properties DataBase. http://sitem.herts.ac.uk/aeru/ppdb/en/Reports/168.htm. Accessed 15 December 2023

Pryor D, Saarman E, Murray D, Prell W (2007) Nitrogen loading from wastewater treatment plants to Upper Narragansett Bay. Narragansett Bay Collection. Paper 2. https://digitalcommons.uri.edu/nbcollection/2. Accessed 19 Aug 2024

Resgalla C, Noldin JA, Tamanaha MS, Deschamps FC, Eberhardt DS, Rörig LR (2007) Risk analysis of herbicide quinclorac residues in irrigated rice areas, Santa Catarina, Brazil. Ecotoxicol 16:565–571

Richard P, Pohanish M (2015) Sittig's handbook of pesticides and agricultural chemicals (Second Edition). William Andrew Publishing, pp 518–597. ISBN 9781455731480. https://doi.org/10.1016/B978-1-4557-3148-0.00013-3

Spycher S, Mangold S, Doppler T, Junghans M, Wittmer I, Stamm C, Singer H (2018) Pesticide risks in small streams—How to get as close as possible to the stress imposed on aquatic organisms. Environ Sci Technol 52(8):4526–4535

Tran ATK, Hyne RV, Doble P (2007) Determination of commonly used polar herbicides in agricultural drainage waters in Australia by HPLC. Chemosphere 67:944–953

Ueji M, Inao K (2008) Rice paddy field herbicides and their effects on the environment and ecosystems. Weed Biol Manag 1:71–79

Vidotto F, Fogliatto S, Carmagnola L, De Palo F, Milan M (2021) Off-site movement of quinclorac from rice fields. Ital J Agron 16:1798. https://doi.org/10.4081/ija.2021.1798

Voccia D, Lamastra L, Fragkoulis G, Facchi A, Gharsallah O, Ferrari F, Tediosi A, Trevisan T (2024) Improving a herbicide risk assessment model in paddy rice cultivation. Heliyon 10(5):e26908. https://doi.org/10.1016/j.heliyon.2024.e26908

Wakida F, Lerner D (2005) Non-agricultural sources of groundwater nitrate: a review and case study. Water Res 39(1):3–16. https://doi.org/10.1016/j.watres.2004.07.026

Weng S, Zhu W, Dong R, Zheng L, Wang F (2019) Rapid detections of pesticide residues in paddy water using surface-enhanced Raman spectroscopy. Sensors 19:506. https://doi.org/10.3390/s19030506

Zampieri M, Scoccimarro E, Gualdi S, Navarra A (2015) Observed shift towards earlier spring discharge in the main Alpine rivers. Sci Total Environ 503–504:222–232. https://doi.org/10.1016/j.scitotenv.2014.06.036

Zampieri M, Ceglar A, Manfron G, Toreti A, Duveiller G, Romani M, Rocca C, Scoccimarro E, Podrascanin Z, Djurdjevic V (2019) Adaptation and sustainability of water management for rice agriculture in temperate regions: the Italian case-study. Land Degrad Dev 30. https://doi.org/10.1002/ldr.3402

Zimdahl RL (2018) Chapter 16 - Properties and uses of herbicides. In: Fundamentals of weed science (fifth edition). Academic Press, pp 463–499. ISBN 9780128111437. https://doi.org/10.1016/B978-0-12-811143-7.00016-0